PhD Thesis
2016

Repair mortars for stone : Increased compatibility through optimised development

Aurélie Isebaert

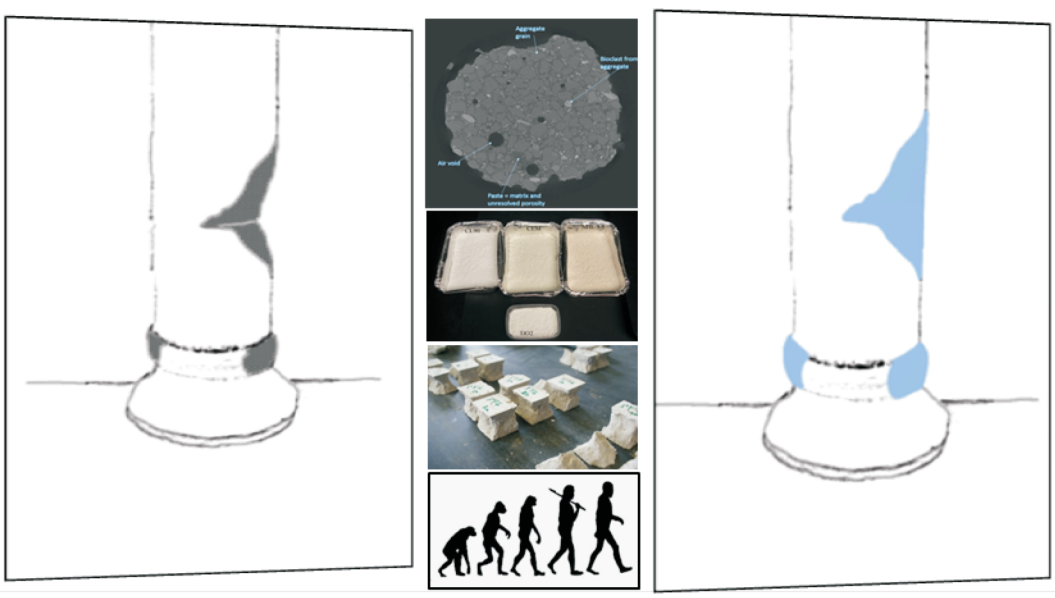

UMONS Université de Mons
POLYTECH MONS
GHENT UNIVERSITY

UMONS

GHENT UNIVERSITY

Repair mortars for stone: Increased compatibility through optimised development

Aurélie Isebaert

A doctoral thesis submitted in partial fulfilment of the requirements
for the joint doctoral degree in
Doctor in Architecture and Urban Planning (University of Mons)
and Doctor of Science: Geology (Ghent University)

Supervisors
Professor L. Van Parys, University of Mons
Professor V. Cnudde, Ghent University
Jury
Professor T. Descamps, University of Mons
Professor J.M. Baele, University of Mons
Professor M. De Bouw, University of Antwerp
Dr. H. Derluyn, Ghent University
Dr. J. Hughes, University of Glasgow
Professor D. Laplume, University of Mons
Professor W. Quist, Delft University of Technology

This thesis was funded by both the Materials Research Institute, University of Mons and the Special Research Fund at Ghent University

Abstract

Built heritage often demands interventions in order for it to resist weathering and deterioration. The materials applied on built heritage are aimed to be compatible with the original building material. Repair mortars for stone also need to fulfil this demand: the properties of every mortar should thus depend on the properties of the stone. Repair mortars are however not always chosen for their adapted properties, mainly because time and budget do not permit to determine what mortar recipe is (most) compatible and durable.

In this thesis, a new system is introduced which, based on the requirements of the stone, will propose several potentially compatible mortar recipes. The number of potential mortar recipes which should be produced and tested is as such reduced. The system focuses on three properties of the mortar -permeability, colour and elasticity- since in terms of performance they proved to be the most influential for compatibility. As the system should be able to present mortar recipes, this thesis discusses the effect of the mortar components on each of these three properties. Their effect is determined by theory and experimental campaigns. This knowledge is used in this thesis for the development of an estimation method for both permeability and elasticity and the adaptation of an estimation method for colour. These estimation methods were implemented into an optimisation algorithm, able to create mortar recipes based on a database and the established estimation methods. Finally, this system as a whole was tested on various natural sedimentary stones.

The thesis leads to the conclusion that the system presented here sets a solid base for an optimised mortar development. Future research can improve the system through the implementation of mineralogy as a compatibility parameter or by elaborating the estimation methods by including the effect of ageing.

Samenvatting

Bouwkundig erfgoed kan enkel verwering en alteratie weerstaan door de interventies die er op worden uitgevoerd. De materialen die worden toegepast op dit bouwkundig erfgoed moeten daarom compatibel zijn met de originele bouwmaterialen. Ook herstelmortels voor natuursteen moeten aan deze eis voldoen: de eigenschappen van elke mortel hangen dus zo af van de eigenschappen van de natuursteen. Maar herstelmortels worden niet altijd gekozen voor hun aangepaste eigenschappen. Dit is voornamelijk vanwege tijds- en budgetbeperkingen die niet toelaten om mortelrecept te ontwikkeln dat (het meest) compatibel en duurzaam is.

In deze doctoraatsthesis wordt een systeem voorgesteld dat, gebaseerd op de eigenschappen van de steen, verschillende potentiële compatibele mortelrecepten voorstelt. Het aantal mortelrecepten dat zo geproduceerd en getest moet worden, wordt aldus gereduceerd. Het systeem concentreert zich op drie eigenschappen van de mortel - permeabiliteit, kleur en elasticiteit - aangezien ze vanuit het standpunt van gedrag het meest de compatibiliteit beïnvloeden. Aangezien het systeem mortelrecepten moet kunnen voorstellen, presenteert deze thesis het effect van de mortelingrediënten op elk van deze drie eigenschappen. Hun effect op de finale morteleigenschappen werd bepaald op basis van theoretische modellen en experimentele studies. In dit onderzoek werd deze kennis gebruikt voor de ontwikkeling van inschattingsmethodes voor permeabiliteit en elasticiteit en de aanpassing van een inschattingsmethode voor kleur. Deze inschattingsmethodes werden samen met een databank van zanden en bindmiddelen in een optimalisatiealgoritme geïntroduceerd, zodat het in staat is om mortelrecepten te ontwikkelen. Dit systeem werd in zijn geheel getest op verschillende sedimentaire natuurstenen.

De thesis leidt tot de conclusie dat dit systeem een solide basis vormt voor een geoptimaliseerde mortelontwikkeling. Toekomstig onderzoek kan het systeem verbeteren door de implementatie van de mineralogie van de mortel als compatibiliteitsparameter of door de uitbreiding van de inschattingsmethodes met de veroudering van steen en mortel.

Preface

To research repair mortars for stone might seem a very specific topic, but it came quite naturally to me. I chose this topic because of my interest in materials, and, due to my background of conservator-restorer, more specifically into the new materials used to restore something which has 'lived' so long. The reasons for which we choose to use these materials and not others, the knowledge we have about them and what we expect from them versus what reality tells us, has fascinated me throughout my studies.

The thesis presents the study of mortar components and their influence on the mortar properties, and sets a base for future research into the optimisation of compatible mortar recipes. In order to achieve this, this work presents the subject of repair mortars out of one angle, the optimisation of compatible mortars, but more than one field of research was required in order to bring this research forward and understand these materials better. Consequently, this thesis was written as a joint doctoral thesis between the Faculty of Engineering at the University of Mons and the Faculty of Sciences at Ghent University. The search for improved mortar recipes is mainly fed by an engineering approach, while the understanding of the mortar components, chemically and physically, are more appropriate to the natural sciences field. The subject required thus a multidisciplinary approach, and the reader will find himself looking at, for example, various measuring techniques for pore-related properties, as well as Darwin's principle of survival of the fittest.

I hope the reader with an interest in built heritage and natural stones will find this work and the conclusions it draws worthwhile and valuable, that it will help understand the behaviour and improve our expectations of these new materials we apply on old buildings.

This preface cannot go by without thanking a number of persons who have helped me from close or from far these past four years.

First of all, I would like to thank my two supervisors, Laurent Van Parys and Veerle Cnudde. Without them, this research would not be what it has become today. Their guidance, their questions and their suggestions have led me further than I thought myself capable of. Each in their own specific style, most likely inherent to their point of view as engineer or natural scientist, have reached out elements on occasions important for either fields. As the researcher performing a joint PhD, I have to admit that the combination of these two point of views was sometimes hard to reconcile. As a result, the thesis is neither a pure scientific work, nor a work completely written as an engineer. Perhaps, it also requires someone with another

background to attempt to study a subject as this one. I have great respect for both my supervisors, since it is mainly their belief in me that has allowed me to perform this research, demanding and exciting at the same time. During my four years as doctoral student, I was also guided by my doctoral advisory committee: Thierry Descamps, Jean-Marc Baele, David Laplume and Hannelore Derluyn, who had pertinent questions and remarks ready whenever I laid out results or questions.

I would like to thank Marjorie Olivier and the Materials Research Institute at the University of Mons as well as the Special Research Fund at Ghent University for the funding of my research.

I also have to thank the various students who have performed their Master thesis in the light of my research and whose results are included in this thesis. Quentin, Sandrine, Sophie, Laurent and Ivan, please know that without your contributions, some experimental campaigns would not have existed.

Due to the multiple disciplines required for this research, I have had the opportunity to meet and work with many interesting persons from various fields. I would like to thank Michel Renglet for his invaluable advice concerning colour and colour measurements, Fanny Descamps and the department of Mining Engineering at the University of Mons for the use of the water permeameter, Jeroen Dils, Philip Van den Heede and Geert De Schutter from Labo Magnel at Ghent University for the use of their MIP equipment, Matthieu Boone and the entire team of UGCT for the use of the micro-CT scan and Mathijs Dumon and Eric Van Ranst for the XRD analysis at Ghent University. I also have to thank INISMA for the laser grain size analysis, and the BRRC for the use of their spectrophotometer. A thank you goes as well to Francis Tourneur who was willing to discuss with me all possibilities for these building stones of the Ursuline Convent in Mons.

A special word goes out to my colleagues and ex-colleagues at both research groups. Mijn collega's en ex-collega's in Gent: Jeroen, Tim, Tom, Hannelore, Victor en Danielle, maar ook Wesley, Jan, Delphine en Marijn, zou ik willen bedanken voor de leuke momenten tijdens de middagpauzes, jullie grappen en de streken die jullie uithaalden, voor de tijd die jullie maar al te graag wilden steken in het scannen of de uitleg die jullie gaven bij een techniek die ik nog niet onder de knie had. Mes collègues à Mons, au début, cette petite flamande a dû travailler pour avoir un niveau suffisant en français pour comprendre vos histoires et vos blagues. Coralie, Anass, Bertrand, Sélim, Thierry, Lucia, Patrick et Michaël, mais aussi Laurent, Jérôme, Dhouha et Elodie, j'aimerais tous vous remercier pour votre aide, soit technique, soit au niveau de logiciels, soit mentale avec vos mots de soutien. Un grand merci à Coralie pour avoir relu des parties de ma thèse.

Last but not least, I would like to thank my family and friends. Jullie waren er steeds voor mij, luisterden naar me als dat nodig was of praatten over volstrekt andere dingen als ik afleiding nodig had. Jullie hebben me gesteund op verschillende vlakken doorheen dit vierjarig avontuur, met zachte woorden, motiverende woorden, grappige woorden. Mama, papa, dit is ook een beetje jullie werk: jullie steun heeft er mee voor gezorgd dat dit werk hier nu op tafel ligt. Daniel et Monique, merci pour la confiance et cet appui logistique qui me permettait d'aller de Gand à Mons à Anvers à… : vous avez fait en sorte que je pouvais mieux me concentrer sur les

choses principales. Bedankt Julie en Thomas om jullie zelf te zijn, een zus en schoonbroer zonder gelijk zijn jullie. En, natuurlijk, om mijn teksten door te nemen als twee gemotiveerde, professionele editors. Als laatste, maar zeker niet de minste, Vincent, zou ik je willen bedanken voor je geduld, je grappen, je steun: je geeft me de kans altijd meer en verder te ontdekken.

Aurélie Isebaert
September 30th 2016

Table of Contents

List of symbols

This list of symbols is not exhaustive: all symbols used only locally in the text are not represented in this list.

Roman symbols

A	Cross-sectional area [m]
D	Pore diameter [m]
D_1	1st modal pore throat diameter [m] by MIP
D_2	2nd modal pore throat diameter [m] by MIP
D_{50}	Aggregate grain size diameter at 50% passing
$D_{critical}$	Critical pore diameter [m]
D_{max}	Maximal aggregate grain size [m]
D_{tube}	Diameter of the tube (packing density test) [m]
E	Elasticity modulus [N/m²]
F	Force [N]
f	Porosity [m³/m³]
F_c	Compressive strength [MPa]
h_{tube}	Height of the tube (packing density test) [m]
I	Intensity [photons/s]
KI	Compacting index [-]
k	Permeability [m³s/kg]
k'	Intrinsic permeability [m²]
L	Length [m]
L*a*b*	CIELAB colour coordinates
m	Mass [kg]
M	Molar mass [kg/mol]
MPT	Maximum Paste Thickness [mm]
$p_{aggregate}$	Adherence factor aggregate grains [-]
p	Pressure [N/m²]
q	Stiffness [N/m]
Q	Volume flow rate [m³/s]
R	Gas constant [J/(mol K)]
r_a	Anhydrated cement grain radius [m]
R_c	Resistance binder [MPa]
r_h	Hydrated cement grain radius [m]

r_{mean}	Mean aggregate grain radius [m]
S	Surface [m²]
$S_{<80\ \mu m}$	Volume percent smaller than 80 µm [-]
T	Temperature [K]
T_{ITZ}	ITZ thickness [m]
u	Volumetric flow velocity [m/s]
V	Velocity [m/s]
V	Volume [m³/m³]
xyY	CIE1931 colour coordinates
XYZ	Tristimulus colour coordinates, from CIE1931
ΔE*	Difference in colour [-]
ΔE_{stat}	Difference in static elasticity [% of target]
Δk	Difference in permeability [% of target]
ΔL	Elongation [m]

Greek symbols

γ	Virtual packing density [-]
δ	Displacement [m]
ε	Strain [N/m²]
η	Viscosity [kg/(m s)]
ν	Poisson ratio [-]
ρ	Apparent mass density [kg/m³]
σ	Stress [N/m²]
φ	Real packing density [-]

Abbreviations

B/A	Binder to aggregate ratio
BSE	Backscattered electron
C-A-H	Calcium aluminate hydrate
CIE1931	Colour space as defined in the CIE report of 1931
CIELAB	Colour space as defined in the CIE report of 1986
C-S-H	Calcium silicate hydrate
ITZ	Interfacial transition zone
micro-CT	Micro-computed tomography
MIP	Mercury intrusion porosimetry
NHL	Natural hydraulic lime
NSGA II	Non dominated sorting genetic algorithm II
RF	Resonance frequency
RH	Relative humidity [%]
W/B	Water to binder ratio
XRD	X-ray diffraction

Chapter 0 Introduction

0.1 Context

The building stones present in our built heritage are subject to the weather conditions they are exposed to. Weathering of the stone can be induced by the migration of water and dissolved agents in the water, such as salts, but stones can also weather due to the action of wind and rain. The stone can also be damaged through its use, the function it has in the building, such as a step of a staircase, corner stone or architectural detail. Both function and environment lead to the deterioration of stone and create deterioration patterns visible on the stone [1]. In order for the built heritage to be in good condition, restoration interventions are necessary which include the implementation of new materials such as repair mortars.

Repair mortars generally consist of a binder, aggregates and sometimes additives or adjuvants. The binders used for these repair mortars can vary from lime to cement to resins. Empirical results show they can attain a life expectancy of 30 years [2,3]. Repair mortars are used to fill in building blocks, or complete architectural details and sculptures. These mortars can be used for restoration, given that the stone itself is still in sound condition, i.e. the repair mortar could only prevent up to a certain level future deterioration, it cannot protect against any deterioration agents already present in the stone, such as salts.

The mortars used for restoration practice must satisfy very specific requirements, since a repair mortar is used in an already existing structure, adjacent to other materials with their own properties, such as in Fig. 0.1. Since the aim of repair mortars is to preserve the original stone material, these materials are (ideally) self-sacrificing [4,5]. Essentially, in order to be compatible, the mortar's properties should be as such that the new repair mortar does not damage the original or older material and building, or any of the values it withholds (such as cultural or historical value) [6]. Only then, the material can be called sacrificial: it is sacrificed for the better preservation of the building. Naturally, the durability of the intervention is important as well, but it is ideally subjected to the concept of self-sacrificial materials.

In order to know whether or not a repair mortar is compatible with a natural stone, this concept of compatibility should be quantified in some way. Looking at repair mortar and its behaviour in a building, the mortar can 'damage' the stone and, in extension, the building, in multiple ways, going

from disturbance of the visual aspect to the physical behaviour of the mortar and the durability of the intervention. This leads to the idea that compatibility of a repair mortar could be determined through two concepts: the comparison of various properties of repair mortar with those of the stone and the quality control of the (application) techniques used. For the latter, both choice of application and the skill of the practitioner are important for the success of the intervention. The first concept would on his turn identify the 'intrinsic' compatibility of the mortar, by researching the mortar's properties. From this point of view, mortars should be adapted to the surrounding materials, e.g. the mortar's colour should be adapted as such that it is compatible with the stone in colour. This work starts thus from the principle that every property of a mortar contributes to the mortar's total (intrinsic) compatibility, and that as such, compatibility can be increased by aiming to change properties of the mortar which were not compatible before.

Following the aspect of self-sacrificing, this concept of *compatibility* is not by definition equal to *similarity* in properties: the mortar's properties should be adapted to the stone's values in order not to harm the stone. For example, one might ideally aim for the same colour but a different surface finish for example, for ethical reasons, as one might ideally aim for the same moisture transfer capacities but a higher deformability for a higher durability.

Fig. 0.1. Restoration of architectural details with repair mortar at the entrance of the St. Anne church, Bottelare, Belgium. The plinth, ornamental detail and column have been restored with repair mortar.

At present, it is difficult to design or adapt repair mortars for stone in a successful and efficient way. First of all, mortar components are often chosen out of experience, and not necessarily because their effect on the mortar's

final properties are all known and wanted for. In addition, there are commercial repair mortars available, which are designed for the repair of one stone type. Most users of these mortars have to trust the information given by the producer of this readily-available mortar mixes, since the list of components is company property and is therefore not made public. A list of properties of the mortar is often presented by the producer, but might lack certain information (e.g. test methods, age of testing), or is incomplete (e.g. the user might need a property not given by the producer). These commercial mortars are assumed to have a colour which is more or less similar to the natural stone it is designed for, but it might be that the final colour is different from the stone the user would like to repair. This might be because of previous interventions which took place on the stone, or because the stone variety is not very homogeneous in colour naturally.

In both situations, commercial repair mortar and experience-based mortar, the user can only assure himself of the quality and/or compatibility of the repair mortar by testing the mortar. For this testing, several steps are necessary before the mortar can be judged to be compatible or not (Fig. 0.2). After a mortar mix or mortar recipe is chosen, the mortar is made and left to cure, a process which might take several months before completion due to the setting reactions of the binder components. The mortar is tested on properties, such as porosity, depending on available time and budget. If testing reveals the mortar recipe has to be adapted, the entire process might start again. Unfortunately for the stones in built heritage, processes as described above are time-consuming and expensive. Performing multiple cycles as presented here is thus quite uncommon and reserved for some specific significant projects. Conclusively, the development of mortars as it exists now is not efficient. Often as well, not enough cycles are made due to a lack of time or budget, making such a mortar development process not adequate either.

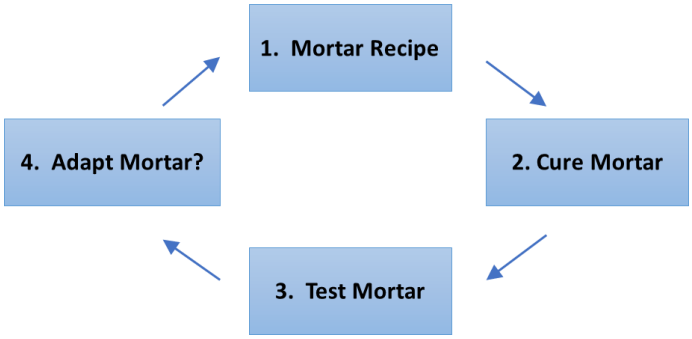

Fig. 0.2. Sketch of a typical mortar design process.

Conclusively, we can state that a vacuum exists in the current research field. At present, most of the research concerning compatible mortars only discuss pointing mortars, e.g.[7,8], and only a few also include repair mortars for stone [9]. No general approach for repair mortars is present: the current studies for the development of adequate compatible repair mortars all focus on mortars for one particular stone, based on experimental campaigns, e.g.

[10–12]. Other articles only confirm the problem, by reporting on failed restoration interventions with repair mortars, due to a lack of knowledge of the used materials [13,14] or because priority was set on visual appearance [15–17].

Previous research performed at the University of Mons has laid foundations to develop efficient mortars by using an optimisation algorithm which narrowed down the choice to some mortar recipes [18,19]. The optimisation algorithm selected mortar recipes based on estimated colour and compressive strength, and was designed for cement mortars only.

0.2 Purpose

The general purpose of this study is to improve the development of repair mortars. The methodology will be improved by creating a system (Fig.0.3) based on the previous research by [18,19] and by adding knowledge concerning mortar components through experimental campaigns and by adding new criteria such as permeability. The purpose of the system is to present mortar recipes close to the 'ideal properties' the mortar should have. The system would as such serve as a computer-aided decision tool, where the user can decide to use the mortar recipes proposed by the algorithm. The implementation of the algorithm serves to reduce the number of cycles necessary to find a compatible mortar to only one cycle (Fig. 0.2).

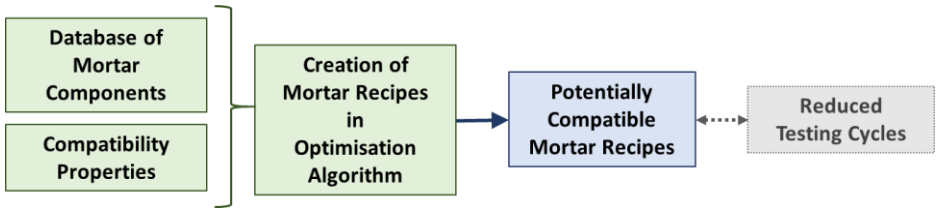

Fig. 0.3 Optimized mortar development represented as a system, where mortar recipes are generated based on information from the stone, the database of binders and sand, using an algorithm. The outcome of a set of potentially compatible mortar recipes will strongly reduce the number of testing cycles required to find the compatible mortar recipe.

The methodology itself will be improved by the algorithm in order to narrow down the number of recipes that have to be tested before finding a compatible mortar. In order to make this approach work, the properties of a mortar recipe should thus be estimated *before* the mortar is actually made. Consequently, the estimation methods the algorithm will rely on, are based on the mortar components, the only elements known before making a mortar. The algorithm is designed to propose suitable mortar recipes, leaning on knowledge of mortar components and on property estimation methods.

The properties which are to be estimated, are set to the three properties which influence most the decision of compatibility in the technical sense of

the term, i.e. mechanically or physically. The approach in this thesis is thus a performance-based approach, and will not take the mineralogical content into account. Consequently, the research will encompass the study to each of these three properties and methods for their estimation based on mortar components. Various experimental campaigns will be carried out in order to understand the main influence of the various mortar components, such as aggregate grain size distribution or binder resistance, on the final properties of the mortar.

The estimation methods for each of these properties will have to fulfil some requirements, too. The first one demands the method to be based on properties from the mortar components. Secondly, since the estimation method will serve later in an algorithm, methods are not allowed to be too complex. These estimation methods have thus to be simple enough so they can be easily implemented into the algorithm, but still provide reliable estimations.

The primary focus of the research is to obtain a compatible mortar in performance by using the three primary components of a mortar: binder, sand and water. The focus of this research is set on mortars made with Natural Hydraulic Lime (NHL), at 90 days of age, since lime mortars have been used frequently for conservation purposes, e.g. [20–23].

The number of primary components is kept limited for this research because a very large database of sands and binders would include extensive experimental campaigns, increasing the risk that the influence of every mortar component is not well understood.

The addition of various adjuvants might seem advantageous in order to obtain very specific properties, and might be useful in future research, but will not be used here in order to be able to determine the influence and boundary limits of the primary mortar components.

The research will not include the effect of weathering or ageing on the variation in mortar properties, since it is assumed more appropriate to make the system function well for mortars in good condition. The research is limited to repair mortar development only, and will not include the application and other elements which might influence the compatibility of the intervention. This is considered to be an additional complexity of the repair mortar problem, since it includes many factors extrinsic to repair mortar itself (e.g. the condition of the stone, the craftsmanship from the restorer, how the stone surface is prepared, or the climate and weather conditions).

Finally, the entire system is aimed to be transparent for the user, starting from the database which could be adapted by the user, to the estimation methods and functioning of the algorithm explained in this thesis. Moreover, the approach is as such that the general set-up of this system will permit to extend the database and include the mineralogy of each aggregate. Consequently, following research questions will be answered throughout this research:

1. *What are the physical and mechanical properties of a repair mortar that determine the compatibility?*
2. *Can a certain tolerance range for each compatibility property be allowed?*
3. *How do the mortar components influence these compatibility properties?*
4. *Can these compatibility properties be reasonably estimated based on the mortar components?*
5. *Can the process of mortar development be made efficient by introducing an optimisation algorithm which proposes mortar recipes, based on information from previous answers?*

0.3 Set-up

The research is split up into seven chapters and systematically tries to answer the questions defined above (Fig. 0.4).

Chapter 1 discusses compatibility properties between repair mortar and stone. This discussion is held from a practical point of view, fitted to the compatibility of a repair mortar in technical properties. This chapter also relates on possible tolerance ranges for every compatibility property. This chapter finally discusses what and how compatibility properties can be ranked.

Chapter 2 details on the various mortar components and the reported effect they have on the properties of the hardened mortar. The various types of binders which are used for repair mortars are discussed, as well as the influence of aggregates and mixing ratios (water/binder, binder/aggregate). In addition, this chapter includes the research towards the binders and aggregates used for the experimental campaigns in this research, and lists the various mortar mixes of these experimental campaigns.

The *third, fourth* and *fifth* chapter are each devoted to one of the three compatibility properties selected for this research: the permeability, the colour and the elasticity, respectively. The final goal of each of these chapters is the proposal of an estimation method for each property. The set-up for each of these chapters is similar: first, the theory is discussed, followed by a discussion concerning possible measuring techniques and an experimental study. Accordingly, it is followed by the study and adaptation or development of an adequate estimation method and its exploitation based on the experimental study.

Chapter 3 discusses the permeability and other pore-related properties of lime mortars. Since this property is deemed as determining for the final compatibility of the mortar, and since the information concerning pore-related properties of lime mortars found in literature was deemed insufficient, a

detailed experimental study was performed for this thesis. Moreover, no valid existing estimation method could be found for permeability for lime mortars, hence, this chapter will detail on the development of a new method for the estimation of permeability, using mortar components.

Chapter 4 discusses the colour of mortars and the influence the mortar components have on this property. The estimation method for this property was adapted for this thesis from the Grassmann theory for colour mixing.

Chapter 5 discusses the elasticity and relating mechanical properties of lime mortars. In addition, the influence of the mortar components on the mortar's elasticity is looked into by means of an experimental study. The estimation method used for this property was adapted from an already existing method.

Chapter 6 relates the use of a genetic algorithm for the development of repair mortars, created based on the knowledge of mortar components, leading to a more compatible mortar recipe. The choice for the specific algorithm is expound on and the architecture of the algorithm, including the various estimation methods, is explained. The robustness of the algorithm is illustrated in the final section of this chapter.

These six chapters explain thus in total the functioning of the repair mortar development system.

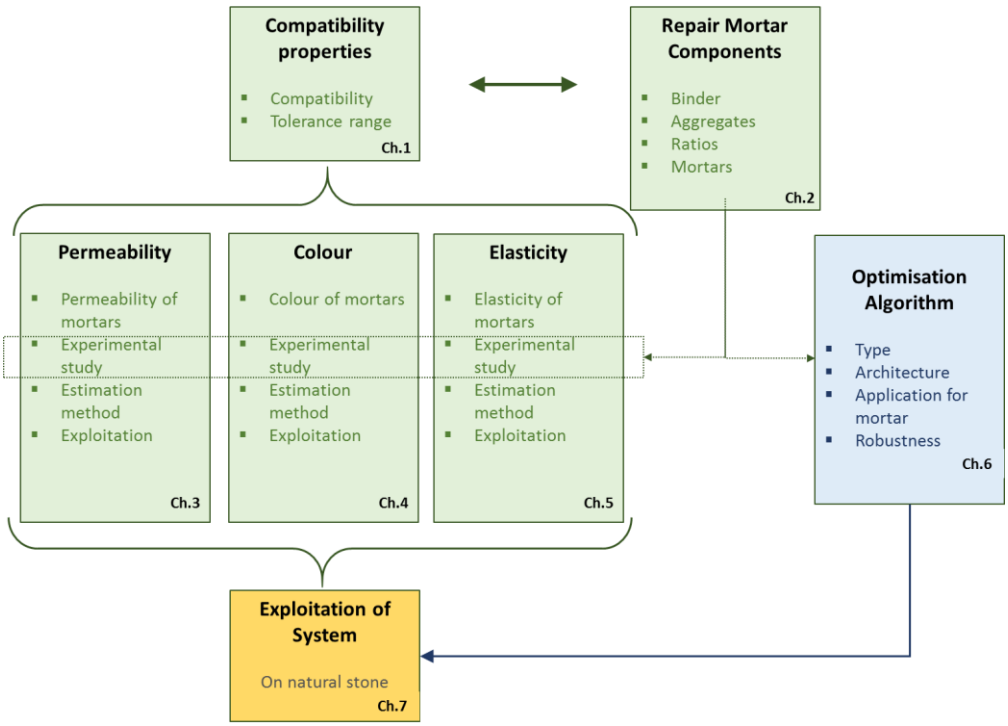

Fig. 0.4 Lay-out of the thesis. Each unit represents one chapter (indicated in the right lower corner). The arrows present the relation of each unit towards the other.

Chapter 7 has as goal to exploit this newly developed system, and test it on four sedimentary stones used as building stones. The produced mortars made were recipes proposed by the system. The estimated property values and the measured property values are compared and discussed into detail, as well as the measured mortar and stone property values. Based on the

information and data gained from previous chapters, an innovative method for the improvement of repair mortars was developed.

Chapter 8 presents the overall discussion of results, the conclusions of this study, accompanied by perspectives for future research. The conclusions of the thesis point out the influence of the actual resistance of the binders (in chapter 2) on the mortar properties (chapters 3 and 5), as well as the added value of the experimental campaigns for all three properties (chapters 3, 4 and 5) on the estimation methods. Finally, chapter 8 discusses the implementation of the estimation methods into an optimisation algorithm (chapter 6), and the conclusions which can be drawn from its application on natural stones (chapter 7).

Bibliography

[1] ICOMOS, ISCS. Illustrated glossary on stone deterioration patterns. Champigny: Ateliers 30 Impression; 2008.

[2] Torney C, Forster AM, Kennedy CJ, Hyslop EK. "Plastic" repair of natural stone in Scotland: perceptions and practice. Struct Surv 2012;30:297–311. doi:10.1108/02630801211256643.

[3] Ashurst J, Dimes F. Conservation of building and decorative stone. 1998.

[4] ICOMOS. International charter for the conservation and restoration of monuments and sites (the Venice charter 1964). 1964.

[5] ICOMOS. The Nara document on authenticity (1994). 1994.

[6] Munoz-Vinas S. Contemporary Theory of Conservation. Routledge; 2012.

[7] Groot C, Hughes J, Van Balen K, Bicer-Simir B, Binda L, Elsen J, et al. RILEM TC 203-RHM: Repair mortars for historic masonry. Mater Struct 2012;45:1277–85. doi:10.1617/s11527-012-9916-0.

[8] Van Balen K, Papayianni I, van Hees RPJ, Binda L, Waldum A. RILEM TC 167-COM: Characterisation of old mortars with respect to their repair: Introduction to requirements for and functions and properties of repair mortars. Mater Struct 2005;38:781–5. doi:10.1617/14319.

[9] Griswold J, Uricheck S. Loss compensation methods for stone. J Am Inst Conserv Hist Artist Work 1998;37:89–110.

[10] Bromblet P. Evaluation of durability and compatibility repair limebased mortars. Int Zeitschrift Für Bauinstandsetz Und Baudenkmalpfl 2000.

[11] Beck K, Al-Mukhtar M. Formulation and characterization of an appropriate lime-based mortar for use with a porous limestone. Environ Geol 2008;56:715–27. doi:10.1007/s00254-008-1299-8.

[12] Szemerey-Kiss B, Török Á, Siegesmund S. The influence of binder/aggregate ratio on the pore properties and strength of repair mortars. Environ Earth Sci 2013;69:1439–49. doi:10.1007/s12665-013-2413-0.

[13] O'Brien P, Bell E. Role of mortars in the decay of granite. Sci Total Environ 1995;167:103–10. doi:10.1016/0048-9697(95)04573-J.

[14] André M, Phalip B, Voldoire O, Roussel E, Vautier F, Morel D. Quantitative assessment of post-restoration accelerated stone decay due to compatibility problems (St. Sebastian's abbey church, Manglieu, French Massif Central). 12th Int. Congr. Deterior. Conserv. Stone, New York: 2012, p. 7p.

[15] Kulle C, Goretzki L, Kraus K. Steinergänzungsmörtel im Vergleich. Bausubstanz WTA

Rev 2012.

[16] Ramge P, Kühne H, Meng B. Entwicklung von modularen Instandsetzungsmörteln für den Einsatz an denkmalgeschützten Natursteinbauwerken. Tagungsband 52. DAfStb-Forschungskolloquium, Berlin: BAM; 2011, p. 247–55.

[17] Schueremans L, Cizer Ö, Janssens E, Serré G, van Balen K. Characterization of repair mortars for the assessment of their compatibility in restoration projects: Research and practice. Constr Build Mater 2011;25:4338–50. doi:10.1016/j.conbuildmat.2011.01.008.

[18] Leoskool L, Vanparys L, Renglet M, Rouge S. Compatible mortar for masonry restorations: discrete optimization for equivalent strength and colour prescription. ICDS12 - Int. Conf. durable Struct., 2012, p. 1–11.

[19] Van Parys L, Léoskool L, Rouge S, Isebaert A, Renglet M. Targeting Colour and Modulus of Resistance for a repointing mortar through a genetic algorithm. In: Hughes J, editor. 3rd Hist. Mortars Conf., Glasgow: University of the West of Scotland; 2013, p. 1–8.

[20] Maravelaki-Kalaitzaki P, Bakolas A, Karatasios I, Kilikoglou V. Hydraulic lime mortars for the restoration of historic masonry in Crete. Cem Concr Res 2005;35:1577–86. doi:10.1016/j.cemconres.2004.09.001.

[21] Gulotta D, Goidanich S, Tedeschi C, Nijland TG, Toniolo L. Commercial NHL-containing mortars for the preservation of historical architecture. Part 1: Compositional and mechanical characterisation. Constr Build Mater 2013;38:31–42. doi:10.1016/j.conbuildmat.2012.08.029.

[22] Kalagri A, Karatasios I, Kilikoglou V. The effect of aggregate size and type of binder on microstructure and mechanical properties of NHL mortars. Constr Build Mater 2014;53:467–74. doi:10.1016/j.conbuildmat.2013.11.111.

[23] Costigan A, Pavía S. Influence of the mechanical properties of lime mortar on the strength of brick masonry. In: Válek J, Hughes JJ, Groot CJWP, editors. Hist. Mortars. Charact. Assessment, Repair, Dordrecht: Springer Netherlands; 2012, p. 359–72. doi:10.1007/978-94-007-4635-0.

Chapter 1 **Compatibility**

The main goal of this thesis is to optimise compatible mortar development. For this optimisation, this thesis is focused on compatibility in terms of the mortar's (technical) properties, or the 'performance' of the cured mortar. This first chapter tries to answer the question which of these properties are primordial in order to create a compatible mortar. The conservation ethics required for this specific technical problem, will also be discussed. The answer will be presented based on findings in literature of both the repair mortar research domain as of the restoration of mortar joints. Since finding a suitable repair mortar for mortar joints was found to raise similar questions as in stone repair mortars, e.g. colour and durability are both key parameters in the choice for the right mortar. This chapter is a reworked version of the review article published in Construction and Building Materials, 'Composition and compatibility requirements of mineral repair mortars for stone – a review' [1].

1.0 Introduction

During restoration of heritage buildings, mortars are frequently used for the repointing of joints or for the "plastic" repair of stone, which is designed to fill in missing parts of stone. Stone repair mortar, reconstitution mortar or 'plastic' repair mortar as it is also called, is a mouldable mortar that can be applied in situ, and 'sets into place by its own adhesion to the substrate' (Fig. 1.1A-B & 1.2) [2].

One of the advantages of repair mortar is that it allows preserving as much of the original material as possible [3]. Although roughening or cut-outs are required in order for the mortar to attach itself mechanically to the stone, more original material can be saved. The original stone can as such be kept longer in its original position. Another advantage that is often claimed is the lower cost compared with other approaches such as replacing the stone with another one [3], certainly when these repair mortars are used for casting replicas of repetitive architectural elements [4]. A third advantage is that they can be adapted to the condition and appearance of the stone. The use of repair mortars will allow for a better understanding of the architectural lines and details, as opposed to no restoration, and it will therefore positively influence the perception of the building.

Fig. 1.1A Example of a failed repair mortar intervention on a church portico, Metz: the stone is sanding, while the mortar still appears to be in good condition.

Fig. 1.1B Example of an acceptable repair mortar intervention on a column of the opera house, Strasbourg.

Generally, repair mortars can exist next to the replacement of stones: repair mortars are used when damage to the original material is limited, and replacement occurs where whole blocks or larger parts have to be restored. Repair mortars can furthermore be used where replacement would only be possible with an unsuitable stone, i.e. a stone that is incompatible with (any of) the properties of the original stone. However, the requirements of repair mortar and replacement stone is not fixed, and varies from country to country [5].

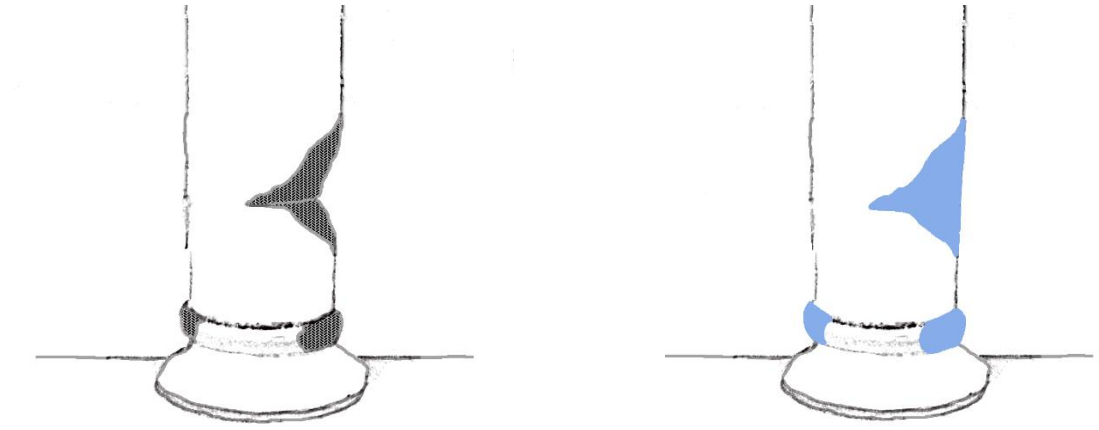

Fig. 1.2 On the left, a sketch of a damaged column for which a plastic repair mortar might be used to fill in the missing parts, as suggested in the right sketch.

1.1 Incompatibility features and following alterations

A repair mortar is a man-made, and possibly, standardized material, which is designed to be compatible with a naturally heterogeneous material. This makes it difficult to develop a good repair mortar. Interpreting the

philosophical and ethical guidelines of both the Venice Charter and the Nara Document, an ideal repair mortar for natural stone should be durable enough, but self-sacrificing on the long run [6–8]. The performance of the mortar should be close to the stone it is repairing, but overall less durable than the stone. It is therefore important to study which properties are considered important (e.g. permeability, colour), and which elements of a mortar (e.g. binder, sand) determine these properties. Each stone type is different, and requires a specifically adapted restoration mortar. It might well be assumed that for each stone type, (a combination of) different binder types should be used, and each binder (lime, cement, or commercial variety) behaves differently in application and setting therefore obliging the restorer to adapt the application techniques and methods. It might be that a certain combination of binder and aggregates leads to properties which are suitable to repair a dense and resistant sandstone, but are not suited for the repair of a soft limestone.

Fig. 1.3 A repair with a cement-based mortar has failed to smoothen and restore the weathered surface of these stone ashlars in Glasgow, from [12]. Both illustrations show the render loosening from the stone façade, allowing weathering of the stone beneath.

Many repair mortars have proven to be incompatible with the stone they had to repair: the stone was damaged instead of being restored and preserved for the future (Fig. 1.3). O'Brien et al. (1995) describe a lime mortar damaging granite: a correlation was made between areas of disrupted granite and a source of calcium ions in solution (run-offs, mortar joint) [9]. In the end, the calcium-ions led to the deposition of gypsum in the granite [9,10]. Report has also been made of cement mortar used for the repointing of gneiss and arkoses: the original stone surface receded 100 times faster in the zones which were repointed with cement and replaced with a new stone, than in the other zones [9]. Schueremans et al. (2011) suggested compatible mortar recipes after thermal and chemical analysis of each repointing mortar [8]. However, these new repair mortars did not show a good visual compatibility with the original mortar, and the final recipe was then adapted until visual appearance did match. It is safe to assume that the change in recipe will have had an impact on the other properties of the mortar as well. Schwengelbeck (2002), finally, draws our attention to the mode of application and the use of

rods in the mortar [11]. Although application techniques for repair mortar are also an important topic, they are beyond the scope of this research and will not be further discussed here.

1.2 Critical parameters for compatibility

These examples of incompatible use of repair mortars for natural stone illustrate that badly chosen repair mortars can have serious consequences for the preservation of the stone [8,9,11,13,14]. They attest that some elements can lead to damage. The example of cement causing the receding of original stone might be related to the properties of the mortar, induced by the cement in the mortar. In addition, the example from Schueremans et al. (2011) illustrates that the visual aspects of the repair mortar are not to be neglected in terms of *compatibility* with the stone, even though one might assume that visual aspects *in se* are inferior in terms of *durability* than, for example water vapour migration: the repair mortar has to re-evoke a certain type of authenticity to the building and should therefore have a comparable colour and structure, but it might not necessarily lead to a more durable intervention.

In order to avoid any damage to the original material and/or re-intervention, following durability determining properties should be considered:

First of all, the actual colour or appearance of a repair mortar is no predictor for the durability of the stone. Also, the mortar might not be chosen if it is not colour compatible. Making the decision in the other direction might perhaps lead to a compatible mortar in terms of colour, but not in other properties, and might lead to a failed restoration intervention. It cannot be neglected that colour of the repair mortar is found an important criterion [8,15,16]. For some interventions, repair mortars with variability in colour are used on the same building. By using various mortars, the aim is to adapt to the colour variability in the façades of the building, caused by weathering, previous treatments, or just by natural variability in colour of the stone itself. For the same reason, the compatibility in colour is sometimes aimed for by painting the surfaces of the repair mortar.

Ramge et al. (2011) also included the aspect of ‘texture’ in their development for a repair mortar for sandstone (Fig. 1.4) [17]. Ruling conservation theories demand that the intervention can still be distinguished from the original [6,18]. Therefore, the mortar can differ slightly from the stone in colour or it can slightly differ in texture. The difficulty lies not only in making the matching colour with the stone’s current condition, but also with the stone’s future colour. Some stones are known to discolour (e.g. due to oxidation of minerals) and this should ideally be taken into account when developing or choosing its repair mortar.

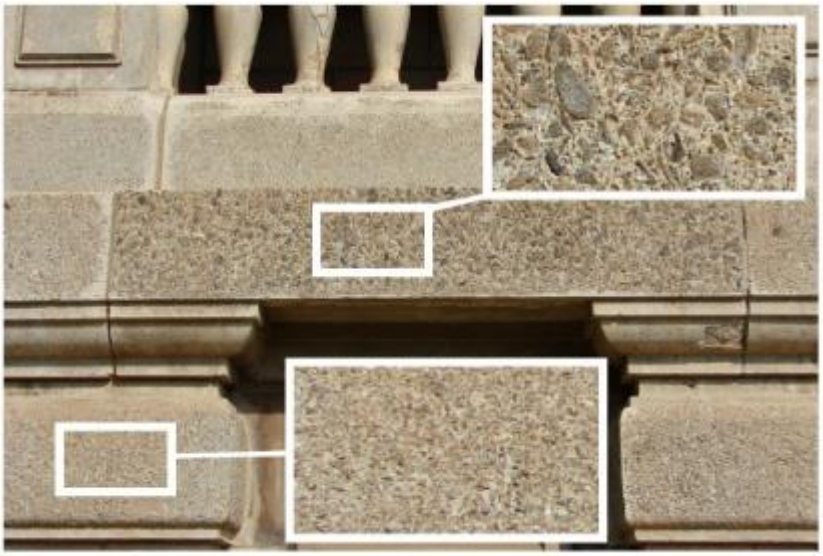

Fig. 1.4. Texture variability due to differential erosion between the concrete element and the natural stone element it is supposed to imitate, from [17].

Following aspects of a mortar are judged to determine the *durability* of the repair mortar intervention:

Water transfer properties: the presence of water contributes greatly to the deterioration of stone, since it can cause stress fractures, erosion and favour biological colonization. Therefore, the possibility of the mortar to transfer water (vapour) has to be equal or possibly higher than the stone since it will allow water trapped in the stone to migrate faster out of the stone than a mortar with a lower water vapour transmission rate than the stone. A key factor is the pore structure of the mortar [19].

Modulus of elasticity and deformability: if the repair mortar will be used for the filling-in, a good balance between strength and deformability has to be found to avoid the formation of cracks, since structures can be subjected to external actions inherent to their use. If in that case the repair material is too rigid, fractures can arise [4].

Bonding strength and adhesion: a good adhesion to the substrate is crucial. The bonding can be assured mechanically and/or chemically, with aid of prime coatings or reinforcement dowels. When looking into adhesion, not only the adhesive strength needs to be taken into account, but also other aspects which can influence the bond strength through time, e.g. water vapour diffusion [4]. Following EN 1015-12:2001, one can conclude that the bond strength should be lower than the tensile strength of the stone, a parameter that is almost never tested on natural stone.

Response to high temperature differences: high temperature differences on sun-faced walls cause the minerals in stones to expand and contract. The internal stresses in the stone due to the consequent cycles of temperature differences can lead to detachment, deformation or cracking of stone and/or mortar [4]. Groot & Gunneweg (2012) state that for soft masonry, a large thermal expansion means a low hydric expansion, and vice versa [14]. For stone, however, this might not be the case: Koch et al. (2004) investigated marbles that both show a high thermal and hydric expansion [20]. They tested

several stone samples and concluded that thermal processes catalysed hydric expansion and enhanced decay [20]. In comparison to the other aspects, this takes place on the mineralogical level, but has a direct influence on the durability of the whole repair mortar intervention.

Next to physical aspects, also the chemical aspects determine the durability of the stone after conservation interventions. Repair mortars can contain, create or attract materials that are harmful for the stone. Repair mortars made with organic polymers, or that contain organic polymers as additive or adjuvant, are more susceptible for biological organisms and can be a nutrition source for biological colonization on the stone [21]. Ageing tests taking into account biological growth can therefore give insight in the durability and compatibility of resin-based mortars.

1.3 Compatibility tolerance on performance-indicating properties

Several authors have discussed compatibility requirements for repair mortars, e.g. [4,22–24]. When searching the right repair mortar, it might prove difficult to find the ideal recipe, e.g. the right colour might impede that the mortar is sufficiently cohesive. It is therefore vital to know which properties influence a compatible, durable intervention more than others and whether or not they could be ranked in a certain way. Additionally, a compatibility tolerance should indicate up to which level the mortars needs to possess the desired properties. If a certain tolerance is allowed, more mortars might make a possible compatible repair mortar for a certain type of stone.

Sasse & Snethlage (1997) suggest compatibility estimations for stone repair. Interestingly, the original material, the natural stone, is taken as reference level: as such, the determination whether or not a mortar is compatible, is defined based on the stone's properties [25]. The requirements for the repair material are divided per property: rigidity, (compressive) strength, adhesion to the substrate, water (vapour) diffusion and thermal expansion (Table 1.7). Surprisingly, colour or any other surface feature does not appear on this list. This method was also used by Sasse & Schulze (1997) and Bromblet (2005) [25,26]. Bromblet (2005) used the method to evaluate six different repair mortars, and added hydric dilation to the list of properties to be evaluated, but no tolerance percentage was suggested. This method takes into account the heterogeneity of stones and the large range of type of stones which were used as building material. This methodology seems therefore to allow a repair mortar to be more adapted to the specific type of stone which is to be repaired.

Table 1.7. Evaluation method for repair materials for natural stone, after [25]. The requirements for each property are given in difference % of the actual stone property value.

Property	Requirement	Requirement after 1 year
Dynamic E-modulus	20-100%	60%
Compressive strength	20-100%	60%
Thermal dilatation coefficient	50-150%	100%
Water uptake coefficient	50-100%	-
Value of water vapour resistance	50-100%	-
Pull-off strength	50-80%[1]	-

[1] Or to be defined in special cases
The adhesion is desired to fail in the stone repair material or in the contact area, but not in the stone.

Other studies set requirements for repair mortars, but do not discuss up to which (quantifiable) level a difference in properties between mortar and stone is acceptable [4,8,27]. Nevertheless, looking at the list of compatibility-indicating properties given by Sasse & Snethlage (1997), also Van Balen et al. (2005) [27] and Hayen et al. (2010) [4] rank deformability or elasticity, porosity properties and water vapour diffusivity, thermal dilatation and strength on the list. They place colour and surface features first and composition of the mortar second, which is more detailed as 'grain size distribution' [27] or as 'containing damaging components for stone', such as gypsum-forming reactants in the binder [4]. Also Veiga et al. (2001) indicate some value ranges that should make good repair renders or repointing mortars [23]. Their focus concerns mechanical resistance, water transfer properties and shrinking behaviour of the mortar. Delgado Rodrigues et al. (2007) took this even further and ranked the properties according to the role they play in the compatibility of a mortar with a stone [24]. These properties include e.g. the chemical composition, the porosity, the colour and the salt content of the mortar. The method proposed by Delgado Rodrigues et al. (2007) is however less interesting for this research than the approach proposed by Sasse & Snethlage (1997), since it makes a comparison between an existing repair mortar and specific stone. Sasse & Snethlage (1997) propose a more general system, where the tolerance range indicated can be used to create mortar recipes for a certain type of stone.

1.4 Discussion & conclusion

From this chapter it can be concluded that repair mortars can be advantageous (e.g. preservation of original material, cost) for conservation and restoration interventions. Conservation principles such as the Nara document or the Charter of Venice indicate that repair mortars should be compatible with the original building material, i.e. the stone. Nevertheless, this study has also indicated that ill-chosen mortar recipes, e.g. in terms of colour or stiffness, have led to bad repairs. The choice for one or other mortar

recipe should be well considered and funded on specific parameters which indicate a compatibility between mortar and stone.

For example, the approach of using various mortars for the repair of one stone type in one building, or applying paints on the repair material can be acceptable, if other parameters which are also important for the compatibility of the mortar with the stone, are not left behind. The colour difference of the mortars should not lead to a difference in water vapour transport for example, when all stones in the building have a similar water vapour transport behaviour. Similarly, the paints seem a good solution for compatibility in colour, but the composition of the paint may not impede a compatible behaviour in water vapour transmission, for example.

Various parameters have been mentioned before which play a role in the compatibility, such as elasticity, colour, or pore-related properties. As stated in the introduction, the focus of this research lies on the technical compatibility of the mortar, the performance, and not on the chemical compatibility of the mortar with the stone. This choice was made in order to comprehend and attain 'technical' compatibility with the stone before including any other element. Naturally, future research could expand the research towards the influence of certain minerals in mortar components (e.g. sands) which might improve/impede a good compatibility. Following the same logic, the technical compatibility will not include properties which are determined by external conditions, such as the thermal dilation or frost resistance or even the influence of weathering on any ageing of the technical compatibility properties which are considered (e.g. colour change due to weathering, water vapour diffusivity changes due to external factors). Again, these are elements which are important for a good compatibility, but are out of the scope of this research: the focus here lies on the intrinsic properties which can be determined at a certain point in the lifetime of a repair mortar.

In this study, an attempt has been made to distinguish the three most influential technical properties, called compatibility properties hereafter, which are determined at one specific point in the lifetime of a mortar.

Visual appearance proved to be an important factor for the success rate of a repair mortar in terms of compatibility, however, a good mortar in colour does not imply a durable mortar.

The pore-related properties of a mortar are important, since they indicate the possibility of fluid flow through the mortar. The elasticity of the mortar was also judged important for the compatibility and durability of the intervention, since it influences the deformability a mortar can be exposed to in a structure which is subject to stresses and strains.

Yet, when searching for the right repair mortar, it is often difficult to answer to all of these parameters, and compromises have to be made. These three properties were chosen since proportionally, they influence compatibility most.

Regarding these technical properties, in literature, several authors have tried to place these compatibility parameters in their 'right' order (see 1.3). In principle, they all mostly agree with each other: mechanical properties (elasticity, strength), pore-related properties (porosity, water (vapour) migration), colour and appearance are considered important, although the representation is variable. Sasse & Snethlage (1997) present a method which allows a tolerance range for properties, which is depending on the stone's properties. This makes this method applicable for all projects and restoration interventions with various stone types [25]. The compatibility of repair mortars can as such be assessed by comparing their properties with the properties that are required for the intervention.

Following the rankings made by previous authors, the author's interpretation of property ranking is presented in Table 1.8. The first column presents the ranking of the property: a higher ranking indicates the property is more important in terms of compatibility. In the column 'recommendation' the recommended compatibility with the stone is given, hereby following Sasse & Snethlage (1997) in their evaluation methods. The tolerance ranges proposed by Sasse & Snethlage (1997) are rather large. However, literature research and the further absence of specific upper and lower boundaries for compatibility properties indicate the difficulty of defining this tolerance range of compatibility for these various properties. Until further research has been performed on the properties of a series of natural stones and their repair mortars, these tolerance ranges are therefore maintained for this research. Therefore, in this research, it would thus be up to the user of the system to choose precisely the properties the mortar should have in order to be considered 'compatible'.

Pore-related properties were ranked first since they are more indicative for a durable intervention than colour. Visual appearance is placed second, due to its importance for the building's uniformity and the public's perception of the building. Texture of the mortar was not selected, since it might prohibit to find a relevant mortar compatible in the other properties. The demand in texture, in order to be compatible with the stone, might demand only coarse sand to be used, to have a similar outlook, while the properties of the stone would perhaps demand a finer grain size distribution. Elasticity was placed third, due to its influence it has on the stiffness of the mortar, which also determines the durability of the intervention.

The reader should be aware that these compatibility properties are defined by the composition of the mortar, i.e. the type of binder is likely to be of influence for the pores in the mortar, and thus for the pore-related properties of the mortar. In that sense, chemical composition of the mortar is of importance, but not to create a chemical compatibility, i.e. the same type, and a similar amount of minerals present in the mortar as are present in the stone. The following chapters will discuss the composition of a mortar and its influence on these compatibility properties into more detail.

Table 1.8. Compatibility properties in the development of a repair mortar. These properties depend on the grain size distribution and mineral components present in the mortar. The influence of properties indicated with a ° on the compatibility depend on other external factors as well such as the application technique and the skill of the restorer, and are thus not considered further in this thesis. Recommended values for each tolerance range from [25] expressed in difference percentage from the stone values, except for colour, which is based on the colour difference (absolute difference) [28].

Ranking	Property	Recommendation	Recommendation after 1 year
1	Pore-related properties:		
	Porosity		
	Pore size distribution		
	Water vapour resistance	50-100%	
	Water absorption coefficient		
2	Visual appearance:		
	Colour	100 ±5%	
	Texture°		
3	Elasticity	20-100%	60%
4	Adhesion°	50-80%	
5	Thermal expansion°	50-150%	100%
6	Compressive strength	20-100%	60%
7	Ageing°		

Bibliography

[1] Isebaert A, Van Parys L, Cnudde V. Composition and compatibility requirements of mineral repair mortars for stone - A review. Constr Build Mater 2014;59:39–50. doi:10.1016/j.conbuildmat.2014.02.020.

[2] Griswold J, Uricheck S. Loss compensation methods for stone. J Am Inst Conserv Hist Artist Work 1998;37:89–110.

[3] Ashurst J, Dimes F. Conservation of building and decorative stone. 1998.

[4] Hayen R, De Clercq H, editors. Versteend Erfgoed omgaan met herstelmortel en kunst steen, Brussels: KIK-IRPA; 2010.

[5] Feilden B. Conservation of historic buildings. 2003.

[6] ICOMOS. International charter for the conservation and restoration of monuments and sites (the Venice charter 1964). 1964.

[7] ICOMOS. The Nara document on authenticity (1994). 1994.

[8] Schueremans L, Cizer Ö, Janssens E, Serré G, van Balen K. Characterization of repair mortars for the assessment of their compatibility in restoration projects: Research and practice. Constr Build Mater 2011;25:4338–50. doi:10.1016/j.conbuildmat.2011.01.008.

[9] O'Brien P, Bell E. Role of mortars in the decay of granite. Sci Total Environ 1995;167:103–10. doi:10.1016/0048-9697(95)04573-J.

[10] Silva B, Aira N, Martínez-Cortizas A, Prieto B. Chemical composition and origin of black patinas on granite. Sci Total Environ 2009;408:130–7. doi:10.1016/j.scitotenv.2009.09.020.

[11] Schwengelbeck O. Fallobst. Ausführungsmängel bei der Verwendung von Steinersatzmasse. Bauhandwerk 2002;6:50–2.

[12] Torney C, Forster AM, Kennedy CJ, Hyslop EK. "Plastic" repair of natural stone in Scotland: perceptions and practice. Struct Surv 2012;30:297–311. doi:10.1108/02630801211256643.

[13] Forster AM, Szadurski EM, Banfill PFG. Deterioration of natural hydraulic lime mortars, I: Effects of chemically accelerated leaching on physical and mechanical properties of uncarbonated materials. Constr Build Mater 2014;72:199–207. doi:10.1016/j.conbuildmat.2014.09.015.

[14] Groot C, Gunneweg J. Rapportage Deelproject voegherstelmortels voor Historisch Metselwerk. Delft: Faculteit Civiele Techniek en Geowetenschappen, TU Delft; 2012.

[15] Ramge P, Kühne H, Meng B. Entwicklung von modularen Instandsetzungsmörteln für den Einsatz an denkmalgeschützten Natursteinbauwerken. Tagungsband 52. DAfStb-Forschungskolloquium, Berlin: BAM; 2011, p. 247–55.

[16] Ramge P, Kühne H, Meng B. Development of repair mortars for the restoration and reprofilings of natural stone elements in listed buildings and monuments. In: Ferreira A, editor. 16th Int. Conf. Compos. Struct., 2011.

[17] Ramge P, Kühne H, Meng B. Repair mortars for the restoration and reprofiling of natural stone elements in cultural heritage. Eur. Work. Train. Day Cult. Herit. Preserv., Berlin: 2011, p. 281–8.

[18] Munoz-Vinas S. Contemporary Theory of Conservation. Routledge; 2012.

[19] Klisińska-Kopacz A, Tišlova R, Adamski G, Kozłowski R. Pore structure of historic and repair Roman cement mortars to establish their compatibility. J Cult Herit 2010;11:404–10. doi:10.1016/j.culher.2010.03.002.

[20] Koch a., Siegesmund S. The combined effect of moisture and temperature on the anomalous expansion behaviour of marble. Environ Geol 2004;46:350–63. doi:10.1007/s00254-004-1037-9.

[21] Warscheid T, Braams J. Biodeterioration of stone: a review. Int Biodeterior Biodegradation 2000;46:343–68. doi:10.1016/S0964-8305(00)00109-8.

[22] Groot C, Hughes J, Van Balen K, Bicer-Simir B, Binda L, Elsen J, et al. RILEM TC 203-RHM: Repair mortars for historic masonry. Mater Struct 2012;45:1277–85. doi:10.1617/s11527-012-9916-0.

[23] Veiga M, Aguiar J. Methodologies for characterisation and repair of mortars of ancient buildings. In: Lourenço PB, Roca P, editors. Hist. Constr., Guimaraes: 2001, p. 353–62.

[24] Rodrigues JD, Grossi a. Indicators and ratings for the compatibility assessment of conservation actions. J Cult Herit 2007;8:32–43. doi:10.1016/j.culher.2006.04.007.

[25] Sasse HR, Snethlage R. Methods for the evaluation of stone conservation treatments. In: Baer NS, Snethlage R, editors. Dahlem Work. Sav. our Archit. heritage, Conserv. Hist. stone Struct., John Wiley & Sons Ltd.; 1997, p. 223–43.

[26] Bromblet P, Martinet G, Martin F. Approach for compatible mortars for restoration purposes: stone repairs of the roman amphitheatre of Arles (France). Int. RILEM Work. Repair mortars Hist. Mason., Delft: 2005, p. 73–81.

[27] Van Balen K, Papayianni I, van Hees RPJ, Binda L, Waldum A. RILEM TC 167-COM: Characterisation of old mortars with respect to their repair: Introduction to requirements for and functions and properties of repair mortars. Mater Struct 2005;38:781–5. doi:10.1617/14319.

[28] Mokrzycki WS, Tatol M. Color difference Delta E - A survey. Mach Graph Vis 2011;20:383–411.

Chapter 2 Components of repair mortars

While Chapter 1 indicated which parameters are vital for a *compatible* and *durable* repair mortar intervention, this second chapter discusses how the mortar composition, i.e. its components and its mixing ratios, can influence the mortar's properties and therefore, ultimately, the mortar's compatibility. The first part of this chapter is largely based on the review article 'Composition and compatibility requirements of mineral repair mortars for stone – a review', which was published in Construction and Building Materials, 2014 [1].

Furthermore, this chapter discusses the components that have effectively been used for the experimental part of this doctoral study. The production of the mortars is described in detail. Most of the content of this second part of the chapter was previously discussed in two scientific manuscripts, both published in the journal Materials and Structures [2,3].

2.0 Introduction

Plastic repair mortars are often subdivided based on their binders [4,5]. A difference is made between the inorganic mineral repair mortars, based on either cement, lime or a combination of both, and the organic repair mortars [4,6,7]. Next to these two groups, also chemical mortars exist [5]. Chemical mortars are ready-made zinc hydroxychloride mortars, wherein two components, a zinc chloride fluid and a zinc oxide coated aggregate, react [8,9]. These mortars are reported to have been used from mid-19th C. until mid-20th C., and have known a new surge at the very end of the 20th C. [8]. These mortars are far from the original stone material in chemical composition [8,9]. The organic repair mortars, or resin-based mortars, have organic polymers as binders such as epoxies or acrylics, and have been used since the early 20th Century [10]. Even though they are able to imitate alabaster and marble very well in appearance, due to their completely different chemical composition, they behave and weather differently than stone [4,6,11,12]. The group of mineral binders with lime and cement are closer to stone in composition and they have been used the longest for the repointing and reconstituting of stone. Hydraulic mortars have been used

since Roman period for the repair of buildings, and from the 19th century onwards, (Portland) cement mortars are manufactured and used for the repair of stone [4].

2.1 Influence of the main components of a mineral mortar

The nature of each mortar component determines the behaviour of the whole mortar mix. The following section will discuss the binders and aggregates in detail. Based on literature, an attempt is made to uncover the influence of each of the final mortar properties.

2.1.1 Nature and influence of different mineral binders

In the following part, the differences between lime and cement binders are summed up, as well as their (dis)advantages for their use in mortars.

2.1.1.1 Air hardening lime

Air hardening lime is mainly composed of portlandite ($Ca(OH)_2$ or CH in mortar chemistry) (Table 2.1). Portlandite undergoes a change in shape when placed in water; the hexagonal prismatic crystals turn into thin hexagonal plates [13,14]. Air hardening lime is available as a lime putty, or a lime hydrate. This lime hardens through carbonation: the portlandite reacts with unbound CO_2 present in the environment to form calcite (Table 2.1).

Table 2.1. Summary table of air hardening lime, after [15,16]

Raw material	Chemical composition	Setting
Pure limestone burnt below clinkering point (800 – 1200°C)	$Ca(OH)_2$ – CH	**Carbonation** $Ca(OH)_2 + CO_2 + H_2O \rightarrow CaCO_3 + 2H_2O + 74\frac{kJ}{mol}$

Lime putty therefore has a high water retention capacity and a high sand carrying capacity [14]. Aged putty (of more than one year old) also carbonates faster than non-aged lime putty [17]. The carbonation process is slow mainly due to the fact that the hydrogen carbonate has to be able to reach the portlandite crystals through the mortar pore network [14].

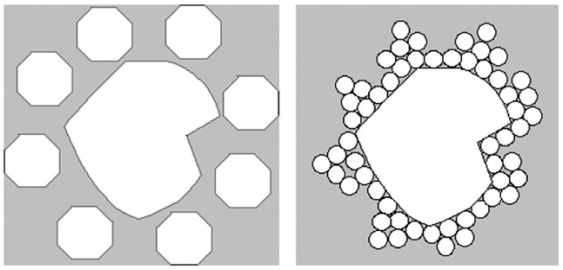

Fig. 2.1. Lawrence et al. (2007) proposed a model representing the interaction of air hardening lime with aggregate particles: (left) portlandite crystals surround the aggregate particle, (right) after carbonation, smaller calcite crystals are more densely packed around the aggregate particle. Figure from [17].

According to SEM analysis performed by Lawrence et al. (2007) calcite crystals seem to be smaller than portlandite crystals, and they attach themselves to surrounding aggregates, which is presumed to explain the higher amount of smaller pores in mortar after carbonation [18] (Fig. 2.1). Calcite also attaches to unreacted portlandite, and due to these smaller pores, carbonation through CO_2 of portlandite becomes therefore very slow and may be self-limiting [18]. Because of its high water retention capacity, air hardening lime is able to take up more water, and it requires a high water-binder ratio (W/B) to make a workable mortar. These two effects, slow carbonation and high water retention, can induce shrinking cracks which are characteristic for this mortar. It depends on application skills and environmental conditions if the subsequent occurring cracks are limited to micro-scale cracks or if they are visible on a macro-scale. In Mercury Intrusion Porosimetry (MIP) data, air hardening lime mortar presents a bimodal pore size distribution, which is due to the two types of pores present: shrinking fissures and air voids [19]. Mortars with this binder have a large pore network and a low density. Their compressive strength is not specified by the EN 459-2010, but lies typically below 2 or even 1 MPa [20].

2.1.1.2 Natural hydraulic lime

Natural hydraulic lime (NHL) consists of portlandite and calcium silicate hydrates (Table 2.2). Due to the presence of portlandite and calcium silicates (belite C_2S and alite C_3S), the lime will set by two means. First, a calcium-silicate-hydrate (C-S-H) is formed, then on a longer term, carbonation induces the formation of calcite. The portlandite then also separates the C-S-H into calcite and amorphous silica [13]. Since a part of NHL also consists of portlandite, the water retention capacity is high, but not as elevated as in air hardening lime. The risk on cracks due to large shrinking is therefore lower, but still present.

Table 2.2. Summary table of natural hydraulic lime, after [15,16].

Raw material	Chemical composition	Setting
(siliceous) limestone burnt below clinkering point (800-1200°C)	$Ca(OH)_2$ – CH 2 $CaO.SiO_2$ - C_2S 3 $CaO.SiO_2$ – C_3S	**Hydraulic setting**: C-S-H $(CaO)_2\ (SiO_2) + 3.3\ H_2O \rightarrow$ $(CaO)_{1.7}.(SiO_2).(H_2O)_3\ + 0.3(Ca(OH)_2)$ $(CaO)_3\ (SiO_2) + 4.3\ H_2O \rightarrow$ $(CaO)_{1.7}.(SiO_2).(H_2O)_3\ + 1.3(Ca(OH)_2)$ **Carbonation** $Ca(OH)_2 + CO_2 + H_2O$ $\rightarrow CaCO_3 + 2H_2O\ + 74\ kJ/mol$

Classification concerning hydraulic lime types is sometimes difficult, and therefore it can be unclear to which type of lime is referred. In this chapter, the classification of EN 459-1 (2010) will be followed [21], wherein natural hydraulic lime (NHL) is lime with hydraulic properties, which was made by burning (siliceous) limestone below clinkering point (between 800 and 1200°C) and does not contain any additives. Research in repair mortar discusses nearly only NHL lime, mainly because, as Smith et al. (2005) describe, NHL is regarded as the 'true' and 'authentic' hydraulic lime as used in the past [22]. Other types of hydraulic lime that are discussed in repair mortar research are formulated lime (FL) and hydraulic lime (HL).

Because of their composition, air lime and NHL mortars have a large connected pore network, with high water vapour diffusivity and permeability. The presence of portlandite allows a better plastic deformation of the mortar, but their large pore network makes them not very resistant to compressive and flexural strength [23]. The presence of the C-S-H will give the NHL a faster and higher resistance than the air hardening lime. EN 459 (2010) standard sets the compressive strength of NHL after 28 days between 2 (minimal authorized limit NHL2) and 15 MPa (maximal authorized limit NHL5) [21].

2.1.1.3 Natural cement

Natural cement is a natural material, and the binder composition is quite variable (Table 2.3). Bayer et al. (2011) presume that the main phases in hardened natural cement are calcium silicate hydrate, followed by calcium aluminate hydrate (C-A-H) and partially carbonated, hydrated calcium aluminate phases, but state as well that more research is needed to explain differences in analytical results [24]. Natural cement was a product used frequently for rendering façades in the 19th century in Europe (France, Austria, Poland), and in that aspect, it is also known as 'Roman cement', although this name can cause confusion with the 'cement' from the Roman period. The pore structure of natural cement is variable, depending on water/binding ratios (W/B) and curing conditions [25], but a dual-phased hydrating mechanism can be detected through a characteristic development of the pore structure [26]. The C-A-H gel is the first to form during setting and produces a relative open pore structure (0.2-0.8 µm threshold pore

diameter in MIP). Only in the second hydration phase the threshold pore width shifts to about 0.02 µm, due to the formation of the more voluminous C-S-H gel. Samples taken from renderings from the 19th century showed low formation of C-S-H gel, and large air pores, with a bi- or tri-modal pore size distribution in MIP-analysis [25]. Gosselin et al. (2008) refer especially to natural cement suited as binder for repair mortars for natural stone due to its high porosity and possibility of water to evaporate; historic natural cement mortars showed porosity values between 22-32% [27]. Natural cement attains a compressive strength higher than 10 or 25 MPa (depending on the classification type) [28]. Maximum values are not given in the work by Gurtner et al. (2012), but research performed for the European Rocare project indicates typical compressive strength values between 20 and 60 MPa [28].

Table 2.3. Summary table of natural cement, after [15].

Raw material	Chemical composition	Setting
Argillaceous limestone burnt below clinkering point (800-1200°C)	C_2S, (C_3S) C_3A_2 C_3S_2 CS CaO	**Hydraulic setting**: C-A-H $3CaO.Al_2O_3 + 6\,H_2O \rightarrow 3CaO.Al_2O_3 6\,H_2O$ **Hydraulic setting** : C-S-H $(CaO)_2\,(SiO_2) + 3.3\,H_2O \rightarrow$ $(CaO)_{1.7}.(SiO_2).(H_2O)_3 + 0.3(Ca(OH)_2)$ $(CaO)_3\,(SiO_2) + 4.3\,H_2O \rightarrow$ $(CaO)_{1.7}.(SiO_2).(H_2O)_3 + 1.3(Ca(OH)_2)$

2.1.1.4 Portland cement

Since the 19th Century, Portland cement appears to have been used more for repair mortars than any other cement type. As can be seen in Table 2.4, many reactions take place in cement. One of the first reactions is the hydration of calcium aluminate hydrates. This is followed by the formation of C-S-H gels, and later, the carbonation of portlandite. Additionally, Portland cement always contains calcium sulphate ($CaSO_4$) (<5%) which is added to slow down the reaction process. The $CaSO_4$ reacts with a part of the C_3A, creating primary ettringite. This primary ettringite may not be confused with secondary ettringite, which causes damage due to volume expansion. Primary ettringite reacts later with calcium aluminate hydrate into calcium alumina sulphate [15].

The larger the percentage of cement in the mortar, the lower the porosity: the calcium silicate hydrate gel takes up all the capillary pore spaces and encloses large air voids in their matrix. Since the formation of C-S-H gels clearly reduces the size of pores, permeability is very low to non-existent, and these mortars present high compressive and flexural strength [16]. Upon ageing, cement also undergoes carbonation. Carbon dioxide, which penetrates slowly in the low permeable matrix, turns calcium compounds into calcite and the silicates and aluminates into amorphous silica and alumina [13]. The carbonation lowers the pH-value of cement from 12 to 8, and will therefore affect the durability of mortars with reinforcements. If metal reinforcements

are used, the decrease in pH-value will facilitate oxidation reactions on the metal, creating as such corrosion and an internal stress in the mortar.

Table 2.4 Summary table of Portland cement, after [15].

Raw material	Chemical composition	Setting
Argillaceous limestone / Clay-limestone mix burnt above clinkering point	C_3S C_3A C_2S, C_4AF $CaSO_4$ .2 H_2O	**Hydraulic setting**: C-A-H $3CaO.Al_2O_3 + 6\,H_2O \rightarrow 3CaO.Al_2O_3 6\,H_2O$ $4CaO.Al_2O_3.Fe_2O_3 + 2Ca(OH)_2 + 10H_2O \rightarrow 4CaO.Al_2O_3.Fe_2O_3.6H_2O$ **Hydraulic setting** : C-S-H $(CaO)_2\,(SiO_2) + 3.3\,H_2O \rightarrow (CaO)_{1.7}.(SiO_2).(H_2O)_3 + 0.3(Ca(OH)_2)$ $(CaO)_3\,(SiO_2) + 4.3\,H_2O \rightarrow (CaO)_{1.7}.(SiO_2).(H_2O)_3 + 1.3(Ca(OH)_2)$ **Primary ettringite**: $3CaO.Al_2O_3 + 3CaSO_4 + 32H_2O \rightarrow 3CaO.Al_2O_3.3CaSO_4.32H_2O$ **Primary ettringite + C-A-H:** $3CaO.Al_2O_3.3CaSO_4.32H_2O + 2(3CaO.Al_2O_3) + 4H_2O \rightarrow 3(3CaO.Al_2O_3.CaSO_4.12H_2O)$

2.1.1.5 Bastard mortars

Bastard mortars have both lime and cement as binders. They harden due to hydration of cement particles and carbonation of portlandite [23].

Studies mainly point out that there is no linear relation between lime and cement properties. Arandigoyen et al. (2006) illustrated that the decrease or increase in compressive strength is not proportional to the percentage lime-cement: the addition of 25% air lime to a cement mortar means a decrease in strength by 50% [29], and a lime addition of more than 10% would alter the microstructure of the cement-lime mortar and create micro-cracks [30]. An increase in cement percentage decreases porosity, and vice versa [19,23]. Winnefeld et al. (2006) indicated that lime-cement mortars were more resistant to sulphate attacks and freeze-thaw actions than lime mortars [31].

Even though Mosquera et al. (2006) found that the tested air lime-cement mortars approached hydraulic lime (NHL 3.5) in pore size range, results show that this is relative: 0.02-0.33 µm in comparison to 0.05-1.50 µm [22]. It can therefore logically be assumed that the more cement is added, the more problems can rise concerning the diffusion of fluids, creating a similar situation to that of pure cement mortar [29].

The blended lime-cement mortars have as main advantage their early strength development. Additionally, the resistance and porosity can be adapted by varying the lime/cement ratio [23] (Fig. 2.2). The amount of lime also makes a certain elastic-plastic deformation possible before failure [23].

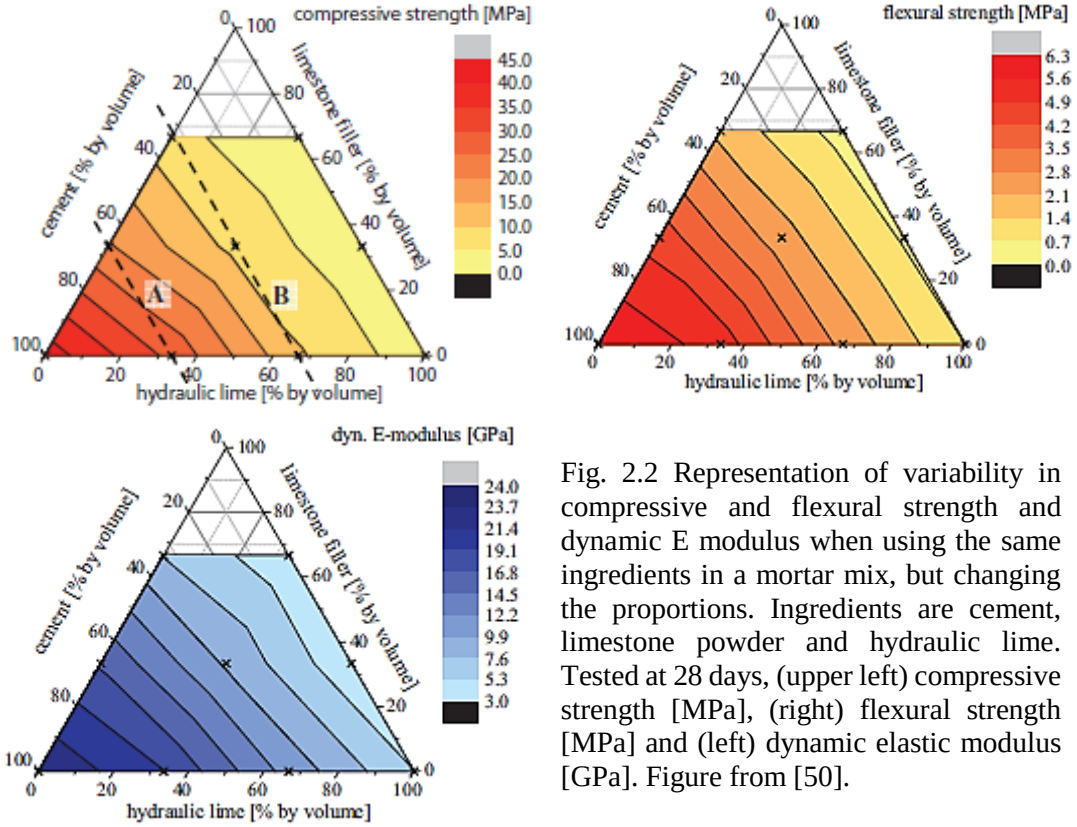

Fig. 2.2 Representation of variability in compressive and flexural strength and dynamic E modulus when using the same ingredients in a mortar mix, but changing the proportions. Ingredients are cement, limestone powder and hydraulic lime. Tested at 28 days, (upper left) compressive strength [MPa], (right) flexural strength [MPa] and (left) dynamic elastic modulus [GPa]. Figure from [50].

Table 2.5. Technical properties of mortar binders versus the classification of the mortar. Values are on a relative scale. Table based on information from [32].

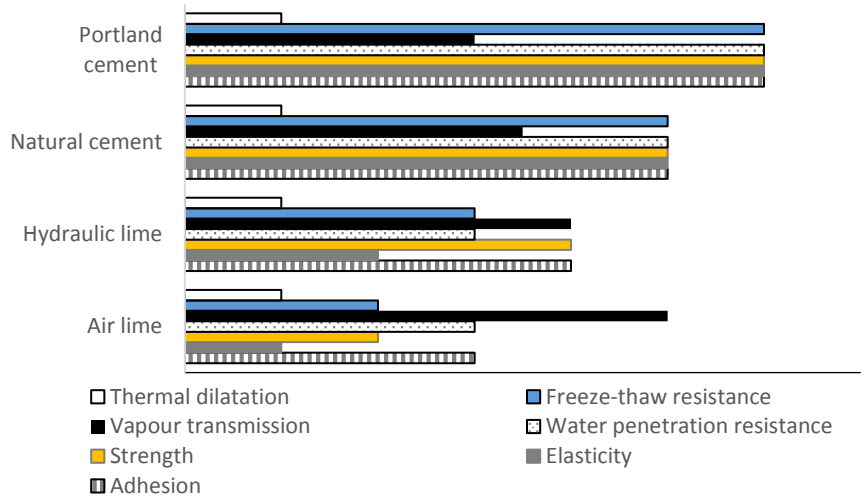

2.1.1.6 Conclusion

Based on the information given above, it becomes clear that every binder behaves quite differently. Each binder has its own strengths and weaknesses. The properties of each binder can as such be represented in a summarizing Table 2.5, based on [32]. All binders are equal when coping with thermal dilatation. Portland cement mortars are more likely to resist freeze-thaw cycles better, however, their water vapour transmission should be lowest of

all binder types. Air lime mortars are weakest of all, and combined with that, their E modulus is expected to be lower than those of cement mortars.

2.1.2 Impact of aggregates

Next to the binders, the aggregates play an important role in the mortar's characteristics. Depending on the aggregates, an air lime mortar can be made more resistant to compressive strength, or a cement mortar can be made less resistant. Most of the (natural) aggregates added to mortars are siliceous or calcareous of nature. Their origin (river, quarry...) and possible processing method (crushing) also affect the form and behaviour of each aggregate. The aggregates influence the mortar on two levels: both the material (mineralogical composition, porosity, resistance) and the size and the shape of the aggregate are of importance. In general, in order to have a qualitative mortar, the aggregates should have a well-dispersed grain size distribution: Allen (2003) refers to the standard sand grading curve from the European Standard EN 13139 (2002) and Ashurst & Dimes (1998) stated that 'sand should be well graded, ranging from fine to coarse' and that this may require mixing aggregates from different sources [6,33].

Ingham (2013) stated that rounded aggregates are easier to work with, but mortars with rounded aggregates are more likely to be less performant in mechanical properties; increased angularity of the aggregate will increase the compressive strength [34].

The rougher the aggregate's surface, the higher the bond strength. When the aggregate size increases, the specific surface area of each grain is proportionally less important, hence, the impact of the surface roughness decreases. The bonding strength is thus more important for smaller sized aggregates [35]. However, fine aggregates have a strong influence on the water demand and workability of the mortar, and might lead to water retention on the substrate's surface when only fine aggregates are applied.

Aggregates in a mortar can play an important role, both in the fresh mortar state as in the hardened mortar properties. However, even though some experimental studies have already been performed concerning the influence of the aggregate grain size distribution, some results are contradictory to what one might expect. For example, the elastic modulus for fine-grained mortars should be higher than for coarser-grained mortars [36], which would also imply that the compressive strength of the finer-grained mortars is higher, while on the other hand coarser grains are more dense and form large nods in the mortar paste; the higher compressive strength should thus be expected with the coarser aggregates, as in [37].

In addition, for repair mortars, the visual appearance and colour of the mortar will also be influenced by the colour and grain size distribution of the sand, e.g. a repair mortar for a coarse grained stone will have to be coarser grained as well in order to show compatibility in visual appearance.

The mineralogical composition of the aggregates is also a determining factor for the durability of the intervention. The primary mineral of the sand is generally quartz, although crushed limestone 'sand' also can be used in mortars. Aggregates also have secondary minerals. The effect of clay minerals (illite, muscovite, kaolinite, clinochlore) in the form of loam and kaolin (grain size <63 µm) on lime-cement mortars was tested by Winnefeld et al. (2006) [31]. They found these additions to decrease strength and elasticity, led to shrinking, and increased freeze-thaw susceptibility was presumed. In addition, mortars with fine clay minerals and lime showed ettringite crystals on the clay minerals of both kaolin and loam addition, after a sulphate attack, and considered these clay minerals as an alumina source which could favour secondary ettringite in the mortar [31]. The EN13139 (2002) standard about additives for mortar for example allows the presence of maximum 3% clays in sand for (masonry) mortars. Because of the high specific surface of clays, a large amount of water is needed to make the mortar. In addition, when the mortar is hardened, mortars with a high amount of clays show a high water retention capacity. So, although clay-rich sands are frequently used because they can increase workability and/or help finding the right colour for the restoration mortar, the durability of the mortar itself can be affected due to the addition of certain clays. Winnefeld et al. (2006) therefore recommend to first examine the type and amount of clays present in the unwashed sands [31].

Other secondary minerals such as chalcedony and opal are reactive silica, meaning they can form an alkali silica reaction (ASR) when in contact with alkali minerals such as sodium and potassium hydroxides [34]. Marine dredged aggregates contain (sodium) chlorides that can favour corrosion in reinforced mortars. Ingham (2013) also reported other minerals such as marine shells, chalk, organic matter and mica as unsuitable for normal cement mortars, following European standards [34]: chalk and other porous materials could lead to increased frost susceptibility, organic matter might retard or prevent the setting of the cement and both shells and mica increase the demand of water for workability, which decreases the mortar's strength [34].

Lanas et al. (2004) found that the use of fine, sand-sized limestone aggregates in a lime mortar increased the strength, and attributed this to a better chemical bonding of the mortar [38]; the calcite aggregate used was however less coarse grained than the quartz aggregates. On the contrary, Lawrence (2007) found that mortars with silicate sand and air hardening lime carbonate faster than the same mortars with an oolite limestone powder as aggregate [18] which might be due to a difference in pore size created by the different grain size used in both mortars.

2.1.3 Complementary aspects

In a mortar, variations in mechanical and physical characteristics can be made as well by changing some variables. These variables have to be approached with moderation. The following can be changed:

- Binder: aggregate ratio (B/A). For example, an increase in B/A in an air hardening lime mortar induces higher porosity and higher strength [38].
- Water: binder ratio (W/B). An increase in W/B means an increase in porosity (capillary pore spaces due to evaporation of water), although a too high W/B ratio can induce shrinking and shrinking fractures can appear. The W/B ratio is one of the main factors affecting concrete permeability [39]. In natural cement mortars a low W/B ratio causes unimodal pore size distribution, while a high W/B ratio creates a bimodal pore size distribution [23].
- Curing conditions influence the setting of the mortar. They therefore influence the bonding strength and the pore volume of the mortar, and can influence the durability of the intervention greatly [40].
- Mixing method: the method of mixing (by hand or mechanically), the speed and the time of mixing, can have an influence on the behaviour of the mortar and on its properties [41].

2.2 Mortars and materials chosen for this research

The previous subchapter discussed various binders and aggregate types which might be used for repair mortars. Various experimental campaigns have been performed on lime mortars.

The mortars in this research were deliberately kept simple in composition, and only binder, aggregates and water were used to produce the mortars. The use of only a few materials will help identify the influence that each mortar component has on the final mortar properties. The materials used for these mortars and the mortar production method are explained below. The mortars studied in this research are all produced with NHL binders, since section 2.1 pointed out that mainly these binders are interesting to use in order to have the better vapour transmission, water penetration and deformability. Two varieties of NHL binders were used: NHL 3.5 and NHL 5. The aggregates, all sands certified for use in construction, were chosen on their variability in colour and in grain size.

2.2.1 Binders

The binders used are the Chaux Pure Tradi 100 and Chaux Pure Blanche LC, both from St Astier, France, and respectively classified as NHL5 and NHL 3.5 according to EN 459-1 (2010).

The anhydrous binders were analysed using powder X-ray Diffraction (XRD). NHL 5 contained about 23 m% portlandite, 18 m% belite and 14 m% alite. NHL 3.5 contained 30 m% portlandite, 23 m% belite and 11 m% alite. All other elements were present in less than 5 m% or are inert. Table 2.6

represents the composition of the anhydrous binders. The complete X-ray diffraction analysis can be found in Appendix 2.1. *(This part was shortened)*

Both binder types were analysed on their grain size distribution through laser grain size analysis with a Mastersizer 2000. The binders were dissolved in propan-2-ol for the analysis. The grain size distribution of both binders can be found in Appendix 2.2. The diameter at 50 % passing was 16.5 µm for NHL5 and 12.5 µm for NHL 3.5.

Table 2.6. Rietveld XRD analysis of NHL5 and NHL3.5 binder in anhydrous condition, in weight percent with C=Ca, H=OH, S=SiO_4, Ĉ=CO_3, A=Al_2O_3 and HT for high temperature.

		NHL 5	NHL 3.5
		m%	m%
Portlandite	CH	23	30
Belite	β-C_2S	18	23
Alite	C_3S	13	11
Calcite	CĈ	31	22
Tilleyite	$C_5S_2Ĉ_2$	7	7
Spurrite	$C_5S_2Ĉ$	<5	<5
Quartz	SiO_2	<5	trace
Tridymite	HT SiO_2	trace	trace
Aluminate	C_3A	trace	trace

Both binders were also tested on their actual compressive strength, according to EN 196-1 (2005) and EN459-2 (2010). For this purpose, both binder types were mixed with reference sand EN 196-1 (2005). The W/B ratio was 0.5 for the NHL5 mortar and 0.6 for the NHL3.5 mortar, the B/A ratio was 0.33. Mortars were stored under conditions of 20 °C and >99 % Relative Humidity (RH). During the uniaxial compressive strength test, a loading rate of 400 N/s was applied. These results can be found in Table 2.7. Results were found to be very low. Both binder types did not have a compressive strength higher than 3 MPa, even though, according to the label, NHL 3.5 minimally should have a compressive strength of 3.5 MPa, and NHL5 a compressive strength of 5 MPa. In addition, the compressive strength of NHL 3.5 was almost nearly as high as NHL 5. Although this is theoretically possible, since NHL 5 should vary between 5 and 15 MPa, and NHL 3.5 between 3.5 and 10 MPa, it is contrary to what one might assume. It might be that the RH for these mortars was too elevated in order to have the full strength development and/or that 28 days of curing is simply not enough to develop the full strength development of these mortars (see 2.2.3 for carbonation tests on other mortars).

A lime mortar of each binder type cured for 90 days, with the same mortar recipe as these reference mortars, was therefore tested on its compressive strength. The difference in testing was the EN standard: EN 1015-11 (1999) was followed for curing conditions (18 ± 2 °C, 75 ± 5 %RH) and load applied (100 N/s). Mortars were tested after 90 days of curing (Table 2.7). Compressive strength is already more elevated, but NHL 3.5 is slightly more resistant than NHL 5.

Table 2.7. Resistance measurements on both lime binder types. The second column indicates the resistance according to EN 459-2, the second column according to EN 1015-11 (1999), after 90 days curing.

	F_c 28 days curing [MPa]	F_c 90 days curing [MPa]
NHL 3.5	2.41 ±0.37	10.07 ±0.61
NHL 5	2.86 ±0.77	9.14 ±0.93

2.2.2 Aggregates

For the experimental campaigns in this research, various lime mortars were produced. For these lime mortars, five different types of sands were used (Fig. 2.4A-E). Apart from the reference sand, all sands are sold for construction purposes.

1. Reference EN 196-1 (2005) sand
2. Rhine fin sand
3. Rhine gros sand
4. Yellow sand
5. Green sand

The cumulative grain size distribution, obtained through sieving of the sands, of all sands is presented in Figure 2.5. The shape of all aggregates was verified through length and width measurements of the loose grains under a light microscope Zeiss Axio Scope A.1. Based on these values, their shape was then defined according to [42]. This microscope was also used to study the minerals in the sands.

The first sand is a reference sand according to EN 196-1 (2005), and was delivered by Normensand GmbH, Germany. The sand consists of quartz and lithological fragments of magmatic origin. This is a well-dispersed sand, with grain sizes varying between 80 µm and 2 mm. The larger grains between 1.5 mm and 2 mm diameter consist of subrounded lithic fragments, the other grains are subangular to subrounded and are monomineralic grains.

A commercial sand named Rhin fin river sand from Groupe Roosens, Belgium, is a frequently used sand type in Western Europe. Quartz is the main mineral present in the sand, but contains also feldspar, lithological fragments and, in low quantities, biotite, muscovite and glauconite. It has a grain size between 0 and 2 mm, of which 50 m% lies between 500 and 630 µm. The larger grains between 1 and 2 mm are subrounded shell fragments. Below the limit of 1 mm, shell fragments and monomineralic grains occur together, with an angular to rounded prolate shape.

The third sand is the Rhin gros river sand from the same manufacturer. The sand is composed of quartz, fossil remains such as shells and lithological fragments. Also some muscovite and biotite were detected in low quantities (< 2%). The sand can indicate the influence of larger grains in the mortar's properties. The grain size varies between 0 and 5 mm. Over 60 m% of the grains have a grain size between 500 and 800 µm. Lithic fragments are present in the region of 300 µm to 5 mm and are subrounded with a variable shape.

Monomineralic grains are present in the range from 0 to 800 µm and are subrounded and equant in shape.

Two fine quarried sands, a yellow and a green, from Groupe Roosens, Belgium, are the fourth and fifth type of sand. 50 m% of the yellow sand has a grain size between 500 and 630 µm and has subrounded to subangular grains. It is finer than the Rhin fin sand. The yellow sand is composed of quartz, lithological fragments, feldspars and biotite. The green sand has a more important part of fine sands, about 40 m% of the green sand lies between 630 to 800 µm. Its grains are subangular to subrounded, and equant in shape. The sand is mainly composed of quartz, biotite and glauconite.

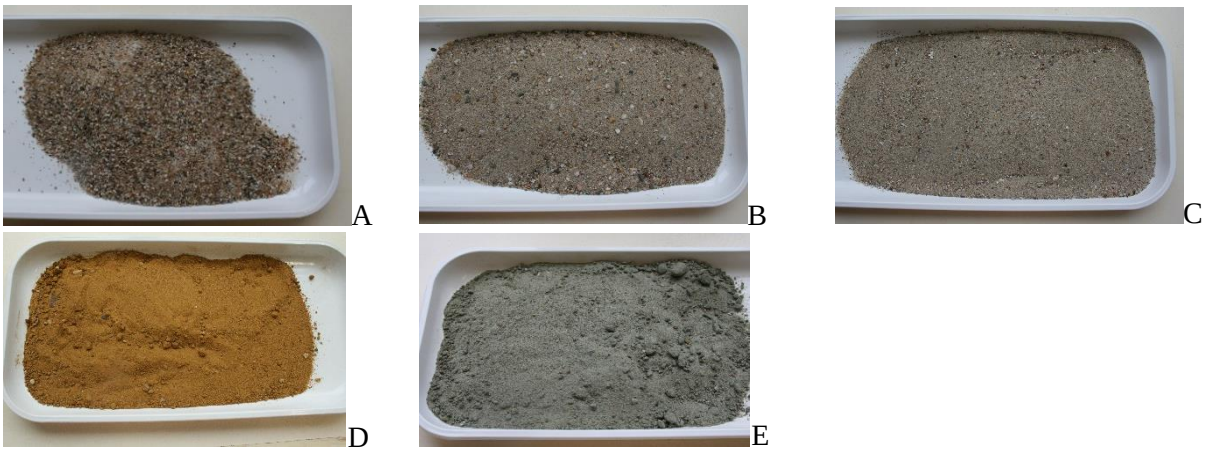

Fig. 2.4. Photographs of the sand used. A reference sand, B Rhin gros sand, C Rhin fin sand, D Yellow sand, E green sand.

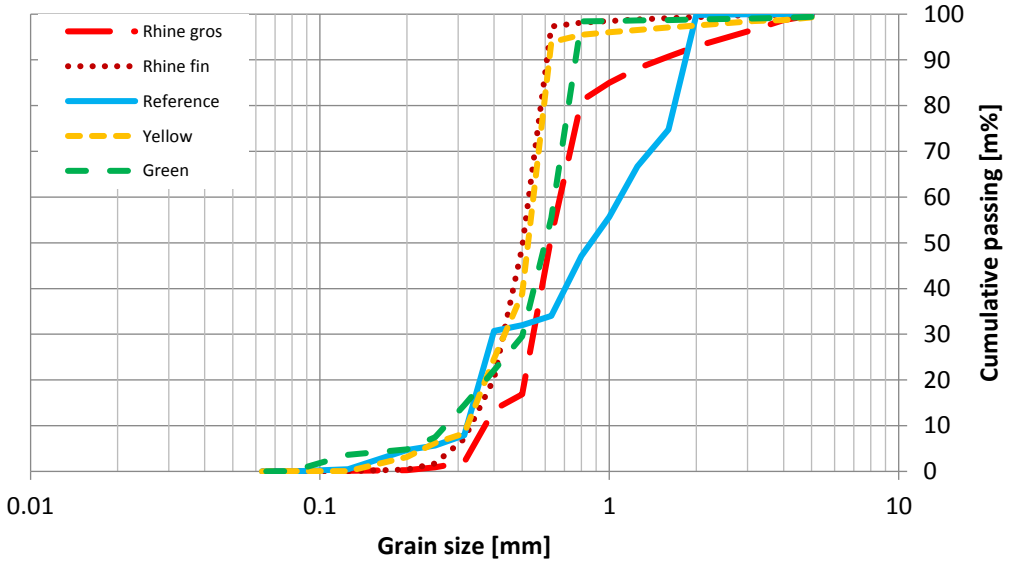

Fig. 2.5 Cumulative grain size distribution of each selected sand.

2.2.3 The mortar series

For the production of the mortars, various approaches were chosen. The first one included a variation of the W/B ratio and the sands, in order to determine their influence on the mortar properties. The second series involved the variation of the B/A ratio.

The W/B-series are made by varying the choice of sands as well as the W/B ratio. Four mortars were made per sand type, according to four spread values 120, 140, 160 and 180 mm, making the W/B ratio dependent of the spread to be obtained. Per binder type, a total of 16 mortars were made. The spread was measured with the flow table test according to EN 1015-3 (1999). Table 2.8 and 2.9 represents the recipe for each mortar mix in mass and the measured spread. When looking at the W/B ratio for the different mortars, the yellow-green sand mortars demand more water than the other mortars for the same spread (Fig. 2.6A-B). This can be explained by its higher amount of fine sand present in the sands. The reference sand has a grain size distribution which allows for a better packing of the grains, consequently, the added water has fewer cavities to fill. The water is thus more effectively used and permits to achieve the desired spread with less water.

All sands were dried at 100 °C, for 48 h. After drying, the Rhin gros sand was sieved so it would only contain grains between 63 µm and 3.15 mm. The Rhin fin sand was sieved with an upper limit of 2 mm. Both the yellow and green sand were sieved with an upper limit of 1.5 mm.

A fixed binder-aggregate ratio (B/A) of 1/3 in mass was maintained for all the mortars, regardless of their water-binder W/B ratio. The mixing ratio in mass of the green and yellow sand was 1:5 (G:Y).

Table 2.8. Mortar mix data for NHL5 W/B series. Mortars are named according to binder, sand and spread, e.g. the name 5-N-2 refers to the 120 mm spread mortar of the NHL 5 Reference sand.

Name	Sand mix	Binder [g]	Sand [g]	Spread (± 3 mm)			
				120	140	160	180
				Water [g]			
5-N-2 / 4 / 6 / 8	Reference	1000	3000	460	600	610	850
5-G-2 / 4 / 6 / 8	Rhin gros	1000	3000	620	651	670	700
5-F-2 / 4 / 6 / 8	Rhin fine	1000	3000	634	680	740	780
5-Y-2 / 4 / 6 / 8	Yellow : green	1000	2400 : 600	910	990	1030	1150

Table 2.9. Mortar mix data for NHL3.5 W/B series. The name construction is the same as for the NHL 5 W/B series.

Name	Sand mix	Binder [g]	Sand [g]	Spread (± 3 mm)			
				120	140	160	180
				Water [g]			
3.5-N-2 / 4 / 6 / 8	Reference	1000	3000	633	649	700	733
3.5-G-2 / 4 / 6 / 8	Rhin gros	1000	3000	640	670	710	820
3.5-F-2 / 4 / 6 / 8	Rhin fine	1000	3000	640	700	760	820
3.5-Y-2 / 4 / 6 / 8	Yellow : green	1000	2400 : 600	910	990	1100	1150

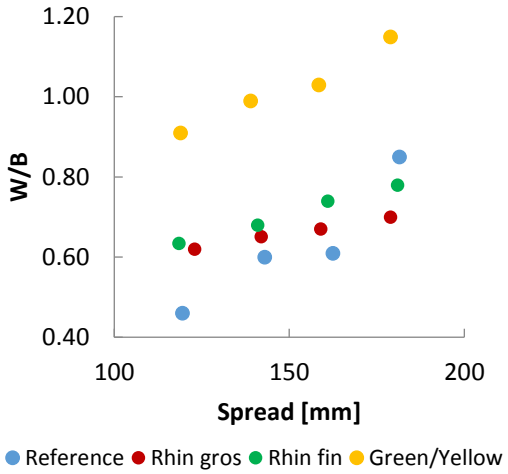

Fig. 2.6A NHL5 W/B series. The influence of the W/B ratio on the actual spread is clearly visible per sand type.

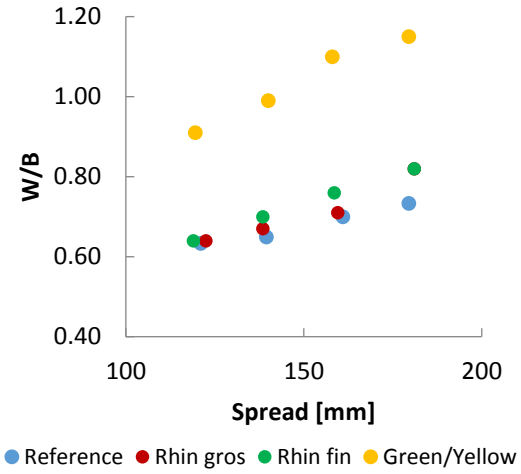

Fig. 2.6B NHL3.5 W/B series. The influence of the W/B ratio on the actual spread is visible, but is different from the NHL5 series.

The B/A-series is the second set of mortars, in which the binder-aggregate ratio is allowed to vary. NHL5 lime was used for these mortars. In order to add information of the influence of the B/A ratio, two other series were made, one with Rhin fin sand, the other one with a mix of Rhin gros-Yellow sand. Table 2.10 represents the mortar mix data for the B/A series. The B/A variation did not alter the spread greatly, and remained more or less stable.

Table 2.10. Mortar mix data for NHL5 B/A series. The spread of all mortars was 160 (± 3) mm. The name refers to the binder (5), the sand used (RF or RGY) and the B/A ratio

Name	Sand mix	Binder (g)	Sand (g)	Water (g)
5-RF-25	Rhin fine	750	3000	1000
5-RF-30	Rhin fine	1000	3000	1000
5-RF-45	Rhin fine	1350	3000	1000
5-RGY-25	Rhin gros : yellow	750	} 1500 : 1500	1000
5-RGY-30	Rhin gros : yellow	1000		1000
5-RGY-45	Rhin gros : yellow	1350		1000

For mixing, recommendations were followed made in EN 1015-11 (1999). It was verified that after every stage the elements were well mixed and no concentrations of one or other component were still visible. Per mix, sand and binder were mixed for 30 s at 63 rpm. Water was added while mixing, the first 30 s at 63 rpm and the following 60 s at 100 rpm. The mortar was cast in pre-oiled prismatic steel moulds of 40 x 40 x 160 mm³ and in cylindrical steel moulds of 25 mm diameter by 50 mm in height. The filled-in moulds were placed on a vibrating table for 15 s. The moulds were covered with thin film and the samples were left to rest for three days. The mortars were then demoulded and cured for three months in conditions of 18 ± 2 °C and 75 ± 5 % RH, following EN 1015-11 (1999). These conditions were

believed to be appropriate for NHL mortars, since both the carbonation as well as the hydraulic setting have to be promoted at the same time.

After curing, each mix was tested with a phenolphthalein indicator to verify their carbonation (Fig. 2.7A-C). The phenolphthalein still coloured the interior of the samples, but carbonation might already have been complete, when taking [43] into account, that stated that the actual carbonation depth is twice the phenolphthalein-indicated depth.

Rhin gros mortar, 120 mm spread

B. Rhin fin mortar, 180 mm spread

C. Yellow and green mortar, 140 mm spread

Fig. 2.7 A-C Carbonation depths for the various mortar mixes as indicated by a phenolphthalein indicator. These samples are representative examples for the carbonation depths of all mortar mixes.

2.3 Conclusion

Through the discussion of the main components of a mortar, more insight was created in the behaviour of repair mortars for stone. In general, all binders behave quite differently. Table 2.5 summarizes this: lime mortars are more advisable to use when fluid migration and a large pore network are considered important, while on the other side of the spectrum Portland cement has its advantageous compressive strength and high elastic modulus to account for. In the case of repair mortars for stone however, a very elevated compressive strength is not necessary. A high elasticity is of course interesting, but for repair mortars, deformability is even more important. Portland cement mortars are generally brittle, and therefore do not allow deformation. Lime mortars are therefore the more interesting option to use.

This study also pointed out that natural cement might be a new binder to use for repair mortars: their reported higher porosity and their possibility for a variation in compressive strength merit more attention, and might prove a good binder type for the repair of stones with an elevated compressive strength and elasticity, without losing too much fluid migration capacity. Nevertheless, this type of binder needs more research (e.g. pore size network, reaction components, workability). Parallel to this type of binder, also bastard lime-cement mortars could be used for the same purpose. Despite the fact that much research has been made on this type of binders, also here, additional studies are required in order to gain the full comprehension of these mixed

binders (e.g. influence of the ratio lime/cement on the pore network and fluid migration).

Conclusively, for this thesis, two NHL binders were chosen to make the experimental mortar studies. The XRD analysis of the binders showed that NHL 3.5 did not have significantly less reactive components, but mainly a larger volume of calcite. The resistance of both mortars was lower than what might be expected according to the standard. It is therefore concluded that (a) both binders do not belong to the most hydraulic kind of NHL binders, and that (b) the NHL 3.5 binder does not differ significantly from the NHL 5 binder.

Aggregates influence the mortar properties as well, i.e. more angular aggregates are to be preferred over very rounded aggregates if more cohesion (and/or more resistance) is desired. More fine aggregates demand more water in the mix for the mortar to be workable, which in its turn influences properties. The mortars chosen in this research contain very fine-grained sands and it was indeed noted that for the same spread, their W/B was elevated in comparison to the other mortars.

The most frequently used sands are mainly composed of quartz, even though also crushed limestone aggregates might be used for the repair of natural stone. In that case, an increased bonding is expected due to chemical similarity. It might also be expected that the (parts of) fossils present in the limestone aggregate would have an influence on the pore network of the mortar. Literature studies and EN standards warn against the use of minerals which are not stable or might react with water. The sands used in this research are certified for use in construction, and microscopic analysis did not show any of the minerals which are reported to be problematic.

Additional aspects proved to be important as well, not only W/B influence the mortar properties, but the mixing method used and the curing regime applied have an impact on the final mortar properties. The preparation of and curing conditions for the mortars made in this research were thus well-considered.

Bibliography

[1] Isebaert A, Van Parys L, Cnudde V. Composition and compatibility requirements of mineral repair mortars for stone - A review. Constr Build Mater 2014;59:39–50. doi:10.1016/j.conbuildmat.2014.02.020.

[2] Isebaert A, Derluyn H, Cnudde V, Van Parys L. Exploring a basic estimation approach for permeability of lime mortars 2015. doi:10.1190/1.3033217.

[3] Isebaert A, De Boever W, Cnudde V, Van Parys L. An empirical method for the estimation of permeability in natural hydraulic lime mortars. Mater Struct 2016:1–13. doi:10.1617/s11527-016-0829-1.

[4] Griswold J, Uricheck S. Loss compensation methods for stone. J Am Inst Conserv Hist Artist Work 1998;37:89–110.

[5] De Naeyer A. New materials for safeguarding cultural heritage. 1998.
[6] Ashurst J, Dimes F. Conservation of building and decorative stone. 1998.
[7] Feilden B. Conservation of historic buildings. 2003.
[8] Oliveira TP. Investigation on whether a zinc hydroxychloride mortar is suitable as a filling material for the conservation of architectural Portuguese azulejos - adhesion and compatibility analysis. West Dean College, 2012.
[9] Moens F, De Witte E. Optimalisation of mineral repair mortars for historic buildings (lithos arte (r) mortars). In: Brandt-Grau A, Pérez-Vitoria S, Chapuis M, Leissner J, editors. Res. Prot. Conserv. Enhanc. Cult. Herit. Oppor. Eur. Enterp., Strasbourg: European Communities; 2002, p. 118–21.
[10] Podany J, Garland KM, Freeman WR, Rogers J. Paraloid B-72 as a Structural Adhesive and as a Barrier within Structural Adhesive Bonds: Evaluations of Strength and Reversibility. J Am Inst Conserv 2001;40:15. doi:10.2307/3180010.
[11] Warscheid T, Braams J. Biodeterioration of stone: a review. Int Biodeterior Biodegradation 2000;46:343–68. doi:10.1016/S0964-8305(00)00109-8.
[12] Roig-Salom J-L, Doménech-Carbó M-T, de la Cruz-Cañizares J, Bolívar-Galiano F, Pelufo-Carbonell M-J, Peraza-Zurita Y. SEM/EDX and vis spectrophotometry study of the stability of resin-bound mortars used for casting replicas and filling missing parts of historic stone fountains. Anal Bioanal Chem 2003;375:1176–81. doi:10.1007/s00216-003-1826-0.
[13] Torraca G. Lectures on materials science for architectural conservation 2009.
[14] Elert K, Rodriguez-navarro C, Pardo ES, Hansen E, Cazalla O. Lime Mortars for the Conservation of Historic Buildings 2008;47:62–75.
[15] Moir G. Advanced Concrete Technology. In: Newman J, Seng Choo B, editors. Adv. Concr. Technol., Oxford: Elsevier; 2003, p. 3–45. doi:10.1016/B978-075065686-3/50277-9.
[16] Cizer Ö, Van Balen K, Van Gemert D. A comparative study of hardening reactions, porosity and mechanical properties of cement-lime mortars. 8th Int. Mason. Conf. 2010, Dresden: International Masonr; 2010, p. 1133–42.
[17] Cazalla O. Aging of lime putty: effects on traditional lime mortar carbonation. J Am Ceram Soc 2000;83:1070–6.
[18] Lawrence RM, Mays TJ, Rigby SP, Walker P, D'Ayala D. Effects of carbonation on the pore structure of non-hydraulic lime mortars. Cem Concr Res 2007;37:1059–69. doi:10.1016/j.cemconres.2007.04.011.
[19] Arizzi A, Cultrone G. The difference in behaviour between calcitic and dolomitic lime mortars set under dry conditions: The relationship between textural and physical–mechanical properties. Cem Concr Res 2012;42:818–26. doi:10.1016/j.cemconres.2012.03.008.
[20] EN. Building lime- Part 1: Definitions, specifications and conformity criteria. 2010.
[21] BLA. Technical: Lime in mortars n.d. http://www.britishlime.org/technical/lime_in_mortars.php (accessed September 30, 2015).
[22] Mosquera MJ, Silva B, Prieto B, Ruiz-Herrera E. Addition of cement to lime-based mortars: Effect on pore structure and vapor transport. Cem Concr Res 2006;36:1635–42. doi:10.1016/j.cemconres.2004.10.041.
[23] Cizer O, Balen K Van, Gemert D Van, Elsen J. Blended lime–cement mortars for conservation purposes: microstructure and strength development. 6th Int. Conf. Struct. Anal. Hist. Constr. Preserv. Saf. Significance, Bath: CRC Press, Taylor & Francis Group; 2008, p. vol2 : 965–72.
[24] Bayer K, Gosselin C, Hilbert G, Weber J. Microstructure of historic and modern Roman cements to understand their specific properties. Proc 13th Euroseminar Microsc Appl to Build Mater 2011:1–9.
[25] Klisińska-Kopacz A, Tišlova R, Adamski G, Kozłowski R. Pore structure of historic and repair Roman cement mortars to establish their compatibility. J Cult Herit 2010;11:404–10. doi:10.1016/j.culher.2010.03.002.

[26] Wilk D, Bratasz L, Kozlowski R. Reducing shrinkage cracks in Roman cement renders. Prepr. 2nd Hist. Mortars Conf. RILEM TC 203-RHM Repair mortars Hist. Mason. Final Work., Prague: 2010, p. 22–4.
[27] Gosselin C, Verges-Belmin V, Royer A, Martinet G. Natural cement and monumental restoration. Mater Struct 2009;42:749–63. doi:10.1617/s11527-008-9421-7.
[28] Gurtner C, Hilbert G, Hughes D, Kozlowski R, Weber J. Manual on best practice in the application of roman cements. Roman cement, past and present. Conservation theory and practice. 2012.
[29] Arandigoyen M, Alvarez JI. Blended pastes of cement and lime: Pore structure and capillary porosity. Appl Surf Sci 2006;252:8077–85. doi:10.1016/j.apsusc.2005.10.019.
[30] Sébaïbi Y, Dheilly RM, Beaudoin B, Quéneudec M. The effect of various slaked limes on the microstructure of a lime–cement–sand mortar. Cem Concr Res 2006;36:971–8. doi:10.1016/j.cemconres.2005.12.021.
[31] Winnefeld F, Böttger KG. How clayey fines in aggregates influence the properties of lime mortars. Mater Struct 2006;39:433–43. doi:10.1617/s11527-005-9023-6.
[32] Hughes J, Members RT 203-R. The role of mortar in masonry: an introduction to requirements for the design of repair mortars. In: Válek J, Groot C, Hughes J, editors. 2nd Conf. Hist. Mortars-HMC 2010 RILEM TC 203-RHM Final Work., Prague: RILEM Publications sarl; 2010, p. 1323–9.
[33] Allen G. Hydraulic Lime Mortar for Stone, Brick and Block Masonry: A Best Practice Guide. Donhead Publishing Ltd; 2003.
[34] Ingham JP. Geomaterials Under the Microscope. Elsevier; 2013. doi:10.1016/B978-0-12-407230-5.50020-0.
[35] Caliskan S, Karihaloo BL. Effect of Surface Roughness, Type and Size of Model Aggregates on the Bond Strength of Aggregate/Mortar Interface. Interface Sci 2004;12:361–74. doi:10.1023/B:INTS.0000042334.43266.62.
[36] Konow T Von. Aggregate grain size distribution—A major influence on many properties of lime mortars for restoration. EUROMAT 2003 Symp. P2–Materials Conserv. Cult. Herit., Lausanne: EPFL; 2003, p. 1–9.
[37] Haach VG, Vasconcelos G, Lourenço PB. Influence of aggregates grading and water/cement ratio in workability and hardened properties of mortars. Constr Build Mater 2011;25:2980–7. doi:10.1016/j.conbuildmat.2010.11.011.
[38] Lanas J, Pérez Bernal JL, Bello MA, Alvarez Galindo JI. Mechanical properties of natural hydraulic lime-based mortars. Cem Concr Res 2004;34:2191–201. doi:10.1016/j.cemconres.2004.02.005.
[39] Sanjuan M, Muñoz-Martialay R. Influence of the water/cement ratio on the air permeability of concrete. J Mater Sci 1996;31:2829–32.
[40] Papayianni I, Stefanidou M. Strength-porosity relationships in lime-pozzolan mortars. Constr Build Mater 2006;20:700–5. doi:10.1016/j.conbuildmat.2005.02.012.
[41] Zheng S, Tian B, Wang D, Hou Z. Cement Mortar Liquidity Testing Method by Rheological Properties. J Highw Transp Res Dev (English Ed 2013;7:11–7. doi:10.1061/JHTRCQ.0000326.
[42] Nichols G. Sedimentology and Stratigraphy, 2nd Edition. Wiley-Blackwell; 2009.
[43] Chang C-F, Chen J-W. The experimental investigation of concrete carbonation depth. Cem Concr Res 2006;36:1760–7. doi:10.1016/j.cemconres.2004.07.025.

Chapter 3 Compatibility in permeability

The first compatibility property concerns the possibility of fluid migrating through the stone and mortar. Since this property can determine the durability of the restoration and of the preservation of the original material, this property was given specific attention in this thesis compared to the other two compatibility properties.

The final aim of this chapter is to present an estimation method for the estimation of permeability. In order to achieve this goal, the theory necessary to understand fluid migration and permeability more specifically, will be discussed. Some well-chosen pore-related characterization methods will be discussed in relation to results in permeability measurements. The experimental campaign presented in this study will illustrate the influence of the mortar components and the mixing ratios on the pore-related properties, such as porosity and permeability. Conclusions of these sections will be used to explore existing estimation theories and to support the development of an estimation method, which will be presented as final section in this chapter.

This chapter is based on the publications of Isebaert et al. (2015), Isebaert et al. (2016a) and Isebaert et al. (2016b) [1–3].

3.1 Pore-related properties in lime mortars

3.1.1 Introduction

The presence of moisture in a (historic) building material can cause deterioration due to the generation of hydric stress (at low temperatures), due to water's transporting capacities or due to its potential reactivity with the building material (hydration, dissolution). Consequently, moisture presence might lead to a variety of water-related problems such as salt crystallisation, freeze-thaw damage and dissolution reactions or hydration reactions [4]. More specifically in built heritage, moisture transport is a key parameter in the quest for compatibility between new and old, original material. Previous studies demonstrated that the permeability and fluid transport in the restoration mortar is primordial in achieving an acceptable compatibility between mortar and stone [5–9]. It is necessary to know how this compatibility is best defined and assessed. A thorough understanding of the fluid migration in mortars is therefore essential. Past research has shown interest in the pore connectivity and permeability of air lime [10–13] and in

cement research. Mortar pore connectivity has been given a lot of attention as well [14–19]. At present, the use of lime mortars for restoration purposes is gaining popularity, because they prove to have a higher porosity and larger pores [11,20,21], and are thus chosen over cement mortars for restoration because of their promising properties.

More research into the fluid transport behaviour of lime mortar is however necessary. Air lime mortar pore-related properties have been researched, e.g. [10–12,22], but pore size distribution and permeability of natural hydraulic lime mortars have not yet been studied to a great extent [23,24]. NHL mortars are often discussed as a comparison material in studies of bastard mortars of air lime and cement or as a starting point for metakaolin-lime mortars (for marine environments) [21,25–29]. There is however a difference in curing between air lime, NHL and cement mortars, since hydraulic lime hardens through both carbonation and hydration.

Therefore, additional research into the microstructure and gas and water permeability of NHL mortars is recommended, even more so since the more hydraulic types of NHL would be able to replace the use of Portland cement in the restoration of structural masonry according to [23].

3.1.2 Theory concerning pore-scale related properties

3.1.2.1 Porosity and pore size distribution

Hall & Hoff (2011) formulate porosity f [-] as the volume of the pore space divided by the bulk volume of the sample, or as the volume fraction of open and closed porosity, in which $0 < f < 1$ [30]. Porosity can be subdivided into open and closed porosity. Open porosity indicates the amount of pores connected as a network towards the outside of the material, through the percolation path, i.e. the connection between voids throughout the matrix of the material. Below the critical porosity f_p, the percolation path no longer exists, since pores become more isolated: there is only closed porosity, which does not contribute to the transport of gases and liquids. It is therefore difficult to detect and is often counted as part of the solid matrix of the material [30]. Above f_p , open and closed porosity exist [30]. Porosity was since long the only way to have an indication of the network of pores inside a porous medium. Although the open porosity of a porous medium can be a first indicator for possible fluid flow, the information it gives is not sufficient: it gives no idea about the repartition of the detected pore volume into the various pore sizes, nor does it give information about the connectivity of the pores.

The pore size distribution on the other hand, gives a more complete idea of the network in the material and possible fluid migration. For example, Moonen & Carmeliet (2013) stated that the moisture capacity of a material is proportional to the pore size distribution, since during water uptake, entrapped air voids decrease the amount of fluid that can be absorbed by a material, while during drying, entrapped fluid can lengthen the time needed to fully dry a material [4].

Table 3.1. IUPAC Classification of pores based on their size quantified through their diameter D [31].

Micropores	$D \leq 2$ E-6 m
Mesopores	2 E-6 m < D < 50 E-6 m
Macropores	$D \geq 50$ E-6 m

Depending on the size of a pore, it is catalogued as a micropore, mesopore or macropore (Table 3.1) [31]. Each type of pore influences the behaviour of the medium towards fluid migration differently. Various techniques can be used to assess the sizes of the pores present in the material. Depending on the technique used, both connected and unconnected or closed voids are determined. Kaufmann et al. (2009) describe the pore network of a *cement*-based system as a network of ink-bottle pores: large chambers interconnected by smaller throats (Fig. 3.1) [14].

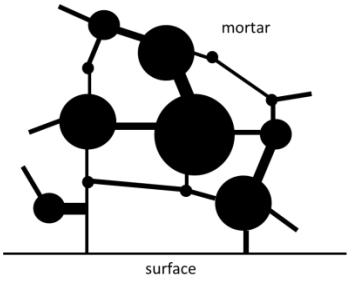

Fig.3.1 Simplified sketch of an ink-bottle pore structure in a cement mortar.

3.1.2.2 Fluid transfer in saturated materials

Along the centuries, the interest of scientists for explaining fluid migration in porous materials was initially focussed on saturated materials. They proposed a theory for liquids that was later transposed to gases. In both cases, the existence of a "flow driving condition" is required which can be associated with a differential potential [30]. At a given point in the material, the associated potential value may be obtained by combining several aspects derived from Bernoulli's law: pressure contribution, velocity contribution and altitude contribution. Once a differential potential exists between two points, a flow will take place (from the highest potential to the lowest one), with which the amplitude can range from very low to very high depending on the network architecture between the two points. In the summarized theory below, the pressure contribution will be considered as the only origin of flow, since every other aspect from Bernoulli's law can be translated into an equivalent pressure concept.

In the following paragraphs, both liquid transfer and gas transfer in saturated materials will be discussed.

- Liquid transfer in saturated materials

In a material saturated with liquid, the pores will be filled with the liquid (Fig.3.2). The amount of liquid content θ [-], i.e. the volume of water per bulk volume, is therefore equal to θ_{sat}. The liquid content is at its maximum, and

remains unchanged. The liquid content does not influence the driving flow and does not make up the driving force of the flow.

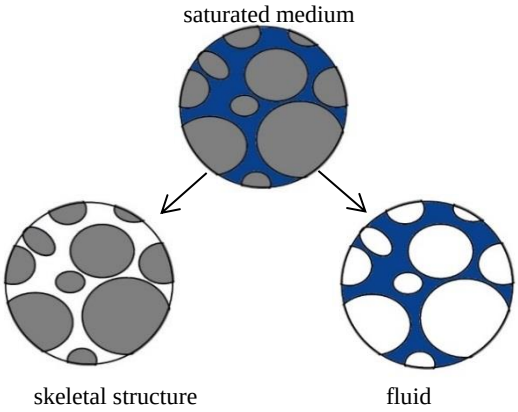

Fig. 3.2 Sketch of a saturated medium, composed of the material's skeletal structure and the fluid.

For such configurations, Darcy established in 1855 a basic law to link the flow of water (liquid) with the pressure difference and introduced the permeability, k [m^3s/kg], of a material [30]. Darcy's law is limited to liquid saturated flow where the volume flow rate Q [m^3/s] through the flow tube is sufficiently low to induce a laminar flow. But turbulent liquid flows do not generally occur in constructions [30]. Turbulent *gas* flow can occur on the other hand. The classical Darcy law expresses the volumetric flow velocity u [m/s] as the volume flow rate Q divided by the cross-sectional area A [m^2] (eq. 3.1), L [m] being the length associated with the considered flow tube (or sample) and Δp [N/ m^2] as the difference between p_1 (inflow) and p_2 (outflow) [30].

$$u = \frac{Q}{A} = k\,\frac{\Delta p}{L} \qquad \text{(eq.3.1)}$$

The Darcy permeability k depends on the liquid viscosity η_{liquid} [kg/ (m s)] for (incompressible) Newtonian liquids in laminar flow in inert non-swelling materials. Accordingly, an intrinsic permeability k', solely dependent on the porous material's properties, can be established. k' [m^2] is independent of the liquid that migrates through the medium [30].

$$k' = k\,\eta_{liquid} \qquad \text{(eq.3.2)}$$

Consequently, Darcy's law can be written as:

$$\frac{Q}{A} = \frac{k'\,\Delta p}{L\,\eta_{liquid}} \qquad \text{(eq.3.3)}$$

Besides the classical expression in SI-units, the intrinsic permeability k' is often expressed in Darcy units (D). 1 D is 1000 mD, or 9.8692 E-13 m^2 (~1 μm^2). In most of the materials, one can assume that the intrinsic permeability is a constant over time. Nevertheless, this assumption should be approached

with care when considering cementitious materials, since they seem to have a decreasing water permeability with increasing test duration [30]. Cementitious materials contain hydrating materials that have water bound in their structure. If these hydrated materials are not yet fully hydrated, or dehydrated due to oven drying, they would (re)hydrate when exposed to water [30]. This explains the phenomenon of decreasing permeability over time: the pores decrease in size and/or the percolation path increases in length.

- Gas transfer in saturated materials

Since gas is constant in mass, but variable in volume, Darcy's law had to be adapted. The ideal gas law of $\rho = p\ M\ (R\ T)^{-1}$, allows managing the evolution of apparent density ρ [kg/m³] with pressure where M [kg/mol] is the molar mass, R the gas constant [J/ (mol K)] and T [K] the temperature. In addition, gas viscosity is independent of pressure over a wide range, it can therefore be considered a constant: the gas viscosity is particular for one gas at a certain temperature. The extension of eq.3.3 in terms of mass flow allows then an expression for gas saturated samples, with $\bar{u}$ the vector flow velocity as (adaptation from [30]):

$$\rho\bar{u} = -\frac{k'\rho}{\eta}\nabla p \qquad \text{(eq.3.4)}$$

Following the ideal gas law,

$$\frac{M}{RT}p\,\bar{u} = -\frac{M}{RT}\frac{k'}{\eta}\frac{\nabla p^2}{2} \qquad \text{(eq.3.5)}$$

Translating eq.3.6 to the scalar field, $\frac{\nabla p^2}{2}$ becomes the more comprehensible $\frac{(p_2^2-p_1^2)}{2L}$

$$u_2 = \frac{k'}{\eta}\frac{(p_2^2-p_1^2)}{2p_2 L} \qquad \text{(eq.3.6)}$$

for steady one-dimensional flow, through a uniform porous material of length L, in which u_2 is the flow velocity at outflow pressure p_2.

3.1.2.3 Moisture transfer in unsaturated materials

Stone, mortars and combined systems used in the exterior of a building cannot be considered as completely dry materials, since they absorb moisture from the soil, the air or by rain (moisture can remain due to capillary trapping). Most building materials are in reality unsaturated, and contain moisture, i.e. water in both liquid and gas phase (Fig.3.3). Due to the presence of water in some form (water vapour, trapped liquid water) on or in the material, aspects which were of no importance in saturated materials will influence the fluid migration in unsaturated building materials. In building materials, water in both gas and liquid state are present at the same time. Therefore, not only water content, but also moisture content becomes important [4]. In unsaturated materials, saturated permeability k as in the

Darcian sense is a simplification of the reality, and the total moisture permeability K is best used. The total moisture permeability K is determined by the saturation degree of the unsaturated medium, since there is a unique relation between saturation degree and capillary pressure (without considering hysteresis effects) [30,32].

Nevertheless, the choice was made to study and estimate the permeability of the mortar in saturated condition: calculating the diffusivity or moisture permeability would not permit to study and understand the effect of the *mortar components* alone since they are influenced by a larger range of factors, e.g. the water and water vapour content behave differently, and their content is influenced by the temperature and the relative humidity.

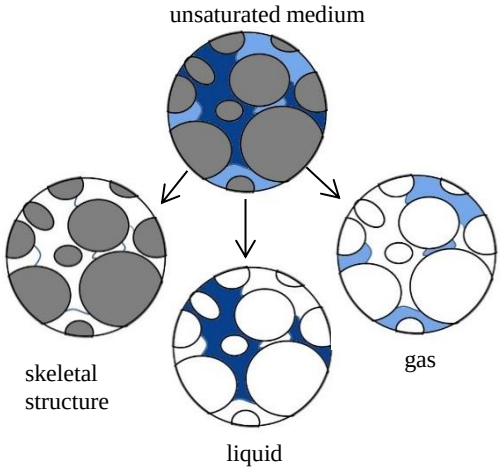

Fig. 3.3. Unsaturated medium, composed of the material's skeletal structure, a liquid and a gas.

3.1.3 Pore-scale related properties: measuring techniques

As stated above, NHL mortars are interesting to use for stone repair due to their combined reaction of hydration and carbonation, and therefore it may be challenging to measure their pore-related properties. A choice was made to discuss and use only some specific techniques, out of all other techniques available to measure fluid migration, since these chosen techniques are used in research disciplines closely related to the lime mortar domain, such as cement mortars or geomaterials in general. Fluid flow was assessed in the mortar through water and gas permeability measurements, while the pore network of mortars was measured and analysed through Mercury Intrusion Porosimetry (MIP) and X-ray micro-CT scanning techniques. The functioning of both MIP and micro-CT techniques has already been discussed in depth by [33–35]. Their use for NHL mortars has only been reported in some studies, for MIP [23,27,36,37], and for micro-CT [37,38]. The fluid-flow assessment techniques operate in the saturated flow regime, and permit to study the effect of the material's intrinsic properties only (intrinsic permeability, pore size distribution) without having to take into account e.g. variation in (atmospheric) pressure or variation in water content. In addition, these techniques were chosen because they can be used to test fluid migration

in mortar, whilst taking into account the material's specific limitations. NHL mortars put a limit on the type of test which can be used: there can always be a possibility that the mortar hydrates when in contact with water, a phenomenon to be avoided during tests, since it can modify the internal structure, and thus also alter the shape of the pore network. As any other porous material, NHL mortars have a certain range in which their pore sizes vary, and this might limit the use of certain analysing methods as well. The sample size is variable depending on the technique used. Most techniques discussed here (permeability, porosity tests) can be performed on samples of several centimetres, while micro-CT and MIP require a much smaller sample size on millimetre scale. Sampling for these two techniques is thus challenging, since a representative volume of the material has to be analysed.

3.1.3.1 Helium pycnometry

In this study, helium pycnometry was chosen since (a) the gas has a small molecular size (31 pm, in comparison to 48 pm for oxygen [39]), (b) is not easily adsorbed onto the mineral surface, and (c) is inert for the mortar. It shows therefore higher accuracy and any hydration effects due to contact with water would be avoided. In helium pycnometry, the solid volume of the sample is calculated by expanding the helium gas into a chamber of known volume, containing the sample. The helium gas is inserted into this chamber and into a reference chamber with another higher pressure. The pressure in the sample chamber is increased and the difference in pressure with the reference chamber is used to calculate the unknown volume present in the sample cell chamber. The small molecules of the helium gas can migrate into the smaller pores of the sample. It can therefore representatively measure the skeletal volume of the sample. The functioning of the helium pycnometer is illustrated in Fig. 3.4. This method is a frequently used technique for stones and mortars alike [30]. For this study, the Accupyc II 1340 (Micromeritcs) was used.

The bulk volume might be calculated based on the geometry of the sample, but in this study a GeoPyc 1360 Envelope & T.A.P. Density Analyzer (Micromeritics) was used to measure the bulk volume. Moreover, the system of the envelope analysis permits accurate results, since it takes the surface irregularities into account. The density analyzer measures the precise bulk volume and allows therefore to calculate the sample bulk density. The sample is inserted into the sample chamber, containing a powder, DryFlo®, which sets itself closely around the sample (Fig.3.5). A piston compresses the sample and the powder up to 145 N. Since the powder has a known density, compressibility and volume, the pycnometer can measure the precise bulk volume and calculate the bulk density of the specimen. Through both measurements, the open porosity is calculated based on the following equation (eq.3.7).

$$f = \frac{(V_{bulk} - V_{skel})}{V_{bulk}} \qquad \text{(eq.3.7)}$$

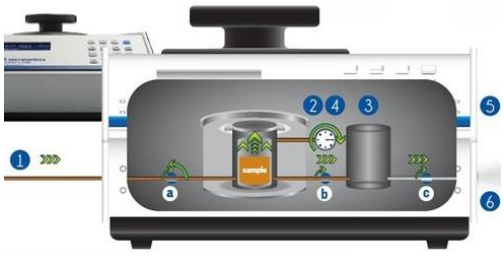

Fig. 3.4. Sketch of the functioning of the helium pycnometer used in this study, figure by Micromeritics.
1. Inert gas flows into a sample chamber - valve *a* opens, then closes
2. An equilibrium is reached
3. Gas flows into second chamber for volume measurement - valve *b* opens
4. Equilibrium is reached again
5. Exact volume occupied by sample is recorded
6. Pressure is vented off - valve *c* opens

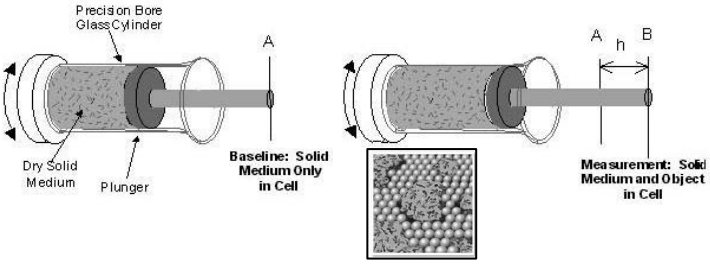

Fig. 3.5. Sketch of the sample holder, containing already the dry powder. The inset image shows a particle to be measured surrounded by the very small particles of the DryFlo ® powder. Figures by Micromeritics.

3.1.3.2 X-ray computed micro tomography (X-ray micro-CT)

With X-ray computed micro tomography, it is possible to visualize the internal structure of a material in 3D, on the micrometre scale [33]. For micro-CT, an X-ray source is placed in front of an X-ray detector. The sample is placed in between the two, on a motorized sample stage, which can make rotational and translational movements.

When the source sends X-rays, the detector captures an image due to the attenuation of X-rays which have passed through the sample. The incident intensity I_0 of a monochromatic X-ray that passes through a homogeneous material with thickness T, will attenuate to a transmitted intensity I, as defined by the Lambert-Beer law (eq. 3.8):

$$I = I_0 \, e^{-\mu T} \qquad \text{(eq.3.8)}$$

μ is the linear attenuation coefficient, and is a function of the atomic density and the microscopic cross-section σ_m, at a specific radiation energy (eq.3.9). The microscopic cross-section indicates the probability that an atom interacts (by transmission, scattering, and absorption) with the X-ray photon, and depends on the energy of the photon and on the specific element.

$$\mu = \sigma_m \, N_{atom} \qquad \text{(eq.3.9)}$$

This technique can be used to distinguish the pores (e.g. the number of pores, the pore size distribution) and the volume of grains present in the mortar [33,34,40]. The polychromatic X-ray radiographs are transformed into a stack of 2D reconstructed slices using reconstruction algorithms [41], image

analysis then permits for example a segmentation of voids present in the sample. The voids, i.e. the pore volume, can be separated in individual objects, and can be quantified (Fig.3.6). This data is collected and, for example, the number of voids with a specific size in the studied sample, can be calculated using dedicated software. Other useful means which can aid in the determination of the sample's pore-related properties are the visual image of the distribution and shape of the pores in the sample, the actual pore size distribution, the maximum opening, sphericity and connectivity of a pore [33,42].

The lower resolution limit is mainly determined by the focal spot size of the X-ray source, and is currently limited to 0.5 µm for traditional micro-CT set-ups, or to 50-100 nm for set-ups using scintillators and magnification optics [33,38]. Pores smaller than the resolution limit cannot be quantified with certainty, and this volume of voids is therefore also called unresolved porosity. Several aspects play a role in the final image achieved from micro-CT analysis, i.e. noise, beam hardening and discretization effects (see e.g. [34]). These discretization effects determine that the lowest achievable voxel size depends on the size of the object. The operator performing the scan should also be vigilant to the parameters which are used as input for the analysis (tube voltage, total exposure time …) and the parameters used for the post data treatment processes: the pores can be segmented using grey-value thresholding, which is very much operator-dependent due to noise and partial volume effects [34]. Because of these effects, quantitative results from micro-CT analysis are to be considered as relative values [34].

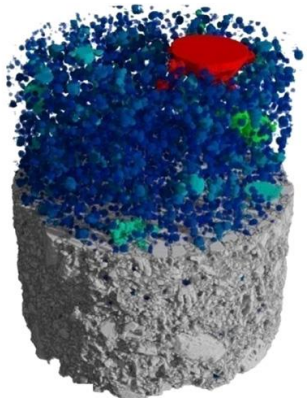

Fig. 3.6. 3D visualisation of a reconstructed and analysed micro-CT scan with VG Studio. The spheres represent various pores, calculated through the equivalent diameters in Morpho+ software. From [38].

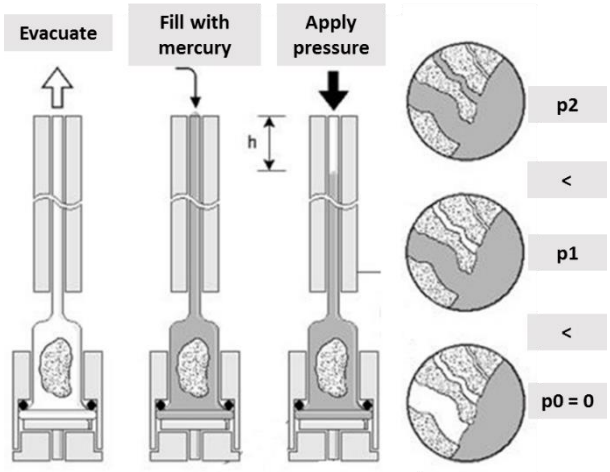

Fig. 3.7. Sketch of the Mercury Intrusion Porosimetry process. The inset shows that smaller pores are intruded last with non-wetting mercury, due to increased pressure. Adapted from Micromeritics.

The HECTOR CT scanner at the Centre for X-ray Tomography (Ghent University, Belgium), was used for the scanning of the mortar sample, at 110 kV tube voltage, and a beam power of 10W [43]. The actual voxel size was 5.39 µm. The images were reconstructed and analysed with Octopus software,

formerly Morpho+ [42]. VG Studio Max was used for the visualisation of the reconstructed images.

3.1.3.3 Mercury Intrusion Porosimetry (MIP)

With MIP, the pressure needed to inject mercury into the sample is used as a proxy for the pore (throat) size distribution [35]. Mercury is a non-wetting liquid and must therefore be forced into the material under high pressure. An increasing pressure allows mercury to intrude smaller throats and finer pores. The Washburn equation can be used to calculate the pore size distribution, and is based on the pressure and the injected mercury volume (eq. 3.10) [44]. This equation is based on the theory that a pore is a cylindrical tube and is entirely accessible from the outer surface of the sample [45].

$$D = -4\gamma\, p^{-1}\cos(\varphi) \qquad \text{(eq.3.10)}$$

D is the pore opening diameter (m), p the pressure applied (N/m^2), γ the surface tension of mercury (0.48 N/m), φ the contact angle of mercury (140°).

Since any material rarely contains (only) cylindrically-shaped pores, the real pore size distribution might deviate from the MIP-presented pore size distribution. In cement mortars, so-called ink-bottle pores are reported with a large pore volume, but a small pore throat entry: a lot of pressure is thus required to inject mercury into this pore (Fig. 3.1, 3.7) [45]. Consequently, through the Washburn equation, it is considered as a very small pore, while in contrast, the pore volume itself might be rather large. MIP should thus be considered more as a means to indicate the pore throat size distribution, rather than the actual pore size distribution [45]. Some studies propose alternative techniques [14,46] which should avoid ink-bottle effects, and should thus represent the actual pore size distribution of the mortar. Kaufmann et al. (2009) propose a multi-cycle mercury intrusion [14]. Assuming that mercury remains trapped in large volume pores with small entry throats, the second injection of mercury after a first one should give a more correct pore size distribution. A pore surface area analysis from nitrogen adsorption tests may then indicate which pores were too difficult to access and were not reached [14]. Zhou et al. (2010) propose one cycle with step-wise increase and decrease in pressure [46]. This should also avoid the ink-bottle effect.

The few studies concerning NHL mortars gave no indication whether or not ink-bottle pores are present, but the experimental campaign later in this study aimed to find an answer through a combination of micro-CT and MIP analysis. The measurements in this study were performed with the Pascal 140 and 440 Series from ThermoScientific.

Typically, the MIP analysis allows to study pores with entry dimensions of 100 µm at the lowest intrusion pressures, and can go up to 2.5 nm at the highest intrusion pressures [30]. However, literature points out that the pressure which is applied during MIP analysis might prove too high for (lime) mortars [30,47]. The MIP analysis in this study was therefore executed until

a maximum pressure of 150 MPa, which should allow to determine the pore size distribution up to 0.01 µm. This is acceptable, since previous studies showed that the pores of NHL mortars are to be situated in the nano to micro millimetre region [21,23,28].

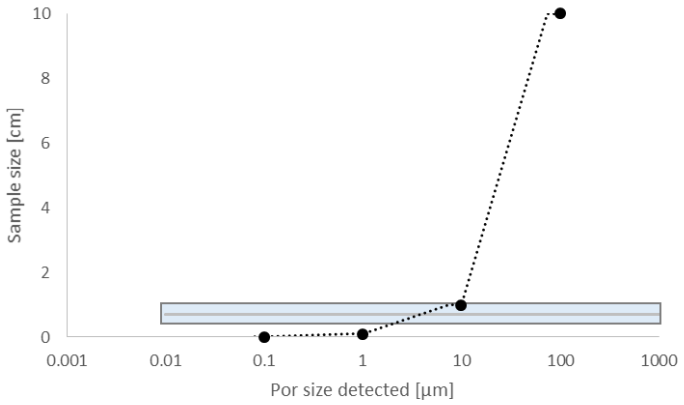

Fig. 3.8. Detectable pore size in MIP and in X-ray micro-CT, based on [33,48]. The bar represents the MIP sample size, the dotted line the micro-CT sample size, required for the pore size which can be detected.

Micro-CT has been compared with MIP [40,48]: although micro-CT is an image analysis technique and MIP an intrusion liquid technique, they overlap in the pore sizes they can detect; minimal detectable pore size is 0.5 µm (or 100 nm for high-end micro-CT) and 3 nm respectively (Fig.3.8). They could thus be regarded as complementary.

3.1.3.4 Gas and water permeability

Permeameters are used to measure flow in materials. They are in general equipped with a Hassler cell, where the (cylinder-shaped) sample is inserted (Fig.3.9). For liquid permeability measurements, the liquid used is often water. The calculation is rather straightforward since this saturated liquid flow follows the Darcy law (eq. 3.3).

For gas flow through materials as well, permeameters can be used. Since gas flow can easily become turbulent in normal testing conditions, an additional effect might take place. The Klinkenberg effect takes place in materials with small pores, where the flow can behave as though there were slippage at the gas-solid interface [30]. This would make the apparent gas permeability decrease while the measured mean pressure increases [16]. To overcome this, the Klinkenberg effect could be taken into account since apparent gas permeability may be different from the intrinsic permeability, by performing a Klinkenberg correction: minimally three subsequent measurements at different backpressure steps but equal flow rates have to be performed with Hassler cell devices to be able to perform the Klinkenberg correction [49]. Filomena et al. (2014) compare the ‘normal’ steady-state permeameters with a Hassler cell with the probe permeameters that can be placed on the surface of a specimen [49]. The probe permeameters have as advantage that they can be used on site or on larger blocks. However, surface

roughness and sealing quality appears to be the biggest Achilles heel. Filomena et al. (2014) therefore suggest a correction on the probe permeameter results [49]. This correction should be established by comparing the probe permeameter results with Klinkenberg corrected results, using the same gas. Naturally, a larger variability of probe permeameter results is likely, since a smaller zone is measured.

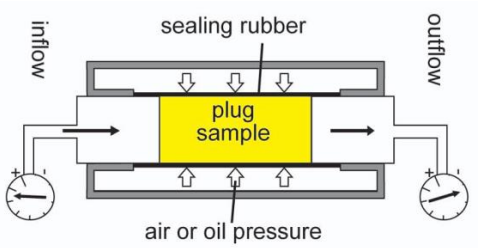

Fig. 3.9. Hassler cell in a permeameter, with a sealing rubber around the sample, confined by oil or air pressure. As such, the gas or liquid injected into the sample can only leave at the other side of the sample. From [49].

Gas permeability was measured here with a steady-state nitrogen GasPermEdu gas permeameter (Vinci Technologies). This device had no built-in back-pressure, but calculated the difference between the measured pressure and the measured atmospheric pressure. The flow rates of six consecutive pressure levels were noted for each sample. Naturally, the lack of a backpressure does not permit a Klinkenberg correction, and the permeability measured is thus the nitrogen permeability of the lime mortar.

The ROP-DBS permeameter was used for measuring the water permeability of the samples. The samples were first immersed in water until saturation point, since preliminary tests indicated that mounting water-saturated lime mortar samples did not show sample fissuring and erroneous results as detected on dry lime mortar samples. As such, any surcharge due to mounting or confinement would also be carried by the water in the sample, and not only by the skeletal structure of the lime mortar itself. Samples were placed in a Hassler cell and consequently subjected to a 2 N/mm^2 confining pressure. Water was then injected at a constant flow rate (on average 2.5 ml/ min) into the cell chamber. Once the flow was stabilised, the permeability was calculated according to the pressure.

In steady-state, laminar flow conditions, permeability can be expressed according to Darcy's adapted law (eq. 3.6) [30].

Additionally, some studies exist which analyse the permeability of the same material, with a liquid and a gas, in order to establish the actual intrinsic permeability of the material: Loosveldt et al. (2002) tested cement mortar on its permeability for argon, ethanol and water [16] and Lion et al. (2004) used ethanol and argon for a Anstrude limestone [50]. Ethanol and the Klinkenberg corrected argon permeability were found to be very close, and both might be considered as the intrinsic permeability of the material [16,50]. Loosveldt et al. (2002) reported that in comparison, the water permeability for the same mortar samples gave a larger scatter, due to a decreasing flow rate [16]. This

is believed to be due to hydration during the permeability test: samples were dried at 60°C (ethanol) and 105°C (water), and indicate again the importance of sample preparation of lime mortars [16].

3.1.4 Conclusion

In this section, several methods to assess the pore-scale properties were discussed in more detail. Throughout the discussion of the various techniques, the element of sample preparation returned. The preparation required for NHL mortars might sometimes complicate the testing technique: NHL mortars are preferably not dehydrated during oven drying, and not (re)hydrated during testing. Moreover, their low strength requires that samples are treated carefully, and preliminary steps such as immersion in water (for water permeability) were undertaken.

The techniques discussed in this section are subdivided based on the subject they actually analyse. First, the permeameters measure the flow of a liquid or a gas through the material, and give therefore only indirectly information about the lime mortar's structure. Remark though, that this is what the user is interested in knowing: the ease with which a fluid can propagate through the lime mortar. Although mortars in buildings are mainly subjected to unsaturated flow, saturated flow is non-negligible in this research. By choosing to test the saturated permeability of lime mortars, a link can be made with the intrinsic permeability, a property solely dependent of the material. Measuring the (saturated) permeability should thus give information about the influence of the mortar components (aggregates, lime type used) or mortar composition (W/B, B/A...). Other studies already demonstrated how the mortar's behaviour can be simulated in the unsaturated flow regime of on-site situations [51–53]. This might include the setting of the mortar together with other building materials, and the influence of each material in this specific configuration on the fluid transport.

The second type of techniques (MIP, micro-CT, porosity) gives information about the actual voids (and their relation towards one another) of the lime mortar. The most common test realised on natural stone and mortars, assessment of the (open) porosity, gives in itself not sufficient information. It is however a widespread well-understood concept and its use might prove useful for a rough estimation of permeability.

MIP gives information about the connection of pores, and micro-CT about the pore size and shape, but are less trustworthy on the exact pore volume present. Based on this information alone, it takes an additional step, such as modelling, to know if the mortar will or will not permit quick fluid transport through its structure, e.g. [33]. Nevertheless, these techniques give information that can be quantified and visualised as well. Moreover, the combination of MIP and micro-CT would allow to define the pore size distribution on a very large range, information which cannot be distilled from permeameters alone. Additionally, the analysis of the pore size distribution and pore structure on various types of lime mortars can help shape the

estimation method for permeability of lime mortars, the actual goal of this chapter.

These techniques listed above are thus best used in combination with each other, in order to have an understanding of the pore-scale properties of the lime mortar out of different point of views. Moreover, the combined use of them also implies that the lime mortars are being investigated on various levels: for micro-CT and MIP, only small samples (< 1cm³) can be analysed, while for both permeability tests and porosity tests, centimetre-sized samples are best used.

3.2 Pore-scale properties of lime mortars: an experimental study

The mortars used for this experimental study were the W/B series of NHL 5 and NHL 3.5 mortars, including tests on 32 different mortar mixes. Both type and size of the sands as well as the spread of the mortar are varied. Remark that all aggregates are sands, and that no fines or gravel were tested. The goal was to be able to indicate the influence of aggregates and water/binder ratio on pore-related properties. In order to be able to illustrate the influence of both as best as possible, two graphs will be presented at every analysis, one where the W/B is regarded to the measured property and one where the sand used is looked into more detail.

All mortars were analysed on their density and open porosity. The pore size distribution was analysed through mercury intrusion. These results are compared with gas and water permeability measurements. In addition, and for comparison means with possible other studies, capillary absorption tests were also executed. These results can be found in Appendix 3.1. In addition to these analyses, one mortar, thought representative for the general behaviour of NHL5 mortars, was analysed through micro-CT.

3.2.1 Open porosity and apparent density

For each mortar mix, 4 to 5 cylindrical samples were tested on their open porosity and apparent density (Fig.3.10-11). In total, 130 samples were subjected to these tests. The tables representing the average and standard deviation per mortar mix can be found in Appendix 3.1.

Fig. 3.10 shows that there is a difference between NHL 3.5 mortars and NHL 5 mortars: the values of open porosity of the NHL 3.5 mortars are much higher than the NHL 5 mortars, and since the two properties are related, the apparent density is lower for the NHL 3.5 mortars than for the NHL 5 mortars. For all mortars, the W/B ratio seems to have a significant influence on the apparent density and open porosity.

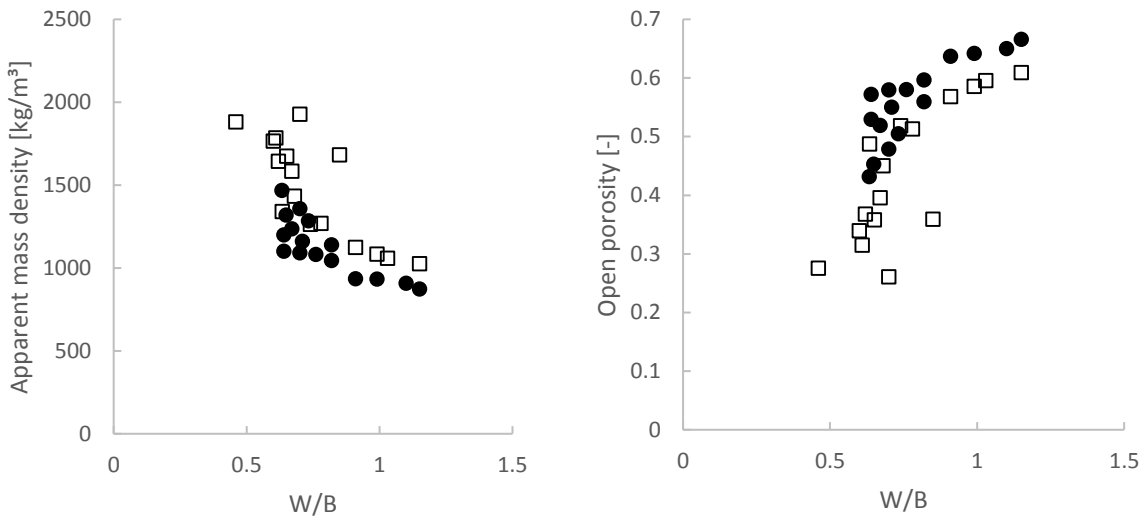

Fig. 3.10. A-B. Porosity shows a clear difference between NHL 5 and NHL 3.5 mortars. The apparent density shows a similar but inverted trend. NHL 5 mortars *(square)*, NHL 3.5 mortar *(circle)*.

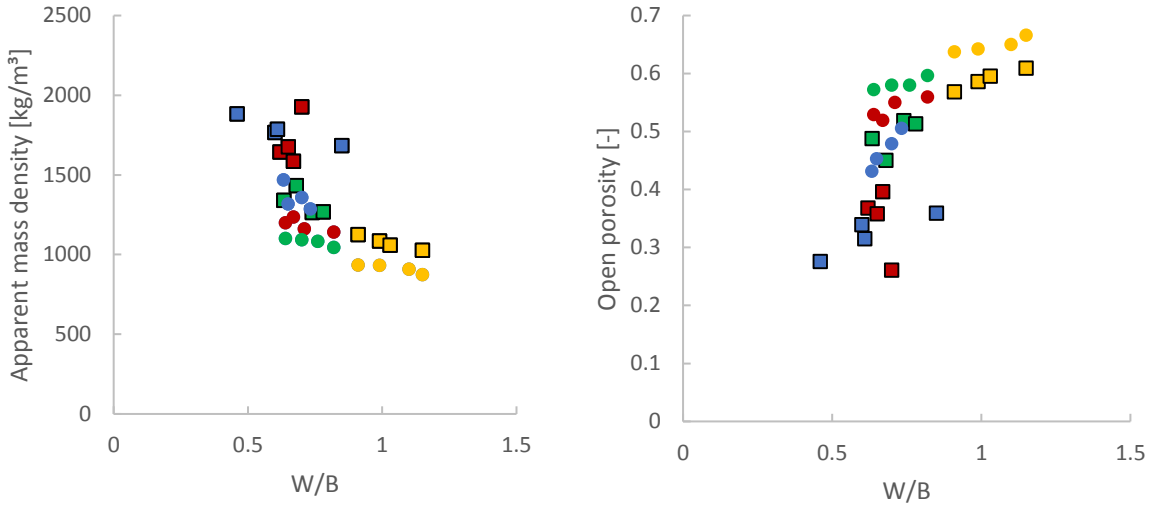

Fig. 3.11. A-B. Apparent density and open porosity of the NHL 3.5 (*circle*) and NHL 5 (*square*) W/B mortar series, subdivided based on the type of sand used. Normalised sand (*blue*), Rhin gros (*red*), Rhin fin (*green*), Yellow-green (*yellow*).

Looking at Fig. 3.11, the effect of the aggregate type on the porosity and apparent density also becomes visible. The finely grained yellow-green mortar series have the highest porosity and lowest apparent density of all mortars. The coarser Rhin gros seem to lead to mortars with lower porosity. The influence of the variable W/B ratio was visible in the reference mortar mixes and in the yellow-green mortar mixes: porosity increased 1.25 times (a difference of 8%) from the lowest spread (120 mm) to the highest (180 mm). The Rhin sand mixes were more stable and were not as much influenced by the increase or decrease of the W/B ratio, which can be linked to the lower variation in added water to achieve the various spreads. The W/B ratio in the Rhin fin mortars was the same as for the reference and Rhin gros mortars: the higher porosity of the Rhin fin is assumed to be due to the finer aggregates. As with the yellow-green mortars, the finer aggregates present in the sand

demanded more water to produce, and this is translated into a higher open porosity and lower apparent density. Remark that the series of both yellow-green and Rhin fin mortar show a rather smooth curve between W/B ratio and open porosity, while there is a larger spread for the Rhin gros and reference sand mortars. This might be due to their larger variation in W/B ratio when producing the mortars.

In this experimental campaign of lime mortars, appears the effect of the grain size distribution to be more important than the binder type on the porosity of the mortar: the slope of the porosity –W/B ratio for some mortars produced with the same sand appears to be similar (Yellow-green, Rhin fin) (Fig.3.10-11). This trend is less distinct to not present in the Reference sand mortars and the Rhin gros mortars.

3.2.2 Pore size distribution

3.2.2.1 MIP analysis

Other studies showed that the pore sizes of NHL mortars are most likely to be situated in the nano to micrometre scale and that the largest bulk of the pores can be situated between 0.1 and 10 µm [21,23,28]. The Pascal 140 and 440 Series from ThermoScientific were used for the analysis of the samples of about 8 x 8 x 10 mm^3. These were sampled at the outer edge of the cast bars so that they would certainly be representative for the cured and carbonated mortar. The laitance was abraded. Taking into account the weaker compressive strength of NHL mortars in general on the one hand and the desired pore size resolution on the other hand (0.01 µm), maximum pressure varied from 130 to 180 MPa. The ‘pressurisation-depressurisation’ technique proposed by [46] could not be performed: this technique requires that the equipment can perform cycles of pressurisation-depressurisation, without losing the information of the previously performed cycles. This was not possible with the equipment available, making it impossible to have the software reconstruct the entire pore size distribution.

The entire pore size distribution of each mortar can be consulted in Appendix 3.1, some representative examples are given in Fig. 3.12-13.

Both NHL 5 and NHL 3.5 mortars have bimodal pore size distributions (Fig. 3.12-13). The influence of the W/B ratio is visible in Fig. 3.14 & 3.15: the mortars with the higher spread have a generally larger intruded volume.

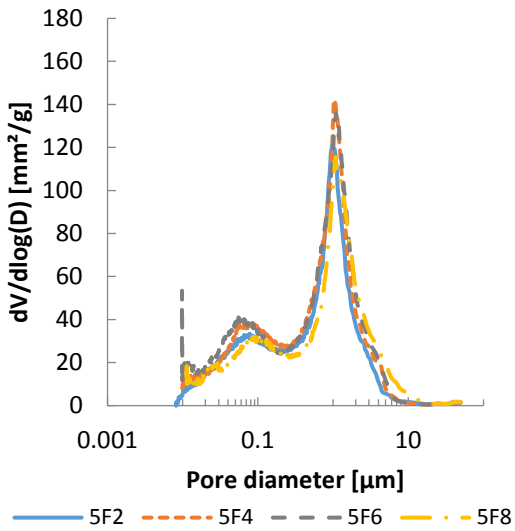

Fig. 3.12. Example of a pore size distribution measured with MIP. The curves represent the pore size distribution of the NHL 5 Rhin Fin mortar mixes, (120, 140, 160, 180 mm). The higher pore volume due to higher W/B ratio is visible in the higher volume of pores detected.

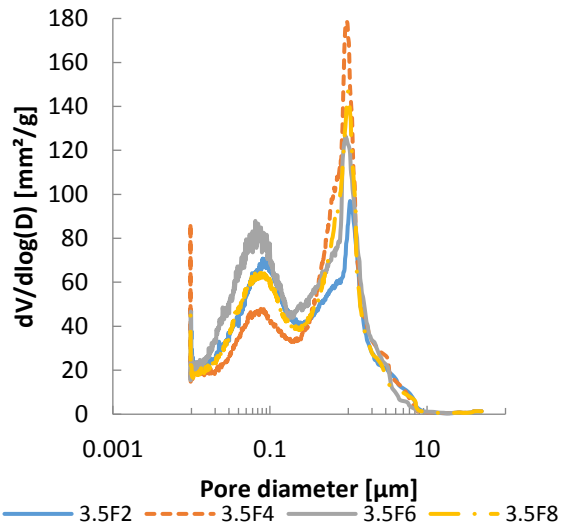

Fig. 3.13. Example of a pore size distribution measured with MIP. The curves represent the pore size distribution of the NHL 3.5 Rhin Fin mortar mixes, (120, 140, 160, 180 mm). The higher pore volume due to higher W/B ratio is visible in the higher volume of pores detected.

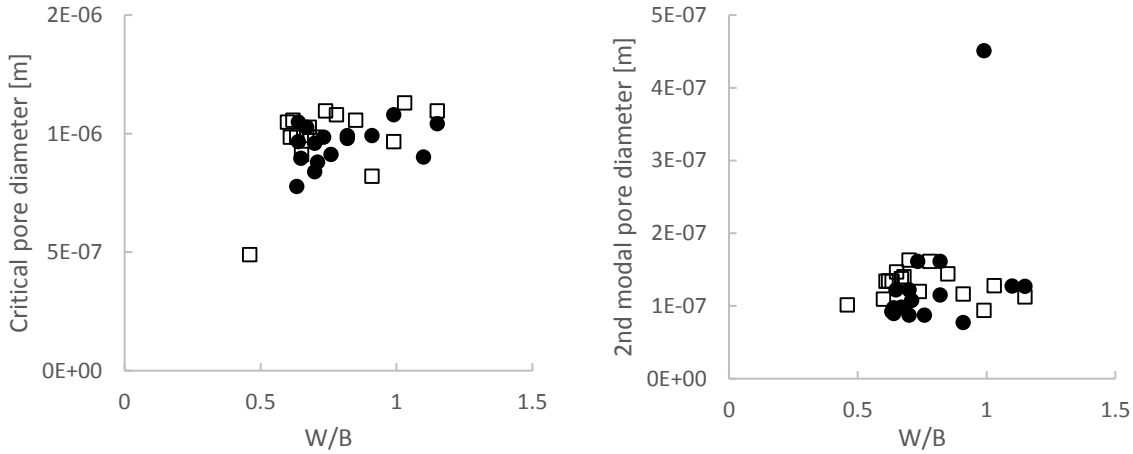

Fig. 3.14. A-B. The critical (A) and second modal (B) pore diameter of each mortar mix in relation to the W/B ratio. NHL 5 mortars *(square)*, NHL 3.5 mortar *(circle)*.

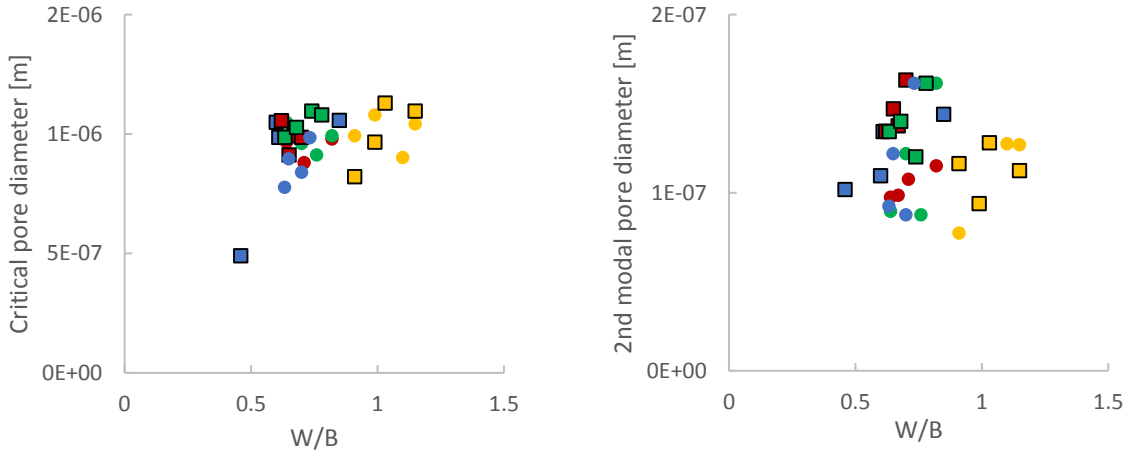

Fig. 3.15. A-B. The critical (A) and second modal (B) pore diameter of each mortar mix related to the W/B ratio, subdivided based on the type of sand used. Normalised sand (*blue*), Rhin gros (*red*), Rhin fin (*green*), Yellow-green (*yellow*). NHL 5 mortars *(square)*, NHL 3.5 mortar *(circle)*. In graph B, the 3.5-Y-4 mix is left out (see graph 3.15B) in order to distinguish the trends better.

In Fig. 3.14, the critical pore diameter of each recorded pore size distribution is represented. The critical pore diameter is the pore diameter at the maximum of the derivative of the pore size distribution curve, as defined by [54], or the first modal pore diameter. The NHL 5 and NHL 3.5 mortars of this experimental campaign seem to behave quite similarly, i.e. the lime type does not seem to influence much and all critical pore diameters vary between 0.8 and 1.2 µm. Comparing figures 3.14 A and 3.15 A, the critical pore diameter seems to be mainly influenced by the type of aggregate used, and on a secondary level by the W/B ratio. Finer grained aggregates (yellow-green and Rhin fin) have on average a higher critical pore diameter than the coarser grained aggregates. Especially the normalised sand shows smaller critical pore diameters for the lower W/B ratio.

The second modal pore size (i.e. the pore with the second largest peak) is represented in Fig. 3.14 B and 3.15 B. This second modal pore size diameter varies between 0.07 and 0.16 µm (with the exception of the NHL3.5 160 mortar). A specific influence of the W/B ratio or of the variation in sands is less distinct.

3.2.2.2 Micro-CT analysis

The pore size distribution of the 5-RF-45 mortar was studied through both micro-CT and MIP analysis. This sample was thought of as representative for the NHL 5 lime mortar series. Considering the fact that the mortar for this analysis could not differ too much in age from the other mortars previously tested, the B/A NHL 5 RF-45 mortar was chosen. At the time of the test, the mortar had cured for 6 months, the other mortars of the W/B mortar series were tested after 3 months curing. Before the micro-CT scan could be made, the sample had to be prepared first. Logically, a cylindrical sample guarantees the same thickness of the sample throughout the scanning of the rotating sample. It proved however difficult to core such a small sample (diameter 4 mm) from a lime mortar bar: the sample crumbled. Two solutions presented themselves, (a) a centimetre-sized sample of the lime bar could be embedded in resin and could be cored afterwards, or (b) a small bar of 1 by 1 by 4 cm^3 long, which had not been used for MIP analysis, could be abraded with sanding paper into a cylinder with diameter 0.4 cm. The last option was chosen and posed no problems.

The mortar used in the micro-CT analysis had an average open porosity of 41.9 %, with a standard deviation of 7 %. Porosity of the mortar showed thus large variation, but followed the trend between W/B ratio and porosity as seen in Fig. 3.11 and 3.12. The 5-RF-45 mortar had an average intrinsic permeability of 5.42 E-12 m^2, with a standard deviation of 5.79 E-13 m^2 (in Darcy, this is 5.49 ±0.59 D). The mortar showed an average nitrogen gas permeability of 4.16E-13 m^2, standard deviation of 8.34E-14 m^2 (0.42 ±0.084 D). Both values are in line with the other mortars measured (see 3.2.3 and 3.2.4).

The pore size distribution of the sample is shown in Fig. 3.16. It has a bimodal pore size distribution with a critical pore diameter of 1.01 µm and a second modal diameter of 0.07 µm, which is representative for the pore diameters of the other mortars previously tested.

The reconstructed images were analysed mainly by the grey-scale values of each voxel. The large air-induced pores were clearly visible in these images, however, it is clear that there is some unresolved porosity present in the paste of the mortar; the voids assumed to be present in the paste cannot be clearly distinguished (Fig.3.17). In order to resolve this problem somehow, the images were analysed twice:

The total volume was first analysed using a dual threshold filter of the grey values with which the largest pores could be distinguished, but not the smallest pores in the paste.

Then, the images were analysed again, using a gradient filter, since unresolved pore volume was assumed to be present next to aggregate grains. The difference in voids and hydrates/carbonates in the paste became as such more defined (Fig.3.18). This technique did not allow an analysis of the air-voids.

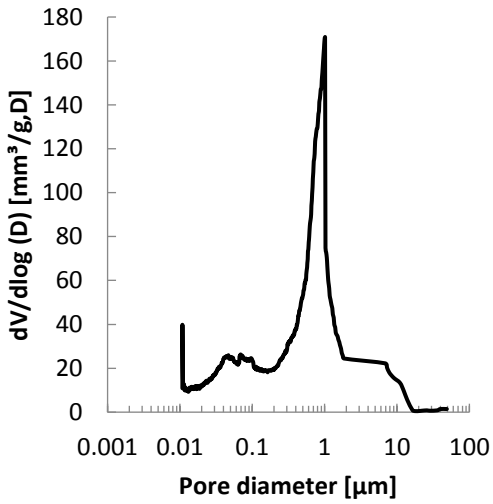

Fig. 3.16. The pore size distribution of the 5-RF-45 mortar as detected by MIP analysis.

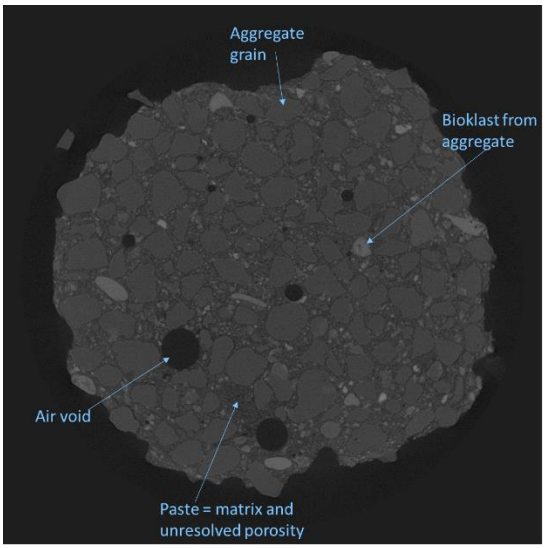

Fig. 3.17 Cross-section of the reconstructed volume, indicating the various elements which can be seen on a slice. The sample is 4 mm in diameter.

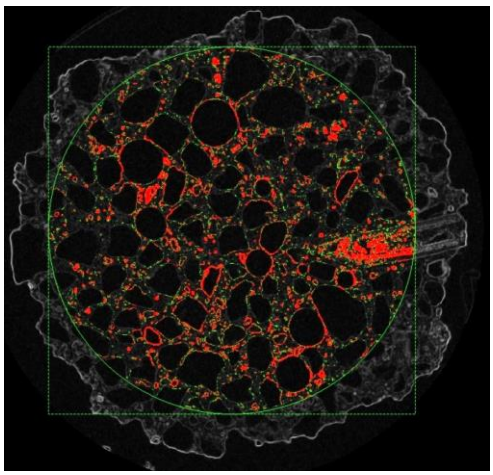

Fig. 3.18. Cross-section of the volume, during the gradient filter operation. The strong threshold (*red*) and weak threshold (*green*) indicate the pores around the grains and air voids. Note that the 'air voids' in this image cannot be distinguished from the aggregate grains. The sample is 4 mm in diameter.

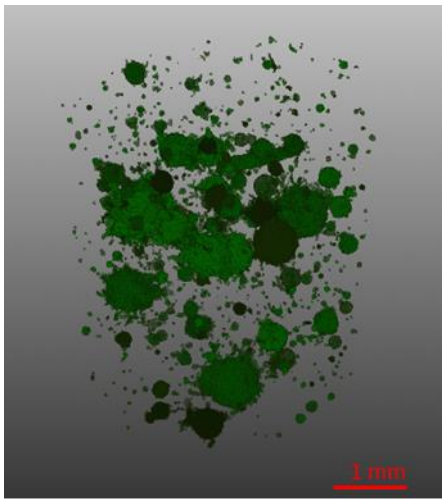

Fig.3.19 The clearly distinguishable (air) voids are mainly spherical, with a small pore throat. Remark that a large bulk of air-voids appear to be well-connected.

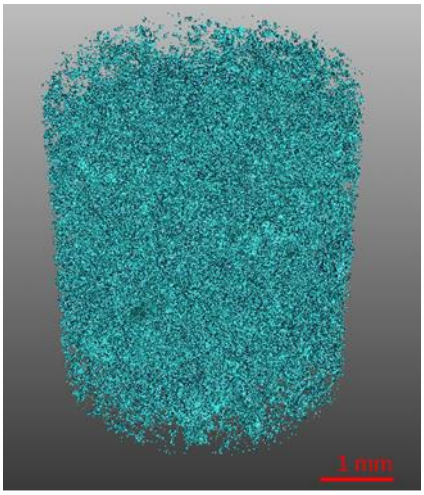

Fig.3.20 The pores assumed to be present in the paste. The air-voids are not represented in this image.

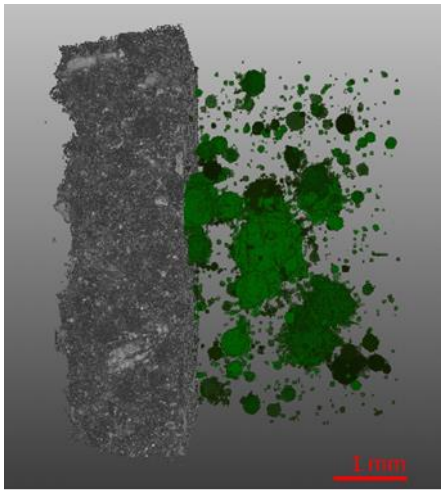

Fig.3.21 Representation of the voids which are clearly distinguishable in the scanned mortar sample.

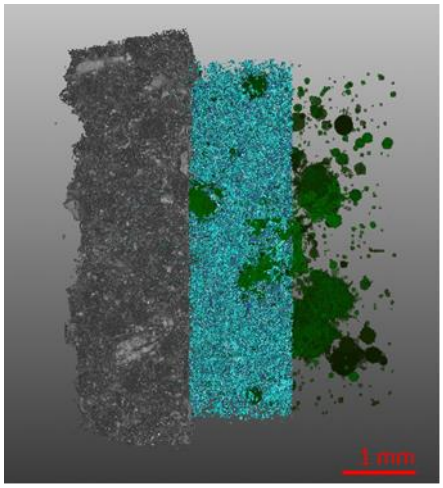

Fig.3.22 Representation of all voids, both clearly distinguishable voids and smaller assumed voids, in the scanned mortar sample.

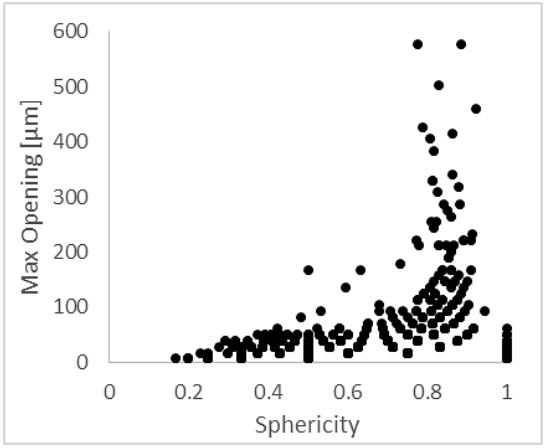

Fig.3.23 A graph of the maximal opening of the distinguishable voids versus their sphericity. The maximal opening is never lower than 5.39 µm, the smallest voxel size of the analysed volume.

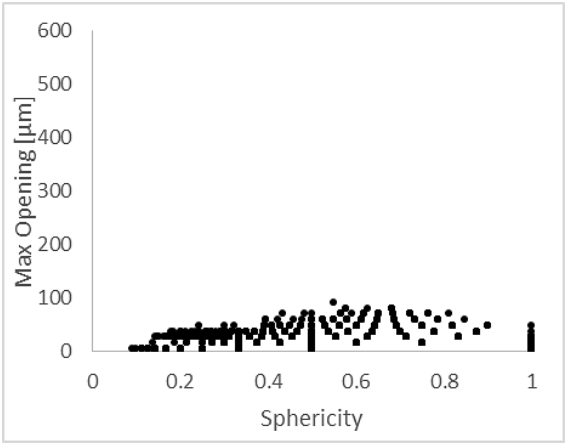

Fig.3.24 A graph of the maximal opening of the gradient filter distinguishable voids versus their sphericity. The maximal opening is never lower than 5.39 µm, the smallest voxel size of the analysed volume.

The voxel size of the images is 5.39 µm: only voids larger than 5.39 µm are thus quantified. Fig. 3.19 & 3.21 show that the large voids that are clearly distinguishable are mainly air-voids, with an ink-bottle shape; and that the largest bulk of these air-voids are interconnected. From collected data, it appears that these air-voids are mainly spherical, and that especially the largest pores are spherical (Fig. 3.23). They have an average maximum opening of 36 µm, and only 5 % of all pores have a maximum pore opening larger than 100 µm.

The smaller pores present in the paste, and detected with the gradient filter, are all very small and very numerous (Fig. 3.20 & 3.24). These smaller pores are on average very low to moderately spherical. There is also an increasing trend between sphericity and maximum opening, but it is less explicit. These smaller pores have in average 10 other pores as neighbour.

It appears this type of mortar touches the limits to detect the entire pore network with the used acquisition and reconstruction parameters as well as the sampling technique. The voxel size of the images does not allow to distinguish the difference between voids and hydrates/carbonates in the mortar paste that is supposed to provide an important part of the pore volume in the mortar.

3.2.3 Water permeability

The samples in this study were tested at 90 days of age, and samples were dried in an oven, at 40°C, in order to avoid hydration during the permeability test. Once the flow was stabilised, the permeability was calculated according to the pressure needed to maintain the flow rate stable. Since preliminary tests showed that dried samples broke in the water permeameter, the samples were saturated with water some 15 to 30 minutes before the test. The water sufficiently relieved pressure on the mortar's structure. In order to avoid erroneous results, one sample of each mix was tested and studied through visual observation on deformation and fissures before and after the test. Nearly all samples from the yellow and green mortar series NHL 3.5-4 and 3.5-6 and NHL 5-8 broke in the permeameter and results of these mixes are thus not taken into account in the discussion. The results represented in Fig. 3.25-3.27 indicate that the water permeability of all lime mortars is influenced by the W/B ratio. An increasing W/B seems to increase water permeability.

3.2.4 Nitrogen gas permeability

The gas permeability was measured through a GasPermEdu gas permeameter from Vinci Technologies. This steady-state permeameter was connected with a nitrogen source. The permeameter had no built-in back-pressure, but calculated the difference between the measured pressure and the measured atmospheric pressure. Permeability was calculated according to equation 3.6. The flow rates of six consecutive pressure levels were logged for each sample. Figures 3.26 & 3.28 show the nitrogen permeability of the

samples. The table with the permeability of each mortar is given in Appendix 3.1.

Fig.3.26 shows that NHL 5 mortars have a certain relationship between the gas permeability and their W/B ratio. An increase in W/B ratio decreases the gas permeability. A similar trend seems to be absent in the NHL 3.5 mortars. For the NHL 5 mortars, the larger permeability values were measured for the lower W/B (and therefore lower spread) mortars. The largest variation in permeability values was seen in the 160-mm-spread mortars.

Remark in Fig.3.28 that the highest permeability was attributed to the reference sand mortars, while the yellow-green mortars are more average, even though porosity was highest in the yellow-green mortars and lowest in the reference sand mortars.

The water permeability values of all lime mortars in this experimental campaign is higher than the gas permeability values. Loosveldt et al. (2002) and Lion et al.(2004) indicate in their study that their gas permeability measurements on cement mortars and limestone were also in general higher than their water permeability measurements, going from 1 to 2 orders of magnitude [16] to 50% higher [50]. Loosveldt et al. (2002) attribute this difference mainly to the chemical activity of water, leading to rehydration, dissolution, precipitation, water adsorption and only in a small level to a possible Klinkenberg effect [16].

As indicated by [30,55,56], for cement mortars, gas slippage is mainly due to small (1-10 nm) pores and low permeability. Water permeability measurements however already showed that this mortar does not have a low permeability, and the pore size distribution indicated the critical pore diameter can be situated around 1 µm. The samples in this study were prepared as such to avoid dehydration and consequent rehydration during water permeability testing. Nitrogen is an inert gas for lime mortars, while water is not an inert fluid, it might therefore be that the water was adsorbed and led to dissolution or precipitation.

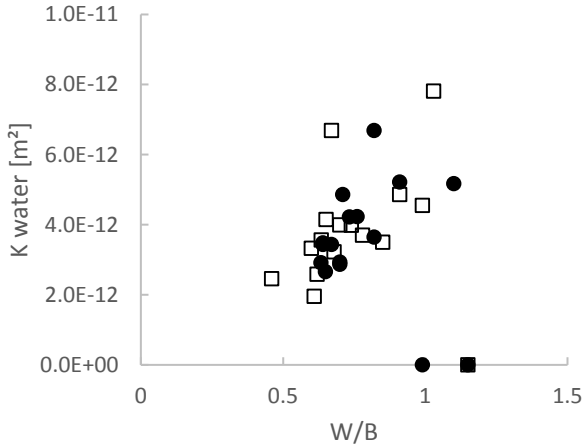

Fig.3.25 The water permeability shows an influence of the W/B ratio. S*quare* NHL 5 mortars, *circle* NHL 3.5 mortar.

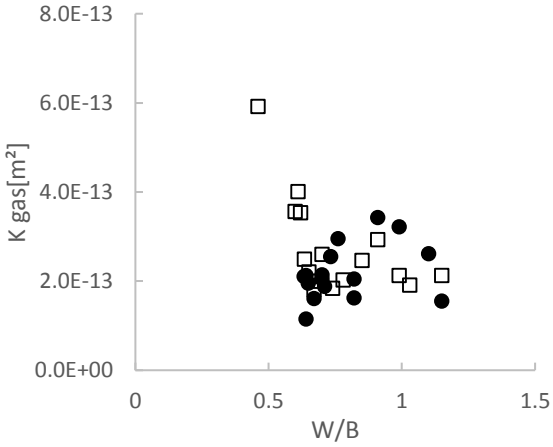

Fig.3.26 The gas permeability in function of the W/B ratio. *Square* NHL 5 mortars, *circle* NHL 3.5 mortar.

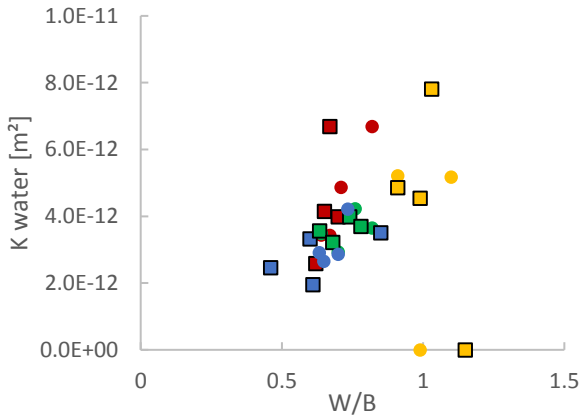

Fig.3.27 The water permeability in relation to the W/B ratio, subdivided based on the type of sand used. Normalised sand (*blue*), Rhin gros (*red*), Rhin fin (*green*), Yellow-green (*yellow*). NHL 5 mortars *(square)*, NHL 3.5 mortar *(circle)*.

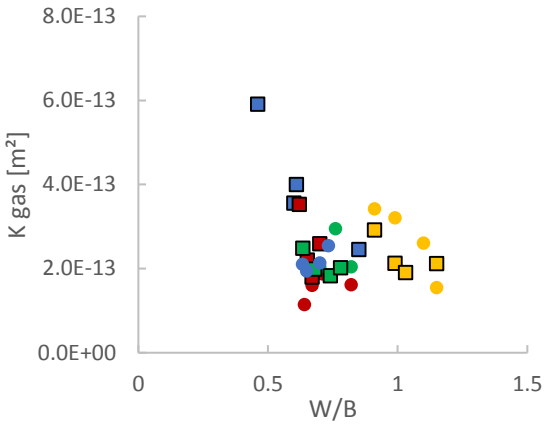

Fig.3.28 The gas permeability in relation to the W/B ratio, subdivided based on the type of sand used. Normalised sand (*blue*), Rhin gros (*red*), Rhin fin (*green*), Yellow-green (*yellow*). NHL 5 mortars *(square)*, NHL 3.5 mortar *(circle)*.

3.2.5 Discussion

The ultimate goal of this chapter is to find a method to estimate the permeability of lime mortars. Based on the experimental study, the grain size distribution of the various sands is thought to influence the final mortar properties. This might prove very useful for the estimation of permeability, since it is something which can be easily established from the sand itself. In this discussion therefore, the experimental study is looked at differently with the grain size distribution of the various sands in mind, leading to results which might be used for the estimation of permeability.

In chapter 2, Fig. 2.5 shows the grain size distribution of the sands used. The reference sand has almost no coarse grains, many medium-sized grains, and some smaller grains. The yellow and green sand have some coarse grains, and many finer grains. The Rhin fin is similar to the yellow sand, and the Rhin gros is the sand with the coarsest grains. If the information of the grain size distribution is compared with the mortars and their pore-scale properties, some elements come forward.

The open porosity of the experimental mortars is influenced by the grain size distribution of the used aggregates, when taking Fig. 3.29 & 3.30 into account. The coarsest grains play a role: even though the reference sand mortar has some fines, it has almost no coarse grains, which makes it has the lowest porosity. The yellow-green mortar has many fine grains, and has the highest porosity. The coarser grains and the smallest grains increase porosity (Fig. 3.29 & 3.30), consistent with results from [23]. Porosity increases when more v% of the aggregates has a smaller grain size. The coarser grains increase the pore volume through the creation of an ITZ zone (see section 3.3), while for the same spread or workability, a high amount of fine grains will increase the water demand, leading to more voids in general left by evaporated water.

Fig. 3.30 represents the measured open porosity and gas permeability of both NHL mortars. The mortars are represented per series of used aggregate. As one should expect, NHL 5 and NHL 3.5 mortars show a porosity increase when the relative amount of fines in the aggregate size distribution increases (see Fig. 3.29), which might be due to the higher demand in water. However, this increase in fine grains decreases the permeability of NHL 5 mortars, but seems to have no effect on the permeability of the NHL 3.5 mortars.

From these graphs, one could deduce an increase in mean grain diameter influences the first modal pore radius. A difference between the two types of NHL mortars is visible, although the difference is less obvious when considering the lowest data point of the NHL5 reference mortars as an outlier.

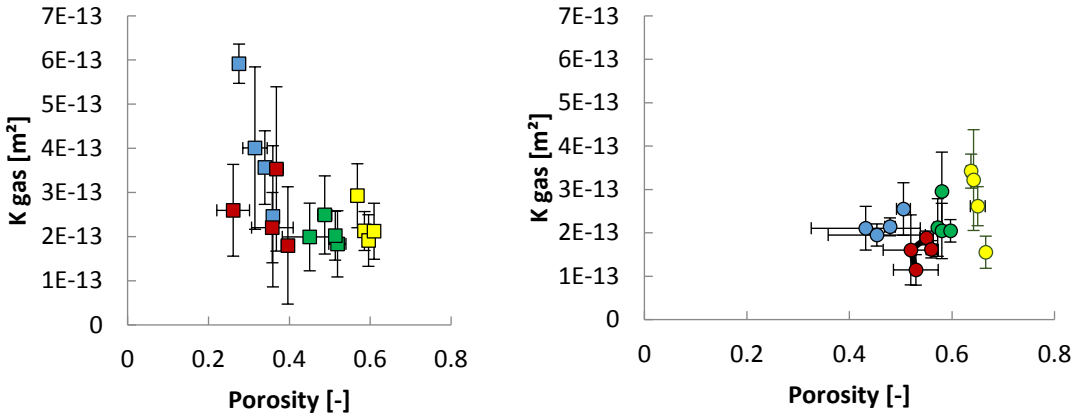

Fig.3.29 A-B. Measured open porosity in function of measured gas permeability from 32 different mortar types. Left graph representing NHL 5 mortars, the right graph represents NHL 3.5 mortars. Normalised sand (*blue*), Rhin gros (*red*), Rhin fin (*green*), Yellow-green (*yellow*).

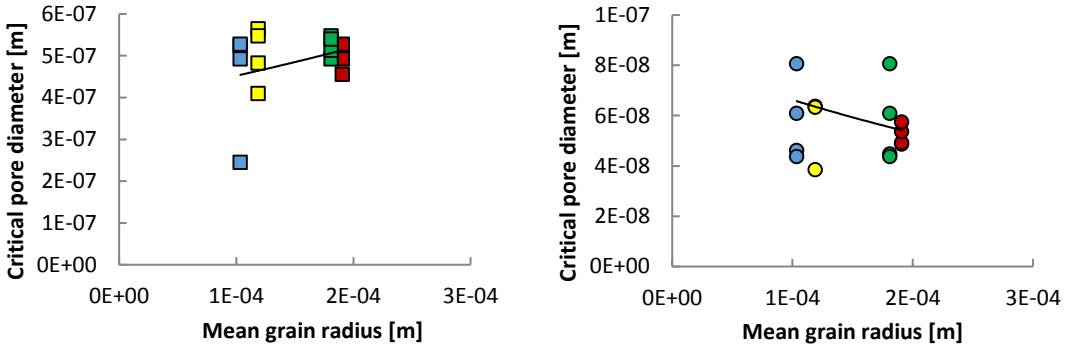

Fig. 3.30 A-B. Measured first modal pore diameter or critical pore diameter in function of the measured mean grain radius of each aggregate type. Left graph representing NHL 5 mortars, the right graph represents NHL 3.5 mortars. Normalised sand (*blue*), Rhin gros (*red*), Rhin fin (*green*), Yellow-green (*yellow*).

Another element in order to understand the permeability of the lime mortars, is the analysis of the pore network and pore size distribution from both MIP and micro-CT.

In this experimental campaign, the maximum opening of the larger, detectable voids was on average 36 µm, and only a negligible amount of these

voids were larger than 100 µm in micro-CT analysis. The MIP analysis however did not show pores larger than 20 µm, and it is therefore logic to assume that the larger, spherical voids which were seen in the micro-CT analysis, were considered as smaller pores in MIP due to the ink-bottle effect. It does however mean that these larger voids are connected to the smaller voids in the mortar.

The smaller voids detected by the MIP are not considered to be only small pore throats, but also finer pores situated around the larger voids and around the aggregate grains. Even though this type of porosity was 'unresolved', i.e. the exact size could not be determined by the standard method, an attempt was made to distinguish these voids in the micro-CT analysis. This method indicated numerous small voids, believed to be connected due to a general high porosity of samples. It could be that these voids take up the bulk of the volume detected by the MIP. This means that in the case of lime mortars, MIP appears to quantify small pores and pore throats.

MIP was measured with pressure increasing continuously, it might be that a pressurisation-depressurisation technique as proposed in [46] would give slightly different results. Assuming the ink-bottle effect could have been reduced to a minimum by using e.g. the technique proposed by Kaufmann (2009) or Zhou (2010), the MIP analysis would presumably show a curve slightly shifted to the larger pore sizes (e.g. to 10 µm) [14,46]. The large air voids effect is believed to be small, since the smaller voids are assumed to be very numerous, and the large voids are very few in proportion to the total amount of pores defined by the micro-CT analysis. More research should point out whether or not the effect is rather minimal as the micro-CT analysis suggests, or if it is still significant.

3.2.6 Conclusion

Not enough information concerning the pore-related properties of NHL mortars was available in literature. Therefore, this study intended to clarify the pore-related behaviour of NHL mortars made with various sands and water-binder ratios. Through the experimental campaign, certain connections between mortar components and properties could be made, and this campaign will thus certainly support the estimation method study which will be discussed further in this chapter. For example, in this experimental campaign on lime mortars, the influence of the binder type could be distinguished clearly in the porosity measurements. The influence of the various aggregates seemed to influence the critical pore diameter size. The W/B ratio also appears to influence the pore diameter, but is considered less important than the influence of the aggregates.

The characterisation of the lime mortars in this experimental campaign allowed a better understanding of NHL mortars at 90 days of age. The mortars show reasonably high porosity values, and are also more permeable than cement mortars. In comparison with properties from other lime types in other studies, e.g. in pore size distribution, the mortars presented in this study show

that NHL is a binder which can be used for restoration mortars: used together with well-dispersed sands, the permeability and pore size distribution are as such that they have characteristics fit for restoration purposes. This study indicates that variation in grain size and W/B ratio allows to 'play' in order to achieve the desired properties. Excess or deficit of water however decreases the quality of the mortars.

A more precise pore size distribution might be obtained using the pressurisation-depressurisation MIP technique or the nitrogen adsorption analysis in combination with MIP. If these tests could have been performed, the measured pore size distribution range is expected to be different: the number of large voids would increase and the total volume of large pores would likely outnumber the small pore volume. In addition, it might be that the amount of smaller pores would be levelled out, since it is likely to contain actual medium-ranged pores. Naturally, only when these tests have actually been performed, a more precise conclusion can be drawn concerning the real pore size distribution of these mortars.

No ethanol permeability tests were performed during this experimental campaign. This testing method on lime mortars would allow additional verification of the water permeability measurements, and would allow to determine, if another permeameter and different confining pressure is used, whether any fissures or hydration effects took place in the mortar sample during the water permeability tests.

3.3 Estimation of permeability

3.3.1 Introduction

Looking at estimation methods for permeability in cement research, two aspects keep reappearing: the porosity f and the square critical pore diameter D^2, the pore diameter at the maximum of the derivative of the MIP pore size distribution curve, as defined by [54]. Remembering from previous sections, the MIP is more representative for the pore throat size distribution: the diameter needed is thus the pore throat diameter, i.e. the diameter of the entrance of the pore. The porosity and square critical pore throat diameter are also often presented together as a product expression [19,57–59]. Other estimation equations from soil permeability research use the sand grain size diameter in combination with porosity [59]. The permeability of natural hydraulic lime (NHL) mortars is indeed influenced by open porosity and pore size as shown in previous experimental studies [19].

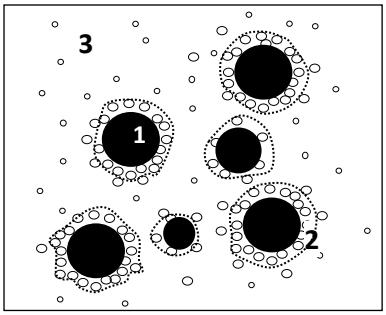

Fig. 3.31 Sketch of a mortar with aggregates (1), ITZ (2) and bulk paste (3). The porosity difference is represented with a different number of small circles. The dotted line represents the border of ITZ-bulk paste, a fictive border, since change in properties is more gradual. Figure after [60].

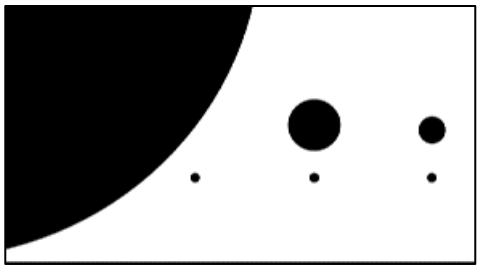

Fig. 3.32 Representation of the binder grain next to a grain of various size. The wall effect is more likely to occur to the binder particle encountering the largest grain (on the left) than to the binder particle on the right.

Basically, permeability is influenced by the pores present in the mortar. In order to be able to link the influence of mortar components to the voids and their structure in the mortar, some research into the theory concerning the formation of the voids in (lime) mortar is necessary. Looking at a mortar, it can be decomposed based on the (very) local variation in properties, and as such, a mortar consists generally of three parts: the aggregates (1), the Interfacial Transition Zone (ITZ) (2), and the bulk of the paste (3) (Fig. 3.31). By definition, both ITZ and bulk of the paste are a part of the paste. ITZ represents a transition zone of the paste enclosed around each aggregate particle, due to a combination of a local 'wall effect' and bleeding around the aggregates [60,61]. The wall effect is considered more important [61]. This wall effect exists, because binder particles are generally much smaller than aggregate particles, which make them behave as if the aggregate particle were a (local) wall (Fig. 3.32). The mean to smaller binder particles place themselves around the wall, decreasing the local binder density around the grains and increasing the porosity in this zone [62–64]. However, aggregate shape (sphericity and roundness) and size influence the ITZ thickness, as demonstrated by [65,66] and reported by [60,67]. Previous studies showed thus an ITZ variation from 10 to 30 or even up to 60 µm in cement mortars [60]. Following this logic, the 'wall effect' would be inexistent where aggregate particles are the same size as the binder particles [61].

3.3.2 Existing estimation methods

Permeability has frequently been the subject of estimation [54,58,68,69]. Permeability is influenced by external factors such as the pressure applied, the saturation degree and the temperature, but that the most important intrinsic factor are the pores present in the material: the pore throat size, the pore network and the total volume of pores all influence the movement of a fluid through the material [30].

Several models, such as the Katz-Thompson model, use mainly hardened mortar properties such as porosity and MIP pore throat size distribution [54,57,58,69]. These existing estimation methods present therefore two

handicaps for their use in lime mortar permeability estimation: they are not adapted for the specific composition of lime mortars and/or they use parameters that can only be measured when the mortar is already made such as in [57,70]. In the latter, permeability can simply be measured since lime mortars, with permeabilities between 1E-10 and 1E-18 m² (or between approximately 100 and 0.000001 D), have a much higher permeability than cement mortars [21]. Only the model proposed by Hamami (2009, 2012) uses solely information from the mortar components, such as the water-binder ratio and the density of the binder [19,71]. The model of Hamami was therefore given more attention in the section below.

3.3.2.1 Hamami model: description, verification and discussion

The Hamami model was developed to estimate the gas permeability of a cement paste, but was extended later to an estimation model for cement mortars [19,71]. It combines grain packing models and their (capillary) cylindrical pore networks with the cement binder properties. The input parameters are the specific density and the specific Blaine surface of the cement used, as well as the water-binder (W/B) ratio.

Assuming these cement grains are spherical, the grains are then placed in a cubic packing and the distance between the grains can be calculated, based on the specific density, the cement grain radius, and the W/B ratio (Fig. 3.33) [71].

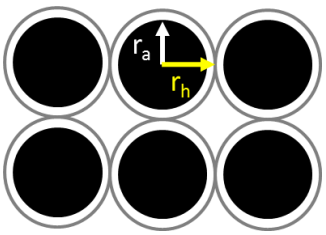

Figure 3.33 Sketch after Hamami (2009) of the cubic packing of anhydrous cement grain with radius r_a and hydrated cement grain with radius r_h. The pore network narrows due to hydration.

In order to validate this method, it was first tried on cement pastes and mortars, since the estimation was initially designed for cement mortars. Permeability for both paste and mortar was largely overestimated. Results are represented in Appendix 3.2.

The Hamami model points out the importance of the use of mortar component properties. Concerning the estimation, following elements can be remarked:

- The model assumes that porosity and permeability of the *paste* are equal to the porosity and permeability of a *paste fraction of the mortar* with the same W/B ratio. However, the properties of the *paste fraction of a mortar* are most likely influenced by the aggregates added to the mortar: the aggregate grains added might

alter the compaction of the paste fraction and therefore the pore network formed in the paste fraction. The estimation model assumes the *mortar* porosity to be equal to the *paste* porosity, while the experimental campaign indicated that the grain size distribution of the aggregates influences porosity (see section 3.2).

- The estimated mortar permeability was higher than the measured value. Additionally, when looking at the estimated permeability values for the cement pastes and mortars, they all lie in the range which can be measured by the permeameter used. Since in reality, their permeability could *not* be assessed, the permeability values are thus overestimated.

Conclusively, the model as such was judged to be insufficient to apply on lime mortars; more research should clarify whether the porosity and permeability of a pure cement paste is representative for the paste fraction of a cement mortar. Due to these conclusions, the method was not applied in this study.

3.3.3 Empirical based model for permeability estimation: Approach by Isebaert et al. (2016) [2]

Previous research indicated no readily adaptable estimation method, and this section therefore presents the study towards an empirically estimated permeability. This study deliberately uses an empirical approach based on mortar theory and on properties of lime mortar ingredients, since this is believed to be easier to understand and to apply by any future users. As such, an estimation is given for NHL mortar permeability at 90 days of age, based on the mixing ratios and relying on the properties of binder, sand and water used for the mortars as essential parameters. The presented method allows to estimate open porosity and two throat pore sizes of the lime mortar, which leads to the estimation of the mortar gas permeability with an equation similar to $f * D^2$. The developed estimation equations were then compared with experimental results and results available from literature.

In the introduction (3.3.1), permeability estimation methods presented in [19,57–59] showed that the product $f*D^2$, sometimes combined with a tortuosity factor, is a frequently-used method to estimate the permeability of cement mortars. Looking more closely at both mortar porosity and critical pore throat diameter, the square product of the critical pore throat diameter D^2 can be seen as the parameter determining the large range in which the mortar permeability is situated, while the porosity f defines the smaller variation in that larger range. For example, if the critical pore throat diameter of one of the studied lime mortars is 3E-7 m (or 0.3 µm), the square product of the diameter, 9E-14 m², would approximate the actual measured gas permeability in orders of magnitude. On its turn, the porosity in the product

lets the estimated permeability value shift higher or lower in the largely defined range.

Therefore, this philosophy was considered an approach that could also be used for the permeability estimation of lime mortars. It implies that permeability can be derived once porosity and pore size are estimated. However few studies present the estimation of porosity [71–73], and the estimation of mortar pore sizes is not frequently developed either [70]. These estimation methods that do exist for porosity and pore size indications are not solely based on elements which can be known before making the mortar, such as the water-binder ratio (W/B), binder-aggregate ratio (B/A), aggregate size distribution. Following sub-sections therefore propose a method based on the estimation methods from literature to estimate the pore size and porosity using mortar components.

3.3.3.1 Estimation of the mortar pore radius

As seen in section 3.2, the pore throat size range of lime mortars varies between 10 nm and 10 µm. Only a few techniques are able to measure the pore (throat) size distribution on this scale. As discussed before, MIP analysis is more significant for the pore throat size of a material, than of the actual pore size [30]. However, the pore throats have significant influence on the transport of fluids in these materials. Additionally, MIP gives information on the volume of pores present on a very wide range, from nanometre to micrometre-scale. Moreover, MIP is also used in other estimation equations to determine the critical pore (throat) size diameter [19,57,58]. It was therefore decided to use this technique with the aim to estimate the lime mortar pore throat diameter.

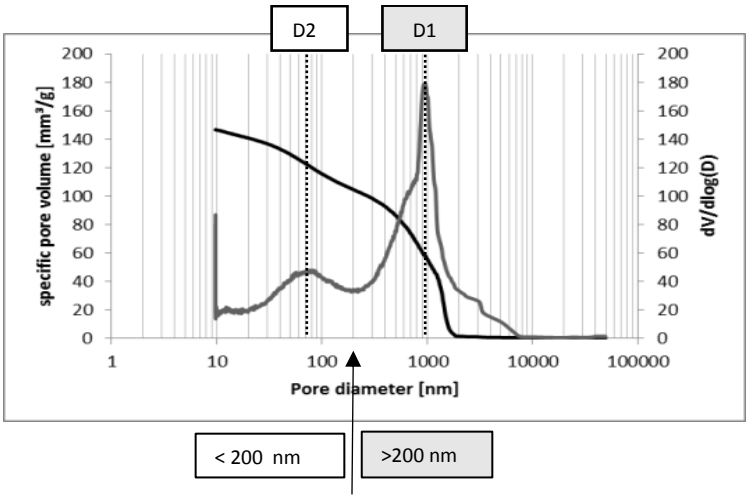

Fig.3.34. Example of the pore size distribution of a NHL mortar. The first modal pore throat size D1 lies above 200 nm, the second modal D2 below 200 nm.

In contrast to afore-mentioned estimation equations, not one critical pore throat diameter, but two can be used. The use of two pore sizes originated

from the fact that many lime mortars have a bimodal pore throat size distribution, as seen in the previous section of 3.2, in contrast to cement mortars and their mostly unimodal pore throat size distribution [13,21,28]. Moreover, it is a set-up which can also be used for mortars with a unimodal pore throat size distribution. The first critical pore throat diameter (D_1) is the modal pore throat diameter, where the incremental volume is largest, which for NHL mortars will be more representative for the larger pore region (>200 nm); the second critical pore throat diameter (D_2) is the second modal pore throat diameter which, in the case of NHL mortars, will mainly be representative for the smaller pore region (<200 nm) (Fig. 3.34).

Experimental results in [60] showed that the smaller pores (<200 nm) can be attributed to porosity in the bulk paste, while the larger pores (>200 nm) are attributed to the ITZ around the aggregates. Also [70] state the smallest pores are created during the hydration process and depend mainly on the type of binder, the W/B ratio and the age of the mortars. Larger pores (>200 nm) are found in the ITZ and the existence of ITZ is influenced by the aggregate size; it can therefore be assumed that the larger pores are influenced by the aggregates as well [60,70]. As stated in the introduction, the ITZ region is influenced not only by the wall effect of the aggregates, but also by the bleeding effect, or in other words, a locally increased W/B ratio [60,61]. Conclusively, both critical pore throat sizes are influenced by the water added to the mix.

For the D_1 diameter, the influence of both mean grain diameter of aggregates and the W/B are represented into one equation:

$$D_1 = 10^{-2}\, r_{mean\ grain} \sqrt{\frac{W}{B}} \qquad \text{(eq.3.11)}$$

As mentioned above, D_2 is influenced by the type of binder and by the W/B ratio [70]. The age of the mortars, as mentioned by [70], is neglected, since this estimation accounts for mortars at 90 days of age. Eq.3.12 could therefore be used for the estimation of the D_2. The type of binder is represented in the form of the mean lime grain size [m]. The lime grain size is used to represent the reactivity of the lime, since a smaller lime diameter implies a higher specific surface.

$$D_2 = 10^{-2} D_{50\ lime} \sqrt{\frac{W}{B}} \qquad \text{(eq.3.12)}$$

3.3.3.2 Estimation of open porosity

Assuming a mortar consists of an aggregate phase and a heterogeneous paste phase, subdivided into bulk paste and ITZ, the volume of the mortar can be defined as follows:

$$V_{mortar} = V_{agg} + V_{bulkpaste} + V_{ITZ} \qquad \text{(eq.3.13)}$$

Considering eq.3.13, the open porosity of the mortar, i.e. the pore volume accessible from the outside, can therefore be defined as the sum of the porosities of each phase multiplied by their volume, divided by the volume of the mortar:

$$f_{mortar} = \frac{f_{agg}V_{agg} + f_{bulkpaste}V_{bulkpaste} + f_{ITZ}V_{ITZ}}{V_{agg} + V_{bulkpaste} + V_{ITZ}} \quad \text{(eq.3.14)}$$

The volume of the aggregates V_{agg}, is a known element when making the mortar. Assuming that the aggregates have none to a negligible amount of voids, the aggregates have no porosity. Accordingly, porosity must all be present in the paste.

The volume of the ITZ and the bulk paste can be calculated according to the geometric model of Lu et al. (1992) [74]. Lu & Torquato (1992) made a model to calculate the nearest neighbour from a certain point with a statistical geometry of composites: for a packing of spherical particles that have any size distribution, an approximate equation for a quantity ev(s) was derived, where s is the thickness of a shell placed on every sphere. It is defined as the volume fraction of matrix material that is outside all the spheres and all the shells (Fig.3.31). The function was designed to take into account the overlap of shells. This method has already been used by Garboczi et al. (1997), Herve et al. (2010) and Caré et al. (2011) [60,62,69] to calculate the presence of grains and their ITZ volume: s becomes then the thickness of ITZ, T_{ITZ}. Following assumptions are made:

- The mortars only contain spherical aggregates.
- The aggregate grain size distribution is known as the number of particles per sieving class, which is not the volume of particles per sieving class. Methods for calculation are presented in [62,75].
- The grains are in an equilibrium arrangement, as if they would be suspended in a liquid and free to move.

The volume of ITZ is represented as follows (eq.3.15 from [62]):

$$V_{ITZ} = 1 - V_{agg} - ev(T_{ITZ}) \quad \text{(eq.3.15.1)}$$

$$V_{ITZ} = 1 - V_{agg} - \left[\left(1 - V_{agg}\right) exp\left(-\pi\, nr\left(c\, T_{ITZ} + d\, {T_{ITZ}}^2 + g\, {T_{ITZ}}^3\right)\right)\right] \quad \text{(eq.3.15.2)}$$

With:

$$c = \frac{4\, r_{mean}^2}{(1 - V_{agg})} \quad \text{(eq.3.15.3)}$$

$$d = \frac{4\, r_{mean}}{(1-V_{agg})} + \frac{12\, z\, r_{mean}^2}{(1-V_{agg})^2} \quad \text{(eq.3.15.4)}$$

$$g = \frac{4}{3(1-V_{agg})} + \frac{8\, z\, r_{mean}}{(1-V_{agg})^2} + \frac{16\, A\, z^2\, r_{mean}^2}{3(1-V_{agg})^3} \quad \text{(eq.3.15.5)}$$

$$z = \frac{2}{3}\, \pi\, nr\, r_{mean}^2 \quad \text{(eq.3.15.6)}$$

In which T_{ITZ} is the assumed thickness of the ITZ [m], and r_{mean} is the mean grain radius [m], based on nr, the number of particles as in [75].

This definition of ev(T_{ITZ}) means that it includes everything of the mortar, except the volume of the spheres V_{agg} and of the shells V_{ITZ}. Consequently, ev(T_{ITZ}) is $V_{bulk\ paste}$.

The calculations involve elements which are all known before making the mortar: the mean grain radius, the v% of aggregates, the number of grains per volume unit and the assumed thickness of the ITZ around each grain. The assumption of spherical aggregates can be omitted when using an adapted version [76,77] of the same calculation method by Lu et al. (1992) [74]. However, numerical simulation [76] demonstrated that the use of spherical aggregates in this calculation (eq.3.15) leads to an underestimation of the volume fraction of ITZ. Following [60,70], this would imply that real mortars might have a higher pore volume and larger pores than estimated. The estimated permeability will therefore most likely be an underestimation of the actual permeability.

Experimental results in 3.2 demonstrate the influence of water and the grain size distribution on the open porosity. This water is partially used for the hydraulic reaction that takes place in the binder particles (mainly belite and alite). NHL mortars also contain a significant amount of portlandite, which also uses water for hardening. However, the water that is not used for reaction is 'in excess' and solely serves for the workability of the mortar. This excess water will eventually diffuse and evaporate in the hardened mortar paste, leaving voids or pores in the matrix. This 'free' water, assumed to turn entirely into voids, is considered to be the total water minus the water used for reaction. The reaction water can be calculated using stoichiometric relations. The reaction for portlandite to calcite was taken from Moorehead (1986) and Cizer et al. (2002) (eq.3.16.1) [78,79]. The reaction for belite and alite to calcium silicate hydrate was taken from Moir (2003) (eq.3.18.2-3) [80]:

$$Ca(OH)_2 + CO_2 + H_2O \rightarrow CaCO_3 + 2H_2O + 74\ kJ/mol \quad \text{(eq.3.16.1)}$$

$$(CaO)_2\,(SiO_2) + 3.3\,H_2O \rightarrow (CaO)_{1.7}.(SiO_2).(H_2O)_3 + 0.3(Ca(OH)_2) \quad \text{(eq.3.16.2)}$$

$$(CaO)_3\,(SiO_2) + 4.3\,H_2O \rightarrow (CaO)_{1.7}.(SiO_2).(H_2O)_3 + 1.3(Ca(OH)_2) \quad \text{(eq.3.16.3)}$$

Both alite (C_2S) and belite (C_3S) reaction use water and generate portlandite (CH). This secondary generated portlandite was considered to react with available water (H). On its turn, portlandite not only uses water for reaction, but produces water as well. Considering mass of lime and water are known, the quantities of reaction water, produced portlandite and produced water can be calculated from stoichiometry.

$$\frac{m_{C2S}}{M_{C2S}}\, a\, M_H = m_{wC2S} \qquad \text{(eq.3.17.1)}$$

$$\frac{m_{C3S}}{M_{C3S}}\, b\, M_H = m_{wC3S} \qquad \text{(eq.3.17.2)}$$

$$\frac{m_{C2S}}{M_{C2S}}\, g\, M_{CH} = m_{CH2} \qquad \text{(eq.3.17.3)}$$

$$\frac{m_{C3S}}{M_{C3S}}\, h\, M_{CH} = m_{CH3} \qquad \text{(eq.3.17.4)}$$

$$\frac{m_{CH}+m_{CH_2}+m_{CH3}}{M_{CH}}\, c\, M_H = m_{wCH} \qquad \text{(eq.3.17.5)}$$

$$\frac{m_{CH}+m_{CH_2}+m_{CH3}}{M_{CH}}\, i\, M_H = m_{wprod} \qquad \text{(eq.3.17.6)}$$

With M molar mass [kg/mol], m mass [kg]; the constants represent the ratio of reactants needed to complete the reaction, e.g. a is ratio of water molecules needed to react with one alite molecule, and is thus 3.3/1 (eq. 3.16); a is the H:C2S reaction ratio; b the H:C3S reaction ratio; c the H:CH reaction ratio; g and h the CH:C2S and CH:C3S reaction ratio; i the H_{prod}:CH reaction ratio.

The volume fraction of water not used for binding is considered to transform into pores, and can be calculated according to:

$$V_{freewater} = \frac{V_w}{V_{tot}} - \frac{(m_{wCH}+m_{wC2S}+m_{wC3S}-m_{wprod})}{\rho_w V_{tot}} \qquad \text{(eq.3.18)}$$

With V_{tot} the sum of volume of binder, water and aggregates, and ρ_w the water density [kg/m³].

The ITZ porosity is defined by porosity induced by water in the mix ($f_{freewater}$), and by the aggregate size distribution. The ITZ porosity is explained by [61] as a local higher W/B ratio than in the bulk of the paste, where the W/B ratio would be smaller than the nominal one. However, this local W/B increase is dependent of the aggregate size, according to [81,82]: a larger aggregate usually results in a more porous ITZ, assumed to be because of enhanced micro-bleeding [82]. The correlation between aggregate grain size and added porosity due to the wall effect can then be represented as a $\sqrt{x}$ – function. This seems to be confirmed by the findings of [81] (Fig. 3.35).

Assuming that a local wall for a small lime particle will remain a wall no matter how large its size, it can be assumed that at a certain point a volume increase of coarser aggregate sizes will not be as significant for the porosity as a volume increase of the finest aggregate sizes. The estimation equation for the theoretical porosity in the ITZ region would then be:

$$f_{ITZ} = \sqrt{10^3 2 r_{mean}} + V_{freewater} \quad \text{(eq.3.19)}$$

with r_{mean} [m] the mean grain radius as defined in [75].

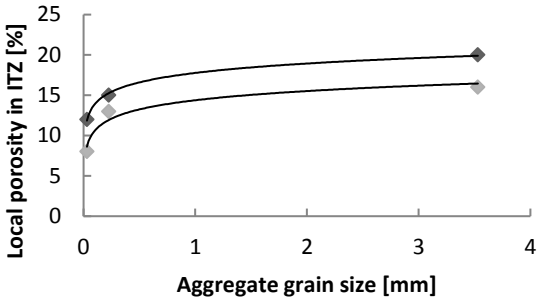

Fig. 3.35 The influence of the grain size on the local porosity in the (whole) ITZ region, with varying W/B ratio (black: 0.55, grey: 0.4). Values from [81].

The porosity of the bulk paste depends on the water in the paste. However, the voids added through water evaporation ($V_{freewater}$) only seem partially accountable for the porosity present in the bulk paste. It could be possible that not all reaction took place, and that more portlandite is present in the bulk paste matrix, making it less dense than if all portlandite would have reacted into calcite. The influence of the W/B ratio was therefore increased:

$$f_{bulkpaste} = \sqrt[3]{\frac{W}{B}} + V_{freewater} \quad \text{(eq.3.20)}$$

Every element of porosity has now been discussed; hence the estimation equation for open porosity is:

$$f_{mortar} = \frac{1}{V_{mortar}} \left[f_{agg}\, V_{agg} + \left(\sqrt[3]{\frac{W}{B}} + V_{freewater} \right) V_{bulkpaste} + \left(\sqrt{10^3 2 r_{mean}} + V_{freewater} \right) V_{ITZ} \right] \quad \text{(eq.3.21)}$$

3.3.3.4 Estimation of gas permeability

Gas permeability can be empirically estimated as the product of the porosity and the critical pore throat diameter [19,57–59]. Both elements, pore throat diameter and porosity, have been estimated in the previous sections and can therefore be used in eq.3.22:

$$k = f_{mortar}\, D_1 D_2 \qquad \text{(eq.3.22)}$$

Both parameters in this equation are set up as such that they implicitly also incorporate the pore connectivity, an approach also present in [54,58,75]. Some existing equations for cement mortars also introduce tortuosity factors [19,69], which are based on experimental correlations of the cement mortar campaign from each author respectively, and is used as a tool to improve the estimation. The use as such of a tortuosity factor will not be incorporated in this study, initially, the method will be compared with experimental studies without the tortuosity factor. If judged necessary future research might define what tortuosity factor should be incorporated and how it should be defined.

3.3.4 Confrontation of the estimation method to measured lime mortar permeability

The estimation methods were used to estimate the open porosity, the critical pore radius and the gas permeability. The estimation methods were validated using values from experimental campaigns found in literature and from the experimental W/B campaign of NHL 5 and NHL 3.5 mortars previously discussed in this chapter.

3.3.4.1 Confrontation of the estimation method using available literature

Table 3.2 shows the measured and estimated values for D_1 and porosity based on the information available in the articles. Although these articles presented no comparable water permeability estimation values, they gave other essential information for the estimation such as aggregate grain size distribution and the lime binder type. The mortars chosen for comparison were selected based on their recipe (i.e. sensible mortars, without extreme proportions) and on their curing conditions (60-80% RH, ± 20°C). Articles which presented water permeability values, gave insufficient information on the type or composition of the mortars tested, and could therefore not be used for validation.

The open porosity and pore size values of the mortars described in these studies were then compared with the estimated porosity and critical pore size according to the method presented in 3.3.3 (published in [2]). When comparing the estimated values with the values found in literature [23,27,83], the open porosity estimation, as well as the D_1 estimation for the critical pore radius, was rather satisfying for NHL 5 and NHL 3.5 mortars, but showed larger differences for CL90 and NHL 2 mortars. CL90 is a pure air hardening lime and NHL 2 is a feebly hydraulic lime, and so contains more portlandite than the NHL 5 or NHL 3.5 mortars. The larger difference in estimation might thus be explained by the fact that the estimation takes the hydraulic setting more into account than is actually reality for CL90 or NHL 2 mortars.

Table. 3.2 Validation of the estimation methods. Remark that some values had to be estimated based on the lime type description, the EN 459-1 norm, and of the used aggregate type, since (exact) data was not present. As means of control, density was adapted such that the total mortar v% would be 1. These estimated values are presented below (in grey), the aggregate grain size distribution and the specific mortar mixing ratios can be found in the cited articles.

	NHL 5 [27]	CL 90 [27]	NHL 5 [23]	NHL 3.5-Z [23]	NHL 5 [83]	NHL 2 [83]
$f_{measured}$ [-]	0.24	0.26	0.25	0.25	0.25	0.25
$f_{estimated}$ [-]	0.23	0.34	0.30	0.24	0.32	0.36
Δf [-]	<0.01	0.08	0.05	<0.01	0.07	0.10
D_c [m]	9.0E-7	1.5E-5	5.8E-7	3.0E-7	8.2E-7	8.8E-7
D_1 [m]	4.5E-7	6.2E-7	1.3E-6	3.8E-7	9.7E-7	9.7E-7
ΔD_1 [m]	4.5E-7	1.5E-5	6.9E-7	7.9E-8	1.5E-7	9.1E-8
D_2 [m]	8.9E-8	6.1E-8	7.4E-8	6.2E-8	9.4E-8	4.7E-8
$\mathbf{k_{estimated}}$ [m²]	9.4E-15	1.3E-14	2.8E-14	5.7E-14	2.9E-14	1.7E-14
ρ_{binder} [kg/m³]	700	450	700	700	700	550
ITZ [m]	3E-5	5E-5	3E-5	1E-5	3E-5	5E-5
D50 lime [m]	1E-5	5E-6	1E-5	8.3E-6	1E-5	5E-6
m% CH	0.30	0.90	0.27	0.40	0.23	0.45
m% C2S	0.15	0.01	0.25	0.20	0.20	0.15
m% C3S	0.10	0.00	0.05	0.05	0.10	0.00
ρ_{agg} [kg/m³]	1100	1100	1250	1250	1200	1200

3.3.4.2 Confrontation of the estimation method using experimental results

The same mortars were used as previously in section 3.2, the NHL 3.5 and NHL 5 W/B mortar series, to validate the estimation method. The precise estimated values for the various mortars can be found in Appendix 3.3.

In order to gain information about the presence of an ITZ zone around the aggregates in the lime mortars, backscattered electron (BSE) imaging was performed on two samples (Fig.3.36). Information concerning the analysis can be found in Appendix 3.3. The ITZ thickness of the NHL 5 mortar varied between 0.05-20 µm, (av. 15 µm). The ITZ thickness of the NHL 3.5 mortar varied between 0.05 - 80 µm (av. 37 µm). This is an indication of the ITZ thickness, since image analysis of a plane section only discusses one section of an aggregate and its ITZ [65,66].

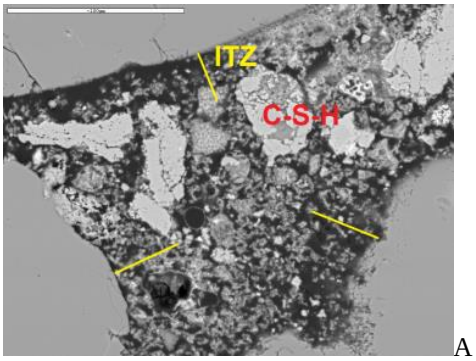

A

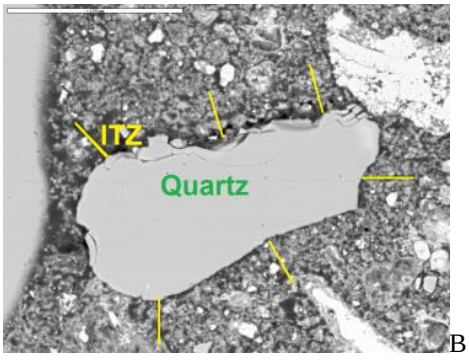

B

Fig. 3.36 A BSE image of NHL 3.5 & B BSE images of NHL 5 showing the zone considered ITZ region based on grey value plots around the aggregate. The white scale bar in the upper left corner represents 100 µm.

Not only the permeability estimation was compared with the measured values, but also pore size and porosity estimation were compared with their measured values:

- Pore size estimation

The measured values in function of the estimated D1 and D_2 are presented in Fig. 3.37. When comparing the estimated values for the two critical pore throat radii with the measured MIP critical pore radii, the estimated values are an overestimation of the measured values. The perpendicular distance between predicted and measured values for D_1 is on average 1 E-7 m for NHL 5 mortars, and 1.2E-7 m for NHL 3.5 mortars.

The perpendicular distance between predicted and measured values for D_2 is on average 2.1E-8 m for NHL 5 mortars, and 1.1E-8 m for NHL 3.5 mortars. Taking into account that only one MIP analysis was performed per mortar batch, a precise agreement between estimated and measured value should not be the direct intent. Until more MIP analyses are made on this type of mortars, the estimated pore throat sizes have to approach the measured values, which serve as indication.

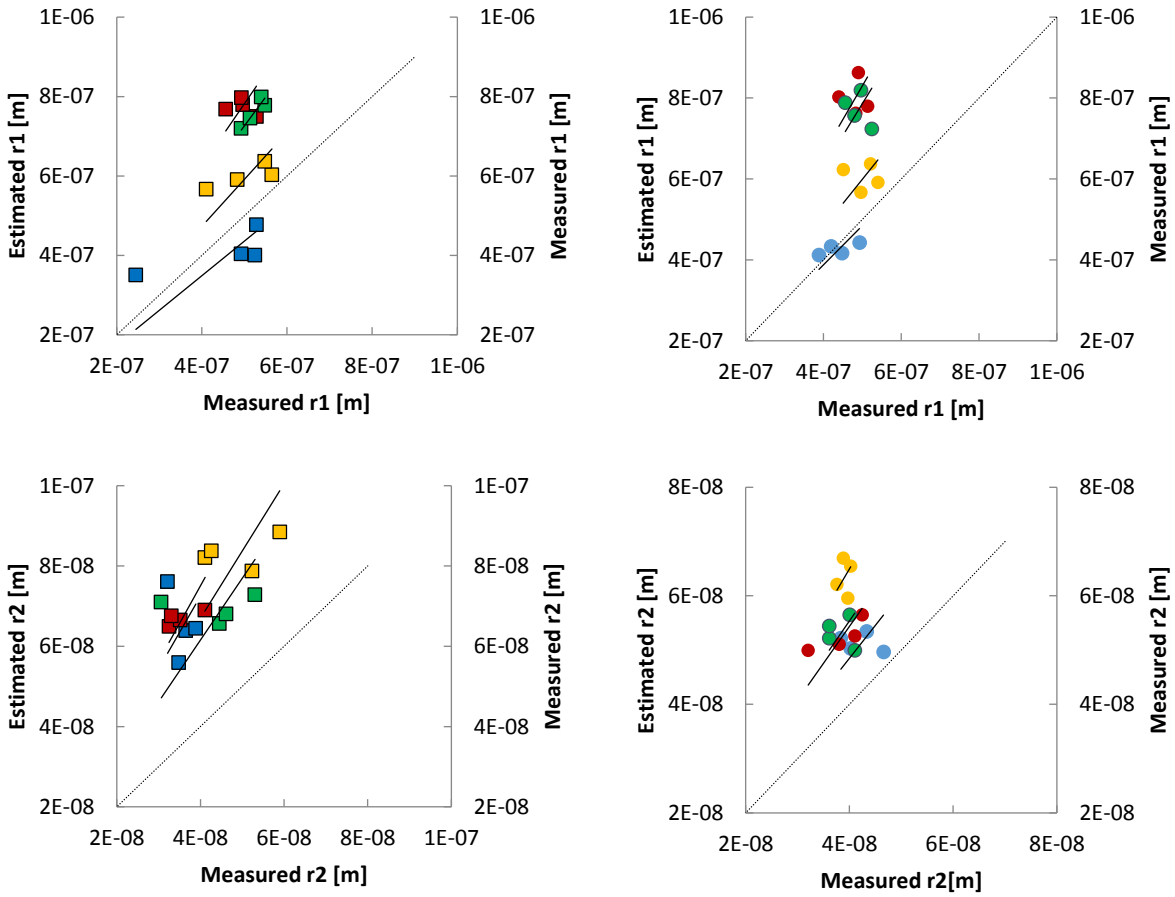

Fig. 3.37 The estimated r1 and r2 pore radii of the mortars in comparison with the measured MIP 1st and 2nd modal pore radius. In the left graph, NHL5 mortars, in the right graph NHL 3.5 mortars. Normalised sand (*blue*), Rhin gros (*red*), Rhin fin (*green*), Yellow-green (*yellow*).

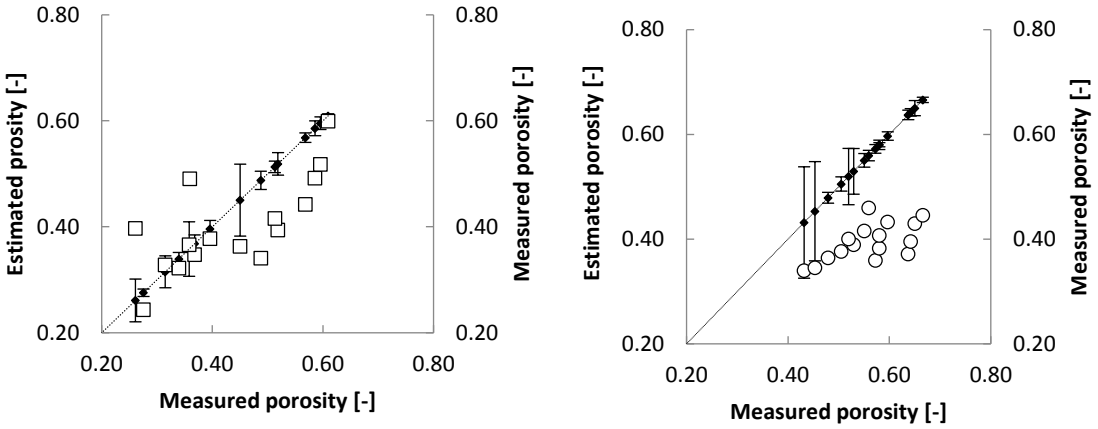

Fig. 3.38 The measured open porosity (*black*) and standard deviation as error bars, in comparison with the estimated porosity (*white*). The overestimated mortars are 180 mm spread mortars. NHL5 is represented in the left graph; the NHL3.5 is represented in the right graph.

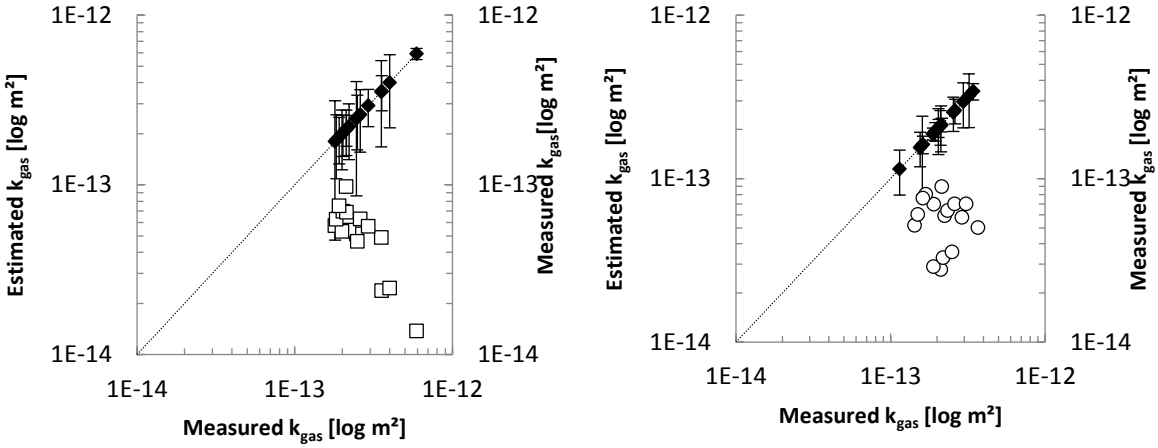

Fig. 3.39 The measured gas permeability (*black*) with standard deviation as error bars in comparison with the estimated permeability values (*white*). Left graph NHL 5 mortars, right graph NHL 3.5 mortars.

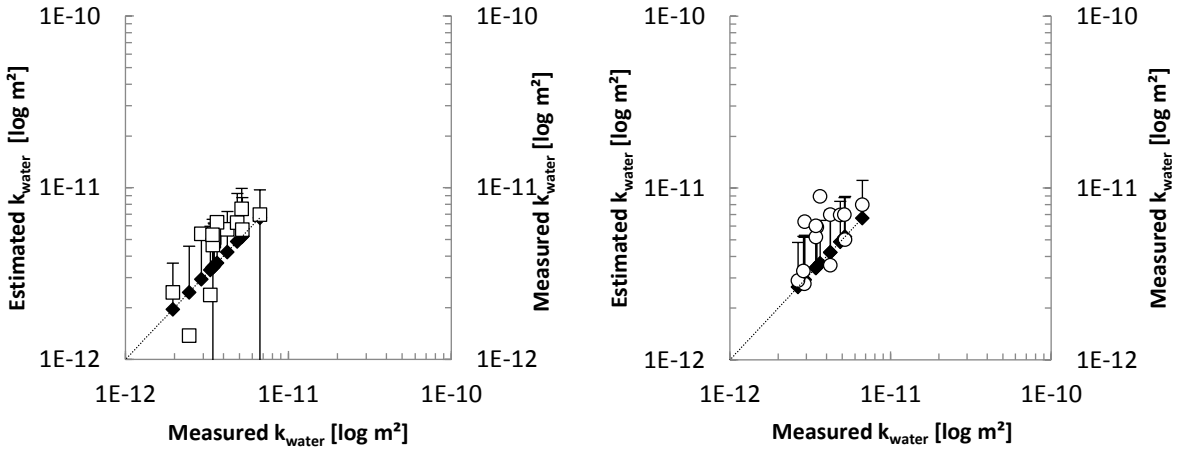

Fig. 3.40 The measured water permeability (*black*) with standard deviation as error bars in comparison with the estimated permeability values (*white*) and the error on the measurements. Left graph NHL 5 mortars, right graph NHL 3.5 mortars.

- Porosity estimation

Fig. 3.38 shows the results of the lime mortar estimation versus the actual measured open porosity values and their standard deviation values. Results are rather satisfying for NHL 5 mortars, but are underestimated for NHL 3.5 mortars. The estimation values for NHL 5 mortars have an average perpendicular distance of 2%, while the NHL 3.5 mortars have an average perpendicular distance of 12%. This large difference for NHL 3.5 mortars will thus certainly influence the permeability estimation.

- Permeability estimation

Results in Fig. 3.39 show that the estimated permeability has a similar order of magnitude as the measured gas permeability values. The average perpendicular distance between estimated and measured permeability of NHL 5 mortars is 1.4E-13 ±9.4E-14 m² (or 0.14 ±0.1 D). For NHL 3.5 mortars, the average perpendicular distance between estimated and measured permeability of NHL 3.5 mortars is 1.1E-13 ±4.7E-14 m² (or 0.12 ±0.05 D).

The gas and water permeability measured during this experimental campaign differed in two orders of magnitude (Fig. 3.39 & 3.40). The authors studied therefore whether this estimation method could approach the measured water permeability, taking this observation into account. The water permeability was estimated using eq.3.23 and compared with the measured values. In the NHL5 mortar series, the average perpendicular distance between estimated and measured values is 2.9E-12 ±2.4E-12 m² (2.95 ±2.4 D). In the NHL 3.5 mortar series the average perpendicular distance is 1.6E-12 ±1.5E-12 m² (1.64 ±1.6 D).

$$k = f_{mortar}\, D_1 D_2 \qquad \text{(eq.3.23)}$$

3.4 Discussion

The estimation of gas permeability was achieved by using the product of the estimated pore throat radii with the estimated open porosity. Experimental results showed both pore throat radii are influenced by the W/B ratio. The 1st modal pore throat radius is also influenced by the mean aggregate radius, in contrast to the 2nd modal pore throat radius, which is influenced by the mean lime diameter. Pore sizes were mostly overestimated, but more quantification of the lime mortar critical pore throat diameter is necessary in order to validate the estimation method.

Porosity was assumed to be inexistent in the aggregates, but considered present in all parts of the paste: in the interfacial transition zone and the bulk of the paste. In both bulk paste and ITZ, open porosity was both influenced by W/B ratio and the mean aggregate radius. This estimation of the porosity was based on observations from experimental results, additional SEM-EDS analysis and earlier estimation models from other studies or research fields.

Open porosity was mostly estimated with a difference of less than 10% for the mortars found in literature and the experimental NHL 5 mortars, while the porosity of the experimental NHL 3.5 mortars showed a much higher porosity than the estimated values.

However, since the pore diameters influence the large range of the gas permeability estimation, the combination of both elements to estimate permeability proved to approach, but underestimate, the gas permeability. It also proved that adding a factor of two orders of magnitude to the equation could estimate acceptably the water permeability. This agrees with results from other studies, namely that an estimation method where spherical aggregates are assumed would lead to an underestimation of the ITZ volume fraction, and might thus underestimate permeability [60,70].

The results from the confrontation with in literature reported values indicate that the porosity estimation becomes more erroneous when the hydraulic setting of the mortar becomes less and less important: the estimation for NHL5 mortar showed better approximation with reality than the estimation for CL90 mortar, with a binder hardening due to carbonation. Also the results from the experimental campaign and their permeability estimation seem to confirm this element.

3.5 Conclusion

The experimental campaign in this chapter focused on the pore-related properties and fluid migration capacity of NHL mortars at 90 days of age. The experimental campaign indicated some important elements for preparation of the samples as well as concerning the interpretation of results in every analysing technique. The campaign was found to be of added value in order to understand and quantify the influence of the mortar components on the final permeability of the mortars: the aggregate grain size distribution, the W/B ratio and the type of binder are important elements for the porosity, pore network and permeability of NHL mortars. A variation in these components would thus allow a variation in properties.

A model for the estimation of lime mortar permeability at 90 days of age is presented. The results of this estimation method are mainly influenced by the grain size distribution and the hydraulicity of the binder. This approach deliberately used an empirical approach using properties of the mortar components and was founded on conclusions from previously published studies and earlier estimation methods. The estimation method proposed here belongs to the same family of these earlier estimation methods (e.g. Katz et al. 1986, Herve et al. 2010, Hamami et al. 2012). Such an approach was chosen since it can be easily implemented into the algorithm and, in addition, no additional calculation time or other software would be required. The advantage of this model over another approach for the estimation of permeability, such as a pore network model for instance, is that the data it

requires to ‘feed’ and improve the model is less time-consuming (permeability, porosity and MIP versus SEM, (environmental) high-quality micro-CT and MIP). In addition, this approach also has as advantage that the estimations can be verified with straightforward testing techniques, either by permeameters or by the combination of porosity and MIP. The largest disadvantage of the method in comparison to more complete (pore network) models, is believed to be the accuracy. Models more representative of the actual pore network might lead to results closer to reality.

In comparison with other similar estimation methods for permeability of (cement) mortars, the quality of the estimation is similar: existing estimation methods have an error of 1-2 orders of magnitude (Katz et al. 1986), or around 40-60% (Wong 2012, Hamami 2009) [54,57,71,84].

The estimation method can thus be used for the estimation of the permeability. Nevertheless, more research will have to be performed, and more validation is necessary to verify its use for other types of mortars, made with a different lime binder and /or different aggregates. The limits of the model lie in its conception, since it is based on mortar theory and empirical results on (lime) mortars.

Still, it would be interesting to extend this model and incorporate the effect of age and curing conditions into the model. More research would then be needed concerning the various factors influencing the permeability with age, such as the combined hydration and carbonation reaction rate of (natural) hydraulic lime mortars and the effect of the relative humidity and temperature on the setting of the mortars.

Bibliography

[1] Isebaert A, De Boever W, Descamps F, Dils J, Dumon M, De Schutter G, et al. Pore-related properties of natural hydraulic lime mortars: an experimental study. Mater Struct 2015. doi:10.1617/s11527-015-0684-5.

[2] Isebaert A, De Boever W, Cnudde V, Van Parys L. An empirical method for the estimation of permeability in natural hydraulic lime mortars. Mater Struct 2016:1–13. doi:10.1617/s11527-016-0829-1.

[3] Isebaert A, Van Parys L, Descamps T, Renglet M, Cnudde V. First steps to computer-aided decision-making in repair mortar recipes: working on three fronts. 10th Int. Conf. Struct. Anal. Hist. Constr. Anamn. Diagnosis, Ther. Control., Leuven: KU Leuven; 2016.

[4] Moonen P, Carmeliet J. Understanding the Tensile Properties of Concrete. Underst. Tensile Prop. Concr., Elsevier; 2013, p. 98–122. doi:10.1533/9780857097538.1.98.

[5] Isebaert A, Van Parys L, Cnudde V. Composition and compatibility requirements of mineral repair mortars for stone - A review. Constr Build Mater 2014;59:39–50. doi:10.1016/j.conbuildmat.2014.02.020.

[6] Rodrigues JD, Grossi a. Indicators and ratings for the compatibility assessment of conservation actions. J Cult Herit 2007;8:32–43. doi:10.1016/j.culher.2006.04.007.

[7] Sasse HR, Snethlage R. Methods for the evaluation of stone conservation treatments. In: Baer NS, Snethlage R, editors. Dahlem Work. Sav. our Archit. heritage, Conserv.

Hist. stone Struct., John Wiley & Sons Ltd.; 1997, p. 223–43.
[8] Torney C, Forster AM, Szadurski EM. Specialist restoration mortars for stone elements: a comparison of the physical properties of two stone repair materials. Herit Sci 2014;2:1–12. doi:10.1186/2050-7445-2-1.
[9] Schueremans L, Van Balen K, Cizer O, Janssens E, Serré G, Elsen J, et al. Compatibility of repair mortars in restoration projects. 8th Int. Mason. Conf. 2010, Dresden: 2010, p. 785–94.
[10] Lawrence RM, Mays TJ, Rigby SP, Walker P, D'Ayala D. Effects of carbonation on the pore structure of non-hydraulic lime mortars. Cem Concr Res 2007;37:1059–69. doi:10.1016/j.cemconres.2007.04.011.
[11] Arandigoyen M, Alvarez JI. Pore structure and mechanical properties of cement–lime mortars. Cem Concr Res 2007;37:767–75. doi:10.1016/j.cemconres.2007.02.023.
[12] Cultrone G, Sebastián E, Huertas MO. Forced and natural carbonation of lime-based mortars with and without additives: Mineralogical and textural changes. Cem Concr Res 2005;35:2278–89. doi:10.1016/j.cemconres.2004.12.012.
[13] Arizzi A, Cultrone G. The difference in behaviour between calcitic and dolomitic lime mortars set under dry conditions: The relationship between textural and physical–mechanical properties. Cem Concr Res 2012;42:818–26. doi:10.1016/j.cemconres.2012.03.008.
[14] Kaufmann J, Loser R, Leemann A. Analysis of cement-bonded materials by multi-cycle mercury intrusion and nitrogen sorption. J Colloid Interface Sci 2009;336:730–7. doi:10.1016/j.jcis.2009.05.029.
[15] Baroghel-Bouny V. Water vapour sorption experiments on hardened cementitious materials. Cem Concr Res 2007;37:414–37. doi:10.1016/j.cemconres.2006.11.019.
[16] Loosveldt H, Lafhaj Z, Skoczylas F. Experimental study of gas and liquid permeability of a mortar. Cem Concr Res 2002;32:1357–63. doi:10.1016/S0008-8846(02)00793-7.
[17] McCarter W., Starrs G, Chrisp T. Electrical conductivity, diffusion, and permeability of Portland cement-based mortars. Cem Concr Res 2000;30:1395–400. doi:10.1016/S0008-8846(00)00281-7.
[18] Sanjuan M, Muñoz-Martialay R. Influence of the water/cement ratio on the air permeability of concrete. J Mater Sci 1996;31:2829–32.
[19] Hamami AA, Turcry P, Aït-Mokhtar A. Influence of mix proportions on microstructure and gas permeability of cement pastes and mortars. Cem Concr Res 2012;42:490–8. doi:10.1016/j.cemconres.2011.11.019.
[20] Mosquera M, Benítez D, Perry S. Pore structure in mortars applied on restoration: Effect on properties relevant to decay of granite buildings. Cem Concr Res 2002;32:1883–8.
[21] Mosquera MJ, Silva B, Prieto B, Ruiz-Herrera E. Addition of cement to lime-based mortars: Effect on pore structure and vapor transport. Cem Concr Res 2006;36:1635–42. doi:10.1016/j.cemconres.2004.10.041.
[22] Arizzi A, Viles H, Cultrone G. Experimental testing of the durability of lime-based mortars used for rendering historic buildings. Constr Build Mater 2012;28:807–18. doi:10.1016/j.conbuildmat.2011.10.059.
[23] Kalagri A, Karatasios I, Kilikoglou V. The effect of aggregate size and type of binder on microstructure and mechanical properties of NHL mortars. Constr Build Mater 2014;53:467–74. doi:10.1016/j.conbuildmat.2013.11.111.
[24] Pavía S, Toomey B. Influence of the aggregate quality on the physical properties of natural feebly-hydraulic lime mortars. Mater Struct 2007;41:559–69. doi:10.1617/s11527-007-9267-4.
[25] Cizer O, Balen K Van, Gemert D Van, Elsen J. Blended lime–cement mortars for conservation purposes: microstructure and strength development. 6th Int. Conf. Struct. Anal. Hist. Constr. Preserv. Saf. Significance, Bath: CRC Press, Taylor & Francis Group; 2008, p. vol2 : 965–72.
[26] Pavia S, Brennan O. Portland cement-lime mortars for conservation. 3rd Hist. Mortars Conf., vol. 1, Glasgow: 2013, p. 1–10.
[27] Silva BA, Ferreira Pinto AP, Gomes A. Influence of natural hydraulic lime content on

the properties of aerial lime-based mortars. Constr Build Mater 2014;72:208–18. doi:10.1016/j.conbuildmat.2014.09.010.

[28] Grilo J, Faria P, Veiga R, Santos Silva A, Silva V, Velosa A. New natural hydraulic lime mortars – Physical and microstructural properties in different curing conditions. Constr Build Mater 2014;54:378–84. doi:10.1016/j.conbuildmat.2013.12.078.

[29] Bianco N, Calia A, Denotarpietro G, Negro P. Hydraulic mortar and problems related to the suitability for restoration 1. Period Di Mineral 2013;82:529–42. doi:10.2451/2013PM0031.

[30] Hall C, Hoff WD. Water Transport in Brick, Stone and Concrete: 2nd Edition 2011.

[31] Sahimi M. Flow and Transport in Porous Media and Fractured Rock: From Classical Methods to Modern Approaches. 2012.

[32] Carmeliet J, Roels S. Determination of the Moisture Capacity of Porous Building Materials. J Build Phys 2002;25:209–37. doi:10.1106/109719602022835.

[33] Bultreys T, De Boever W, Cnudde V. Imaging and image-based fluid transport modeling at the pore scale in geological materials: A practical introduction to the current state-of-the-art. Earth-Science Rev 2016;Accepted:93–128. doi:10.1016/j.earscirev.2016.02.001.

[34] Cnudde V, Boone MN. High-resolution X-ray computed tomography in geosciences: A review of the current technology and applications. Earth-Science Rev 2013;123:1–17. doi:10.1016/j.earscirev.2013.04.003.

[35] Giesche H. Mercury Porosimetry: A General (Practical) Overview. Part Part Syst Charact 2006;23:9–19. doi:10.1002/ppsc.200601009.

[36] Arandigoyen M, Alvarez JI. Blended pastes of cement and lime: Pore structure and capillary porosity. Appl Surf Sci 2006;252:8077–85. doi:10.1016/j.apsusc.2005.10.019.

[37] Mattana AJ, Pereira E, do Rocio de Mello Maron da Costa M. Evaluation of porosity in mortar by X-ray microtomography (micro-CT) as an additional tool fro mercury intrusion porosimetry. Iberoam J Appl Comput 2014;4:18–28.

[38] Lanzón M, Cnudde V, de Kock T, Dewanckele J. X-ray microtomography (μ-CT) to evaluate microstructure of mortars containing low density additions. Cem Concr Compos 2012;34:993–1000. doi:10.1016/j.cemconcomp.2012.06.011.

[39] Clementi E, Raimondi DL, Reinhardt WP. Atomic Screening Constants from SCF Functions. II. Atoms with 37 to 86 Electrons. J Chem Phys 1967;47:1300–7. doi:10.1063/1.1712084.

[40] Cnudde V. Exploring the potential of X-ray tomography as a new non-destructive research tool in conservation studies of natural building stones. Ghent University. Faculty of Sciences, 2005.

[41] Vlassenbroeck J, Dierick M, Masschaele B, Cnudde V, Van Hoorebeke L, Jacobs P. Software tools for quantification of X-ray microtomography at the UGCT. Nucl Instruments Methods Phys Res Sect A Accel Spectrometers, Detect Assoc Equip 2007;580:442–5. doi:10.1016/j.nima.2007.05.073.

[42] Brabant L, Vlassenbroeck J, De Witte Y, Cnudde V, Boone MN, Dewanckele J, et al. Three-dimensional analysis of high-resolution X-ray computed tomography data with Morpho+. Microsc Microanal 2011;17:252–63. doi:10.1017/S1431927610094389.

[43] Masschaele B, Dierick M, Loo D Van, Boone MN, Brabant L, Pauwels E, et al. HECTOR: A 240kV micro-CT setup optimized for research. J Phys Conf Ser 2013;463:12012. doi:10.1088/1742-6596/463/1/012012.

[44] Washburn EW. The Dynamics of Capillary Flow. Phys Rev 1921;17:273–83. doi:10.1103/PhysRev.17.273.

[45] Diamond S. Mercury porosimetry: an inappropriate method for the measurement of pore size distributions in cement-based materials. Cem Concr Res 2000;30:1517–25.

[46] Zhou J, Ye G, van Breugel K. Characterization of pore structure in cement-based materials using pressurization–depressurization cycling mercury intrusion porosimetry (PDC-MIP). Cem Concr Res 2010;40:1120–8. doi:10.1016/j.cemconres.2010.02.011.

[47] Stefanidou M. Methods for porosity measurement in lime-based mortars. Constr Build Mater 2010;24:2572–8. doi:10.1016/j.conbuildmat.2010.05.019.

[48] Cnudde V, Cwirzen a., Masschaele B, Jacobs PJS. Porosity and microstructure characterization of building stones and concretes. Eng Geol 2009;103:76–83. doi:10.1016/j.enggeo.2008.06.014.
[49] Filomena CM, Hornung J, Stollhofen H. Assessing accuracy of gas-driven permeability measurements: a comparative study of diverse Hassler-cell and probe permeameter devices. Solid Earth 2014;5:1–11. doi:10.5194/se-5-1-2014.
[50] Lion M, Skoczylas F, Ledésert B. Determination of the main hydraulic and poro-elastic properties of a limestone from Bourgogne, France. Int J Rock Mech Min Sci 2004;41:915–25. doi:10.1016/j.ijrmms.2004.02.005.
[51] Janssen H, Derluyn H, Carmeliet J. Moisture transfer through mortar joints: A sharp-front analysis. Cem Concr Res 2012;42:1105–12. doi:10.1016/j.cemconres.2012.05.004.
[52] Ramézani H, Jeong J. Environmentally motivated modeling of hygro-thermally induced stresses in the layered limestone masonry structures: Physical motivation and numerical modeling. vol. 220. 2011. doi:10.1007/s00707-011-0463-5.
[53] Derluyn H, Janssen H, Carmeliet J. Influence of the nature of interfaces on the capillary transport in layered materials. Constr Build Mater 2011;25:3685–93. doi:10.1016/j.conbuildmat.2011.03.063.
[54] Nokken MR, Hooton RD. Using pore parameters to estimate permeability or conductivity of concrete. Mater Struct 2007;41:1–16. doi:10.1617/s11527-006-9212-y.
[55] Hooman K, Tamayol A, Dahari M, Safaei MR, Togun H, Sadri R. A theoretical model to predict gas permeability for slip flow through a porous medium. Appl Therm Eng 2014;70:71–6. doi:10.1016/j.applthermaleng.2014.04.071.
[56] Zheng Q, Yu B, Duan Y, Fang Q. A fractal model for gas slippage factor in porous media in the slip flow regime. Chem Eng Sci 2013;87:209–15. doi:10.1016/j.ces.2012.10.019.
[57] Katz AJ, Thompson AH. Quantitative prediction of permeability in porous rock. Phys Rev B Condens Matter 1986;34:2–4.
[58] Glover PW, Walker E. Grain-size to effective pore-size transformation derived from electrokinetic theory. Geophysics 2009;74:E17–29. doi:10.1190/1.3033217.
[59] Nelson P. Permeability-porosity relationships in sedimentary rocks. Log Anal 1994:38–62.
[60] Herve E, Care S, Seguin JP. Influence of the porosity gradient in cement paste matrix on the mechanical behavior of mortar. Cem Concr Res 2010;40:1060–71. doi:10.1016/j.cemconres.2010.02.010.
[61] Bentur A, Alexander MG. A review of the work of the RILEM TC 159-ETC: Engineering of the interfacial transition zone in cementitious composites. Mater Struct 2000;33:82–7. doi:10.1007/BF02484160.
[62] Garboczi EJ, Bentz DP. Analytical formulas for interfacial transition zone properties. Adv Cem Based Mater 1997;6:99–108. doi:10.1016/S1065-7355(97)90016-X.
[63] Caré S. Influence of aggregates on chloride diffusion coefficient into mortar. Cem Concr Res 2003;33:1021–8. doi:10.1016/S0008-8846(03)00009-7.
[64] Liu L, Shen D, Chen H, Xu W. Aggregate shape effect on the diffusivity of mortar: A 3D numerical investigation by random packing models of ellipsoidal particles and of convex polyhedral particles. Comput Struct 2014;144:40–51. doi:10.1016/j.compstruc.2014.07.022.
[65] Chen H, Sun W, Stroeven P, Sluys LJ. Overestimation of the interface thickness around convex-shaped grain by sectional analysis. Acta Mater 2007;55:3943–9. doi:10.1016/j.actamat.2007.03.009.
[66] Chen H, Zhu Z, Liu L, Sun W, Miao C. Aggregate shape effect on the overestimation of ITZ thickness: Quantitative analysis of Platonic particles. Powder Technol 2016;289:1–17. doi:10.1016/j.powtec.2015.11.036.
[67] Garboczi E, Bentz D. Computer simulation and percolation theory applied to concrete. Annu Rev Comput Phys VII 1999.
[68] Berg R. Method for determining permeability from reservoir rock properties. Trans - Gulf Coast Assoc Geol Soc 1970.

[69] Care S, Derkx F. Determination of relevant parameters influencing gas permeability of mortars. Constr Build Mater 2011;25:1248–56. doi:10.1016/j.conbuildmat.2010.09.028.
[70] Gong F, Zhang D, Sicat E, Ueda T. Empirical Estimation of Pore Size Distribution in Cement, Mortar, and Concrete. J Mater Civ Eng 2014;26:04014023. doi:10.1061/(ASCE)MT.1943-5533.0000945.
[71] Hamami AA. Vers une prédiction de la perméabilité au gaz à partir de la composition des matériaux cimentaires. Université de la Rochelle, 2009.
[72] Lafhaj Z, Goueygou M, Djerbi A, Kaczmarek M. Correlation between porosity, permeability and ultrasonic parameters of mortar with variable water/cement ratio and water content. Cem Concr Res 2006;36:625–33. doi:10.1016/j.cemconres.2005.11.009.
[73] Hernández MG, Anaya JJ, Ullate LG, Cegarra M, Sanchez T. Application of a micromechanical model of three phases to estimating the porosity of mortar by ultrasound. Cem Concr Res 2006;36:617–24. doi:10.1016/j.cemconres.2004.07.018.
[74] Lu B, Torquato S. Nearest-surface distribution functions for polydispersed particle systems. Phys Rev A 1992;45:5530–44.
[75] Garboczi EJ, Bentz DP. Multiscale Analytical/Numerical Theory of the Diffusivity of Concrete. Adv Cem Based Mater 1998;8:77–88. doi:10.1016/S1065-7355(98)00010-8.
[76] Xu W, Chen W, Chen H. Modeling of soft interfacial volume fraction in composite materials with complex convex particles. J Chem Phys 2014;140. doi:http://dx.doi.org/10.1063/1.4861664.
[77] Xu W, Chen H, Chen W, Jiang L. Prediction of transport behaviors of particulate composites considering microstructures of soft interfacial layers around ellipsoidal aggregate particles. Soft Matter 2014;10:627–38. doi:10.1039/c3sm52718b.
[78] Cizer Ö, Van Balen K, Elsen J, Van Gemert D. Real-time investigation of reaction rate and mineral phase modifications of lime carbonation. Constr Build Mater 2012;35:741–51. doi:10.1016/j.conbuildmat.2012.04.036.
[79] Moorehead DR. Cementation by the carbonation of hydrated lime. Cem Concr Res 1986;16:700–8. doi:10.1016/0008-8846(86)90044-X.
[80] Moir G. Advanced Concrete Technology. In: Newman J, Seng Choo B, editors. Adv. Concr. Technol., Oxford: Elsevier; 2003, p. 3–45. doi:10.1016/B978-075065686-3/50277-9.
[81] Elsharief A, Cohen MD, Olek J. Influence of aggregate size, water cement ratio and age on the microstructure of the interfacial transition zone. Cem Concr Res 2003;33:1837–49. doi:10.1016/S0008-8846(03)00205-9.
[82] Xie Y, Corr DJ, Jin F, Zhou H, Shah SP. Experimental study of the interfacial transition zone (ITZ) of model rock-filled concrete (RFC). Cem Concr Compos 2015;55:223–31. doi:10.1016/j.cemconcomp.2014.09.002.
[83] Winnefeld F, Böttger KG. How clayey fines in aggregates influence the properties of lime mortars. Mater Struct 2006;39:433–43. doi:10.1617/s11527-005-9023-6.
[84] Wong HS, Zimmerman RW, Buenfeld NR. Estimating the permeability of cement pastes and mortars using image analysis and effective medium theory. Cem Concr Res 2012;42:476–83. doi:10.1016/j.cemconres.2011.11.018.

Chapter 4 Compatibility in colour

Next to compatibility in fluid migration, which is important for the durability and preservation of both mortar and stone, the repair mortar should also be compatible in colour. As discussed in chapter 1, the colour of a repair mortar is an important factor for compatibility. Even though it does not influence the durability of the intervention *per se*, it influences the choice made for one repair mortar or another.

This chapter encompasses first a short discussion on colour principles necessary for the understanding of the colour of mortars, and is followed by a description (and discussion) of the measuring set-up used. The aim of the chapter was to find a colour estimation method for lime mortars when cured at three months of age. This estimation method is discussed in the last part of the chapter.

The discussion concerning existing estimation methods in this chapter is based on a peer-reviewed article for the proceedings of the Structural Analysis of Historical Constructions conference [1]. Elements from the estimation method have been researched during a Master thesis at Mons University by Dessoy (2015), which was co-supervised by the author [2].

4.1 Colour theory for mortars

Mortars are matte, which means that the reflection of incident light from the mortars surface is diffuse: the light is scattered in all directions. The colour of the mortar is then 'produced from the internal absorption and scattering of the incident light in the material' [3]. However, the colour of a mortar does not only depend on the mortar alone. The incident light on the mortar also plays a role, by emitting for example only a part of the visible spectrum. The observer himself also plays a determining role; his perception of the mortar's colour can only be made by analysing the received light. As such, colour depends on the mortar, the incident light and the observer's eye.

4.1.1 The visible spectrum and its perception

The visual light that humans can detect, is created by electromagnetic waves with a wavelength between 380nm and 780 nm (Fig.4.1). Perceived light can be monochromatic, only representing one specific wavelength, or

can be polychromatic, composed of multiple wavelengths. The emitted light, such as sunlight, is often polychromatic.

The spectral luminous efficiency is the luminous flux perceived by the eye and the strength of the electromagnetic wave received. The human eye has the ability to perceive the entire visible spectrum, but due to the colour receptors present in the eye, it is more sensitive for colours situated at about 555 nm (yellow-green) [4]. The perceived colour not only depends on the physical properties of the electromagnetic waves, but also on the physiologic properties of the vision the specific observer has, such as the (well-)functioning of the receptors, nerves and fibres, and also the memory associations made with a certain colour [4,5]. Perceiving colour is thus subjective.

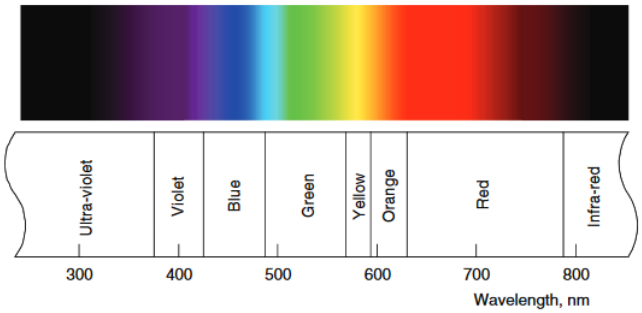

Fig. 4.1. The wavelengths of radiation, their names and their colour, from [5].

Historically, man has since long been trying to express and measure colour in some way or another. One of the problems is that colour is perceived by the human eye, an instrument which is very well developed, but as discussed above, also subjective. Various studies on colour, such as the research by Munsell for example, find that three independent variables are necessary to compose one unique colour [3]. The most logical three dimensions are called lightness, hue and saturation (Fig.4.2). These principles are defined here, from [5]:

- *Lightness* is used to describe the visual perception according to which an area appears to exhibit more or less light, relative to that of a similarly illuminated white. Lightness is a relative value.
- *Hue* is the attribute of a visual perception according to which an area appears to be similar to one, or to proportions of two of the perceived colours red, yellow, green and blue.
- *Saturation* is the colourfulness of an area judged in proportion to its lightness.

The distinction between lightness and saturation is difficult to make, especially when at minimal or maximal lightness, where colours tend to be desaturated. The hue and saturation are therefore often grouped together into chromaticity attributed to a certain level of lightness.

4.1.2 Colour representation & colour difference

Previous theories concerning colour, such as the Munsell theory, showed that nearly all colours can be reproduced by mixing, in appropriate proportions, three primary lights of a very saturated red, green and blue [4]. Colorimetry systems can be subdivided into three different types [3]:

- A perceptual system, based on visual appearance, with the dimensions of hue, saturation and lightness
- A psychophysical system, based on *additive* colour mixing of three primary colours
- A physical system, based on *subtractive* colorant mixing of three primary colorants

Additive laws govern mixes of light: the resulting flow contains the spectral contribution of each member and becomes more and more powerful so that the chromaticity tends to white (Fig.4.3). Liquid paint mixes on the other hand are governed by *subtractive* ones: the resulting product reflects the spectral part of incident light that no member has absorbed and becomes less and less powerful so that the chromaticity tends to black (Fig.4.3). For example, mixing yellow and blue watercolours will result in green, simply because the watercolour perceived as yellow absorbs the violet and blue regions of the spectrum, and the watercolour perceived as blue, the orange and red regions (Fig.4.1). Only green is not *subtracted* from the spectrum and is left to be reflected. If, on the contrary, little dots or squares of yellow and blue paint would be painted neatly next to each other, and the observer would stand far enough, the observer would see the additive mixture of light, resulting from the blue and yellow squares. The resulting colour perceived is lighter than any of the two colours, and, in this example, would be a more neutral grey colour (Fig.4.3) [3].

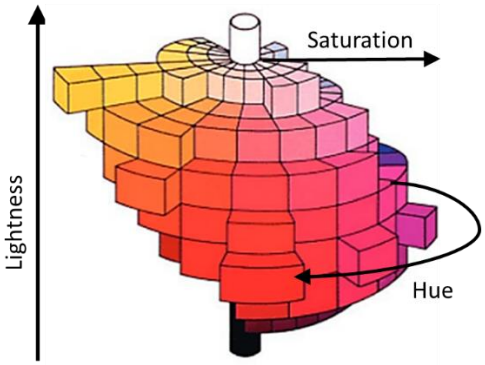

Fig. 4.2 Munsell colour system. Lightness is called ‘value’ in this system. In the Munsell system, saturation is also subject to the comparison with a similar illuminated white area, and is called chroma. Both terms are closely related [3]. Adapted from Konica Minolta.

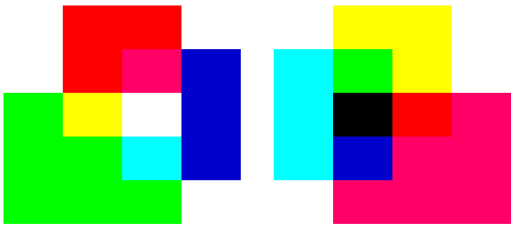

Fig. 4.3 The additive (left) versus subtractive (right) colour theory.

The additive mixing of colours is best described according to the laws of Grassmann:

- Principle of trichromacy

Any colour can be reproduced by a mixture of three coloured lights independent of each other. Three colours are independent of each other when neither of them can be reproduced by a mixture of the two others.

- Linear law of additivity

A colour can be reproduced by the sum of primary colours that compose the additive mixture. The luminance of an additive mixture is the sum of the three primary colours needed to produce the mixture.

- Proportionality principle

If the intensity of a colour varies, the three primary components should be adapted in the same proportions.

Several representation methods proposed by the International Commission on Illumination (CIE) are a practical way of representing the spectral reflection of an object. The CIE put a psychophysical system forward in 1931 for a CIE 2° standard observer, based on additive colour mixing [3]. This 1931 system was initially proposed by Mac Adam, and starts from the fact that colour is essentially the product of three elements: (a) the spectral distribution of the object, (b) the spectral force of the light source and (c) the spectral distribution received by the observer. In Fig.4.4, the example is given of a blue object (R) under a light source of daylight type (P). The product PR is then observed by a standard observer ($\bar{x}$,$\bar{y}$, $\bar{z}$). The $\bar{y}$ curve is representative for the luminance. The final colour perceived is the surface area below the curves PRx, PRy and PRz, and are called X, Y and Z (Fig. 4.4). X, Y and Z can be measured with a colorimeter or determined from a spectrophotometer. Y indicates the reflectance of the surface, X and Z are needed for the calculation of x and y (eq.4.1-2).

$$x = \frac{X}{X+Y+Z} \qquad \text{(eq.4.1)}$$

$$y = \frac{Y}{X+Y+Z} \qquad \text{(eq.4.2)}$$

The coordinates x and y can then be represented in a diagram, which is a two dimensional representation of the chromaticity, and is inherently linked to a certain reflectance Y (Fig.4.4-5). This colour space is the CIE 1931 colour space. The area that is used by the colour system is limited by the spectrum locus, a line of coordinates of only saturated, monochromatic colours (Fig.4.5). White is situated at the point W in the diagram. Adding white to a monochromatic, saturated colour would create an unsaturated colour, situated between the white and the saturated colours.

Remark that, in this system, the distance between two points is not the same in every direction, its gradation is dilated in the yellow-green direction, the zone in which the eye has its optimal efficiency. Conclusively, this

colour system is not perceptually uniform, i.e. the diagram does not present the same gradation of colour change in every direction. It would thus be wrong to calculate the Euclidean distance between two points in order to know the difference in colour between the two points. This non-uniformity can be illustrated by placing the Mac Adam ellipses on this diagram (Fig. 4.5). Mac Adam calculated the just-not-perceivable colour differences by the human eye per region in the diagram. Since this system is not perceptually uniform, the differences are ellipsoidal and not spherical, and vary in size depending on the wavelength region [4].

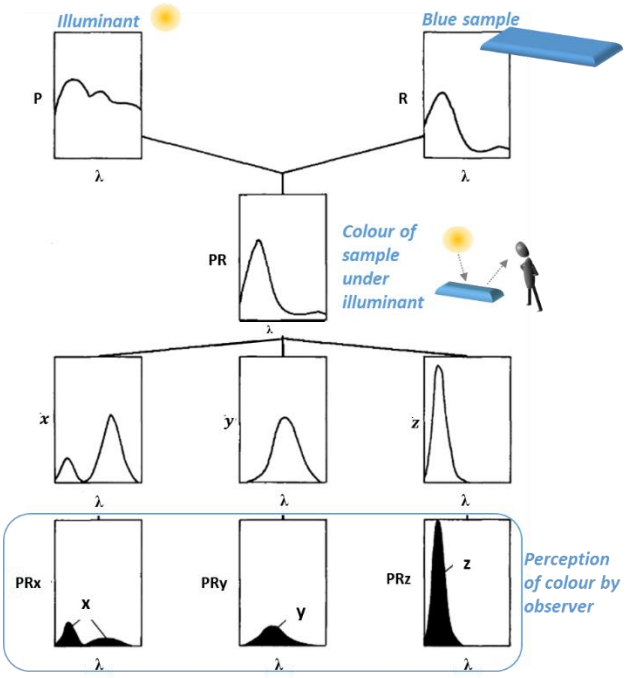

Fig. 4.4 Creation of the tristimulus values for the CIE standard observer CIE 1931, looking at a blue object R under a day light type light source P. The black surface areas are used to calculate XYZ. Adapted from [6].

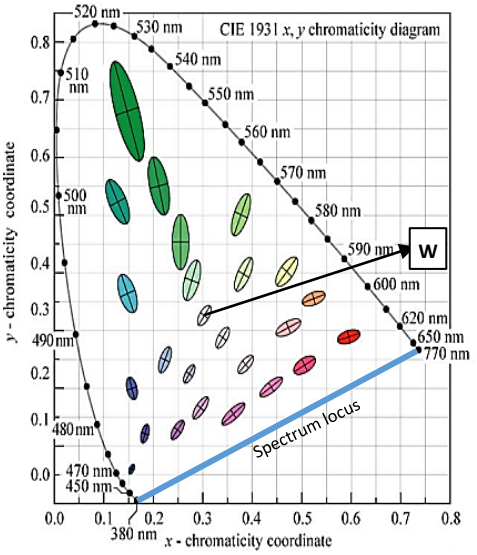

Fig. 4.5 CIE1931 x,y chromaticity diagram for a given Y value. Remark that the ellipses are ten times their actual size. Adapted from [7].

In 1976, the CIE introduced a new colour system, based on the colour system proposed by Hunter in the 1940's [4]. This system is known as the L*a*b* or the CIELAB system and is used very frequently in the research of colours of art objects and mortars. In this system, three parameters L*, a* and b* are used for the representation of a colour (Fig.4.6-7). The L* coordinate indicates the lightness of the colour, and goes from black (0) to white (100). The a* coordinate determines the colour on the red (+a*) to green (-a*) scale, while the b* coordinate determines the colour on the yellow (+b*) to blue (-b*) scale (Fig.4.6-7).

The CIELAB coordinates are calculated using the XYZ values (eq. 4.3-6). The subscript 0 refers to the XYZ values of a perfect reflecting diffuser for the illuminant and observer used. For illuminant type D65 and CIE 2° standard observer, a perfect reflecting diffuser has values X_0 =95.047,

Y_0=100.000, Z_0=108.883. These equations are only valid when the ratios X/X_0, Y/Y_0 and Z/Z_0 are larger than 0.008856 [8]. Conclusively, the L*, a*, and b* values are relative to the reference point in the XYZ data they were calculated from, and represent therefore a proportion between measured value and reference value. Absolute values can only be known once the reference illuminant is stated as well.

One of the reasons for the widely spread use of this system is its reasonably uniform distribution of colour gradation that permits to calculate the difference between two colours with a reasonable accuracy. This chromatic difference is calculated by the Euclidean distance between two points 1 and 2 for all three coordination points, and is called ΔE* (eq.4.6). According to Mokrzycki et al. (2011) a ΔE* varying between 2 and 3.5 indicates that an inexperienced observer can notice the difference [7]. Higher than 3.5 should indicate that a difference is visible. A value higher than 5 indicates an obvious and clear colour difference [7]. According to Johnston-Feller (2001), differences in hue are most important, differences in saturation are less important and differences in lightness (L*) are least important [3].

$$L^* = 116\left(\frac{Y}{Y_0}\right)^{1/3} - 16 \qquad \text{(eq.4.3)}$$

$$a^* = 500\left(\frac{X}{X_0}\right)^{1/3} \qquad \text{(eq.4.4)}$$

$$b^* = 200\left[\left(\frac{Y}{Y_0}\right)^{1/3} - \left(\frac{Z}{Z_0}\right)^{1/3}\right] \qquad \text{(eq.4.5)}$$

$$\Delta E^* = \sqrt{(\Delta L^*)_{1-2}{}^2 + (\Delta a^*)_{1-2}{}^2 + (\Delta b^*)_{1-2}{}^2} \qquad \text{(eq.4.6)}$$

The CIELAB system is closer to being perceptual uniform than the CIE1931 system. In the CIE1931 system, colour difference is represented as ellipsoids that vary in size depending on the region in the CIE1931 space. In the CIELAB space, colour difference is the same in every direction, and thus spherical, and has the same size in every region of its space. This indicates that the total colour difference is determined equally by lightness differences and chromaticity differences. So, if difference in colour is mainly attributed to a difference in lightness L*, but not in a* or b*, the total colour difference will still represent a large total colour difference.

Improvements have been made in the colour difference calculation of the CIELAB system for small colour differences: ΔE* (eq.4.6) is not as able to calculate colour differences between close-related colours [7,9].

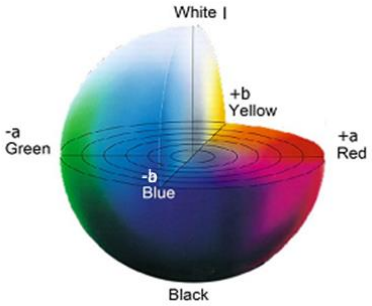

Fig. 4.6 The CIELAB colour space

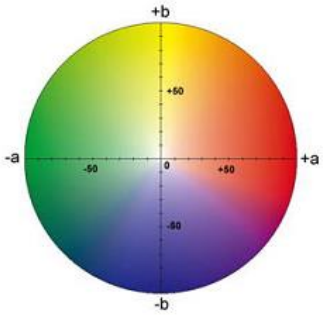

Fig. 4.7 Slice of the CIELAB space at L*=50

4.1.3 Conclusion

If a mortar is regarded as a mixture of small particles of different colours, as in the example of squares of yellow and blue paint, a mortar mix might be considered a material following additive mixing theories. As such it is interesting that colour theory includes the Grassmann laws, which states that any colour can be created by mixing three independent colours.

The perception of colour is subjective, and should thus be neutralised as much as possible, that is, eliminating the 'appreciation' or association persons have with a certain colour, and use a system which contains no deficiencies and for which results can easily be reproduced. The colour systems presented before (CIE1931, CIELAB) both try to represent objectively the colour as analysed by the observer. The CIE1931 method lies closest to the actual analysis of colour by the observer, so one could argue that measurements are best performed in this colour system. On the other hand, this system is not suited for the representation of colour differences, since the space is non-Euclidean. Therefore, colour differences are best expressed in CIELAB.

4.2 Colour measurement

4.2.1 Measuring equipment

In order to estimate the colour of mortars, it is essential to measure colour correctly and quantify it in absolute values. Hence, comparative charts, such as the Munsell chart, the Pantone or NCS or RAL will not be used here. The three techniques discussed below regroup the most frequently used methods to measure colour.

The spectrophotometer measures the relative amount of electromagnetic power reflected by the sample at individual wavelengths of the entire (visible) spectrum [3]. The spectrophotometer has an embedded light source, usually a tungsten, tungsten-halogen or xenon flash-tube lamp, and is equipped with a monochromator with a slit, which serves to isolate a narrow band of wavelengths [3]. The (diffuse) reflectance for the entire visible

spectrum (400-700 nm) is recorded per 10 or even 20 nm. The spectrophotometer will therefore give very precise information about the colour of the sample. The spectro*colori*meter has the more specific additional ability to convert the measured spectral distribution into tristimulus values using built-in numerical integration abilities, emulating data concerning the standard light sources and standard observers. These measuring techniques are accurate, but provide voluminous data. Additionally, samples have to meet certain conditions, which might be considered limiting for the research on lime mortars, e.g. only small samples can be tested, the material may not abrade the optical eye or holder, and for some colorimeters, the material should be placed upright. In that case, mixes of fine binder particles and larger sand grains would lead to a heterogeneous mix: fine particles are concentrated below and larger grains are concentrated in the upper region.

Tristimulus filter colorimeters are filter radiometers [3]. They have a built-in light source, normalised according to CIE standards. Three photocells are incorporated into the equipment, which are filtered as such that they imitate the CIE1931 colour matching distributions of ($\bar{x}$,$\bar{y}$,$\bar{z}$) as a function of wavelength [10]. Since this data is proportional to the XYZ tristimulus values, the output can be transformed into the desired colour space, such as (xyY) or CIELAB. Colorimeters were initially designed to compare materials with similar spectral curve shapes and similar appearance, such as surface reflection and uniformity. The colorimeter is easier to use than the spectrophotometer, but may be less accurate, since it has three integral values, without determining the entire spectral distribution presented by the sample.

The luxmeter-colorimeter is similar to a tristimulus filter colorimeter, with the exception that it does not have a built-in light source. Instead, it measures the reflection of the sample from the incident light. Provided that the light source is regularly verified, it might be considered that the luxmeter- colorimeter approaches well how humans translate colour objectively, that is, without interfering elements such as memory or colour association. Additionally the luxmeter- colorimeter can be placed as such that it permits to measure loose particles such as sand and lime at a small distance (e.g. 2-5 cm) without having to fear abrasion of the optical eye.

4.2.2 Experimental set-up

The method that is the most complete in results appears to be the spectrocolorimeter. Its greatest disadvantage however are the practical limitations which are difficult to combine with the properties of the materials which should be tested in this thesis: its measuring technique does not allow a guarantee for an even distribution of both lime binder and sand, and therefore, of an acceptable and reproducible measurement. The same disadvantage is valid for the colorimeters. The luxmeter-colorimeter does not have this disadvantage: since it can be placed at a certain distance above

the mix, representative and reproducible samples can be guaranteed. Additionally, it measures the incident light reflected by an object and as such approaches more the perceived reality.

The equipment chosen for the colour measurements in this study is a luxmeter-colorimeter CL 200 by Konica-Minolta. The equipment was calibrated by the manufacturer with a measuring error of ±0.002 and a reproducibility error of ±0.0005.

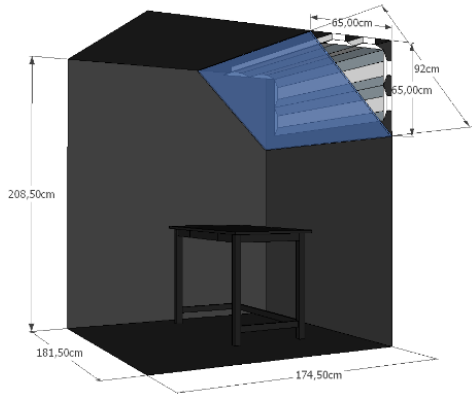

Fig. 4.8 Sketch of the incident light source in and the dimensions of the black room

Fig. 4.9 Experimental set-up. The optical eye, attached to a stand, is situated some 4 cm above the sample. The device with the display of the measured values can be placed outside of the black room.

Since the colorimeter would be placed at a certain height above the sample, it would receive light reflected or transmitted from more than just the mortar sample. Since the materials surrounding the sample would influence the perceived colour of the sample, the environment had to be made as neutral as possible.

All measurements on the individual mortar components (sand, binder) or on the final mortar were therefore performed in a black room, specially designed for this purpose (Fig.4.8). Everything from walls to table was painted in matte black paint, so that the only light in the room would come from specially installed lights. Eight Philips Master TL-D 90 Deluxe 58w/965 1SL light tubes were placed in one upper corner of the black room (Fig.4.8), and placed behind an acrylic diffusion screen. This screen was placed in an angle of 45° with the soil in the upper corner before the light tubes. The temperature of the white incident light was measured and proved to be near the CIE65 temperature (6500K) (Appendix 4.1). It can thus be defined as very close to daylight. Initial results of measurements with this set-up indicated an influence of the luminance on the sample. The stability of the light emitted from the tubes was therefore verified by measuring the xyY values of the light in relation to the temperature of the light tubes (Appendix 4.1). The emitted light evolved in a linear and reproducible manner once 50°C was achieved. A correction factor on the flux can as such be applied systematically.

The set-up of the luxmeter-colorimeter is as such that the operator can be outside the black room (Fig.4.9). Any influence of the operator (e.g. clothes) is as such excluded. The optical eye was detached from the luxmeter-colorimeter and placed on a mechanical lifting arm which was on the table in the middle of the room. The optical eye was placed in a horizontal position, at approximately 4 cm above the sample's surface. With the current experimental set-up, measuring in a neutral environment, under daylight, with a calibrated colorimeter; measurements were considered relatively reproducible.

Measures were also taken to avoid any effects due to the specific surface finish of the samples: the surface finish also influences the reflected light. A surface finish difference between two samples will thus give an erroneous colour difference, since the total colour difference (eq. 4.6) does not consider the influence of the surface finish and the surroundings.

If all samples, mortar, stones and bulk ingredients (sand, binder) are in powder form, a more uniform database is created than if all samples had a different surface finish. Moreover, sands and binders were to be measured in loose, bulk form. As such, the side-effect of surface finish or gloss on colour differences was excluded. Appendix 4.1 illustrates colour measurements on grinded and non-grinded mortar samples. Difference in chromaticity was low (av. 0.0035), while the measured lightness was, as could be expected, different for the two types of samples (av. 0.11).

Additionally, the xyY-values of a grinded cured mortar and the dry powder mix (before adding water) were compared. The dry powder mix indicated very closely the chromaticity of the cured mortar (difference on average 0.008). In contrast, the Y coordinate of the powder was less representative for the Y coordinate of the mortar (on average 0.041 difference) (Appendix 4.1). Fig.4.10 A-B represent a crushed mortar and its powder mix under the microscope. Based on these figures, both grinded mortar and initial binder-sand mix appear similar, e.g. in the positioning of fine grains towards larger grains. In this research, the chromaticity of the mortars is thus more representative for the colour of the mortar than the lightness.

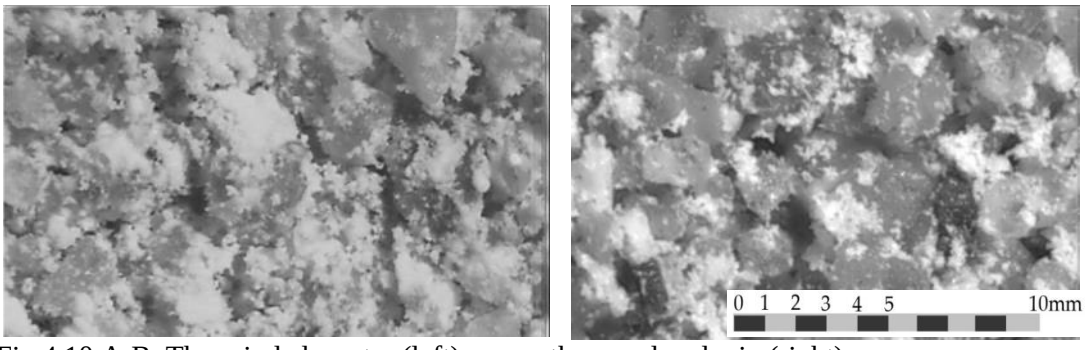

Fig.4.10 A-B. The grinded mortar (left) versus the powdered mix (right).

4.3 Estimation methods of colour

4.3.1 Kubelka-Munk method

The estimation method developed by Kubelka and Munk in 1931 has already successfully been used in the domain of pigments, for the estimation of colours for inks and paints. It is a method based on the subtractive colour theory [11]. The theory proposed by Kubelka and Munk was thought out for diffuse surfaces. Diffuse surfaces, such as mortars, are matte, i.e. the reflectance is isotropic and thus the same regardless of the observer's viewpoint. The Kubelka-Munk method appeared thus an interesting method to estimate the colour of a mortar recipe, based on the components alone. For detailed information concerning the Kubelka-Munk method, the reader is referred to specialized literature [4,12].

The input data needed for this estimation method are the full spectral distribution curves of all mortar components (sands, binders) and of several binder-sand and sand-sand mixes. For example, component A, in a mix with components A and B, makes out 0, 20, 40, 60 or 80 % of the mix. The influence of a component on the absorption and reflectance curve has to be determined very precisely. Once this is established, the colour of any given dry mortar mix can be established.

Due to technical limitations, this method was not explored into detail. First of all, only spectrophotometers can establish the spectral distribution curve, but they were found to be incompatible with the material that is studied in this thesis: binders and sands were available in loose bulk form, and the sample measuring technique employed in a spectrophotometer did not guarantee an even, homogeneous distribution of the mixture. On top of that, a very extensive research with a large database of binders and sands, and mixtures of these binders and sands in various concentrations would be necessary in order to be able to use this method for the prediction of the colour of mortars.

4.3.2 Grassmann method

4.3.2.1 Estimation method according to Grassmann laws

According to Grassmann laws, the colour of binary mixes with similar grain sizes can be easily predicted. In the CIE xyY system for example, the resultant triplet (x_3,y_3,Y_3) is located on the 3D straight line, linking (x_1,y_1,Y_1) and (x_2,y_2,Y_2). At each step *i* a parameter p_i, the relative proportion of volume V_i to ($V_1 + V_2$), can be defined which represents the position of the mixture on the 'segment' linking each two initial components, set out in a colour coordinate x,y graph (Fig.4.11). The principles of Grassmann are then applied in following equations, assuming the mixing of components with colour coordinates 1 and 2 leads to a mixture with colour coordinates 3, where p_i is $V_2/(V_1 + V_2)$ (eq.4.7):

$$x_3 = x_1 - p_i(x_1 - x_2) \quad \text{(eq.4.7.1)}$$
$$y_3 = y_1 - p_i(y_1 - y_2) \quad \text{(eq.4.7.2)}$$
$$Y_3 = Y_1 - p_i(Y_1 - Y_2) \quad \text{(eq.4.7.3)}$$

In order to validate Grassmann's model, several experimental studies were performed.

First, a preliminary test was executed to evaluate the suitability of Grassmann's method for predicting the colour of heterogeneous surfaces. Using a Monte-Carlo approach, a deterministic algorithm, randomly dispersed patterns with arbitrary distributions of two colours were generated and used to create test cards (Fig.4.12) with an inkjet printer. The global CIE xyY color of these cards was measured and compared to the CIE xyY triplets predicted with Grassmann's method based on the measurement of only completely yellow and completely blue test cards. This proved that a heterogeneous surface does behave as many small individual reflective particles and that the Grassmann's method can be used.

Secondly, the Grassmann theory was applied on a mix of two aggregates with similar grain size. The first aggregate was composed of crushed and sieved grey-blue limestone, the second was composed of crushed and sieved red ceramic bricks. Both aggregates were sieved on size, and divided into 5 groups: >1.6 mm, >1.25 mm, >800 µm, >500 µm and >200 µm. Each grain size group of the ceramic bricks was mixed with the corresponding group of the blue limestone. For each mix, five volume proportions were produced (100/0, 75/25, 50/50, 25/75, and 0/100). The measured results are given in Fig.4.13. The results indicate that the influence of the volume ratio is linearly related to its chromatic effect on the mix.

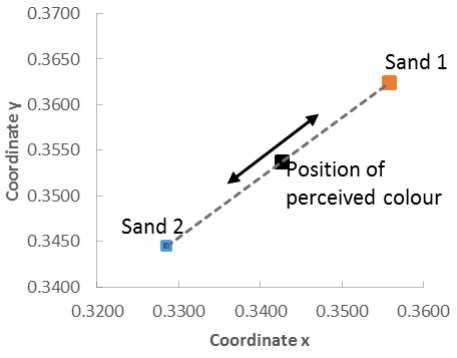

Fig. 4.11 Varying position of colour depending on the volume ratio of the two components.

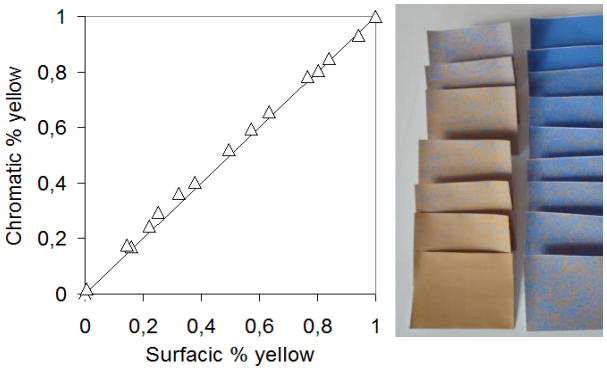

Fig. 4.12. Left: An example of the test cards used. Right: The measured values (triangle) and the estimated values (solid line).

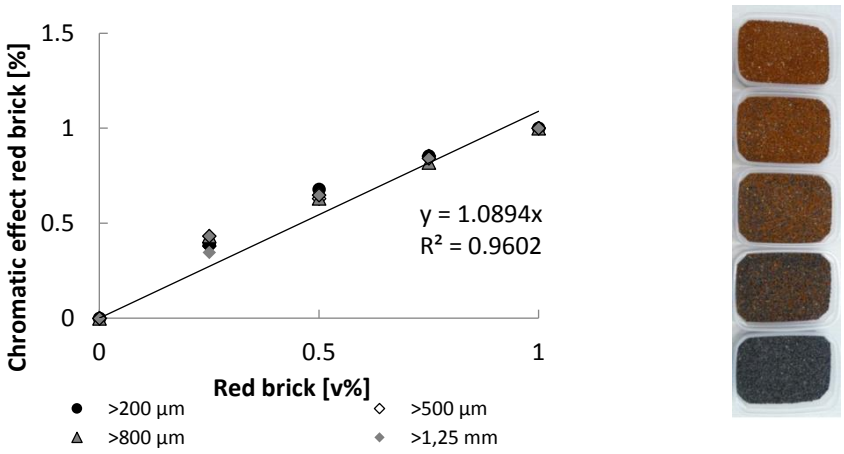

Fig. 4.13 Trendline of 1.25 mm mixes showing the linearity of the mixes of red brick and blue limestone sand-sized grains.

Since the Grassmann theory worked well for mixes with the same aggregates size, a second mix was made, where a green sand was mixed with a white cement binder. The binders used in this study are more or less white, while the sand used is coloured (green, yellow, and beige): adding more binder decreased the saturation of the mix. The colour of the binder added changed the colour of the mixture significantly (Fig. 4.14 A-B).

Until a certain threshold value, ±10% of the sand volume, the adding of more binder would not change the colour of the mix significantly anymore. The binder-sand mix did not follow the predicted theory by Grassmann anymore. A non-linear correlation could as such be established between volume % of binder added and its chromatic influence on the mix. The more binder volume was added, the more the mixture would have the colour of the binder particles. This led to assume that the binder 'polluted' the sand particles. This effect was already assumed in Fig.4.10, where small cement particles appeared to be attached to the surface of the sand particles.

After this threshold, called V_{tr} hereafter, the smaller binder particles had placed themselves around the sand particles, and the colour would not be the mix of a sand and binder, but the colour of a thin film around the sand particles (Fig.4.15).

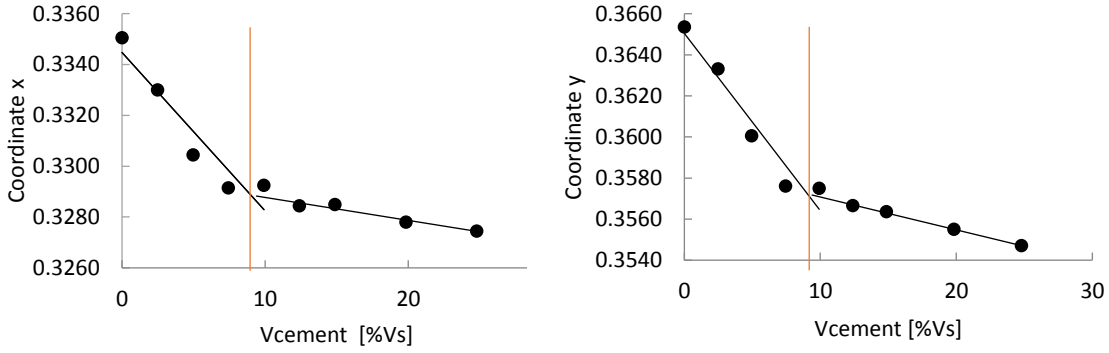

Fig. 4.14 A-B. V% binder and actual chromaticity for green sand-cement mixes. The V_{tr} can be set at just below 10 % of the sand volume.

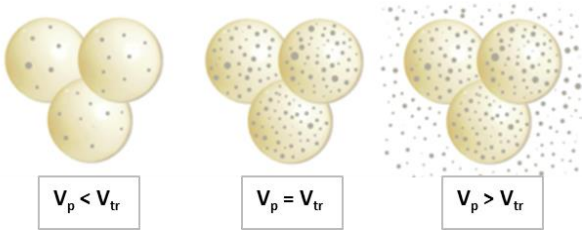

Fig. 4.15 Sketch of the assumed pollution effect of the smaller particles of the binder on the sand particles.

Additional research to this effect of pollution of the binder particles was performed and it was studied if a geometrical projection model could be used in order to estimate the threshold value V_{tr} for different aggregate sizes.

Assuming both binder and aggregate particles are spherical, and that the skeletal density ρ, the medium grain size D_{50} and the mass quantity Q is known, the volume of each component can be defined (eq. 4.8.1-11).

The total aggregate volume V_a

$$V_a = \frac{Q_a}{\rho_a} \qquad \text{(eq.4.8.1)}$$

The volume of 1 aggregate particle $V_{a,g}$

$$V_{a,g} = \frac{4}{3}\pi\left(\frac{D_{50,a}}{2}\right)^3 \qquad \text{(eq.4.8.2)}$$

The lateral surface of 1 aggregate grain S_{lat}

$$S_{lat} = 4\pi\left(\frac{D_{50,a}}{2}\right)^2 \qquad \text{(eq.4.8.3)}$$

The number of aggregate grains N_a

$$N_a = \frac{V_a}{V_{a,g}} \qquad \text{(eq.4.8.4)}$$

The volume of 1 binder particle $V_{b,g}$

$$V_{b,g} = \frac{4}{3}\pi\left(\frac{D_{50,b}}{2}\right)^3 \qquad \text{(eq.4.8.5)}$$

The projected surface of a binder grain S_{proj}

$$S_{proj} = \pi\left(\frac{D_{50,b}}{2}\right)^2 \qquad \text{(eq.4.8.6)}$$

In order to know the volume of binder particles necessary to cover the aggregate particles, the total surface of both binder and aggregate particles S_{tot} is considered to be equal to

$$S_{tot} = N_a\, S_{lat} \qquad \text{(eq.4.8.7)}$$

And the number of binder particles N_b would then be

$$N_b = \frac{S_{tot}}{S_{proj}} \qquad \text{(eq.4.8.8)}$$

The volume of binder particles V_b is then

$$V_b = N_b \, V_{b,g} \qquad \text{(eq.4.8.9)}$$

The volume of binder particles needed to completely cover the aggregate grains is

$$V\%_{cov} = \frac{V_b}{V_a} = 4\frac{D_{50,b}}{D_{50,a}} \qquad \text{(eq.4.8.10)}$$

Implementing the definitions of eq.4.8.1-9 in eq. 4.8.10, the volume of binder particles needed to cover aggregate grains completely can then be defined as:

$$V_{cov,b} = V\%_{cov} \, V_a \qquad \text{(eq.4.8.11)}$$

The experimental study and validation of this geometrical model is available in Appendix 4.2.

Figure 4.16 illustrates that for a smaller aggregate grain size, a larger percentage of binder volume is necessary to cover the aggregates completely.

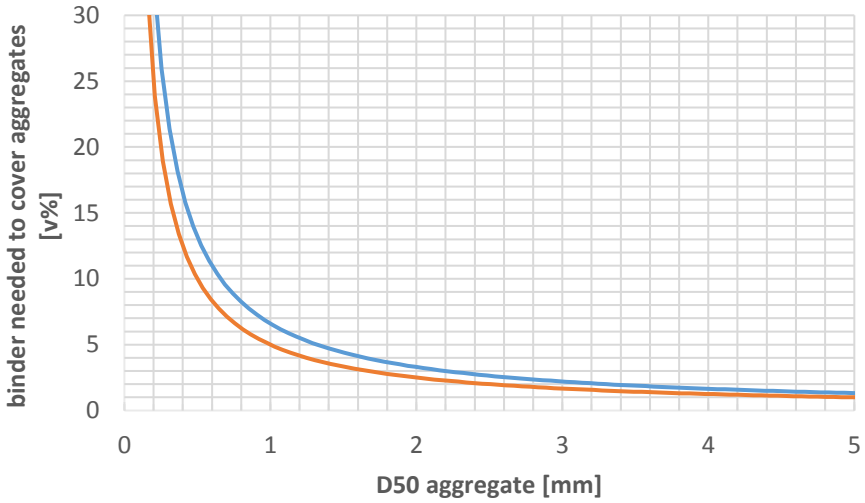

Fig. 4.16 Geometrical model indicating the threshold vol% of binder, necessary to cover the aggregates, in function of the aggregate size. The *blue* line indicates the threshold line in the situation where the binder is NHL5, the *orange* line for NHL3.5.

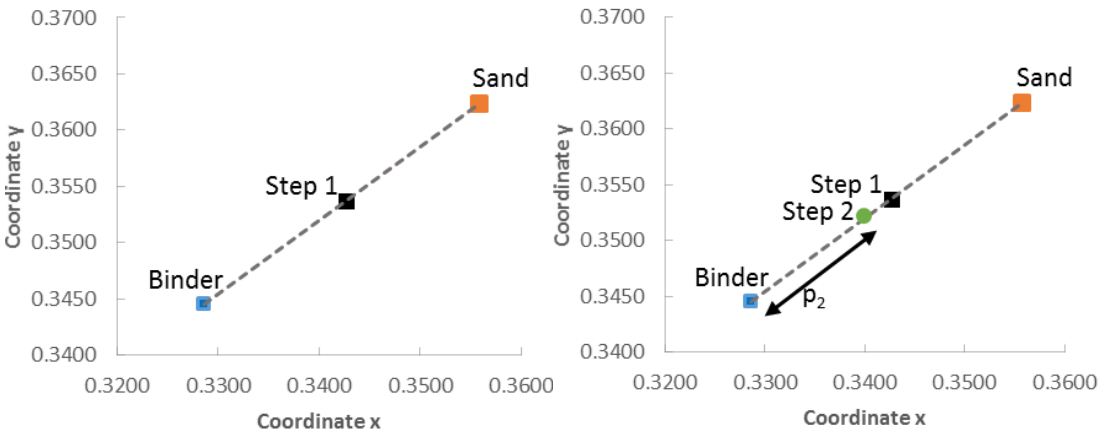

Fig. 4.17 Diagram of x,y, with the position of the mixtures issued from steps 1 and 2 of the estimation method.

4.3.2.2 Adapted Grassmann laws

Since normal Grassmann laws were not able to estimate a binder-sand mix, the Grassmann method was adapted so that the effect of the binder pollution would be included into the method. This process can be split up in two steps (Fig. 4.17-18).

The first step is the mixing of the total volume of sand and a part of the cement volume, which is the part needed to cover the sand. The volume of cement needed to cover the sand is called the maximal pollution volume percentage.

The second step is the mixing of the first mixture and the remaining volume of cement.

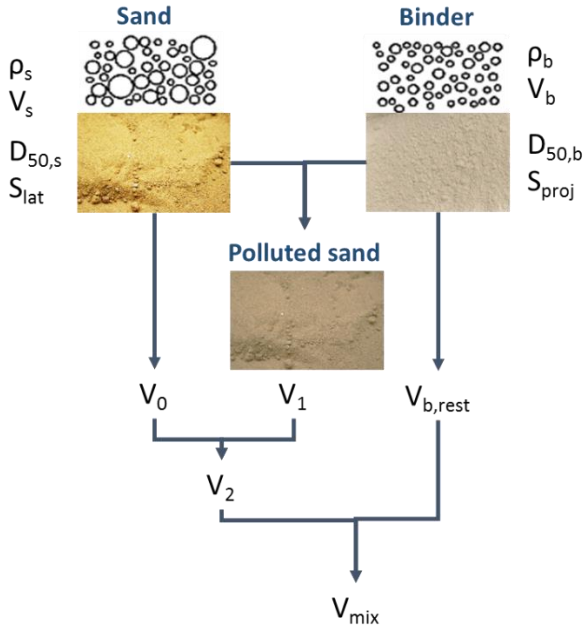

Fig. 4.18 Sketch of the calculation steps needed to perform the estimation according to Grassmann laws.

In the **first step** it is assumed that for both binder and sand, the xyY coordinates, the skeletal density ρ, the medium grain size D_{50} and the mass quantity Q are known so the volume of each component can be defined (eq.4.9.1-13).

In this manner, the number of sand grains covered by binder can be calculated, by taking into account the number of binder grains covering sand, and the number of binder grains necessary to cover one sand grain:

$$N_{a\ cov} = \frac{V_{cov,b}}{V_{b,g}} \frac{S_{proj}}{S_{lat}} \qquad \text{(eq.4.9.1)}$$

The non-polluted sand volume can then be calculated according to

$$V_0 = V_{a,g}\left[\frac{V_a}{V_{a,g}} - N_{a\ cov}\right] \quad \text{(eq.4.9.2)}$$

The polluted sand volume is then

$$V_1 = N_{a\ cov}V_{a,g} + V_{cov,b} \quad \text{(eq.4.9.3)}$$

Finally, the parameter p_1 can be defined as the proportional volume of the polluted sand on the volume of sand:

$$p_1 = \frac{V_1}{(V_1+V_0)} \quad \text{(eq.4.9.4)}$$

The colour coordinates x_1,y_1,Y_1 of the mixture of binder and sand particles can then be described as

$$x_1 = x_s - p_1(x_s - x_b) \quad \text{(eq.4.9.5)}$$
$$y_1 = y_s - p_1(y_s - y_b) \quad \text{(eq.4.9.6)}$$
$$Y_1 = Y_s - p_1(Y_s - Y_b) \quad \text{(eq.4.9.7)}$$

Now that a part of the sand has been completely polluted by the binder particles, the remaining volume of binder $V_{b\ rest}$ is mixed with the mixture of step 1, V_2,

$$V_{b\ rest} = V_b - V_{cov,b} \quad \text{(eq.4.9.8)}$$

$$V_2 = V_a + V_{cov,b} \quad \text{(eq.4.9.9)}$$

The parameter p_2 is then

$$p_2 = \frac{V_2}{(V_2+V_{b\ rest})} \quad \text{(eq.4.9.10)}$$

The colour coordinates x_2,y_2,Y_2 can then be described as

$$x_2 = x_b - p_2(x_b - x_1) \quad \text{(eq.4.9.11)}$$
$$y_2 = y_b - p_2(y_b - y_1) \quad \text{(eq.4.9.12)}$$
$$Y_2 = Y_b - p_2(Y_b - Y_1) \quad \text{(eq.4.9.13)}$$

This adapted Grassmann method could also be used for ternary (or even more) mixes, assuming that they are linear combinations of binary mixes.

4.3.3 Validation of the adapted Grassmann method

The experimental campaign from 4.2.2 indicated that for a given recipe, chromaticity (CIE xy) remains generally unchanged, between the dry powder mix and the fresh mortar paste, while luminance (CIE1931 Y) can change considerably. This experimental study therefore focuses on the chromaticity aspect of the mortar mixes and uses primarily dry powder mixes to measure the chromaticity. The estimation method according to

Grassmann laws, only uses eq. 4.7.1-3 with $p_1 = V_{cement} / V_{tot}$. Fig. 4.19-21 present all calculated values for various mixtures. It is clear that the original Grassmann equation is not sufficient to estimate the colour of the mixture, but that eq. 4.9.1-13 approach the actual measured value much closer. The tolerance ranges in x and y direction indicate the Mac Adam ellipses in the (x,y) domain. Since these ellipses indicate the just-no-perceivable difference, it demonstrates that one out three estimations falls in this range.

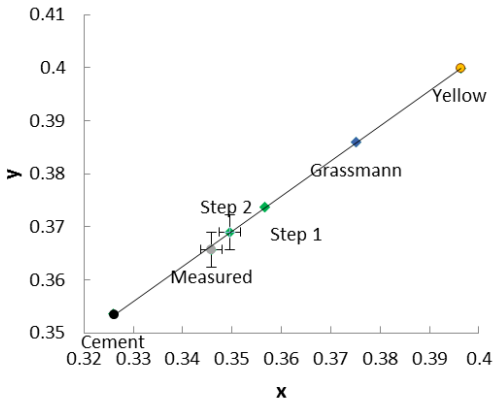

	x	y	Y
Yellow sand	0.3963	0.3998	261.5
White cement	0.326	0.3535	671.4
Measured	**0.3458**	**0.3657**	**496.7**
Calcul step 1	0.3566	0.3737	492.8
Δ	0.0108	0.0080	3.9
Calcul step 2	**0.3495**	**0.3690**	**534.1**
Δ	0.0037	0.0033	37.4

Fig.4.19 Diagram x,y and table representing the values for cement and sand, the original Grassmann estimation and the steps to achieve the final estimation (step 2- *light blue*) of the adapted Grassmann estimation. For a mix of yellow sand –white cement (2:1 ratio)

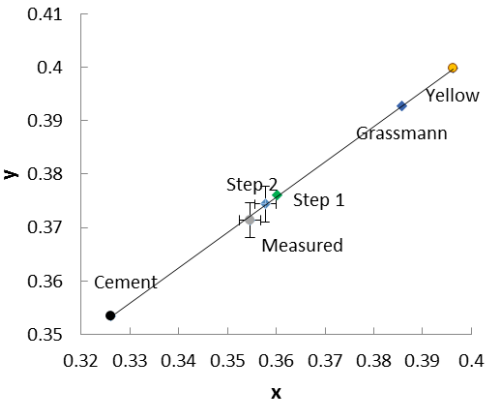

	x	y	Y
Yellow sand	0.3963	0.3998	261.5
White cement	0.326	0.3535	671.4
Measured	**0.3546**	**0.3714**	**411.5**
Calcul step 1	0.3603	0.3761	471.6
Δ	0.0057	0.0047	60.1
Calcul step 2	**0.3577**	**0.3744**	**486.3**
Δ	0.0031	0.0030	74.8

Fig.4.20 Diagram x,y and table representing both the values for cement and sand, the original Grassmann estimation and the steps to achieve the final estimation (step 2 - *light blue*) of the adapted Grassmann estimation. For a mix of yellow sand –white cement (4:1 ratio)

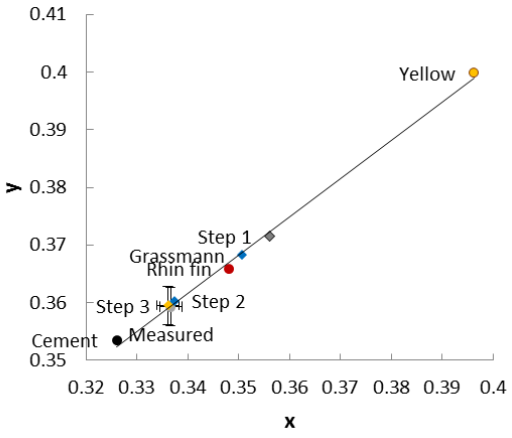

	x	y	Y
Yellow sand	0.3963	0.3998	261.5
Rhin sand	0.3481	0.36585	316.75
White cement	0.326	0.3535	671.4
Measured	**0.3366**	**0.3593**	**521.2**
Calcul step 0	0.3561	0.3715	307.6
Δ	0.0195	0.0122	213.6
Calcul step 1	0.3373	0.3603	534.8
Δ	0.0007	0.0010	13.6
Calcul step 2	**0.3361**	**0.3595**	**549.2**
Δ	0.0005	0.0002	28.0

Fig.4.21 Diagram x,y and table representing both the values for cement and sand, the original Grassmann estimation and the steps to achieve the final estimation (step 3 -*yellow*) of the adapted Grassmann estimation (*dark blue*). For a mix of yellow sand –Rhin fin sand (1:5) with white cement (B/A=1:4)

4.4 Discussion & conclusion

The experimental set-up used for this test permits to measure the colour of binder, sand and mortar mixes in a reproducible way: a neutral environment, a standardized light source and an equipment which allows it to be positioned as such that powders and loose mixes can be measured. By only measuring powder mixes, the effect of the surface finish was excluded, and it permitted to have the same colour measurement for every sample, binder, sand, mortar, stone. A disadvantage of this technique for stones would be that heterogeneities in colour, such as veins or bioturbations, would not be measured: the veins would be blended with the rest of the sample. A possible solution for this problem might be to separate bioturbation or vein rich regions from other zones in the stone, and grind them separately.

Dry powder mixes were found to be representative for the chromaticity of hardened mortars.

The estimation method following Grassmann theory was considered applicable for repair mortars, because mortar might be seen as a mixture of binder and aggregate particles, all influencing the total perceived colour of the mortar by their own specific colour.

The Grassmann theory proved to be valid for grain mixes of any size, as long as all grains on one mix had the same size. The estimation method based on Grassmann laws proved to be insufficient once a binder was combined with larger aggregates, due to a pollution effect of the binder. In its original configuration, the model is thus not able to estimate the colour of the actual mortar mixes tested in this campaign.

The volume of binder necessary to cover the sand grains was determined according to a geometrical calculation model, assuming that a part of the

binder particles ‘project’ themselves onto the surface of the aggregate grains. This theoretical approach fitted well with experimental results. The geometrical model can thus be applied on other mixes as well, since it depends only on the grain size of binder and aggregate.

The adaptation of Grassmann method made in this research, taking into account the pollution effect, showed very good results for one of the mixes tested. The other mixes showed results which were already better than the normal Grassmann theory, but where the estimation was still situated outside of the just-not-perceivable colour difference. This difference might be due to the fact that the Grassmann method does not take the diffusion of light by the aggregates into account.

Mortars are diffuse surfaces, and the Kubelka-Munk theory seemed therefore a very good estimation method. Unfortunately, the method could not be tested and validated due to practical limitations. This method is likely to be more precise in results than the Grassmann method, since a) the input data is already more complete than the Grassmann method, by using the entire spectral distribution curve, and b) the theory is created for materials with similar light reflecting properties than mortars. The largest disadvantage of this Kubelka-Munk method would be the immense input of data required. For the Grassmann method, data of only the individual elements are required, while for the Kubelka-Munk method, the spectral distribution curve of mixes of sand-sand and sand-binder would have to be known. Additionally, for now, an adapted measuring technique for this specific type of materials has not been found yet.

This chapter concerning colour leaves additional possibilities for future research, e.g. the effect of texture on the colour of the mortar, or the effect of ageing and weathering on the colour difference between mortar and stone, both elements which have been deliberately left out of the scope of this research, in order to focus on the colour of the mortar as determined by the mortar in a fresh, unweathered, state. However, such research should probably include knowledge about the specific minerals in natural stone which can play a determining role in their change in colour during time, such as glauconite. These minerals may be added purposefully to a mortar mix, given that ageing tests would be performed in order to determine the durability of such a specialized mix. Ageing of repair mortar and stone might as such be more parallel.

The surface finish is not taken into account, mainly because this method, as well as the Kubelka-Munk method, starts from the *mortar components* and their colour. Surface finish is inherently related to the application technique and should also be linked to the skills of the user. Future research might implement the surface finish as additional aspect. In that situation, a relationship between mixes of sands and binders on one hand and various surface finishes (sanded, chiselled etc.) on the other hand can be established.

Bibliography

[1] Isebaert A, Van Parys L, Descamps T, Renglet M, Cnudde V. First steps to computer-aided decision-making in repair mortar recipes: working on three fronts. 10th Int. Conf. Struct. Anal. Hist. Constr. Anamn. Diagnosis, Ther. Control., Leuven: KU Leuven; 2016.

[2] Dessoy Q. Vers une maîtrise colorimétrique du béton. University of Mons, 2015.

[3] Johnston-Feller R. Color science in the examination of museum objects. Non-destructive procedures. J. Paul Getty Trust; 2001.

[4] Kowaliski P. Vision et mesure de la couleur. 2nd ed. Paris: Masson; 1990.

[5] Hunt RWG, Pointer MR. Measuring Colour. 4th ed. 2011.

[6] Delamare F. Vision et mesure de la couleur. Datation-Caractérisation Des Peint Pariétales Murales 1987:195–222.

[7] Mokrzycki WS, Tatol M. Color difference Delta E - A survey. Mach Graph Vis 2011;20:383–411.

[8] Bartleson CJ, Bertrand G, Chalmers AN, Fink X, Gentile C, Hunt RWG. CIE 15.2:1986 Recommendations on Colorimetry. 1986.

[9] Cheung V. Uniform Color Spaces. In: Chen J, Cranton W, Fihn M, editors. Handb. Vis. Disp. Technol., Berlin, Heidelberg: Springer Berlin Heidelberg; 2012. doi:10.1007/978-3-540-79567-4.

[10] Gardner JL. Comparison of calibration methods for tristimulus colorimeters. J Res Natl Inst Stand Technol 2007;112:129–38.

[11] Kubelka P, Munk F. Ein Beitrag Zur Optik der Farbanstriche. Zeitschrift Für Tech Phys 1931;12:593–601.

[12] Capo-Chichi KTE. Materiaux complexes et couleur: hiérarchisation des paramètres et prévision de la couleur dans un béton coloré. Université Montpellier II, 1996.

Chapter 5 Compatibility in elasticity

Next to the compatibility in colour and permeability, the mortar should also be compatible in elasticity to the stone it is supposed to repair. As in the previous two chapters, this chapter will first discuss the theory necessary to understand the property, followed by possible characterization techniques for mortars. The chapter concludes with the discussion of existing estimation methods and elaborating on the estimation method chosen for this study. The aim of this chapter is to find an estimation method using the mortar components for elasticity.

The experimental study of the compressive strength of lime mortars was published in Isebaert et al. (2015) [1]. The experimental study was further enriched with results from the master thesis study of Ecrepont (2014) at the University of Mons, performed under the author's supervision [2]. The part concerning the estimation methods contains elements from Isebaert et al. (2016) [3].

5.1 Elasticity in building materials

5.1.1 Theory

A material subjected to a deformation will follow several stadia of material behaviour. Depending on the type of material, only some or all stadia can be run through. Elastic behaviour is the first stage, where, after the material was subjected to stress, it can return to its initial state and shape once the stress has been cancelled. Elastic behaviour is described by a linear relation between constraint and deformation; and can be described by Hooke's law (eq. 5.1.1) [4],

$$\delta = \frac{F}{q} \qquad \text{(eq.5.1.1)}$$

where δ [m] is the relative displacement or the resulting elongation following the direction of the force, F [N] is the applied force, q [N/m] is the stiffness of the material. The stiffness is a constant for a certain geometry and material, assuming that the material is elastic. Hooke's law can be generalized to define a correlation between stress σ [N/m²] and strain ε [m/m], for an isotropic material subjected to a single stress σ_x (eq. 5.1.2).

$$\varepsilon_x = \frac{\sigma_x}{E} \quad \text{(eq.5.1.2)}$$

where E [N/m²] is the elasticity modulus. This equation (5.1.2) is a simplification from the general theory of Hooke and is therefore only valid if it links stress and strain in one given direction. As can be seen in Fig. 5.1, the relation between strain ε and stress σ is linear until a certain value, the proportionality limit S [N/m²], after which the sample cannot return to its initial state. After the elasticity stage, the material will be permanently deformed, even when the applied stress is cancelled. The material now shows plastic behaviour. The relation between ε and σ for a material with plastic behaviour is non-linear (Fig. 5.1).

Various studies exist on the mechanical properties of cement mortars and cement-lime mortars, e.g. [5–8]. Costigan et al. (2012) have studied the elasticity of mortars made with various lime binders elasticity: lime mortars with a feebly to higher hydraulicity showed a predominantly elastic behaviour [5]. These values are represented in Fig. 5.2. These results are consistent with other studies [6,7]: all lime mortars demonstrate an elastic-plastic deformation before failure. Lime mortars are consequently different from standard cement mortars, which are brittle, and show only elastic behaviour [6]. These studies support therefore the use of lime mortars in historic masonry instead of cement mortars, since they will allow to adapt to a differential setting and more deformation under critical stress in the masonry [6]. Hayen et al. (2004) attribute the failure of lime mortars to an initial pore-collapse mechanism, leading to a deformation before failure [8]. One can assume this pore-collapse mechanism to be more important in lime mortars with a higher porosity. Lime mortars with a lower hydraulicity have a higher porosity e.g. [6,9]. This corresponds to the graph represented in Fig. 5.2.

The influence of the W/B ratio and the grain size distribution has also been studied by Haach et al. (2010) [7]. A clear relation was present between W/B and elastic modulus. Mortars with a higher W/B showed a decrease in compressive strength and a decrease in static E modulus, and was attributed to the fact that an increase in W/B induces a higher porosity, which is held responsible for the decrease in mechanical properties.

The grain size distribution of the sands added in the mortars also showed an influence on the elasticity, albeit less distinct than the W/B ratio. The mortars made with the coarser sand led to higher compressive strength and higher elastic modulus values. The coarser sand also led to a more ductile and deformable behaviour, behaviour attributed to the non-uniform distribution of the (coarser) sand particles [7].

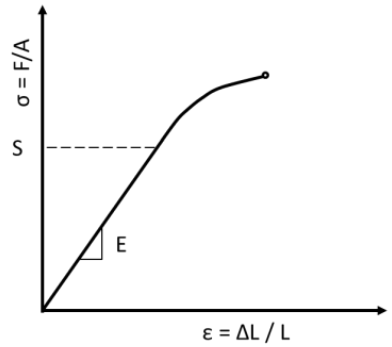

C

Fig. 5.1. An idealized uniaxial stress-strain curve of a plastic material. Elasticity E is the linear relationship between stress and strain, S represents the proportionality limit, F is the applied force, A the undeformed surface area, L the undeformed length, ΔL the elongation.

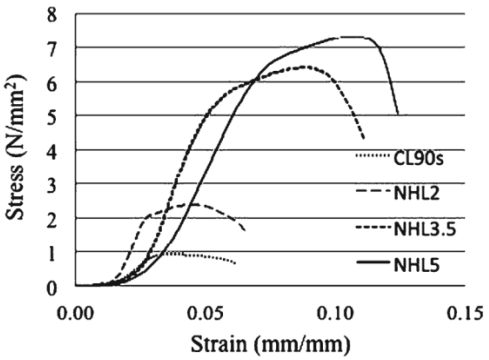

Fig. 5.2 The stress-strain curves for mortars produced with the same sand, but with different lime binders, tested after 56 days of curing. The mortars show elastic-plastic behaviour. Figure by [5].

5.1.2 Elasticity measuring techniques

To measure elasticity, two main approaches can be used: the static and dynamic E modulus. In terms of measuring elasticity on lime mortars, not many standards exist on the subject. In contrast to European standards for the determination of the compressive strength, no European standard exists to determine the elastic modulus for mortars. The testing of the elastic modulus for *concrete* can be tested according EN 12390-13 (2013) for the secant modulus of elasticity in compression, which is the slope of the secant from the origin to a particular stress-strain combination. Additionally, American standards describe tests methods for concrete as well, e.g. ASTM C597-09 (2009) for the determination of the pulse velocity measurements, ASTM C215-02 (2002) for the fundamental transverse, longitudinal and torsional frequencies and ASTM C469M-14 (2014) for the testing of the static elasticity by compression.

The static E modulus can be measured using a three point bending test with a stress-strain gauge [10] or through a calculation using the slope of an uniaxial compressive strength curve, e.g. in EN 12390-13 and ASTM C469M-14 (Fig. 5.3-4). The first method is a direct method, measuring exact stress and strain. However, perfect measurements are complex since perfect alignments are asked for, and, for low strength materials such as lime mortars, gauges have to be quite sensitive. The latter is an indirect method where the slope of the stress-strain couple can be obtained based on results from a compression test: the compressive strength is measured and simultaneously, the overall deformability should be measured. The static E modulus can then be calculated according to eq.5.2. Two stress values σ_x and σ_y are set as percentages from the maximal stress σ_{max} [N], i.e. the stress at which point the material breaks. When set out in a (σ, ε)-graph, the interval between (σ_x, ε_x) and (σ_y, ε_y) should be linear.

$$E_{stat} = \frac{(\sigma_x - \sigma_y)}{(\varepsilon_x - \varepsilon_y)} \quad \text{(eq.5.2)}$$

with E_{stat} the static modulus of elasticity [N/mm²], σ_i the applied stress [N] at a point *i* associated with its elongation ε_i [mm].

The dynamic E modulus can be measured by either the ultra-sonic pulse velocity test (UPV), according to ASTM C579-09 or the resonance frequency (RF) test according to ASTM C215-02 [10,11] (Fig. 5.5-6). Research on cement mortars indicated that the UPV-determined E_{dyn}, the dynamic E modulus [N/m²], gave lower values than the RF-determined E_{dyn} for almost all tested mortars [10].

The velocity V [m/s] from the UPV test can as such lead to the E_{dyn}, given that the apparent density ρ [kg/m³] and Poisson ratio ν [-] are known (eq.5.3.1).

$$V^2 = \sqrt{\frac{E_d(1-\nu)}{\rho\,(1+\nu)(1-2\nu)}} \quad \text{(eq.5.3.1)}$$

For the calculation of the E_{dyn}, the Poisson ratio should be known. The Poisson ratio ν represents the ratio between transversal and longitudinal deformations (eq.5.3.2), when the applied charge is directed along the longitudinal axis. The Poisson ratio theoretically can vary between 0 and 0.5. Building materials have generally a Poisson ratio varying around 0.2 [12]. It is however rarely determined, due to the complexity of the test and the required precision.

$$\nu = -\frac{\varepsilon_y}{\varepsilon_x} = -\frac{\varepsilon_z}{\varepsilon_x} \quad \text{(eq.5.3.2)}$$

For the same material, the values of the dynamic modulus of elasticity are reported to be higher than the static modulus of elasticity [13]. A relationship between both results can only be established per material type and a general equation is thus not available. Various rocks, when measuring their stress and strain, show a hysteresis between increasing stress-strain values and decreasing stress-strain values [13]. This hysteresis indicates that the elastic behaviour of these rocks is non-linear, i.e. a linear elastic material should show no difference in loading and unloading cycles. Yale et al. (1995) found that the hysteresis can be related to the difference in the static and dynamic value of the Young's modulus [13]. The difference in static and dynamic values is mainly attributed to strain amplitude differences between the two measurements. Since different strain amplitudes are applied for both tests, the tests measure a different field of deformation. It is assumed that if the strain amplitude would be decreased to levels similar to acoustic wave propagation, the static E modulus would increase to a value close to the dynamic E modulus [13]. However, no such correlations for lime mortar were found in published studies.

In addition, some practical aspects are to be considered when comparing studies of elasticity on lime mortars. Firstly, lime mortars are susceptible for the temperatures at which they are dried. Mortars are best dried at 40°C to avoid dehydration, but for tests on elasticity this is sometimes not applied for lime mortars [14], and seems absent in studies of cement mortar elasticity [10,15,16]. Moreover, lime mortars are not smooth and the contact between measuring devices (gauges, compressive surfaces, transducer and receptor) and the sample is therefore lower. To this purpose, wax, an epoxy coating or Vaseline are often added to this contact area, influencing thereby the results [14].

Some tests require a different sample size than other tests. As stated in 5.1.1, the geometry of the sample is of importance for the apparent stiffness of the material. A comparison between various tests is therefore only possible when taking a certain geometrical factor into account.

Last but not least, dynamic E measurement set-ups are logically non-destructive and those for a static E modulus destructive. Therefore, the dynamic E modulus is often used in built heritage, where destructive techniques are preferably avoided in order to keep a maximum of original material.

Fig. 5.3 Example of a static E modulus measurement set-up with stress-strain gauges fixed on the sample, which is placed in compressive strength test cell. Figure adapted from Controlsgroup.

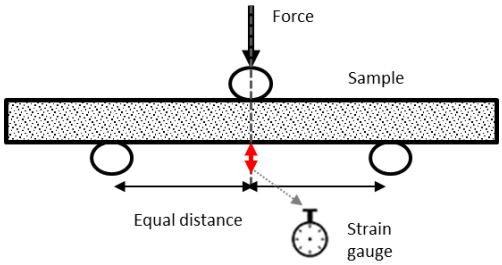

Fig. 5.4 Example of a static E modulus measurement set-up, using the three-point bending test with a stress-strain gauge.

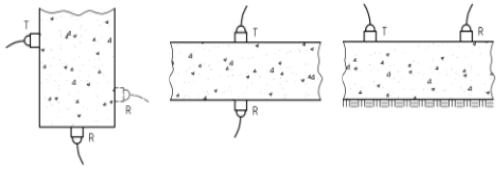

Fig. 5.5 Sketch of the various set-ups possible for transducer and receiver for a dynamic E modulus measurement using the UPV test. Semi-direct transmission (left), direct transmission (middle) and indirect transmission (right). Fig. by EN 14579 (2004)

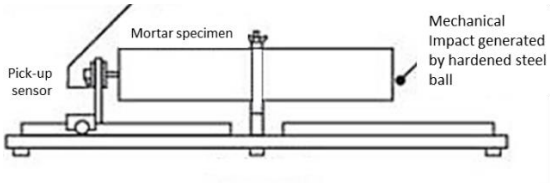

Fig. 5.6 Dynamic E modulus measurements using the RF test in longitudinal mode. The sample can be tested in longitudinal, flexural and torsional vibration.

5.1.3 Conclusion

Porous building materials are reported to demonstrate elastic-plastic behaviour. Elasticity is measured on the material in its elastic region, i.e. the material returns to its initial shape, and a linear proportionality should be present between applied stress and strain. Once a non-linear relation exists between stress and strain, the material would have changed to the plastic region. The dynamic E modulus is determined using only very low strain amplitudes and is therefore used where non-destructive testing is required. The static E modulus is determined using higher strain amplitudes, approaching the maximal stress a brittle material such as mortar can manage, leading to a destructive test. Previous experimental studies and available European standards point out that there is no uniform manner to measure either of the two moduli (static or elastic E modulus) for lime mortars, nor as there is an established (verified and validated) correlation between the static and elastic E modulus.

The dynamic test only measures very small strain amplitudes, while the static E modulus takes into account larger strain amplitudes. Since in built heritage, the building materials might well be solicited on larger strain amplitudes, up to millimetre or even centimetre-scale, static tests are considered more representative for this study. Therefore, the rest of this chapter will be dedicated to the static E modulus of lime mortars.

5.2 Elasticity in lime mortars: experimental study

The static modulus of elasticity was measured on the W/B and B/A lime mortar series described in chapter 2, as well as values from [2], called E14 mortars hereafter. The composition of this mortar series can be found in Appendix 5.1. The static E modulus was calculated using eq.5.2 by performing a compressive strength test. The compressive strength test was set up according to EN 1015-11 (1999), and the elongation was deduced from the change in distance between the loading plates during the compressive strength test, including a correction factor which takes the deformability of the plates into account during the test. Using strain gauges would have allowed to measure strain directly. The recourse to the distance in loading plates was however used, since no strain gauges were present with the sensitivity needed for these low strength materials (e.g. in comparison to concrete).

5.2.1 Sample preparation and testing method

For this test, mortar bars of 40 x 40 x 160 mm^3 were used after approximately 90 days of curing. The bars were dried at 40 °C for minimally 48 h, until constant mass was achieved.

A 300 kN Tira test 28300 testing device was used for these tests. Previous calibration tests confirmed that the precision of this equipment is sufficient to be able to read the variations in small force applied on the samples. Each bar was first subjected to a flexural strength test, after which each half of each bar was placed in a mounting apparatus. The surface area subjected to stress was 40 x 40 mm² (Fig. 5.7). This sequence of tests is generally performed for the testing of mortars, even though it might be remarked that the use of this sequence might have an influence on the final elasticity values, and that testing cubes with the same dimensions as the pressure head would lead to perhaps more deformable mortars. All samples were subjected to a load at a constant rate of 100 N/s. Test duration varied between approximately 60 and 130 s. The static E modulus was defined using eq.5.2 in which σ_x is 0.8 σ_{max} and σ_y is 0.2 σ_{max}. Fig. 5.8 shows the elongation of a lime mortar sample due to the applied force: the behaviour of the mortar remains elastic, that is, the mortar breaks before entering in the plastic domain.

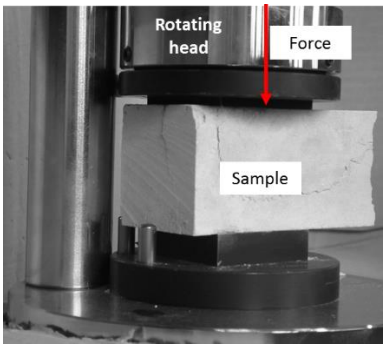

Fig. 5.7 Set-up used for the compressive strength test, using equipment standardized for EN 1015-11 (1999).

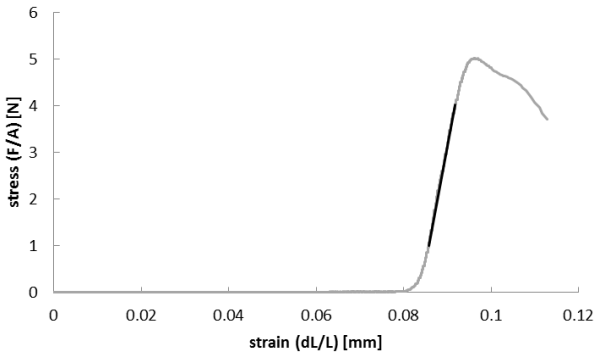

Fig. 5.8 Example of a 5-G-6 lime mortar's strain depending on the stress applied (in grey). The black line represents the distance over which the static modulus of elasticity was calculated.

5.2.2 Results

Around 260 tests on 45 different lime mortar recipes were used to find a relation between the measured E_{stat} value and other parameters which might influence the E modulus. The results were analysed on the influence of binder type, aggregate type and W/B ratio on the measured elasticity. The values for open porosity used for following figures were obtained according to Helium pycnometry as in chapter 3.

The mortars either show elastic-plastic behaviour or elastic behaviour. Fig. 5.9, 5.11 and 5.12 demonstrate representative examples of the stress-strain curves seen on the 260 tests made, the exact elasticity values can be found in Appendix 5.2.

In this experimental campaign, the influence of the binder type, NHL5 or NHL3.5, appears to be minimal. Fig. 5.9 shows that the NHL3.5 mortars seem to support less strain, but a similar or higher level of stress. There is however no difference in deformation behaviour: both binder types created mortars with elastic to elastic-plastic behaviour. Regarding the static E modulus values, mortars from both binder types vary in the same range (Fig. 5.13).

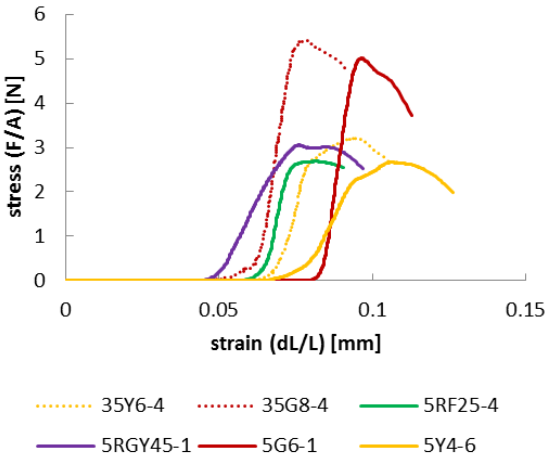

Fig. 5.9 Typical stress-strain curves of NHL mortars tested. Both elastic and elastic-plastic behaviour is visible. The recipe of each mortar can be found in Chapter 2.

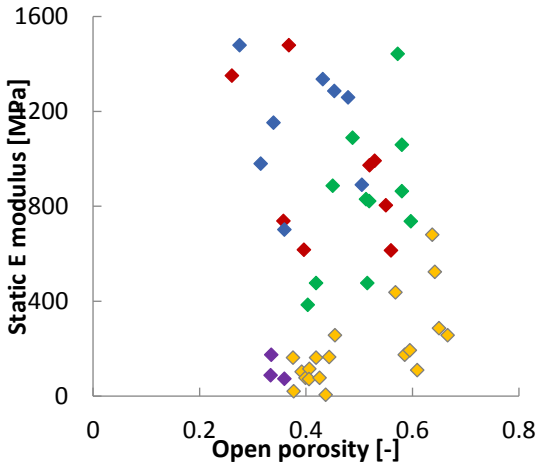

Fig. 5.10 The static E modulus in function of the porosity, per aggregate type. Reference sand (*blue*), Rhin gros (*red*), Rhin fin (*green*), yellow-green (*yellow*), Rhin gros-yellow (*purple*).

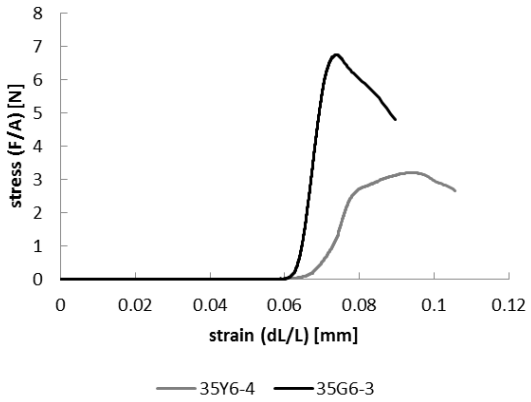

Fig. 5.11 Comparison of representative stress-strain curves for two NHL3.5 mortars with the same spread, one with yellow-green sand (Y), the other Rhin gros sand (G). The G mortar has a higher elasticity and is less deformable than the Y mortar.

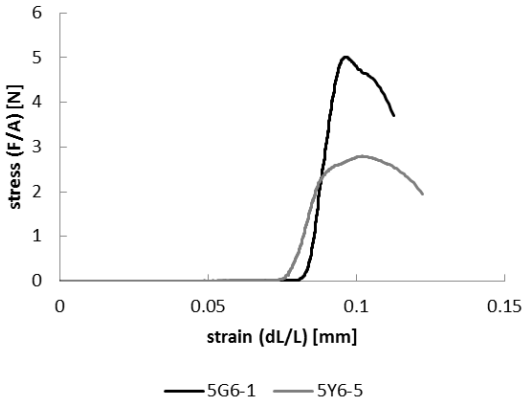

Fig. 5.12 Comparison of representative stress-strain curves for two NHL5 mortars with the same spread, one with yellow-green sand (Y), the other Rhin gros sand (G). The G mortar has a higher elasticity and is less deformable than the Y mortar.

The influence of the grain size distribution is visible when comparing the mortars with the coarser sand with the mortars with the finer sand. In general, the yellow-green mortars (Y) demonstrated more elastic-plastic behaviour, while the Rhin gros (G) mortars demonstrated nearly exclusively

elastic behaviour (Fig. 5.9, 5.11, 5.12). Fig. 5.10 shows the average static E modulus in relation to the average open porosity for each mortar mix. The static E modulus for Yellow-Green (Y) mortars is lower than the Rhin gros (G) mortars: the E_{stat} of 5-Y mortars are on average only 15% of the E_{stat} of 5-G mortars and the E_{stat} of 3.5-Y are on average 33% of the E_{stat} of 3.5-G mortars. For the same porosity, the coarser sand grains thus appear to lead to higher E modulus values, and elastic behaviour, in contrast to the finer sand grains, which appear to lead to lower E modulus values and elastic to elastic-plastic behaviour. This is in consistency with results from Haach et al. (2010) [7].

The static E modulus was also compared to the water-binder ratio (Fig. 5.14). An increase of the W/B ratio appears to decrease the static E modulus non-linearly. Since the W/B ratio can be related to the porosity, a (similar) correlation might be expected between the measured open porosity and the static E modulus. However, as Fig. 5.10 & 5.13 demonstrate, for all 45 mortar mixes made, no definite and clear correlation can be established between porosity and static E modulus.

Also, a linear relation with good correlation (R^2 = 0.86) between compressive strength F_c and E_{stat} is clearly present (Fig. 5.15). The equation of the trend line for the NHL 3.5 mortars does not differ much from the trend line of the NHL 5 mortars (Fig. 5.16-17).

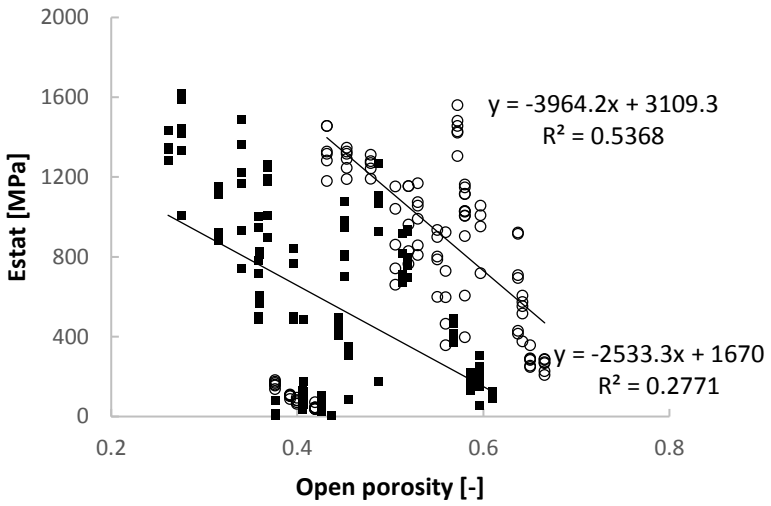

Fig. 5.13 Comparison of the static E modulus for NHL5 (*black square*) and NHL3.5 (*white circle*) mortars in function of their porosity. Note that this is the same graph as Fig. 5.10, only this time mortars are catalogued based on binder type. Even though porosity is higher for NHL3.5 mortars, their elasticity is similar to that of NHL5 mortars. Trend lines show poor correlation for the NHL 5 (R^2=0.53) and for the NHL 3.5 (R^2=0.27).

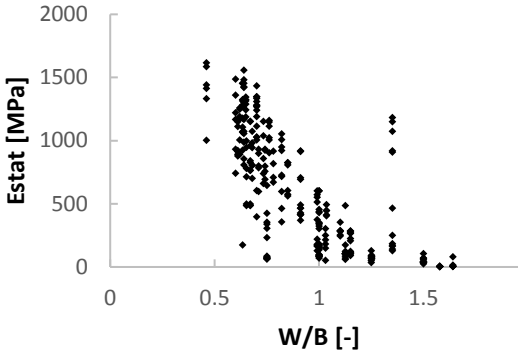

Fig. 5.14 The measured static E modulus in relation to the water-binder ratio of the tested lime mortars

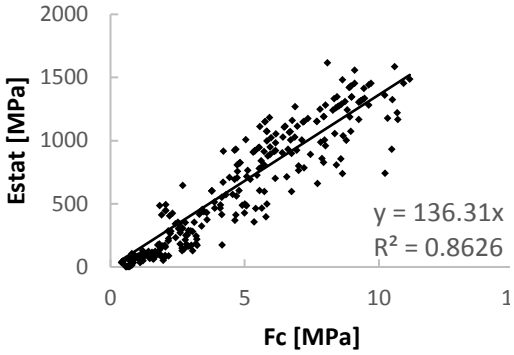

Fig. 5.15 The measured static E modulus in relation to the compressive strength of all tested lime mortars.

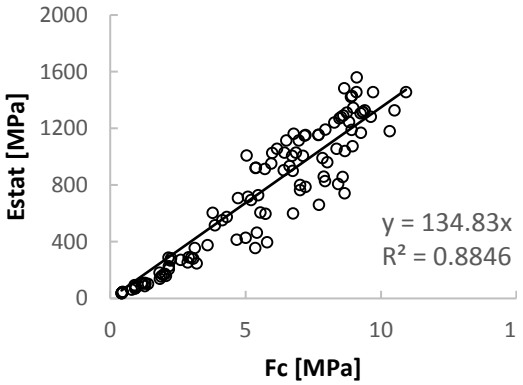

Fig. 5.16 The measured static E modulus in relation to the compressive strength of the NHL 3.5 lime mortars.

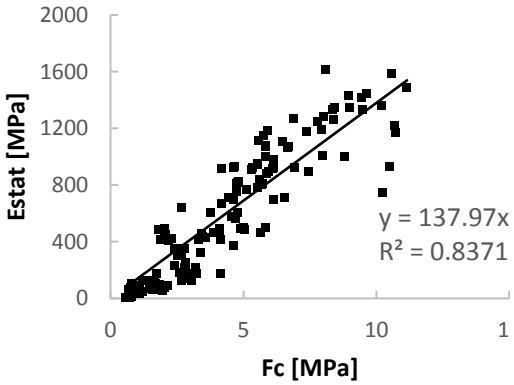

Fig. 5.17 The measured static E modulus in relation to the compressive strength of the NHL 5 lime mortars.

5.2.3 Discussion

All mortars from the experimental campaigns on lime mortars in this study indicated a clear linear trend between the static E modulus and the compressive strength. Furthermore, the static elasticity of NHL5 and NHL 3.5 mortars appeared to be influenced by the components of a mortar: the aggregate grain size distribution, the binder type and the W/B ratio. The W/B ratio increase induced a decrease in mechanical properties. Coarser aggregates increased the static E modulus, a conclusion which was also found influential in the results from Haach et al. (2011) [7]. The influence of the static E modulus by W/B ratio and the grain size distribution might therefore certainly be implemented in possible estimation methods.

Additionally, no clear difference in compressive strength or static elasticity can be made between NHL 5 and NHL 3.5 mortars. Contrary to what might be expected from literature e.g. [5], in this study, the E_{stat} is not dependent of the lime type used. It already became clear in chapter 2 that the two binder types do not have very different volume percentages of reactive minerals, and that their actual resistance is the reverse of what one

might expect. Therefore, a comparative research with other binder types such as NHL2, air lime and cement might still indicate the influence of the binder type on the final elasticity. On top of that, the elastic-plastic behaviour as indicated by other studies was less distinct or present in the mortars of this experimental campaign, which showed mainly elastic behaviour, although testing at lower loading rates would perhaps allow to measure the (small) elastic-plastic behaviour of the hydraulic mortars.

5.3 Estimation of elasticity

5.3.1 Multi-phase models

Some estimation methods for elasticity are multi-phase models [17–20]. These models use the composition of the hardened mortar to estimate the elasticity: the elasticity of each mortar element (aggregates, paste, and voids) is used to estimate the general elasticity of the mortar. The main undeniable difficulty with these models is that they require the elasticity-related properties of every element in the mortar.

Hervé et al. (2010) present a model for cement mortars [21] (Fig. 5.18). They find the properties required for the data input of their model by either estimation or reverse engineering. The paste porosity and ITZ porosity were estimated, the elastic properties of the solid phases were found by reverse engineering and the elastic properties of the sand are taken from literature. More research is considered necessary by the authors of the model to validate it for cement mortars.

In the same line, Nežerka et al. (2011) proposed a model for the estimation of the E modulus for *cocciopesto* mortars, lime mortars with brick dust [17,22]. In this model as well, three phases exist, the lime paste, the aggregates and the ITZ. The volume fraction of each phase (voids, paste, aggregates) has to be known, which is calculated based on geometrical relations [22]. For all phases stiffness, shear modulus as well as their Poisson ratio have to be known (Fig. 5.19).

De Larrard (1999) also suggested an estimation method for the static elasticity for concrete, which is influenced by the ITZ, the paste fraction and the adherence between paste and aggregates [20]. Here as well, the E modulus of both paste and aggregate grain were required.

Both models are based on properties of the composition of the hardened mortar (ITZ, paste, aggregates etc). These models, however, do not link the properties of these components to the raw mortar ingredients. In addition, these models require the modulus of elasticity of each phase to be known separately, or if not, it requires that bulk or shear modulus, and deviatoric stresses must be known. Testing on lime mortars would have to be performed to such an extent that the mechanical properties of each phase, aggregate, lime paste, C-S-H gel, ITZ, can be determined, since the models

described above do not present enough the data to use them for the estimation of the elastic modulus of lime mortars. Both the models of De Larrard (1999) and Hervé et al. (2010) require the calibration of the model with experimental data. Considering the complexity and the variety of tests required, another model was sought to be able to determine the elasticity based on the mortar ingredients.

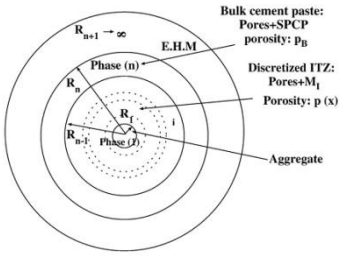

Fig. 5.18 The three-phase model presented by Hervé & Caré (2010) [19].

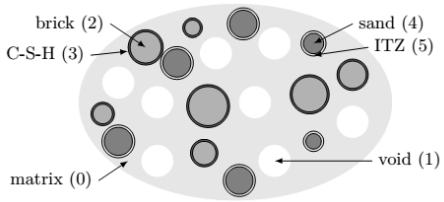

Fig. 5.19 Sketch of the different elements of the mortar incorporated into the model presented by Nežerka et al. (2011) [22].

5.3.2 Estimation methods based on compressive strength

5.3.2.1 Single equation estimations

The most frequently used estimation method for the static modulus of elasticity is the use of a single equation expressing the mortar's compressive strength and, occasionally, a fitting parameter (Table 5.1). Such estimation equations were found mainly in the concrete research field. This method is based on the mortar's compressive strength; a property which can only be measured once the mortar has cured.

From Table 5.1 it becomes clear that all equations proposed are non-linear. The relation between compressive strength and elasticity observed during the experimental campaign was however clearly linear. Nevertheless, the equations were tested for comparison, by using the measured compressive strength in the equation to estimate elasticity. The estimated and measured elasticity are compared in Fig. 5.20. Every estimated elasticity value was higher than the actual measured elasticity. The equations therefore overestimate elasticity.

Table 5.1. Following equations are proposed to estimate the static modulus of elasticity [MPa] for concrete, from [15], with F_c the compressive strength [MPa] and γ the specific weight [kg/m³].

$E_{stat} = 22000\ (\frac{F_c}{10})^{1/3}$	From CEB-FIP, for normal strength concrete and high strength concrete
$E_{stat} = 21000\ \left(\frac{\gamma}{2300}\right)^{1.5}\ (\frac{F_c}{20})^{1/2}$	From Architectural Institute of Japan, for normal strength concrete
$E_{stat} = k_1 k_2 1.486 * 10^{-3}\ \gamma^2 {F_c}^{1/3}$ k1 for coarse aggregate, k_2 for mineral admixtures (table in [15])	From Noguchi et al., using regression analysis on Normal Strength Concrete and High SC

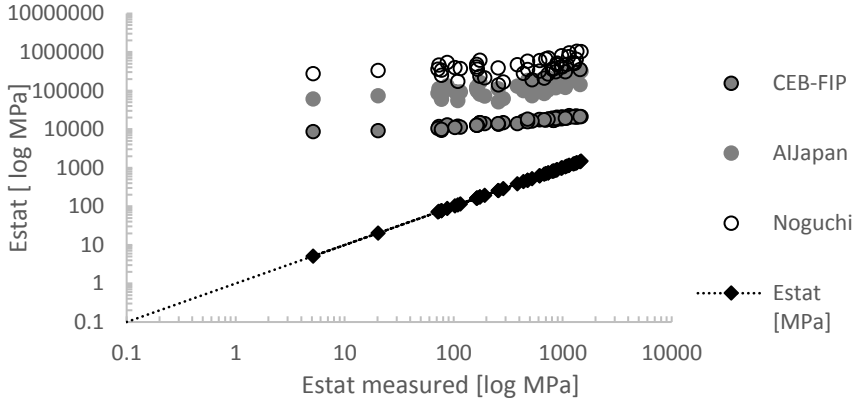

Fig. 5.20 Static modulus of elasticity for the studied lime mortars (see section 5.2) in comparison with the estimated elasticity, calculated using the measured compressive strength.

5.3.2.2 Hybrid method of De Larrard

The work of De Larrard [20] contains another estimation method, dedicated to compressive strength. This estimation is based on the mortar composition and behaviour. De Larrard found that, for his concrete samples, the static modulus of elasticity is influenced by the same phenomena which influence his compressive strength model, i.e. ITZ, paste, adherence between paste and aggregates. He also established following linear correlation between E_{matrix} and $F_{c,concrete}$:

$$E_{matrix} = 226\ F_{c,concrete} \qquad \text{(eq.5.4)}$$

This equation between elasticity and compressive strength approaches the linear relation found between the static elasticity and compressive strength of the studied lime mortars, i.e. $E_{stat}=136.31*F_c$. Since the compressive strength estimation of De Larrard is based on the raw ingredients of the mortar, and the experimental campaign in 5.2.2 established a correlation between static elasticity and compressive strength, the De Larrard method will be explained in more detail below.

The compressive strength estimation proposed by De Larrard gathers and unifies concepts that were proposed by numerous authors before, all

continuing on the theories developed by Feret and Bolomey [20]. At present, the method of De Larrard is widely used, e.g. [23–27] and was also implemented in the BetonLab software, which is used by concrete producers [28]. In practice, it can be seen as complementary with the Dreux-Gorisse method [29]: the Dreux-Gorisse method established the concrete recipe corresponding to a given strength value while the De Larrard method estimates the strength value corresponding to a given concrete recipe.

De Larrard considers the aggregate packing and the nature of the matrix as determining for the compressive strength of the mortar, and pays particular attention to the B/A ratio and W/B ratio, the type of binder and the shape and nature of the aggregates. Conceptually, the De Larrard model considers concrete as a paste (cement, water and air) surrounded by aggregate grains.

A preliminary study on cement mortars using Betonlab software shows that this estimation model estimated the compressive strength of the cement mortars acceptably with an average error of 6.9% (Appendix 5.3).

De Larrard's method relies on data which can be known or measured prior to mortar curing. The effective strength of the binder is required and can be determined experimentally [30] and a parameter depending on the origin of the aggregate is included [20]. The components can be characterized by their grain size distribution through $S_{<80\mu m}$ and D_{max}. In this study of lime mortars, a binary mixture will be used, since the particles in the mortar mix can be subdivided in fines (< 80 µm) and sand (80 µm -2 mm). $S_{<80\mu m}$ is as such the volume of all binder and fine sand grains smaller than 80 µm.

The calculations presented in eq.5.5.1-11 were derived from De Larrard (1999) and adapted to mortars where necessary, e.g. for the definition of γ (eq.5.5.10-11) [20].

$$F_c = p_{aggregate}\, F_{c,matrix} \qquad \text{(eq.5.5.1)}$$

The compressive strength of the mortar F_c [MPa] according to a compression on prismatic samples is based on the matrix compressive strength $F_{c,matrix}$ [MPa], and p [-], an adherence factor based on the shape and type of aggregate which can be established empirically through a method by De Larrard [20].

$$F_{c,matrix} = 11.4\, R_c \left(\frac{V_b}{V_b+V_w+V_a}\right)^{2.85} MPT^{0.13} \qquad \text{(eq.5.5.2)}$$

The compressive strength of the matrix $F_{c,matrix}$ [MPa] is calculated using R_c [MPa], the real resistance of the used binder. V_b, V_a, V_w are the volume ratios of the binder, mixed-in air and water in the mortar respectively [-].

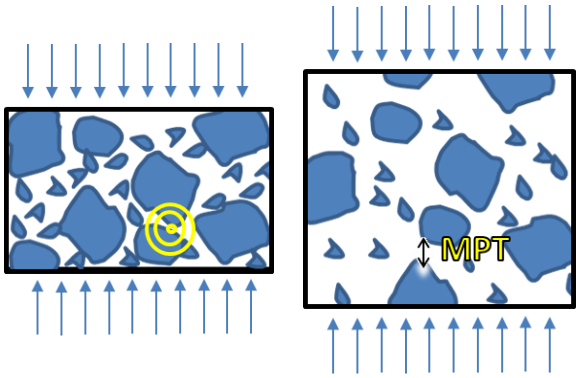

Fig. 5.21 A Dry mix of particles subjected to uniaxial compression. B Mortar seen as a dry mix of particles injected with binder paste. De Larrard assumes the network of gravity centers of particles is uniformly dilated, so that MPT indicates the largest interval between two large grains which were previously in contact. Figure adapted from [20].

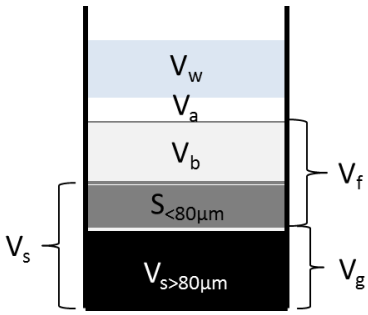

Fig. 5.22 Total volume of components according to De Larrard's estimation method. The volume of sand can be subdivided into a volume of fines, and a volume of coarser grains.

MPT is the maximum paste thickness [mm]. The matrix' compressive strength depends as such on the actual resistance of the binder, the binder content in the paste and the Maximum Paste Thickness (MPT) around the grains (Fig. 5.18-19). The 2.85 value in eq.5.5.2 takes into account the volume increase of the binder paste through hydration reactions, see [20]. The constants of this and following equations were defined based on various experimental studies. It is assumed that these constants can also be used in this study.

$$MPT = D_{max}\left(\sqrt[3]{\frac{\gamma}{V_{g,m}}} - 1\right) \qquad \text{(eq.5.5.3)}$$

MPT, the maximum paste thickness, is used to express the concept that the larger (aggregate) grains have the tendency to support the maximal force, and as such can be considered as hard nods in a rather supple environment, which is composed of a porous packing of smaller grains. When packing is random, some larger, more resistant grains can be in contact with each other, and in these contact points the largest forces occur. If this grain packing is filled up with paste, a larger volume than the available porosity of the dry packing is present. The paste between two large grains is thus very likely to be compressed when under pressure. The distance between the two grains is the maximal paste thickness MPT, because it represents the largest interval which exists between these particles, in a process of constant dilation. The maximal grain size D_{max} [mm] is reported to influence the compressive strength of mortars: an increase of D_{max} decreases water demand, and can therefore increase compressive strength, while, if the W/B ratio should be kept constant, the compressive strength is reported to decrease [31]. γ is the virtual packing density of the aggregate [-], $V_{g,\,m}$ the volume percentage of the largest grains in a mortar volume unit [-].

The *real* packing densities of sand and binder can be measured according to a specific testing method from Laboratoire Central des Ponts et Chaussées (LCPC), involving a tube filled with aggregate subjected to shocks and calibrated according to a specific compacting index K.I. [32].

$$\phi = \frac{4\, m_g}{\pi\, \rho_g\, D_{tube}^2 h_{tube}} \qquad \text{(eq.5.5.4)}$$

The real packing density Φ of the grains [-] depends on the mass of the grains tested, m_g [kg], the skeletal density of the grains ρ_g [kg/m³], the diameter D_{tube} [m] and the height of the tube after the final test h_{tube} [m].

The residual packing density for each sand and binder can as such be calculated, β [-], with K the specific compacting index set for this test at 9 [32].

$$\beta = \phi \left(1 + \frac{1}{K}\right) \qquad \text{(eq.5.5.5)}$$

The virtual packing density γ is the maximal packing density which can be obtained by a given mixture. For a mixture of spherical grains with the same size, this would be $\pi/(3\sqrt{2})$ or 0.74048. If we assume the mixture of sand and binder is a binary mixture of fines and sand, without grain interaction, i.e. the local arrangement of a group of grains of one size is not perturbed by the presence of grains from the other grain size. In this mixture, the binder and a part of the sand are fines, which behave differently in a mixture than the larger grains. Two new volumes [-] can be defined, one for each grain size type: V_f for the fines in the mixture and V_g for the coarser grains in the mixture, with $V_f + V_g = 1$. With V_b the binder volume, V_s the sand volume and $S_{<80\mu m}$ the sand volume smaller than 80 µm, all [-] (Fig. 5.22).

$$V_f = \frac{V_b + V_s\, S_{<80\mu m}}{(V_b + V_s)} \qquad \text{(eq.5.5.6)}$$

$$V_g = \frac{V_s\, (1 - S_{<80\mu m})}{(V_b + V_s)} \qquad \text{(eq.5.5.7)}$$

The residual packing density previously established per sand and binder type can now be divided into a β_f and β_g, residual packing density of the fines and of the coarser grains respectively.

$$\beta_f = \frac{\beta_b V_b + \beta_s V_s\, S_{<80\mu m}}{(V_b + V_s)} \qquad \text{(eq.5.5.8)}$$

$$\beta_g = \frac{\beta_s\, V_s\, (1 - S_{<80\mu m})}{(V_b + V_s)} \qquad \text{(eq.5.5.9)}$$

Now, all elements are assembled to define the virtual packing density γ. Since there is no interaction between the grain classes, the most dominant grain size is assumed to control the behaviour of the mix.

If $V_f < V_g$, then

$$\gamma = \frac{\beta_g}{1-V_f} \quad \text{(eq.5.5.10)}$$

If $V_f > V_g$, then

$$\gamma = \frac{\beta_f}{1-V_g(1-\beta_f)} \quad \text{(eq.5.5.11)}$$

The volume of air, V_a, as used in eq. 5.5.2, is the air introduced into a mortar solely by the action of mixing the ingredients. It does not concern the voids created due to evaporation of water, nor due to the addition of any air-entraining agent. According to De Larrard, a certain volume of air remains trapped after mixing in the spaces between the aggregates, and forms air bulbs. Once the mortar is placed in a mould and vibrated, each air bulb individually ascends, but De Larrard assumes that small air bulbs remain trapped. De Larrard states that sand would favour the entrapment of air bulbs, since this grain size class has both a critical grain size and an elevated specific surface area. The binder is a fine, and has therefore a high specific surface area, but no critical grain size.

There are some side notes to be made on this air volume concept. In reality, a volume of voids into a mortar shall decrease the compressive strength. The resistance of a mortar at 90 days will be more influenced by the volume of voids present in the hardened mortar, but this appears to be represented by water volume V_w in the denominator of eq. 5.5.2. De Larrard introduces the mixed-in air volume, but this appears only important when the mortar is in a fresh state (uncured). In addition, the estimation of the mixed-in air volume by De Larrard includes the estimation of the slump and the shear strength of the fresh mortar, two elements which cannot be measured and should thus be estimated.

A preliminary study was performed in order to know whether the mixed-in air volume would influence the final compressive strength. Results can be found in Appendix 5.4. Excluding the V_a of the estimation equation for the matrix' compressive strength (eq.5.5.2) does lead to a higher estimated compressive strength, which is more important for small estimated F_c values, on average 15% higher, but lower for the higher estimated F_c values (on average 8%).

Due to the limited effect of V_a on the compressive strength, and since its significance for the final cured mortar raises some questions, it was decided not to use it in the experimental study.

5.3.3 Validity of compressive strength estimation for lime mortars

The method proposed by De Larrard [20], given in eq.5.5.1-11, was used to estimate the compressive strength of the lime mortar series W/B, B/A and E14.

The first step was the definition of every parameter required for the estimation. The apparent and skeletal densities for every sand and binder were determined through pycnometry (chapter 3). The real packing density was determined through the LCPC test, and the residual packing density was calculated based on the real packing density (eq. 5.5.5). The grain size distribution of each sand was used to determine the maximal grain size diameter, the grain size at 50% passing and the volume percent smaller than 80 µm. The adherence factor p was adapted based on the type of sand [20]. The real resistance of each binder type was determined in chapter 2. For this validation, the compressive strength value after 90 days of curing was used, the hardening reaction is more complete than after 28 days and thus more representative for the real resistance of the binder. All parameters used in this validity test are given in Table 5.2.

Table 5.2. Table representing the various parameters for each sand type and binder used. The real packing density of the reference sand was not measured, and therefore an estimated value of 0.6 was considered.

	Reference	Rhin gros	Rhin fin	Yellow	Green	NHL5	NHL3.5
ρ_{app} [kg/m³]	1728.2	1607	1462.3	1325.5	1368.6	780.1	759.3
Φ [-]	0.600	0.655	0.698	0.551	0.580	0.537	0.537
β [-]	0.667	0.728	0.776	0.612	0.644	0.483	0.483
D_{max} [mm]	1.987	4.002	1.408	3.622	2.683	-	-
$S_{80µm}$ [%]	0.502	0.100	0.067	0.333	3.619	-	-
p [-]	0.291	0.216	0.230	0.165	0.170	-	-
$R_{c,\ 90}$ [MPa]	-	-	-	-	-	9.14	10.07

The estimated compressive strength for each mortar mix is presented in Fig.5.23 (the values can be found in Appendix 5.2). Mortars from the NHL 3.5 W/B series had their compressive strength generally overestimated by 8.9% on average. The NHL 5 W/B mortar series' compressive strength were generally overestimated by on average 18.5%. The mortars from the B/A series or E14 had a low measured compressive strength: the estimation on these Fc values is therefore overestimated by 57.2% on average (for B/A mortars), and 67.7% (for E14 mortars). The mortars' compressive strength is generally overestimated (Fig.5.23).

Based on the estimation of the compressive strength of each mortar mix, the static E modulus was estimated according to the function $E_{stat} = F_{c\ mortar}$ *136.31 which was established in the experimental campaign (see 5.2). Fig.5.24 shows the results of the estimation of elasticity in relation to the actual measured static elasticity. Logically, the trends seen in the compressive strength estimation also appear here, the estimation for the W/B mortar series perform relatively better with an overestimation of 17.1% for NHL 3.5 mortars and 38.1% for NHL 5 mortars on average. The elasticity

for the B/A mortar series and from the E14 campaign are overestimated with on average 212% for B/A and 200 % for E14 mortars. The mortars with low elasticity are generally overestimated, the mortars with higher elasticity appear to be underestimated in general.

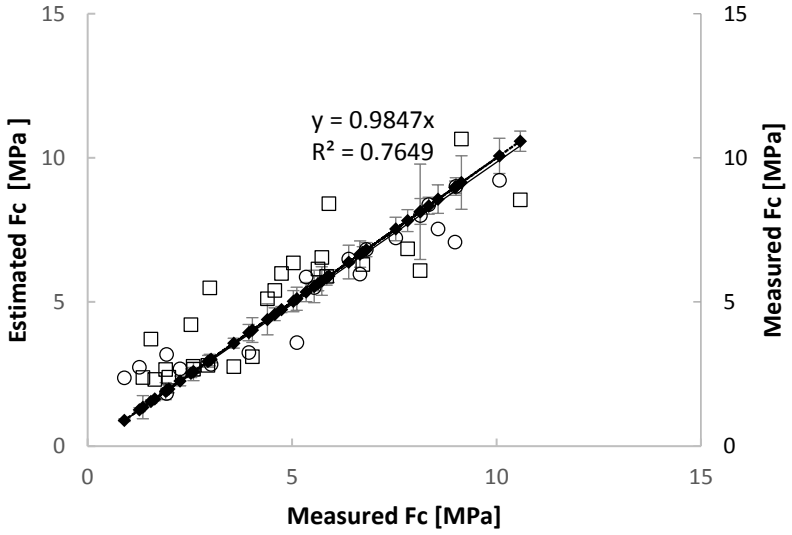

Fig. 5.23 The estimated values in relation with the measured mortar values for compressive strength. *Square* for estimated NHL 5 values, *circle* for estimated NHL 3.5 values, *filled diamond* for all measured values. The standard deviation of the measured compressive strength is indicated as grey error bars. The trend line and equation correspond to all estimated values.

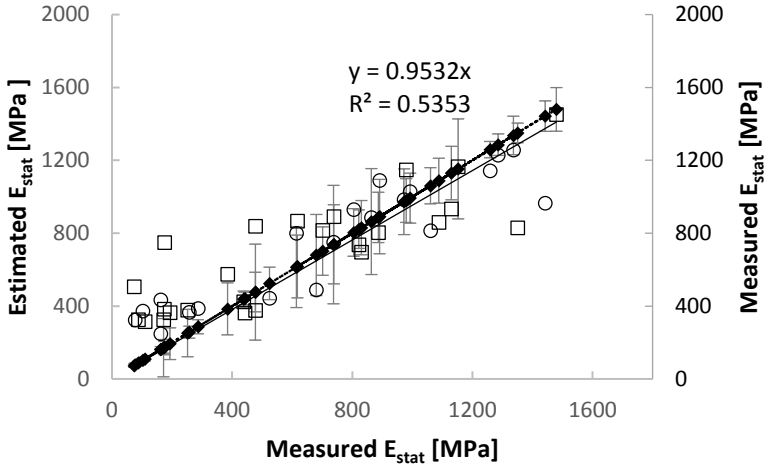

Fig. 5.24 The estimated values in relation with the measured mortar values for static elasticity, based on the estimation of compressive strength, $E_{stat} = F_{c\ m,cube} * 136.31$. *Square* for estimated NHL 5 values, *circle* for estimated NHL 3.5 values, *filled diamond* for all measured values. The trend line and equation correspond to all estimated values.

5.4 Conclusion

Lime mortars demonstrate elastic to elastic-plastic behaviour, due to the internal pore-collapse mechanism. Lime mortars would thus allow more deformability before actual collapse.

The elasticity of the mortars in this study was measured through the static E modulus, which measure the range of strain amplitudes that are interesting for building materials. A large experimental campaign was performed, and indicated that the mortar components can be related to the measured E modulus. As such, an increase of the aggregate grain size increased the static E modulus of lime mortars, while an increase of W/B ratio decreased the static E modulus. The influence of binder type could however not clearly be determined, but this might be due to the fact that both binders used are closely related in terms of real resistance. Therefore, the actual resistance of the binders is considered more important than the class they belong to. No clear correlation was found between the measured open porosity and the static E modulus. In addition, the experimental campaign showed that a good linear correlation could be established between compressive strength and static E modulus for the lime mortars in this experimental campaign.

Conclusively, the experimental campaign gave representative handles which were used for the estimation of elasticity. This elasticity estimation method was found by combining the experimental linear correlation and the estimation method for compressive strength, both adapted from De Larrard. The method of De Larrard was found to combine sufficient properties from mortar components in order to estimate the compressive strength. The method is more correct for higher-strength mortars than low-strength mortars. The estimation method for static E modulus presented here for the W/B series approaches the error range of the estimation model proposed by Hervé et al. (2010), which varies between 0.7 and 11% [21]. In order to find the reason for the different behaviour of both E14 and B/A mortars, the ageing and curing conditions in relation to the measured E modulus might indicate additional elements which have not been explored until now.

The method proposed here is a rather simplified method, but considering that there were no other valid options to estimate the elasticity for lime mortars, results are promising. The De Larrard method as used in this study is entirely based on properties of the mortar components. Moreover, elements from the De Larrard method which were thought to be too adapted to concrete mortars, were left aside. Any future research can thus build on this ‘simple’ model and add the elements which are then deemed necessary. Another advantage of this simplified model is that it is easily encoded into an algorithm, an argument not to be left aside in this study. However, its more simplified approach may also be its largest disadvantage: it might be that the model cannot be improved significantly. Results might then remain

a rough estimation. More research with other lime mortars is therefore required.

It would be more difficult to find the correct input data for other estimation methods such as the method by Nežerka et al. (2011) where the estimation method requires elasticity-related property values for every mortar element (bulk paste, ITZ, aggregate). One should already start using an ITZ volume estimation (such as discussed in chapter 3) in order to have an estimation aggregate, ITZ and bulk paste volume. Also porosity should be estimated. In addition, the elasticity-related property values should be estimated or deduced from experimental campaigns. The combination of errors on the estimation of these various elements might prohibit a good estimation of, finally, the elasticity. Such an approach seemed therefore less advisable.

Another approach might be the use of a 3D model where a simulation of the elasticity is performed upon. For this type of models, the same type of restrictions are applicable (the establishment of the elasticity related property values for every mortar component), and would also require the modelling of the various mortar elements as a 3D structure. Neither of these elements make this method more advantageous for use in this optimisation research.

In the future, research concerning a relationship between static E moduli and dynamic E moduli might provide additional and interesting information for lime mortars used for conservation purposes.

Bibliography

[1] Isebaert A, De Boever W, Descamps F, Dils J, Dumon M, De Schutter G, et al. Pore-related properties of natural hydraulic lime mortars: an experimental study. Mater Struct 2015. doi:10.1617/s11527-015-0684-5.

[2] Ecrepont S. Compatibilité des mortiers de restauration: contribution à l'étude de la migration des fluides. University of Mons, 2014.

[3] Isebaert A, De Boever W, Cnudde V, Van Parys L. An empirical method for the estimation of permeability in natural hydraulic lime mortars. Mater Struct 2016:1–13. doi:10.1617/s11527-016-0829-1.

[4] Bazergui A, Bui-Quoc T, Biron A, McIntyre G, Laberge C. Résistance des Matériaux. 3rd ed. Montréal: Presses internationales Polytechnique; 2002.

[5] Costigan A, Pavía S. Influence of the mechanical properties of lime mortar on the strength of brick masonry. In: Válek J, Hughes JJ, Groot CJWP, editors. Hist. Mortars. Charact. Assessment, Repair, Dordrecht: Springer Netherlands; 2012, p. 359–72. doi:10.1007/978-94-007-4635-0.

[6] Cizer O, Balen K Van, Gemert D Van, Elsen J. Blended lime–cement mortars for conservation purposes: microstructure and strength development. 6th Int. Conf. Struct. Anal. Hist. Constr. Preserv. Saf. Significance, Bath: CRC Press, Taylor & Francis Group; 2008, p. vol2 : 965–72.

[7] Haach VG, Vasconcelos G, Lourenço PB. Influence of aggregates grading and water/cement ratio in workability and hardened properties of mortars. Constr Build

Mater 2011;25:2980–7. doi:10.1016/j.conbuildmat.2010.11.011.
[8] Hayen R, van Balen K, Van Gemert D. The mechanical behaviour of mortars in triaxial compression. In: Roca P, Oflate E, editors. Int. Congr. Arch Bridg. ARCH'04, Barcelona: CIMNE; 2004, p. 1–10.
[9] Silva BA, Ferreira Pinto AP, Gomes A. Influence of natural hydraulic lime content on the properties of aerial lime-based mortars. Constr Build Mater 2014;72:208–18. doi:10.1016/j.conbuildmat.2014.09.010.
[10] Deniz S, Erdoğan S. Prediction of Elastic Moduli Development of Cement Mortars Using Early-age Measurements. J Mater Civ Eng 2014:1–9. doi:10.1061/(ASCE)MT.1943-5533.0001025.
[11] Nežerka V, Slížková Z, Tesárek P, Plachý T, Frankeová D, Petráňová V. Comprehensive study on mechanical properties of lime-based pastes with additions of metakaolin and brick dust. Cem Concr Res 2014;64:17–29. doi:10.1016/j.cemconres.2014.06.006.
[12] Frey F. Analyse des structures at milieux continus: Mécanique des structures. 2nd ed. Lausanne: Presses polytechniques et universitaires romandes; 2006.
[13] Yale DP, Nieto JA, Austin SP. The effect of cementation on the static and dynamic mechanical properties of the Rotliegendes sandstone. In: Daemen JJK, Schulz RA, editors. Proc. 35th U.S. Symp. Rock Mech., Balkema; 1995, p. 169–75.
[14] Ball RJ, El-Turki A, Allen GC. Influence of carbonation on the load dependent deformation of hydraulic lime mortars. Mater Sci Eng A 2011;528:3193–9. doi:10.1016/j.msea.2010.12.070.
[15] Noguchi T, Tomosawa F. A Practical Equation for Elastic Modulus of Concrete. ACI Struct … 2009.
[16] Komloš K, Popovics S, Nürnbergerová T, Babál B, Popovics JS. Ultrasonic pulse velocity test of concrete properties as specified in various standards. Cem Concr Compos 1996;18:357–64. doi:10.1016/0958-9465(96)00026-1.
[17] Nežerka V. Micromechanics-Based Models of Cocciopesto Mortars. Czech Technical University Prague, 2011.
[18] Nežerka V, Němeček J, Slížková Z, Tesárek P. Investigation of Crushed Brick-Matrix Interface in Lime-Based Ancient Mortar by Microscopy and Nanoindentation. Cem Concr Compos 2014. doi:10.1016/j.cemconcomp.2014.07.023.
[19] Caré S, Hervé E. Application of a n-Phase Model to the Diffusion Coefficient of Chloride in Mortar. Transp Porous Media 2004;56:119–35. doi:10.1023/B:TIPM.0000021730.34756.40.
[20] Larrard F de. Concrete Mixture Proportioning: A Scientific Approach. London: E & FN Spon; 1999.
[21] Herve E, Care S, Seguin JP. Influence of the porosity gradient in cement paste matrix on the mechanical behavior of mortar. Cem Concr Res 2010;40:1060–71. doi:10.1016/j.cemconres.2010.02.010.
[22] Nežerka V, Zeman J. A micromechanics-based model for stiffness and strength estimation of cocciopesto mortars. Acta Polytech 2012;52:29–37.
[23] Kooiman AG. Modelling Steel Fibre Reinforced Concrete for Structural Design. TU Delft, Delft University of Technology, 2000.
[24] Ji T, Lin T, Lin X. A concrete mix proportion design algorithm based on artificial neural networks. Cem Concr Res 2006;36:1399–408. doi:10.1016/j.cemconres.2006.01.009.
[25] Domone PL. A review of the hardened mechanical properties of self-compacting concrete. Cem Concr Compos 2007;29:1–12. doi:10.1016/j.cemconcomp.2006.07.010.
[26] Habert G, Roussel N. Study of two concrete mix-design strategies to reach carbon mitigation objectives. Cem Concr Compos 2009;31:397–402. doi:10.1016/j.cemconcomp.2009.04.001.
[27] Nozahic V, Amziane S, Torrent G, Saïdi K, De Baynast H. Design of green concrete made of plant-derived aggregates and a pumice–lime binder. Cem Concr Compos 2012;34:231–41. doi:10.1016/j.cemconcomp.2011.09.002.

[28] Sedran T, de Larrard F. Betonlab Pro2: Computer-aided mix-design 2000.
[29] Dreux G, Gorisse F. Contribution à l'études statistique des contrôles de béton. Ann L'institut Tech Du Bâtiment Des Trav Publics 1973;302.
[30] EN 196-1: Methods of testing cement- Part 1: Determination of strength. 2005.
[31] Sedran T, de Larrard F. Une nouvelle approche de la formulation des betons. Ann Du Bâtiment Des Trav Publics 1999.
[32] Ledee F, de Larrard F, Sedran T. Essai de compacités des fractions granulaires à la table à secousses: Mode operatoire Méthode d'essai n°61. Paris: 2004.

Chapter 6 Optimisation of compatible mortar development

The previous chapters have explained how the three considered compatibility properties can be reasonably estimated. This chapter describes the system that will gather the estimation functions and will finally present mortar recipes close to the desired properties. The first subsections of the chapter discuss what method is used for the creation of mortar recipes close to the properties the user would like to have. These subsections are based on the conference paper 'Compatible interventions on stone systems: an optimisation problem' [1]. Accordingly, following subsections explain more thoroughly the effective functioning and practical set-up of the algorithm.

In the last subsection a validation of the system is proposed by testing the stability of the system: for the same demanded properties, multiple runs were performed, after which the proposed mortar recipes were compared on their fitness and composition.

6.1 Multi-Objective Optimisation

6.1.1 Introduction

Optimisation can be defined as an act, process or methodology that makes a system, concept or decision, as effective, well-functioning as possible [2]. Multi-objective optimisation is more specific and can best be explained by use of an example, such as the search for a route between two points in Brussels. Various means of transportation are available between the Brussels Central train station and Brussels National Airport, which all take a certain time. If duration of the trip is the only objective, then the train would be the best choice. However, this is not a single objective problem. The train may be the fastest, but as a user, you are limited by the train's frequency and timetable. In contrast to the train, you may choose to go by bike. Consequently, this trip will take longer, but you can choose to leave whenever you want. Between these two extremities, there are various other solutions, which are faster than the bike, but are still bound by a certain timetable (bus, tram) (Fig.6.1). Ideally, the gain in flexibility is related to the extent of sacrifice in duration. An optimal set of solutions can thus be

imagined, where a gain in one objective induces a sacrifice in the other objective. This optimal set of solutions in optimisation is commonly denoted as a Pareto front, and are in this example non-dominated, i.e. no other solution is better than the other [3]. As Deb (2001) explains, where there is more than one objective for the same problem, not one of the solutions proposed will be best with respect to both objectives [4]. In multi-objective problems, a set of optimal solutions are thus equally important. More information is required to single out one solution of the whole set of solutions on this curve between the two extremes. If we had remained with only one single objective, e.g. the duration, only one solution would be the optimal one.

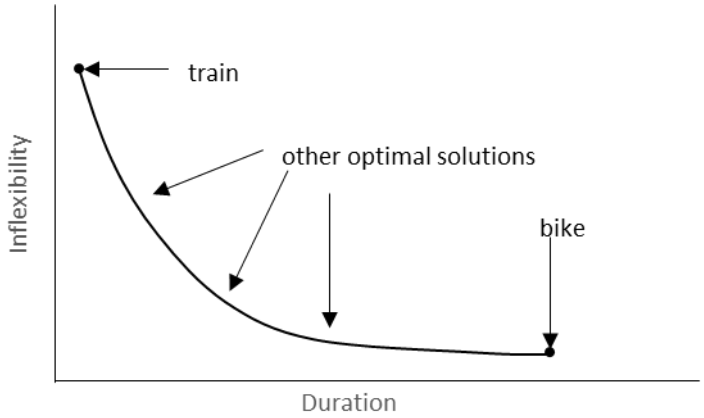

Fig.6.1 Example of a Pareto front: graph representing two minimising objectives, flexibility and duration, to optimise a trajectory between two points.

Previous chapters made clear that a repair mortar is made out of different components (binder, water, aggregates), and that the properties that make out a compatible, durable intervention are influenced by these various components and the ratios used. Based on the previous chapters, the properties determining compatibility of a repair mortar can be estimated.

Chapter 1 indicated that some variability is possible for each property: a certain tolerance can be allowed, which would make it easier to find a compatible mortar. Taking into account the objectives with their respective tolerance range, the influence of the component ratios and the availability of various components, the number of possible combinations to make a mortar is limited by these constraints. The mortar should still be workable, e.g. a sufficient W/B is necessary. This is a constraint to the feasible solutions. Therefore the search space in the optimisation of mortar development is divided by the constraints into feasible and infeasible regions [4].

The development of compatible mortars is determined by the various compatibility properties, which can be looked upon as the objectives which need to be obtained, and by answering to various (practical) limitations, which can be seen as the constraints. As such, the development of compatible mortars can be considered a *constrained optimisation problem*, where mortar recipes could be generated by a system, which calculates their

estimated properties and compares these values with the targets, i.e. desired properties. As such, the user of the entire process can use these suggested mortar recipes for the repair of a natural stone. Notice that the process set up here is developed such that it offers help to the user, by suggesting mortar recipes, estimated to have compatible properties. The judgement of which mortar to use would still be up to the user.

By using such an aid in the optimisation of mortar development, the process and costs of development could be reduced significantly. Previous chapters 3 to 5 proved that the estimation methods for permeability, colour and elasticity are not determined by exactly the same set of parameters, e.g. the permeability estimation is influenced by the reactive components of the binder, an aspect of the binder not taken into account by any of the other property estimation methods. The corresponding three objective functions can therefore not be merged into one, making the problem a *multi-objective constrained optimisation problem*.

6.1.2 Interpretation of the multi-objective optimisation problem

The aim of the system is to produce a set of Pareto-optimal solutions the user can choose from. Intuitively, the user of this system of database linked to an optimised mortar development would like to have the recipes of the mortars optimised to specific targets. This user would like to know exactly the type and the quantity of sand, binder and water he should add to obtain a mortar with these (estimated) properties. Therefore, the choice was made to optimise the mortar recipes in which the type of sands (nature, origin, granularity…), the type of binder (nature, hardening scheme, and strength class) as well as the relative quantities of sands, binders and water will constitute the design variables for the optimisation problem.

The maximal number of different sands and different binders that may be mixed for one recipe are parameters: it is a general condition that might be modified by the programmer of the system. Figure 6.2 illustrates the organisation of 6 design variables defining one string, which is in this specific problem of mortar development an actual mortar recipe. Such a recipe expresses a configuration maximally mixing two different aggregates (sand #1 S_1 and #2 S_2) from a database that could count a number of sands limited to 8 in the present configuration (3 bits), with one single binder (B) from a database that could count a number of binders limited to 2 in the present configuration (1 bits). Larger databases can be created in the future, since the coding can be easily modified to 4 or even 5 bits. Knowing the volume of binder V_b and water V_w in 1 m^3 allows deducing the global quantity of sand while the X_s ratio expresses the respective quantities of sand #1 and #2.

The *quantity* of each constituent has to be represented as a continuous variable (to be chosen from an interval of real numbers), while the *type* of aggregates (allocating 2 bits permits a 4-sand database) and binder

(allocating 1 bits permits a 2-binder database) is best characterized as a discrete variable (to be chosen from a permitted set of discrete values).

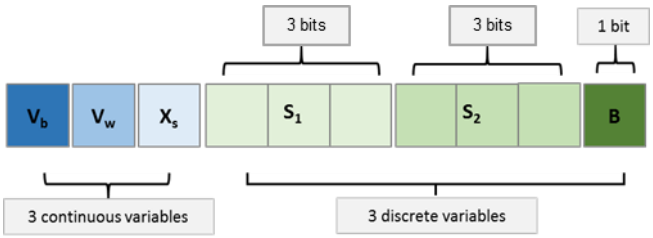

Fig. 6.2 Design variables defining one string, i.e. a mortar recipe, where V is volume in real variables, and S and B indicate the type of sands and binder used in discrete variables.

This intuitive approach helps the user to be conscious of the actual materials used along the entire process: the set of design variables is directly related to reality. As a consequence, the expression of constraints may be directly inherited from European standards for mixing ratios. For example, to achieve a good workability, a first rough limitation can be set on the W/B ratio, which is influenced by the types of binder and aggregates used [11]. These will be very coarse limits, so as to not overconstrain the feasible solutions. If required, the user can eliminate himself mortar recipes based on a more restrained W/B ratio boundary set after the algorithm has run. Nevertheless, introducing too many constraints should be avoided in the algorithm, in order to avoid the problem of it becoming over-constrained, leaving no more degrees of freedom for optimisation [16].

Table 6.1. Tolerance ranges allowed for the three targets. Both permeability and elasticity values are represented in relative percentage of the stone's property, while the colour is given in absolute difference. A specific mortar property after 1 year is specified for the elasticity, while the same tolerance range would then still be applicable for the other two objectives.

		Permeability tolerance [%]	ΔE* tolerance [-]	E_{stat} tolerance [%]
Tolerance	Min	50	0	20
	Max	100	5	100
Requirement	1 year	-	-	60

The objectives or targets in this case, are the desired properties for the mortar the user would like to have. After the system has run, the user can apply the tolerance ranges for compatibility as presented in Table 6.1. These values are based on the suggestions by Sasse & Snethlage (chapter 1) [5]. The objective function can be seen as the gap between target value and the predicted value x of the individual. The distance, or difference between target and individual, has to be reduced to a minimum; therefore the objective functions in this study are minimising functions.

The interpretation of the multi-objective optimisation problem is thus such that the design variables (Fig. 6.2) are the constituents of the *raw* mortar recipe before the mortar is made, while the objectives (as in e.g. Fig.

6.1) are defined as properties of the *hardened*, cured mortar. The minimising objective functions therefore have to rely on the previously established estimation functions.

This system is thus not only challenging to implement for repair mortar development, but also because the objective functions are estimation equations which should be implemented in the algorithm. Therefore, the previous chapters 3 to 5 aimed for an estimation method per property which can easily be implemented in an algorithm and still provides reliable estimations.

6.1.3 The solving architecture

6.1.3.1 General explanation of genetic algorithms

The solving architecture should be capable to treat the fundamentals of the studied optimisation problem. Two solving approaches exist: deterministic solving and stochastic solving. A deterministic approach is often interesting, and might be efficient, once the trend line is known that each objective function will follow. In order to be successful, a deterministic approach requires that every influence of every modification imaginable on each design variable is known. In a real population, all irregularities from the behaviour of a population, its environment and its system conditions at a given point in time are rarely known, and can therefore not be modelled in detail [6]. The deterministic approach is thus quite restrictive, and the optimal individual might not be found. Regarding the design variables and objective functions associated to the proposed mortar compatibility question, a stochastic solving approach, that takes irregularities into account, is believed to be more appropriate.

In parallel, the intuitive interpretation of the optimisation problem imposes a combination of continuous and discrete variables in the string. The use of discrete variables implies that discrete programming capabilities should be embedded in the solving algorithm.

Bearing in mind that the mortar compatibility question implies considering several objective functions, the remaining solving possibilities for this problem are to be restricted to multi-objective approaches. In practice, various methods are available to solve multi-criteria optimisation problems with mixed discrete-continuous variables.

Through a succession of runs, the stochastic *conventional methods* allow to find an optimal set of solutions (e.g. Fig.6.1) [7]. There are always multiple solutions in these multi-criteria optimisation models, and it is thus up to the user to single out the most appropriate one. These conventional methods require successive runs in order to compose a subset of solutions that approaches a (local) minimum. Therefore, only in a limited way, these methods can help decide which individual is an optimal solution. From this subset, the user is obliged to choose the most preferred solution and consider it as satisfactory [7].

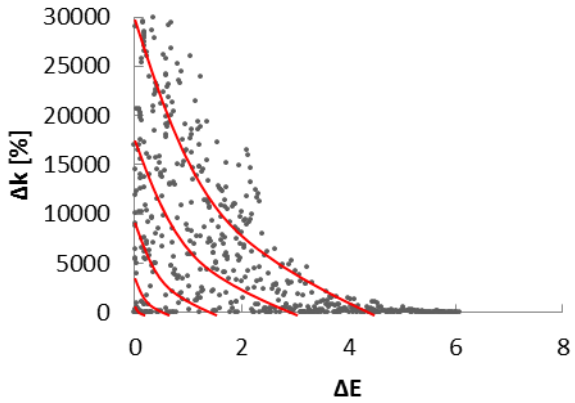

Fig. 6.3. Graph representing a population, where individuals can be subdivided in several fronts (in red). Each front gathers individuals 'dominated' by the same number of individuals, e.g. 0 for the first, optimal, Pareto front, 1 for the second front etc. The Pareto front, closest to the target values, gathers the best individuals of the population.

Genetic algorithms on the other hand are stochastic algorithms based on the evolution processes found in nature, such as the natural selection and the Darwinian principle of survival of the fittest. Following terms are therefore also more in use for these algorithms: 'individual' for a solution, i.e. a single mortar recipe, 'population' for a set of mortar recipes, and 'generation' for a population which is the offspring of another population. Multi-objective evolutionary algorithms aim to find the best individuals, i.e. closest to all targets. In the mortar optimisation problem, other individuals that are not on the Pareto front exist as well. The set of best individuals are present in the Pareto front: they all dominate other, lower-ranked individuals and are themselves not dominated by any better solutions (Fig. 6.3) [7]. Most of the existing evolutionary algorithms do not only try to approximate the Pareto front as accurately as possible, and obtain as such the global minimum, but they also aim an even distribution among individuals (in order to have a good variety in individuals).

The optimisation is achieved in several steps. Generally, there is a random creation of individuals first, taking specified lower and upper bounds on each design variable into account. This random creation is then followed by an iterative operation: the population is updated with new individuals by using 4 main operators: selection, cross-over, mutations and elite-preservation until the goals or the maximum number of generations are met.

When applied to a global population with parents and offspring, the selection operator has as primary goal to duplicate good individuals in a mating pool for the next step, and eliminate bad individuals from the population, whilst keeping the total population size constant. Good individuals can be selected by using various methods, such as the tournament selection, proportionate selection and ranking selection [4]. The tournament selection compares two individuals with each other, and places the best one in the mating pool (Fig. 6.4). If carried out systematically, each

individual can be made to participate in two tournaments [4]. The best individual will win both times, and will be duplicated twice, the worst will lose every time, and will be eliminated from the population. This means that every individual in a population will be duplicated twice, once, or not. The tournament selection is stated to have the best or equivalent results in convergence and computational time in comparison with other selection operators [4].

After the 'winning' individuals of these tournaments have been copied into a mating pool, other operators are used on them:

The crossover operator is applied afterwards and will, at random, take some portion of the string of an individual and interchange it with a portion of the string of another individual, to create two new individuals (Fig. 6.5). Every crossover between any two individuals might lead to a worse or better individual than both parent individuals. If this operation is carried out systematically, the chance of creating better individuals is more than random [4], since the two individuals being crossed are individuals which have already survived the selection. They must therefore have a good combination of strings already present.

The mutation operator maintains the diversity in the population. The mutation operator changes the string locally to generate –hopefully- a better substring (Fig. 6.6). Here as well, it is more than likely to find a better individual after mutation, since the parent individuals were already subjected to the tournament selection operator before [4]. The mutation operator introduces as only operator punctual novelty, which is crucial to be able to explore zones of the design variable domains which were not represented in the initial population.

This is followed by the elitism principle: the individuals subjected to all operations, the 'parents', and their 'offspring' are all compared with each other (Fig. 6.7). This way, the parents can compete with their offspring. If mutation or crossover would have created a worse individual than any of its parents, it would 'lose' during this operation from its parent. The elitism principle guarantees as such that the fitness of the population's best solution does not deteriorate, and increases the probability of creating better offspring [4].

As such, evolutionary algorithms are very efficient, and inherently dominate conventional methods: even the most effective conventional optimisation methods will still stop at a local minimum, while evolutionary algorithms tend to eventually find the global minimum, after a sufficient number of generations [7]. Their architecture is therefore believed to be suitable for this optimisation problem.

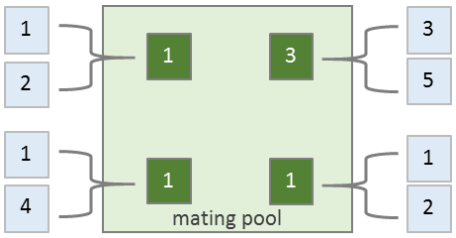

Fig. 6.4 The selection operator performs a tournament selection duplicating the best performing individual in the mating pool.

Fig. 6.5 The crossover operator acts on various individuals (parents) and interchanges sections so as to create offspring.

Fig. 6.6 The mutation operator changes at random one variable in the string.

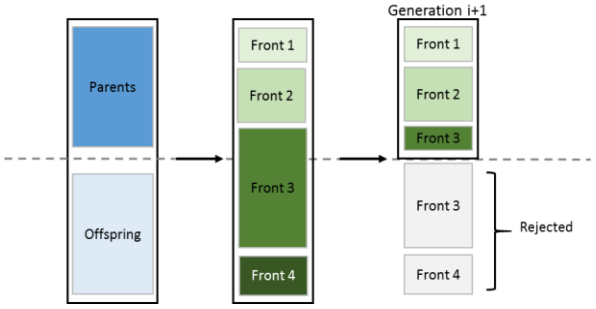

Fig. 6.7 The elitism principle compares and ranks individuals in fronts.

6.1.3.2 Choice for a specific genetic algorithm

In order to find a suitable genetic algorithm (GA) for this mortar compatibility problem of (only) three objective functions, some multi-objective GA that have already proven their success were evaluated on their functioning and possible implementation for the problem.

Algorithm 1: SPEA 2

The Strength Pareto Evolutionary Algorithm 2 (SPEA2) was developed by Zitzler in 2001 as an improvement for the SPEA model proposed in 1999 [8]. The SPEA was one of the first multi-objective algorithms that incorporated elitism. In SPEA, Pareto-ranking is used to determine the probability of duplication [9]. SPEA 2 has an external archive of individuals, in which new individuals compete with the best (non-dominated) individuals found in previous generations [10]. Individuals are well distributed, due to an incorporated nearest neighbour estimation technique and an archive trunking method (to guarantee boundary individuals preservation) [19]. This competition between the newly generated individual and the archived individuals leads to replacement of the archived individual if a newly generated individual dominates it, the maximum archive size is exceeded and the front (or a portion of it) where the individual is located, is overcrowded [8].

First, the initial population and the archive are generated. The fitness value of each individual is calculated, and all non-dominated individuals are copied to the archive, whilst aiming to preserve the initial population size. A new generation of individuals is made by first performing a tournament selection on the individuals in the archive after which recombination and mutation operators act on the selected individuals. Fitness values are

calculated as a sort of ‘strength’ value in the Pareto set, considering the distribution of the individuals, and how much the individual is dominated and dominates [8]. Zitzler concluded that SPEA 2 outperformed its predecessor and obtained similar results as the NSGA II algorithm (see below) [8]. When the number of objectives in simulation models increases, SPEA 2 proved to have a better distribution of points in comparison to NSGA II. However, overall, NSGA II had a broader spread and therefore a better performance.

Algorithm 2: SPEA 2+

The SPEA 2+ algorithm is an improvement of the SPEA 2 algorithm, proposed by Kim et al. (2004) [11]. These researchers introduced not only a cross-over mechanism in the objective space, but also a cross-over mechanism in the design variable space, and they thereby attempted to improve the problem space exploration abilities of SPEA 2 [11]. To achieve these goals, SPEA 2+ contains additional operations, such as the neighbourhood crossover: a crossover of individuals close to each other in objective space applied after sorting, (avoiding cross-over with the same individuals). Also a mating selection is introduced because Kim et al. (2004) state that the binary tournament selection used in SPEA 2 to generate a new population “sacrifices the diversity of non-dominated individuals” [11]. They therefore propose to copy the whole archive to the population used in the search. The third operation added is the introduction of a second archive of best individuals, and this for the variable spaces. Each generation non-dominated individuals are copied to both archives, followed by truncation in each archive, based on the objective and variable space Euclidian distance. A diverse range of individuals will then be present in both spaces [11]. The use of two archives allows to achieve a wider variety of individuals in the variable space without affecting the search ability and performed better than SPEA 2 [11].

Algorithm 3: NSGA II

The NSGA II is an improvement of the NSGA, the Non-Dominated Sorting Genetic Algorithm, an algorithm put forward by Srinivas and Deb (1994) [12]. The NSGA was based on the non-dominated sorting method and a technique to simultaneously locate multiple Pareto-optimal points [12]. The NSGA demanded a lot of computational time when treating larger population sizes. Additionally, the elitism principle present in other algorithms (e.g. SPEA) improved their fitness function [12]. Accordingly, Deb et al. (2000) adapted the NSGA into a fast elitist non-dominated sorting genetic algorithm, the NSGA II [13].

The difference with NSGA is that every individual from the population is checked with a partially filled population for domination. If any other individual dominates the individual, it is neglected, if not, it is placed in the population. In addition, the individuals are ranked according to their crowding distance (elitism). For minimising functions, an individual in a

lower rank is preferred over an individual in a higher rank; and an individual in a less crowded region is preferred over an individual in a more crowded region. This makes the algorithm faster. The original population is used to create an offspring population, after which both populations are combined together. The population size is now twice as large. Only then, a non-dominated sorting is used to classify the entire population in fronts. Truncation is then performed to regain the original population size. The most dominated individuals are eliminated: first, the individuals are ranked into fronts, then, some individuals are favoured over others according to their crowding distance (the distance towards other neighbouring individuals).

NSGA II was very popular in the years after its confection. Its largest disadvantage was probably its difficulty with many-objective problems. It did not always find the entire Pareto optimal set, and Deb (2006) found it was largely due to the fact that an emphasis on all of the non-dominated individuals for a large number of objectives was not sufficient to increase the selection pressure towards the Pareto optimal front. Solutions proposed by Deb were (a) find a preferred smaller range of the Pareto front or (b) find multiple regions of interest. The proposed methods appear to be able to solve a 10-objective problem [14].

6.1.4 Selection of one solution from an optimal set of solutions

The example of the means of transport given in the beginning already illustrated that the optimal Pareto front includes a set of solutions which are equally good, and that they are defined by a trade-off between the conflicting objectives. This of course induces the question which solution of this set should be chosen, and how. As you make your trip from Brussels' Central train station to Brussels' National Airport, you can only use one of the solutions presented. Many other elements will eventually influence the final choice of transport: the cost of the transport or the need to undertake the same trip over a certain period. But physical health, safety in traffic, reliability of the roads and public transport network also play a role in the decision process. This high-level information is often experience-driven, qualitative and non-technical. Even though only one means of transport can be used at a time, the luxury is given to the user: one day you are in a hurry, and you prefer to take the train, the other day, the sun is shining and you prefer to take your bike.

The same can be applied to the mortar optimisation problem: it might be that one repair on a building has to be performed on a very visible spot, which might let the user prefer to choose a mortar which is a little bit better in colour than in any of the other properties. It might also be that the mortar has to have a good consistency for plastic repair. In that example, the mortar might be selected on its W/B ratio for example. It is thus up to the user to choose any or more of the mortar recipes proposed by the algorithm, to test the recipes in the laboratory and make a final decision on compatibility of

colour, permeability and elasticity, performing as such computer-aided mortar development.

6.1.5 Discussion & conclusion

The problem of repair mortar development optimisation is best approached as a multi-objective optimisation problem. A stochastic solving approach with discrete programming capabilities will imply an intuitive, realistic configuration of the problem, and in addition, will take irregularities into account. Each individual in the population made by the GA will represent one mortar recipe, which is composed of the design variables, including the volume of aggregate, binder and water to be used, as well as the type of binder and aggregate to be used. The mixing ratios, such as the B/A ratio and W/B ratio will be considered as the constraints of the functions.

In terms of the actual structure, a comparing study was made of the conventional methods and various evolutionary algorithms. The early conventional approaches are simple and easy to use, but they only generate one individual per run, and therefore, several runs are necessary to generate a Pareto optimal set. SPEA 2 and NSGA II are very successful GA's, although they have a higher computational cost than other, more recent algorithms. However, when considering the reasonable number of objective functions, and what the main reason for the optimisation of the mortar-stone compatibility problem was (trial-and-error), even with a calculation time of several hours, the advantage of this optimisation method would be immense. When comparing SPEA 2, SPEA 2+ and NSGA II, the SPEA 2+ improved SPEA 2 because local optimal individuals were avoided. It generated a wide variety of individuals, and improved diversity and precision of the individuals. The difference in search ability between SPEA 2+ and NSGA II was however small, since in NSGA II, the binary tournament selection in the mating pool ensures that the individual with the smallest crowding distance is chosen [11]. The population in NSGA II is therefore more uniformly distributed than a similar population in SPEA 2+ [11].

The NSGA II algorithm was chosen for this problem, since it is a GA that has proven to find individuals on the Pareto optimal front. Moreover, the algorithm creates solutions that are spread in a broad and well-dispersed range, which is an important element in order to explore the entire available space of continuous variables. The NSGA II is also a faster type and should be able to calculate the optimal front for the three-objective function problem proposed.

6.2 NSGAII Algorithm for mortar compatibility development

6.2.1 Introduction

A general overview of the system is given in Fig. 6.8 and presents how it can be seen in the light of a restoration intervention. This figure shows how a stone column to be restored (on the left) can be repaired with repair mortar, using a mortar developed by this system. First, the column's stone properties are introduced into the NSGAII algorithm. Some of these stone properties can be measured using a non- or less destructive approach. The algorithm based on the Darwinian principle, will then use estimation objective functions to search for mortar recipes, selected on their compatibility with the stone's properties.

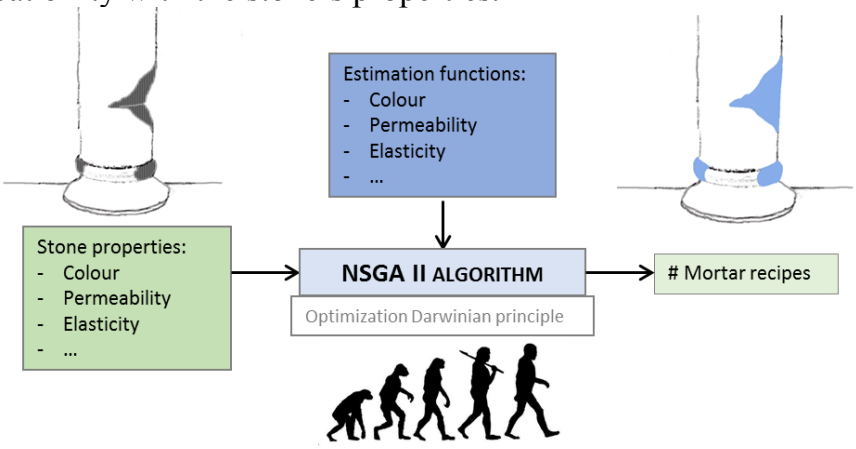

Fig. 6.8. General overview of the system for the repair of natural stone. The example here presents a stone column, but repair mortars proposed by this system could be used for other types of repair as well.

The algorithm is written in MATLAB® 2012 language, allowing the coding to be easily adaptable (Fig. 6.9). Several implementations of the NSGAII algorithm are available on the Internet. The version used here, was initially encoded by C. Versèle at the Engineering Faculty of the University of Mons, in 2008. The routine had already been partially adapted by Van Parys et al. (2012 & 2013) to the needs for the mortar development problem [15,16]. More precisely, they adapted the string to the version represented in Fig. 6.2, and two objective functions had been introduced.

During this research, several modifications have been made. The most important one is undoubtedly the extension of the already existing 2-objective algorithm towards a 3-objective algorithm: the objective function for permeability did not exist in the previous version of the algorithm. This property was judged important for a compatible and durable intervention, and was therefore thoroughly researched in this thesis, in order to be able to implement into the system an estimation method for permeability. This estimation method was then implemented into the algorithm.

Secondly, the objective functions which were present in the previous version had to be thoroughly revised. The objective functions were colour

and compressive strength, designed for the property estimation of cement mortars. Consequently, they were adapted for lime mortars, and the compressive strength estimation method was extended further into an elasticity estimation. In addition, the coding was clarified and corrected where needed.

The third improvement was the storage of data and the storage of solutions. The database was separated from the algorithm and its scripts. Data input is required in various scripts and if this data has to be adapted, the user would have been obliged in the previous version of the algorithm to adapt the data in every script where needed. Separating the database permits the user to adapt the data only once. In this adapted version of the algorithm, the solutions and all their metadata (mortar recipe, distance towards targets, estimated property values, estimated spread) are stored in a tree structure.

The fourth improvement included the creation of a Graphical User Interface (GUI) for both tool and database, and the development of the tool as a standalone application.

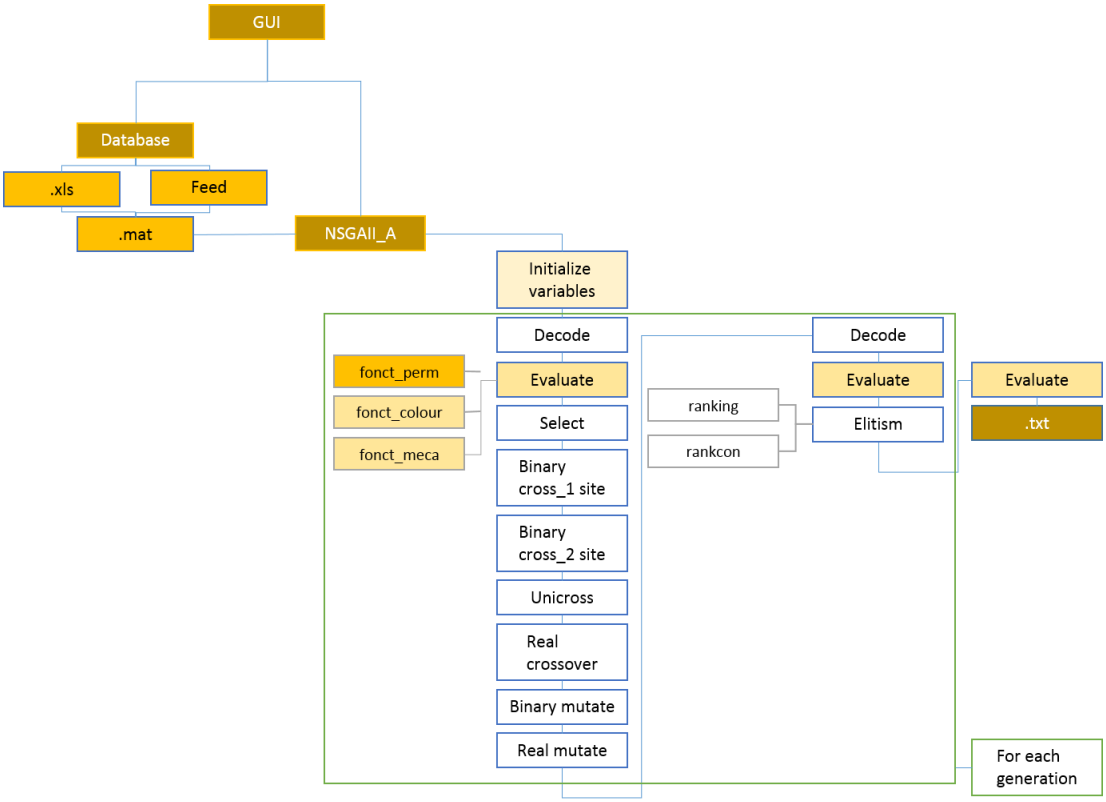

Fig. 6.9. Lay-out of the algorithm. The functions in white with blue rim contain codes of the evolutionary algorithm itself (encoded by Versèle), and have not been adapted throughout this study. The codes in yellow are modified codes (light yellow), or contain newly-written codes (darker yellows). These adapted or new codes only adapted the estimation and the ergonomics of the system. The 'decode' function reappears once, the evaluate function and its subjected functions reappear twice. For specific information concerning the content of each step, see 6.2.2 to 6.2.5 and Appendix 6.1.

6.2.2 Execution of the system

The entire system is encoded in MATLAB®, in various scripts. One of the scripts can be seen as the 'mother' file (called NSGAII_A in Fig.6.9), which uses any of the other scripts, function files, when necessary. The entire system of when which script is called, is shown in Fig. 6.9. The total encoding encompasses some 3500 lines. More information concerning the detailed functioning of the algorithm can be found in Appendix 6.1.

Following steps explain which information is required for the system to function:

Information concerning the database: the database needs to be introduced first. The user can fill in every property necessary for the three estimation methods through questions asked by the automated file. Table 6.2A illustrates some of the questions asked by the system. More information can be found in 6.2.3.

The mother file can be modified when desired, to adapt the size of the population and the number of individuals. However, this is set to a standard value, which has been determined in 6.3.2.

Table 6.2A Some representative questions asked in order to create the database file

Apparent density sand a [kg/m³]:
D50 sand a [m]:
Insert mean ITZ thickness [m] binder 1:
Insert resistance [MPa] binder 1:

Table 6.2B Questions asked by the mother file to the user (*left*) to determine the targets and the boundary limits the input should follow (*right*)

Input the L of LAB:	Input between 0 and 100
Input the a of LAB:	Input between -50 and 50
Input the b of LAB:	Input between -50 and 50
Input kwater in [m²]:	Input between 1E-9 and 1E-14 m²
Input Estat in [MPa]:	Input is positive
Agree with initial population? Y/N:	Input is Y for yes or N for no.

Every element is now 'ready' to be launched. When the mother file is run, the follow-up of scripts will be automatic. Immediately, the user will have to answer several questions:

1. First, the targets are determined. The user has to answer the questions presented in Table 6.2B. If the answer is outside of the two boundaries set, the script is programmed to consider the answer as invalid, and asks the question again. The [L,a,b] triplet represents the colour, the permeability can be introduced by using either the k_{gas} or k_{water}. The desired elasticity is introduced by the E_{stat} value. The targets introduced here, are the mortar property values that are desired.
   The objective functions are based on the estimation equations which were established in chapters 3, 4 and 5. They refer to the separate script files for permeability, colour and elasticity (eq. 6.2.1-3).

Table 6.3 Objective functions as present in the evaluation script file. In these objective functions, there are references towards the function files. Each objective for each objective function was written based on the chapters 3, 4 and 5.

$$\Delta K_{water} = 100\frac{abs(k_{w\ mortar} - k_{w\ stone})}{k_{w\ stone}} \quad \text{(eq. 6.2.1)}$$

$$\Delta E_{stat} = 100\frac{abs(E_{stat\ mortar} - E_{stat\ stone})}{E_{stat\ stone}} \quad \text{(eq. 6.2.2)}$$

$$\Delta E^*_{i-j} = \sqrt{(\Delta L^*)_{i-j}{}^2 + (\Delta a^*)_{i-j}{}^2 + (\Delta b^*)_{i-j}{}^2} \quad \text{(eq. 6.2.3)}$$

2. After the algorithm has created the first population, the population will be shown in a graph, presenting the variation in binder and water, asking the user to confirm whether the distribution is acceptable (Table 6.2B). This question allows the user to judge the quality of the initial population. The initial population is random, and it might thus be that the initial population is not as well distributed as intended. If the population is not as desired, the individuals are created again and the same question will be asked, until the answer is positive. A good distribution of individuals in the population is required in order to find the best solutions faster.
3. The algorithm then indicates the number of generations already processed. For each generation, it illustrates every individual of the population in a ΔE*, ΔK-graph (Fig.6.10).

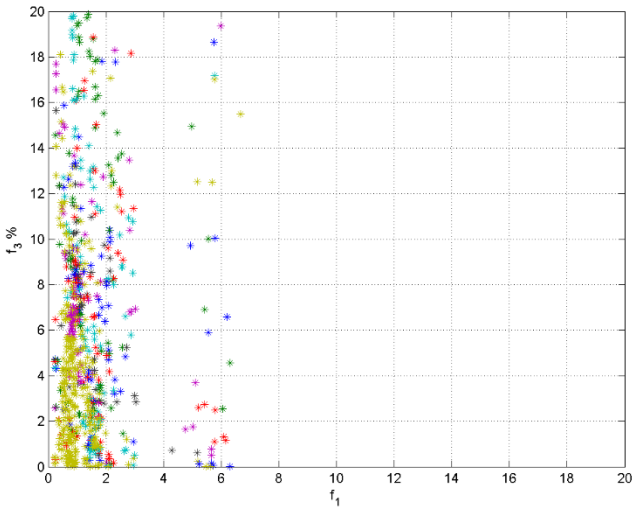

Fig. 6.10 Example of a ΔE*, ΔK-graph representing the individuals of each generation of during one run. ΔE* [-] is f1 and ΔK [%] is f3 on the graph.

4. After the generation loop ends, the mother file accumulates and displays the metadata, e.g. population size, number of generations, the calculation time. It will also display information concerning the final population, such as the mortar recipe of the individual which approaches the targets closest.

5. Finally, every individual of the final population is stored in a *.txt* file. If desired, the user has as such the possibility to have additional information of the final population, and to look for example, other recipes which show good results for one of the targets. This file contains information of the distances towards the targets, as well as the specific mortar recipe and the estimated property values. As complementary data, an indication of the spread is given for every individual. This estimation was made based on the measured spread values from the mortars tested in the experimental campaign of this research (Appendix A6.1). This is a mere indication, and more research should point out the relevance of the estimation for other mortars. In addition, it is of interest to know that this estimation is never used as an objective or constraint in the algorithm. It is mere information, calculated as additional feature after the optimisation is complete.

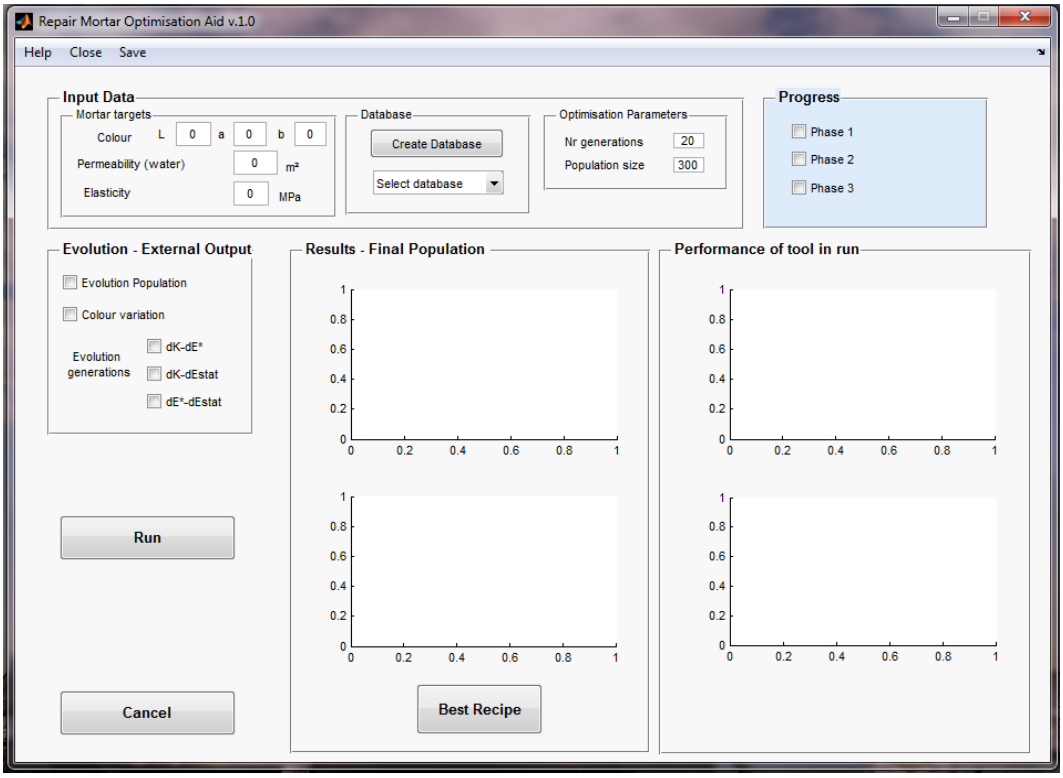

Fig. 6.11 The GUI of ReMO v1.0. The input data panel allows to introduce the mortar targets, create or load a database, and introduce the number of generations and population size. The Progress panel on the right indicates automatically the advancing of the run. The Evolution panel allows the user to check which external graphs he would like to see during the run. The Results panel will give two graphs of distance towards the targets of the final population. The Performance panel allows to determine the well-functioning of the system for the concerned mortar problem.

As can be seen in Fig. 6.9, the system can also be used through a graphical user interface (GUI). The GUI is represented in Fig. 6.11. Users without experience in coding or without access to MATLAB® can as such use the entire system (database, algorithm and GUI's) through a standalone

application. For this *.exe* file to function, the user only needs to download a free package (MATLAB® Runtime).

6.2.3 Database

The algorithm can only propose new mortar recipes using a database of sands and binders. This database comprises the data of the raw mortar ingredients (Fig. 6.12). As Figure 6.9 demonstrates, the database is external and stands alone: the user should decide which database is to be uploaded for that specific run of the algorithm.

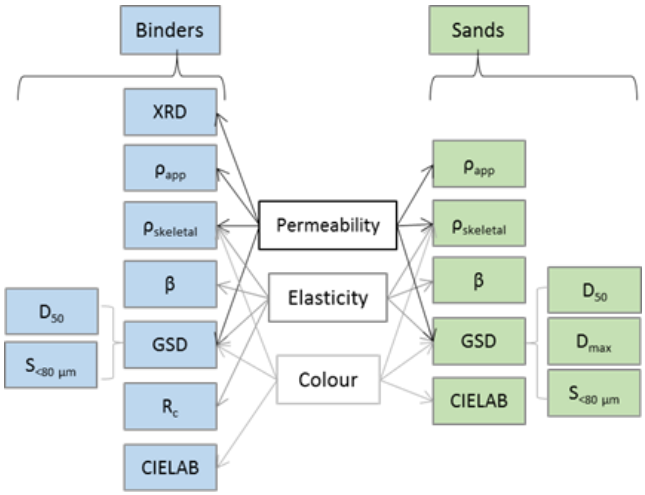

Fig. 6.12 Properties of the raw ingredients needed to complete the database for binders and sands. 'XRD' indicates that the reactive components of the binder have to be known. 'GSD' stands for grain size distribution. The arrows point to the properties needed for each estimated mortar property.

Hence, before the algorithm can run, a database should exist. If the database would not yet exist, a specific automated script was designed in Matlab® which guides the user step by step to establish a convenient database. The database is then saved as an *.xls* file. Saving the file under this format has two advantages: (a) the user can very easily verify afterwards if all data are indeed included (in the right cell) and can modify and save his modifications, and (b) the format of *.xls* permits that, at present, the file can run on any computer, disregarding whether or not the most recent version of Excel or other office software is installed.

Using the *.xls* file throughout the run of the whole algorithm would demand significant calculation time, so in this system, the data will be transferred once, in the beginning of the run, into a *.mat* file, which is easier to read for Matlab®: after verification of the *.xls* database, the *.xls* file is called by a script which handles the input of data in the algorithm, which will transfer the data in a *.mat* file. The several script files can then read this *.mat* file during the running of the algorithm.

6.2.4 Ranking and individuals

In order to facilitate the coding in the algorithm, the individuals are not only composed of the set of design variables, but they have also a set of data with them. These data are for example the results of the objective functions or the actually estimated property value for that individual. On their turn, the individuals are linked to the generation in which they were created. As explained in the previous section, they are incorporated into the newest population after successful ranking.

The individuals, including the information linked to their properties and composition, are stored in a tree structure, which allows a clean architecture. A tree structure is not restrained to a certain size, as such, if in the future it is deemed necessary to enlarge or add branches to the tree structure, this would be possible. The information given in the final *.txt* file after running the tool is directly based on this tree structure. One row of this *.txt* file is thus an offprint of the tree structure of one individual (Fig. 6.13). Initially, the only elements of this tree structure were the first 4 branches which indicate the composition of the individual and the fitness value for each objective function (or the distance towards the target). This study added the 4 last branches, so that the user would know what the exact estimated properties are for each individual, and what its spread is estimated to be.

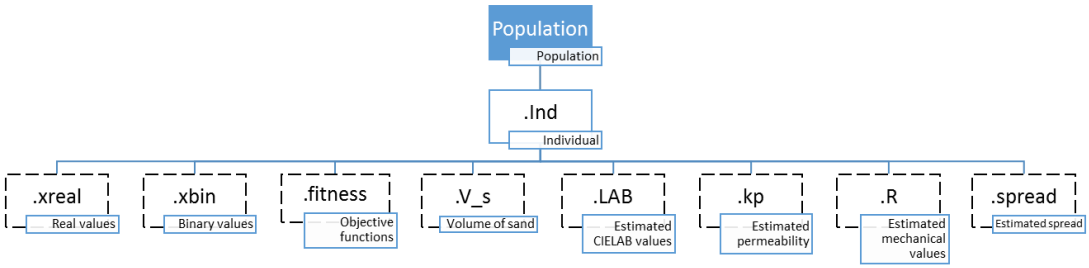

Fig. 6.13 The tree structure of an individual in the final population.

6.3 Validation of the optimisation process

The previous subsection explained the implementation and adaptation of the NSGA II algorithm for the studied problem. The following subsection investigates which pertinent default values for algorithm parameters can be modified, such as the population size and the number of generations of the run. The population size required for this problem was studied in depth. After this parameterisation, the robustness of the algorithm was also studied by testing the reproducibility of its results.

6.3.1 Population size

The choice for the population size is related to the complexity of the problem [4], and therefore, the population size should be chosen with

consideration. Taking into account the functioning of an algorithm, a small population size might calculate faster and reach a (local) optimum, while this would take longer for a larger population size. Moreover, a large population size is better at finding the global minimum, despite the longer calculation time. Indeed, Goldberg et al. (1992) found that the quality of convergence of a small population size is left to chance, and that large population sizes can differentiate more easily between better and worse individuals and thus create an increased convergence of results [17].

In this optimisation problem, it is unknown what can be defined as a sufficiently large population, without spending unnecessary computation time. To answer this question, several runs were performed with various population sizes, in order to determine what population size would best fit this problem. The maximal number of generations was set at 50, the parameter settings concerning crossover and mutation were kept as in Appendix 6.1, and the targets were set to:

- [L*,a*,b*] = [80,0,10]
- K_{water} = 1 E-12 m²
- E_{stat} = 500 MPa

Based on experimental studies in Chapter 3 and 5, the static E modulus and water permeability should be easily obtained with the database used. The database here included NHL 5 and NHL3.5 as binders, and the yellow, green, Rhin gros and Rhin fin sands. Based on this database and the estimation theory of colour presented in Chapter 4, it might prove more challenging for the algorithm to find a mortar recipe with this colour estimation. This was chosen on purpose in order to enlarge the effect of possible convergence throughout the generations.

Three runs per population size N were performed using Matlab® 2012 on 1 core of an Intel i5 Windows 7 64 bit computer (RAM 6 Go, CPU 2.5 GHz). N was defined at 6, 30, 60, 300, 600 and 3000 individuals. The runs were compared on the duration of the calculation, and on the convergence of each towards the global minimum (Table 6.6, Fig. 6.14). Convergence is assumed to take place once the evolution is stabilized, i.e. the largest improvements in terms of genetics are made. Any generation created after this would improve results only on a minor level. The results of N=600 are visible in Fig.6.15, which represent the evolution of the population after each 10^{th} generation, for the combination ΔE^* and ΔK_w, as f_1 and f_3 respectively. The evolution for the other population sizes can be seen in Appendix 6.2.

The smallest population size N of 6 does not induce the convergence of a population to the global minimum after 50 generations. The bulk of the population was trapped in a local minimum. The time spent to a run with N=6 is, as could be expected, very low.

The three runs with N=30 indicated that the population converged towards the targets, but that the bulk of the population did not converge before 50 generations. The population size of 60 individuals showed a faster

convergence. The bulk of the population converged at averagely 42 generations. The duration of the run has nearly doubled in comparison to 30 individuals.

A population size of 300 individuals indicated a convergence of the bulk of the population at averagely 20 generations. The three runs with N=600 designated a convergence of the bulk of the population towards the target values after 16 generations (Fig. 6.15). A population of 600 individuals increased the calculation time per generation by 230% in comparison to the N=300 calculation time per run. The gain in convergence speed (in number of generations) is thus levelled out by the longer calculation time per generation.

The population with 3000 individuals showed a convergence of the bulk of the population after the 14th generation. The stabilization in convergence was already visible starting from the 11th generation, but from the 14th generation onwards, the individuals are less dispersed. A slow convergence is visible through the generations after that, especially starting from the 40th generation. However, this progress is very slow in comparison to the progress made in generations 1-14.

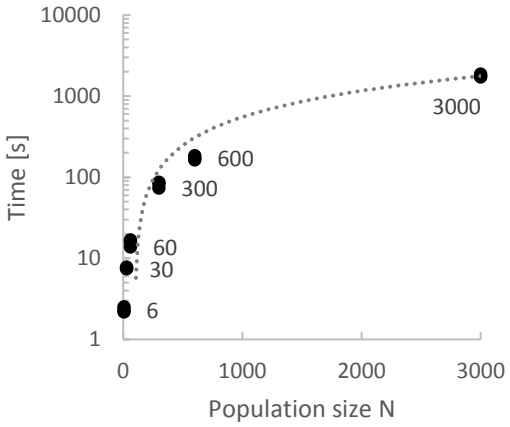

Fig. 6.14 The calculation time per generation for the various population sizes.

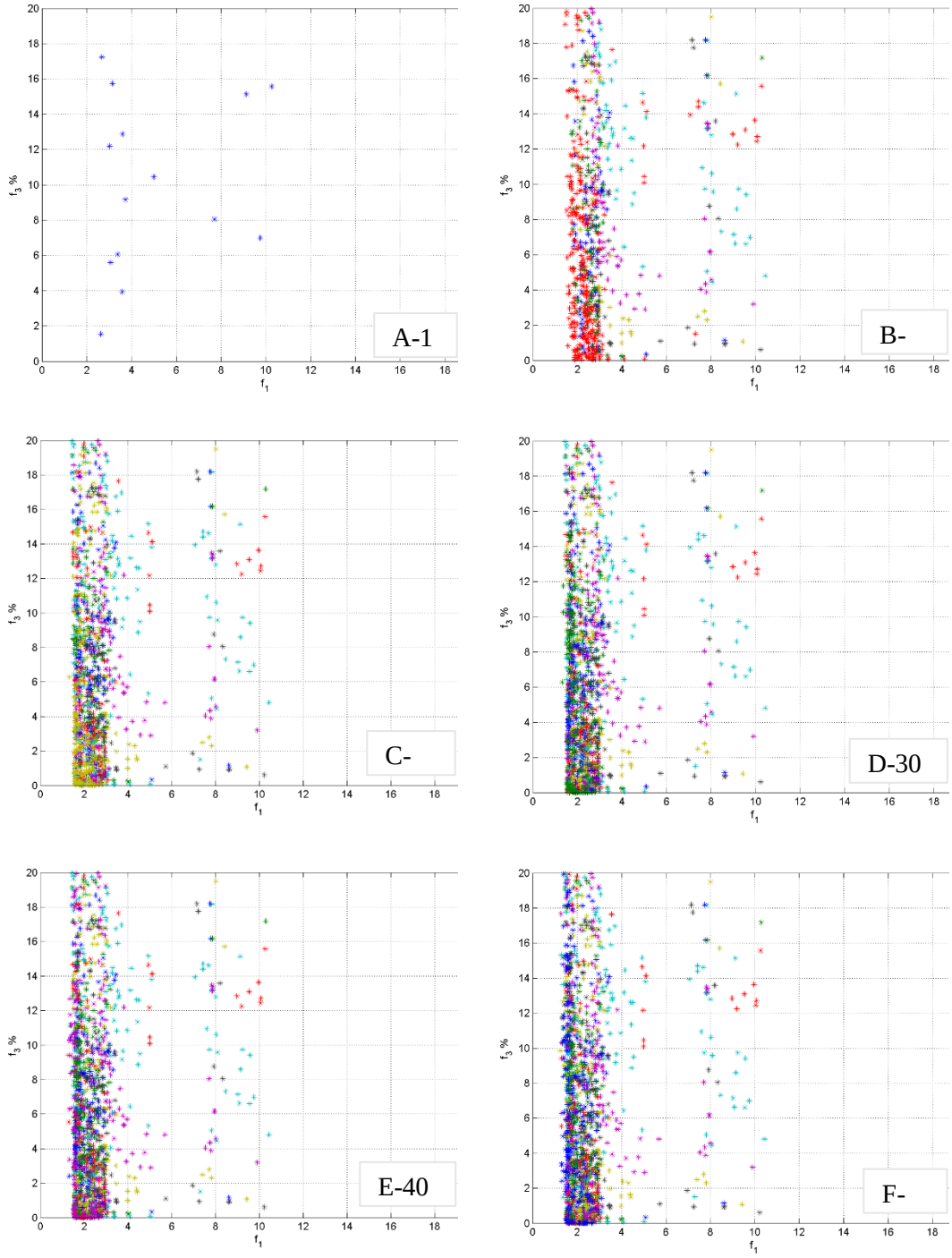

Fig. 6.15 Run 1 of the algorithm with N=600. A-F represent convergence of the individuals towards a minimal distance between the targets, here f1= ΔE^* [-] and f3%= ΔK_w [%], after 1, 10, 20, 30, 40 and 50 generations respectively

Table 6.5 Summary table of the various runs with a different population size.

N size	Calculation time (50 gen) [s]		Calculation time (per gen) [s]		Convergence	Average nr generations before convergence
	Av.	St.dev.	Av.	St.dev.		
6	117	7	2	0	No	>50
30	377	7	8	0	No	>50
60	797	64	16	1	Yes	42
300	4201	286	84	6	Yes	19
600	8681	430	174	9	Yes	16
3000	89277	3133	1786	63	Yes	14

Based on results, a population size of 300 would seem appropriate for the complexity of this problem, with a number of generations approximating 20, the number of generations after which the bulk of individuals will not converge significantly anymore towards the target values. This choice was made, not only to gain in time, but also because the gain in even more successful individuals would be minimal.

6.3.2 Robustness of the algorithm

In order to illustrate the robustness of the algorithm, 10 runs were performed on two different sets of targets, but with the same input data and the same parameters. These setting parameters are those defined in Appendix 6.1. The population size was set to 300 for 20 generations. After each run, the metadata of the run contains information about the 'best' individual, or mortar recipe. The best mortar recipe is defined by the conventional, albeit mathematical, method where each individual is compared to an ideal point X, whose coordinates in the objective function space are the best for all targets (eq.6.3.1-4). Each coordinate can come from various individuals in the population, who have for example the best composition in terms to be the closest in ΔE* of all individuals in the population, but not in any of the two others. His ΔE* coordinate will as such be combined with the ΔK_{water} coordinate from another individual which was best for permeability, and with the best ΔE_{stat}, also possibly from another individual. Logically, point X is different for each run. The coordinates of point X for each run of the two sets of targets is given in Appendix 6.3.

$$X = (f_{1,ideal}, f_{2,ideal}, f_{3,ideal}) \quad \text{(eq.6.3.1)}$$

In which

$$f_{1,ideal} = \min f_1 \quad \text{(eq.6.3.2)}$$
$$f_{2,ideal} = \min f_2 \quad \text{(eq.6.3.3)}$$
$$f_{3,ideal} = \min f_3 \quad \text{(eq.6.3.4)}$$

The distance Δ_i between each individual and the ideal point X is then calculated according to eq.6.4

$$\Delta_i = \sqrt{\sum_{j=1}^{M} \left(\frac{(f_{j,i} - f_{j,ideal})}{f_{j,ideal}} \right)^2} \qquad \text{(eq.6.4)}$$

With M the number of objectives, $f_{j,i}$ the value of the j^{th} objective function of the i^{th} individual, $f_{j,ideal}$ the minimal value obtained during the run for the j^{th} objective function. The individual closest to X, with minimal Δ_i, is selected as the best mortar recipe.

For the first set, the targets are the same as in 6.3.1. The composition of each 'best' mortar recipe is given in Table 6.6 and Fig.6.16. This shows that all mortars contain green sand (100%), and the other sand is 4 out of 10 Rhin gros, and 6 out of 10 Rhin fin. The yellow sand was not proposed. In terms of binder, 60% of these best mortar recipes propose NHL 3.5, and 40% NHL 5. The water volume for all mortar recipes is fairly constant, as well as the binder volume and the total sand volume (Table 6.6). The volume percent of sand 1 and sand 2 are more variable (S1 10.54±7.05%, S2 39.54±7.55%). This variation is thus due to the changing ratio between the two sands: T1-7 is near a 6:4 ratio for the two sands, favouring the green sand. Three mortar recipes propose to add between 20 and 35% of the total sand volume to be green sand (T1-1, T1-2 and T1-10), while 6 other mortar recipes propose less than 16% of green sand for the total volume of sand.

In terms of performance, the mortar recipes showed that the ΔE* for all mortars varied around 3, with a minimum of 2.40 for T1-7. The ΔE_{stat} and ΔK_w can be narrowed down much more (Table 6.8): ΔE_{stat} has 9 out of 10 values below 1% difference, while ΔK_w had 6 out of 10 mortar recipes below 1% difference.

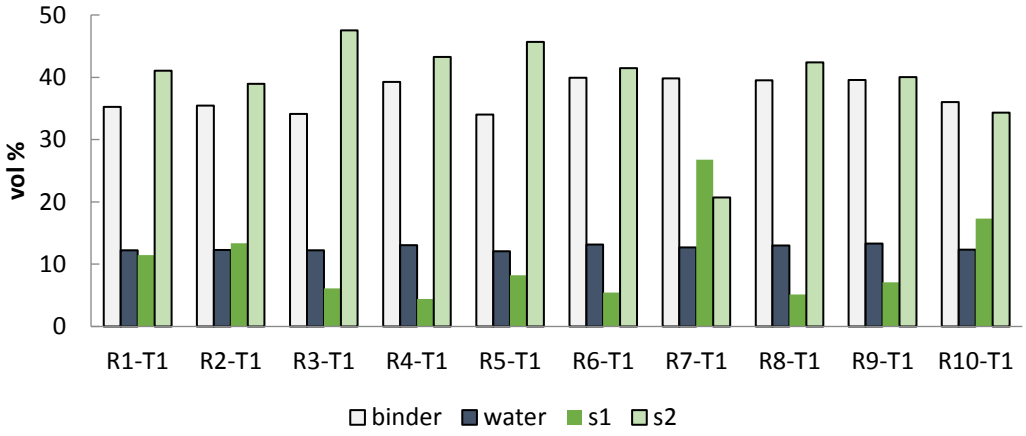

Fig. 6.16. Composition of the best mortar recipes for the 10 runs with T1 targets.

Table 6.6. The 'best' mortar recipes of every run (1-10) for the same targets (T1) set.

Mortar	V_b [v%]	V_w [v%]	V_{s1} [v%]	V_{s2} [v%]	b	s1	s2
Run 1-T1	35.24	12.25	11.47	41.05	NHL3.5	Green	Rhin gros
Run 2-T1	35.45	12.26	13.35	38.94	NHL3.5	Green	Rhin fin
Run 3-T1	34.10	12.23	6.13	47.54	NHL3.5	Green	Rhin fin
Run 4-T1	39.26	13.05	4.44	43.25	NHL5	Green	Rhin gros
Run 5-T1	34.03	12.06	8.22	45.70	NHL3.5	Green	Rhin fin
Run 6-T1	39.91	13.15	5.47	41.47	NHL5	Green	Rhin gros
Run 7-T1	39.81	12.71	26.78	20.70	NHL3.5	Green	Rhin fin
Run 8-T1	39.50	12.98	5.13	42.40	NHL5	Green	Rhin gros
Run 9-T1	39.58	13.31	7.08	40.04	NHL5	Green	Rhin fin
Run 10-T1	36.04	12.32	17.31	34.34	NHL3.5	Green	Rhin fin
Av.	37.29 ±2.52	12.63 ±0.46	50.08 ±2.95		NHL 3.5	Green	Rhin fin

The second set of targets T2 was chosen, as the first set, based on the experimental campaigns on NHL mortars in Chapters 3, 4 and 5. This time, all demanded targets should be able to be achieved by the algorithm, using the same database.

- [L*,a*,b*] = [78,2,12]
- K_{water} = 7 E-13 m²
- E_{stat} = 1000 MPa

The composition of each best mortar recipe is given in Table 6.7 and Fig. 6.17. All mortars contain green sand. Three out of ten mortar recipes contain only green sand, six out of ten also contain Rhin gros, and one mortar recipe combines green sand and Rhin fin sand. The NHL5 binder was proposed six out of ten times. T2-1, T2-5 and T2-10 have the same components (NHL 3.5 and green sand) and are also in volume of each component very similar, with binder volume around 39 % and water volume around 10%. T2-2, -3, -4, -7, -8, and -9 are also all composed of the same components, NHL5, green sand and Rhin gros sand. Their water volume is relatively similar, the other components are more variable.

Water volume is in general for all mortars stable. The binder volume varies a little more, as does the sand volume (Table 6.7). The sand1:sand2 volumes also here vary, but less significantly than for the T1 targets (S1 8.08±4.01%, S2 46.52±4.05%).

The mortar recipes are estimated to have properties close to the demanded colour and water permeability: the largest ΔE* value is 3.14, and the largest ΔK_w value 0.18% (Table 6.8). The demanded ΔE_{stat} proved to be a larger challenge: the smallest difference with the target was 35%. All mortars were estimated to be weaker than the demanded 1000 MPa. The mortar recipe of these ten closest to the demanded static E modulus also performed worst on both of the other two targets set.

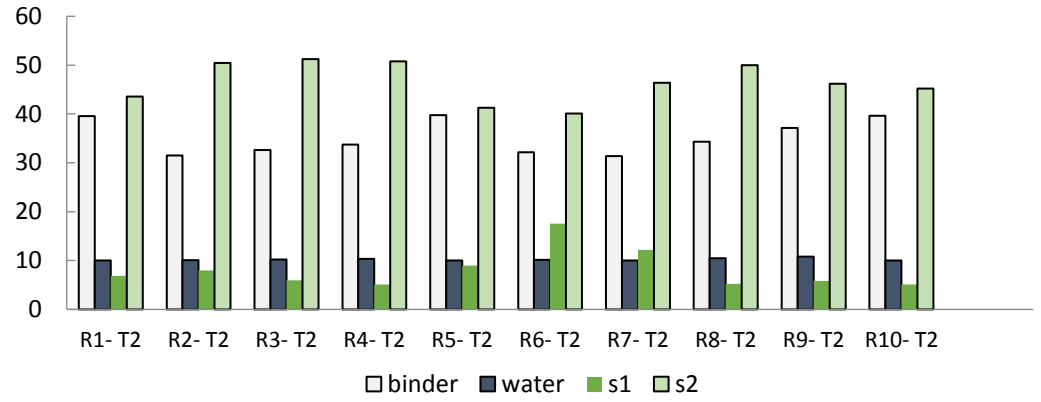

Fig. 6.17. Composition of the best mortar recipes for the 10 runs with T2 targets.

Table 6.7. The 'best' mortar recipes of every run (1-10) for the same targets (T2) set.

Mortar	V_b [v%]	V_w [v%]	V_{s1} [v%]	V_{s2} [v%]	b	s1	s2
Run 1-T2	39.56	10.00	6.85	43.59	NHL 3.5	green	green
Run 2-T2	31.53	10.06	7.99	50.42	NHL 5	green	Rhin gros
Run 3-T2	32.60	10.21	5.94	51.25	NHL 5	green	Rhin gros
Run 4-T2	33.77	10.38	5.07	50.78	NHL 5	green	Rhin gros
Run 5-T2	39.75	10.02	8.98	41.25	NHL 3.5	green	green
Run 6-T2	32.19	10.17	17.55	40.09	NHL 3.5	green	Rhin fin
Run 7-T2	31.38	10.04	12.21	46.38	NHL 5	green	Rhin gros
Run 8-T2	34.31	10.45	5.23	50.02	NHL 5	green	Rhin gros
Run 9-T2	37.14	10.82	5.83	46.21	NHL 5	green	Rhin gros
Run 10-T2	39.66	10.01	5.13	45.21	NHL 3.5	green	green
Av.	35.19±3.50	10.22±0.26	54.60±3.49		NHL 5	green	Rhin gros

Table 6.8. The 'best' mortar recipes of every run (1-10) for the same target set (T1 or T2).

Mortar	ΔE*	ΔEstat [%]	ΔKw [%]	**Mortar**	ΔE*	ΔEstat [%]	ΔKw [%]
Run 1-T1	3.67	0.16	0.19	**Run 1-T2**	1.55	50.81	0.00
Run 2-T1	3.34	0.15	0.09	**Run 2-T2**	0.46	52.18	0.00
Run 3-T1	3.79	0.04	1.28	**Run 3-T2**	0.68	50.73	0.01
Run 4-T1	3.21	0.42	3.12	**Run 4-T2**	0.88	49.50	0.01
Run 5-T1	3.68	0.07	0.81	**Run 5-T2**	1.55	50.64	0.00
Run 6-T1	3.14	0.02	3.05	**Run 6-T2**	1.12	53.35	0.00
Run 7-T1	2.40	0.18	0.65	**Run 7-T2**	0.28	53.29	0.03
Run 8-T1	3.17	0.12	4.75	**Run 8-T2**	0.95	49.07	0.01
Run 9-T1	3.45	2.38	0.13	**Run 9-T2**	1.40	46.84	0.00
Run 10-T1	3.11	0.76	0.00	**Run 10-T2**	3.14	35.08	0.18

6.3.3 Discussion

The NSGA II algorithm adapted to the requirements for repair mortar development uses three objective functions, and creates mortar recipes with a minimal distance towards the targets set. The population size for this

problem was determined to be best around 300, for about 20 generations, after which the population would have converged towards the target values.

For the validation of the system, two sets of targets were used. The runs for the first set of targets showed a reasonable variability in mortar components and ratios. There was a general preference for the use of one sand, and some variability existed in the choice of the second sand (both Rhin sands). The largest variable element was the S1/S2 ratio. Binder, total sand and water volume percentages remained fairly stable. The runs for the second set of targets showed that the recipes could be largely subdivided into two groups which were similar in type of binder, sand, and amounts of water, binder and sand used.

Since only two sets of targets were researched, a definite conclusion of the robustness of the algorithm is difficult to draw. The larger variability in recipes of the first set of targets might be due to the greater difficulty the algorithm has in finding compatible mortars, since some target values were out of the database' range. The combination of both set of targets might indicate that, when the mortar targets are likely to be approximated with the given database, mortar recipes are created which are slightly variable in distances with the targets but show a limited variability. Similar testing has been performed in chapter 7.

This seems to indicate that the population has converged (due to the similarity), but that there is still a level of variability in composition present which might be used to the advantage of the user which would like to choose selectively from the population.

6.4 Conclusion

In order to find a mortar compatible with all three properties (colour, permeability and elasticity) for a given material, a way was searched through optimisation. Considering the optimisation of repair mortar development as a multi-objective optimisation problem, and taking into account that constraints are present (e.g. workability and proper curing of the mortar), several algorithm types were studied. The stochastic approach (e.g. GA) was favoured over the deterministic approach (e.g. Monte Carlo), since it would require to know the most likely behaviour of various components in various mixes. This would require a large database of experimental campaigns on lime mortars in order to feed this model. Moreover, such an approach would only allow a deterministic calculation, i.e. following the previously-established trend or behaviour of the mortars. It was believed that such an approach would limit the possible results. In addition, the genetic algorithm used here applies the advantage of the Monte Carlo approach, i.e. the randomness in the creation of the initial population and of the mutation operator. From the stochastic methods, the genetic algorithms were believed to be more suitable for this type of problem, since these algorithms are quicker in finding an optimal solution than for example the single-generation

optimisation methods. These single-run optimisation methods would require multiple runs in order to find a Pareto front of solutions. Moreover, these single-generation optimisation methods start from nothing with every new run, while genetic algorithms will single out the best performing recipes from the previous generations, which are then used in operations such as cross-over and selection in order to improve the population in general.

The NSGAII algorithm was first adapted so that each individual represents one mortar recipe. In order to optimise them, these individuals are composed of discrete and real values, representing either the type of binder or sand used (discrete) or the amount in volume of binder, sand or water needed to create the mortar (real). By means of cross-overs and mutations of both discrete and real values, 'offspring' of the existing population is generated, after which all individuals are ranked according to the non-dominancy principle. These steps are repeated for a number of generations. The distance between the target and the individual is calculated according to the objective functions. These functions are based on the estimation equations defined in the previous chapters (chapters 3, 4 and 5).

In this thesis, the system was improved by changing the 2-objective algorithm into a 3-objective algorithm. The permeability estimation method as established in chapter 3 was implemented into the system, and the other two objective functions (colour, compressive strength) were adapted to the estimation methods as established in chapters 4 and 5 and focused on lime mortars.

In order to facilitate the use of the algorithm for the user, several aspects were implemented. These modifications allow to speak of a whole, a system, rather than a stand-alone algorithm:

The database is created separately from the algorithm itself, and once the database is created, the algorithm will be fed from that database. This database contains some properties which are elementary (e.g. the grain size distribution of the sand, the colour of the sand), but other elements necessary for the estimation of some of the targets are less straightforward (packing density, expected thickness of the ITZ around the aggregates).

During the run of the algorithm, various graphs appear, which indicate to the user either the variability of the population, the evolution of the individuals towards two of the three targets and the colour of target, sands, binders and individuals.

The implementation of a GUI, or Graphical User Interface allows users without programming experience to use the system. Data and target values can as such be introduced, and follow the run in MATLAB® by graphs which appear after every generation and indicate the convergence of the population. In addition, the users who do not possess a MATLAB® license, are now able to use this system as well through a standalone application.

The algorithm was tested on its robustness, and results were presented and discussed. It was illustrated that, for the same set of target values, the mortar recipes closest to the target values would approach each other, but would not be the same: the mortar recipes as individuals are created at random, and a repetition of the same population should thus not be possible. The last section of this chapter illustrated that the algorithm is capable of creating mortar recipes with estimated properties that converge generation after generation towards the target values. Nevertheless, in order to have a clear overview of the similarity in proposed recipes, a more thorough study would be required.

It should be remarked that, in the tool, the tolerance ranges are deliberately not included in this tool: the target values which have to be introduced are the mortar target values. This leaves the choice to the user to aim for a more adapted approach of every target. The tolerance ranges for each property used in this research are quite large. Future studies might narrow these ranges. For example, it could then be imagined that the user aims more for an optimal permeability than for any of the other two properties. In that situation, the user might interpret results differently by passing results through a narrowed-down tolerance range for permeability.

Future research might also include the introduction of the tolerance range as a 'stop' function for the algorithm. The algorithm is then assumed to stop running before the number of generations is achieved.

It is recommended to enlarge the database of the system. In terms of practicalities, the string with variables will then have to be enlarged. Expanding the range of binder types, and additionally, allowing two (or more) binders to the algorithm to make one mortar recipe, would improve results. But also the enlargement of the sand discrete variables is believed to lead to better or equally good solutions for the same targets in less time, since the system has more materials to its disposition between it can choose and it can combine them more easily.

Bibliography

[1] Isebaert A, Van Parys L, Descamps T, Renglet M, Cnudde V. First steps to computer-aided decision-making in repair mortar recipes: working on three fronts. 10th Int. Conf. Struct. Anal. Hist. Constr. Anamn. Diagnosis, Ther. Control., Leuven: KU Leuven; 2016.

[2] Merriam-Webster Dictionary 2016.

[3] Deb K. Multi-objective optimisation using evolutionary algorithms: an introduction. In: Wang L, Ng AHC, Deb K, editors. Multi-objective Evol. Optim. Prod. Des. Manuf., London: Springer London; 2011, p. 3–34.

[4] Deb K. Multi-Objective Optimization using Evolutionary Algorithms. Chichester: John Wiley & Sons Ltd.; 2001.

[5] Sasse HR, Snethlage R. Methods for the evaluation of stone conservation treatments. In: Baer NS, Snethlage R, editors. Dahlem Work. Sav. our Archit. heritage, Conserv.

Hist. stone Struct., John Wiley & Sons Ltd.; 1997, p. 223–43.
[6] Gustafsson L, Sternad M. When can a deterministic model of a population system reveal what will happen on average? Math Biosci 2013;243:28–45. doi:10.1016/j.mbs.2013.01.006.
[7] Osyczka. Studies in Fuzziness & Soft Computing, Berlin: Springer Verlag; 2002.
[8] Zitzler E, Laumanns M, Thiele L. SPEA2 : Improving the Strength Pareto Evolutionary Algorithm 2001:1–21.
[9] Dabhi VK, Chaudhary S. Empirical modeling using genetic programming: a survey of issues and approaches. Nat Comput 2014. doi:10.1007/s11047-014-9416-y.
[10] Justesen PD. Multi-objective Optimization using Evolutionary Algorithms. University of Aarhus, 2009.
[11] Kim M, Hiroyasu T, Miki M, Watanabe S. SPEA2+: improving the performance of the strength Pareto evolutionary algorithm 2. Parallel Probl Solving from Nat PPSN VIII 2004;3242:742–51.
[12] Srinivas N, Deb K. Multiobjective Optimization Using Nondominated Sorting in Genetic Algorithms. J Evol Comput 1994;2:221–48.
[13] Deb K, Agrawal S. A fast elitist non-dominated sorting genetic algorithm for multi-objective optimization: NSGA-II. Parallel Probl Solving from Nat PPSN VI, Lect Notes Comput Sci 2000;1917:849–58.
[14] Deb K, Sundar J, Udaya Bhaskara RN, Chaudhuri S. Reference Point Based Multi-Objective Optimization Using Evolutionary Algorithms. Int J Comput Intell Res 2006;2:273–86. doi:10.5019/j.ijcir.2006.67.
[15] Van Parys L, Léoskool L, Rouge S, Isebaert A, Renglet M. Targeting Colour and Modulus of Resistance for a repointing mortar through a genetic algorithm. In: Hughes J, editor. 3rd Hist. Mortars Conf., Glasgow: University of the West of Scotland; 2013, p. 1–8.
[16] Leoskool L, Van Parys L, Renglet M, Rouge S. Compatible mortar for masonry restorations: discrete optimization for equivalent strength and colour prescription. ICDS12 - Int. Conf. durable Struct., 2012, p. 1–11.
[17] Goldberg D, Deb K, Clark J. Genetic algorithms, noise, and the sizing of populations. Complex Syst 1992;6:333–62.

Chapter 7 Exploitation of the estimation tool

The previous chapters have one by one looked into possible estimation methods for permeability, colour and elasticity, and discussed how these estimation methods can be set into a larger system of a raw material database coupled to a genetic algorithm. This chapter illustrates how this entire system can be exploited, by creating and testing repair mortars for four sedimentary stones. This chapter mainly aims to determine whether or not the repair mortars which are estimated, indeed also have these properties in reality. Additionally, the mortars will be compared with the natural stones they were targeted for. Since all estimation methods used in this system were developed for lime mortars after 90 days curing, logically, the mortars will also be tested at 90 days of age.

The exploitation of the estimation tool as presented here is twofold. The first part concludes a comparison between estimation and measured mortars, after an experimental campaign was performed. The runs were performed in November 2015 with the Repair Mortar Optimisation tool (ReMO) v0.0: time was calculated in the planning in order to guarantee a curing time of 90 days and to guarantee sufficient time for testing. Consequently, the results presented in this part give an indication of the system's performance in November 2015. Moreover, the results obtained in this chapter have helped improve the estimation methods and the set-up of the algorithm, and have led to the results presented in chapters 3 to 6 and to the development of ReMO v1.0.

The second part presents the runs performed on the ReMO v1.0. For these runs, the same mortar target values were used, and the results were compared with the results from the ReMO v0.0 on both mortar recipe and performance. Due to time limitations, the mortar recipes proposed in this second part could not be produced and tested.

7.1 Natural stone selection

Four sedimentary stones were considered for this exploitation study:

- Avesnes stone, a limestone from the Cambrai-Artois region, France

- Maastrichter stone, a limestone from the Limburg region, Belgium and Netherlands
- Obernkirchener stone, a quartzite from the Hannover region, Germany
- Savonnières stone, a limestone from the Meuse department, France

The selected stones are all sedimentary stones used in the built heritage in Belgium and in bordering countries. In order to test the system on a range of stones, their properties, described in this section, had to vary from one another. Their properties can be found in the next section. A general description and information concerning origin, use and weathering of each stone can be found in Appendix 7.1. The Maastrichter, Obernkirchener and Savonnières stones were blocks from the quarry, from Mergelbouwsteen P. Kleijnen (NL), Obernkirchener Sandsteinbrüche (DE) and Exploitation de Carrières Savonnières (FR) respectively, while the Avesnes stone came from blocks used as pillars in the chapel of the former Ursuline convent in Mons, Belgium. Due to adaptive reuse of the convent's chapel, some blocks of these pillars were removed. The stone block used did not show weathering or deterioration. The inner part of one Avesnes block was sawn into smaller test specimens.

Open porosity, water and gas permeability, colour, static module of elasticity and compressive strength were tested on all stone types. Sample preparation and testing procedures for open porosity and both permeability tests are described in chapter 3, the sample preparation and testing method for colour was described in chapter 4. All CIELAB values presented in this chapter do not include the correction performed on the Y coordinate of xyY. Compressive strength was tested according to the European standard EN 1926 (2007).

7.1.1 Avesnes stone

The stone can be described as a white greyish chalky limestone. The stone from the Ursuline Convent, Mons, is quite homogeneous in its properties (Table 7.1). Despite that its influence as historical building material is well documented, the mechanical properties of this stone are not. Based on the geological description of the stone as a chalk limestone, it is logical to assume that the stone is not very resistant, and should have a high porosity, as was indeed concluded from the tests on the stone from the chapel. It proved much more difficult to obtain reference values in comparison to the other stones. The only property value of this stone found in this research, was the compressive strength, 8 MPa, according to Camerman (1961). The colour of the stone can be seen in detail in Fig. 7.1, the colour coordinates [L*,a*,b*] of the studied stone were [89.393; 1.881; 15.810].

Table 7.1. Properties of the Avesnes stone: author's results compared to results in [1].

App. mass density [kg/m³]	Open porosity [%]	kwater [10^{-12} m²]	Fc [MPa]	Estat [MPa]
1477.12 ± 0.16	45.64 ± 5.95	3.89 ± 0.57	16.58 ± 2.30 8*	1882.97

* Value from Camerman (1961), repeated in [1]

7.1.2 Maastrichter stone

The Maastricht limestone is a well-sorted, yellow coloured, fine to coarse grained limestone. The tested Maastrichter stone presented very homogeneous results (Table 7.2). Compared to Maastrichter stone values from literature, these values are in the range of what is expected: high porosity, low density. Due to its low compaction, this stone has a very high porosity and a very low compressive strength. Only one Maastrichter sample was tested for its water and gas permeability, since samples broke during both permeability tests. The colour of the stone can be perceived in Fig.7.2, its CIELAB coordinates are [92.575; 3.819; 28.793].

Table 7.2. Properties of the Maastrichter stone: comparison of the author's results and results from [2].

App. mass density [kg/m³]	Open porosity [%]	kwater [10^{-9} m²]	Fc [MPa]	Estat [MPa]
1275.4 ± 8.47	52.65 ± 0.36	7.46 ± 2.08	2.05 ± 0.72	338.57± 100.10
1322 ± 18*	51.7 ± 0.8*		3.2 ± 0.7*	

* Values from [2].

7.1.3 Obernkirchener stone

Obernkirchener sandstone is a homogeneous compact sandstone. The stone is homogeneous in its properties and only shows small variations. The open porosity measured on the stone in this study is higher than the values found in literature (Table 7.3). The compressive strength is however similar to results found in literature. The colour of the Obernkirchener stone can be seen in Fig. 7.3, the [L*,a*,b*] colour coordinates are [86.006; 2.685; 12.995].

Table 7.3. Properties of the Obernkirchener stone: comparison of the author's results and results from [1,3].

App. mass density [kg/m³]	Open porosity [%]	kwater [10^{-12} m²]	Fc [MPa]	Estat [MPa]
2009.2 ± 43.1	24.19 ± 1.66	6.30 ± 2.27	94.62 ± 8.87	3225.20 ± 99.96
2260*	16 to 21°		94*	

* Values from [1], ° Value from [3]

Fig. 7.1 Macroscopic image of the stone from the chapel of the Ursuline convent, Mons. The block in this image shows small bioturbations from top to bottom on the right of the image. Other parts of the stone show larger bioturbated zones. The scale is in centimetre.

Fig. 7.2 A macroscopic image of the sawn surface of the Maastrichter stone sample used in this study. The scale is in centimetre.

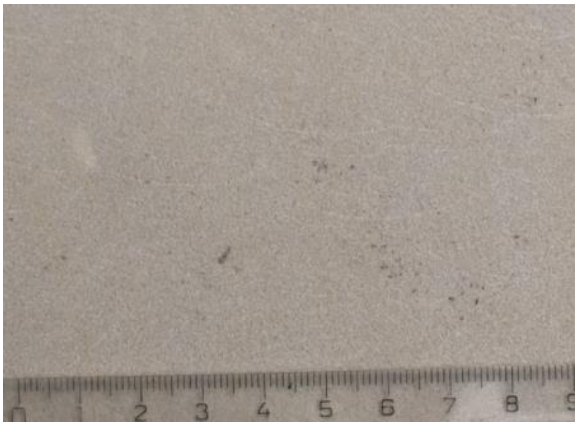

Fig. 7.3 Macroscopic image of the grey variety of Obernkirchener sandstone, used in this study. The scale is in centimetre.

Fig. 7.4. Macroscopic photo of the Savonnières limestone used in this study. The scale is in centimetre.

7.1.4 Savonnières stone

The Savonnières is a grey to yellowish oolithic limestone with a grainstone texture (Fig.7.4). The stone's porosity and apparent density is in line with the values found in literature (Table 7.4). The compressive strength of the stone is also situated in the range normally measured on this type of stone. The Savonnières' elevated porosity is translated into a higher water permeability. The stone's colour with CIELAB coordinates [98.034; 3.419; 19.792] can be seen in Fig.7.4.

Table 7.4. Properties of the Savonnières stone: comparison of the author's results and results from [1].

App. mass density [kg/m³]	Open porosity [%]	kwater [10^{-12} m²]	Fc [MPa]	Estat [MPa]
1810.3 ± 64.61	33.71 ± 2.11	10.30 ± 3.22	12.08 ± 1.50	n.d.
1748 to 1820*	30.6 to 34.7*		11.5 to 17.3*	13200 to
1897 to 2053°	24.0 to 29.7°		25.4 to 30.5°	14600°

The static elasticity of the Savonnières was not determined. * Values from [1], ° values from [4].

7.1.5 Stone properties: overview

The properties of each stone discussed in the previous subsections are listed in Table 7.5. As this table illustrates, the stones vary in properties, mainly in compressive strength and permeability. Two extremes in comparison to the other three stones exist: the Obernkirchener and its high compressive strength, and the Maastrichter with a low compressive strength. In addition, the Maastrichter stone is also very permeable in comparison to the other stones. This high permeability was already discussed in literature [1], where it is assumed to be the reason for the unexpected durability of such an uncompacted stone. The water permeability of the Obernkirchener is similar to the permeability of the Savonnières and Avesnes stone. In terms of porosity, all stones have a medium to high porosity.

The colour of all stones can be roughly described in the green to grey, and beige to yellow area.

All stones were tested on their compressive strength according to the EN standard for natural stones, which is a different standard than for lime mortars. Since the static E modulus was measured during each compressive strength tests, the static E modulus was obtained using the same method, but using other parameters and samples size: 5 x 5 x 5 cm^3 for stone and 4 x 4 x 4 cm^3 for mortars.

Table 7.5. The properties of the selected Obernkirchener (Ober), Savonnières (Savonn), Avesnes and Maastrichter (Maast) stones. E_{stat} was calculated, taking into account elongation, based on results from the Rc tests (EN-1926) (chapter 5). The CIELAB values presented here do not include the correction performed on the Y coordinate of xyY. Only one Maastrichter sample was tested for its gas and water permeability, since samples broke during both tests. The static elasticity of the Savonnières was not established.

Stone	Kwater [10^{-12} m^2]	Kgas [10^{-14} m^2]	f [%]	[L*,a*,b*]			Fc [MPa]	Estat [MPa]
Ober	6.30 ± 2.27	1.50 ± 0.50	24.19 ± 1.66	86.006	2.685	12.995	94.62 ± 8.87	3225.20 ± 99.96
Savonn	10.30 ± 3.22	2.72 ± 0.49	33.71 ± 2.11	98.034	3.419	19.792	12.08 ± 1.50	n.d.
Avesnes	3.89 ± 0.57	67.70 ± 0.14	45.64 ± 5.95	89.393	1.881	15.810	16.58 ± 2.46	1882.97 ± 145.94
Maast	7460 ± 2080	900	52.65 ± 0.36	92.575	3.819	28.793	2.05 ± 0.72	338.57 ± 100.10

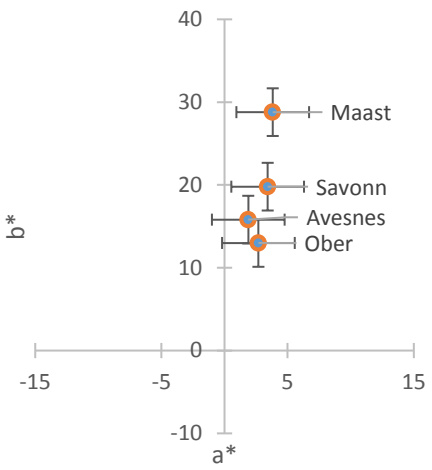

Fig. 7.5 A Tolerance range allowed on the a*,b* coordinates of the mortar (*blue*). The stone's values are indicated in *orange*.

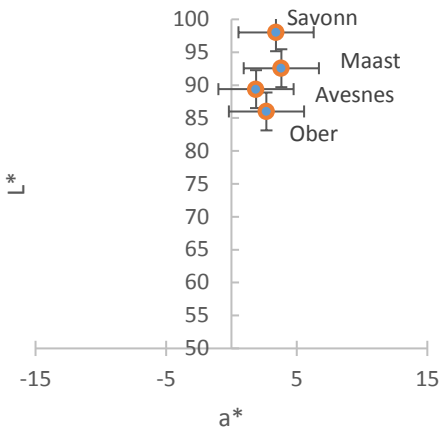

Fig. 7.5 B Tolerance range allowed on the a*,L* coordinates of the mortar (*blue*). The stone's values are indicated in *orange*.

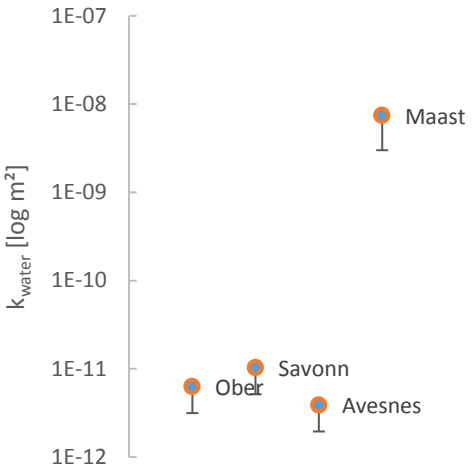

Fig. 7.5 C Tolerance range allowed on the water permeability of the mortar (*blue*). The stone's values are indicated in *orange*.

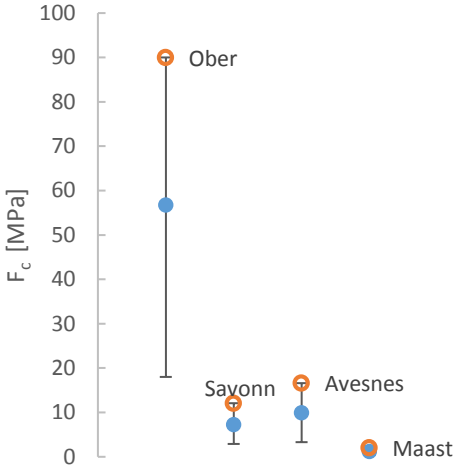

Fig. 7.5 D Tolerance range allowed on the compressive strength of the mortar (*blue*). The stone's values are indicated in *orange*.

7.2 Algorithm exploitation run ReMO v0.0

The developed system was tested on its ability to estimate the properties of the mortars correctly, and on its ability to present mortars close to the target values. At the moment of this first exploitation run, the system was not yet completely finished: the study in compressive strength for example was completed, but not the estimation for elasticity. Therefore the target for a compatible compressive strength was used instead. Since we discussed that the static modulus of elasticity was directly related to the compressive strength, the same (relative) tolerance range for elasticity, as proposed by Sasse & Snethlage (1997), was used for the compressive strength [5]. The targets in the algorithm are the values as stated in Table 7.5, i.e. the maximum permeability and identical colour is demanded, except for the F_c

target, which was set at 0.6 F_c of the stone. In the end, the estimated mortar properties should lie between the minimal and maximal limit of tolerance as stated in Fig.7.5.

The mortars proposed by the algorithm will be composed of the sands and binders present in the database. Therefore, the mortars proposed in this chapter will be judged on their compatibility in terms of performance only (permeability, colour, elasticity), and not on their mineralogical composition. As explained in the Introduction of this thesis, the goal of this research was to improve the general development of repair mortars for various stone types, by improving the compatibility in properties.

Based on the binders and sands present in the database currently available, the repair mortars proposed by the system will most likely not approach the compressive strength of the Obernkirchener, Avesnes or Savonnières. However, the tolerance range for compatibility (Fig.7.5 A-D) demands a lower compressive strength. The minimal value of this tolerance range is believed to be achievable, except for the Obernkirchener repair mortars.

Results in chapter 3 indicated that NHL mortars are in general not as permeable as the Maastrichter stone and it might therefore also prove a challenge to achieve a repair mortar with properties close to the desired permeability.

Fig. 7.6 A-B represent the colour of each database element and the colour of the stones measured. The figures lead us to conclude that three out of four stones have a colour in the area between the colours of the various database elements. According to Grassmann's theory, it should therefore be possible to create mortars in a similar colour as these three stones, but it might prove difficult for the Maastrichter stone.

The parameters chosen for this exploitation study of the system are the same as those discussed in the validation section of chapter 6. For this study, the number of generations was set at 20 for a population size of 600 individuals, assuming the population would have sufficiently converged close to the optimum. The algorithm needed between 45 and 70 minutes to calculate to reach the maximum number of generations. Convergence was achieved without major problems.

Mortar recipes from the last generation of the population were chosen based on their distance towards the ideal point X (chapter 6). Five mortar recipes were selected based on minimal Δk and ΔE^* values combined. In Appendix 7.2, the variation of these 5 mortar recipes proposed by the system is presented per stone type.

Two mortar recipes were selected from these five through a second selection, based on their workability. Both W/B and W/A ratio were calculated for each recipe. Based on this information and the graph Fig.2.6 in chapter 2, an indication of the spread of the mortars was sought. In this way, the very liquid mortars proposed by the tool for the Maastrichter stone

and the very dry mortar recipes for the Obernkirchener stone could be left out. As such the two best mortar recipes per stone in terms of colour and permeability, as well as workability, were chosen.

Table 7.6 represents the recipe for each mortar estimated by the tool. These mortars were produced similar to all other mortars in this thesis (chapter 2). Their spread, measured on the fresh mortar, is represented in the bottom row of Table 7.6. The spread of the Maast-4 mortar could not be determined; it was too fluid after the flow table test. The Ober mortars were very dry, therefore the spread was 100 mm, i.e. the diameter of the cone.

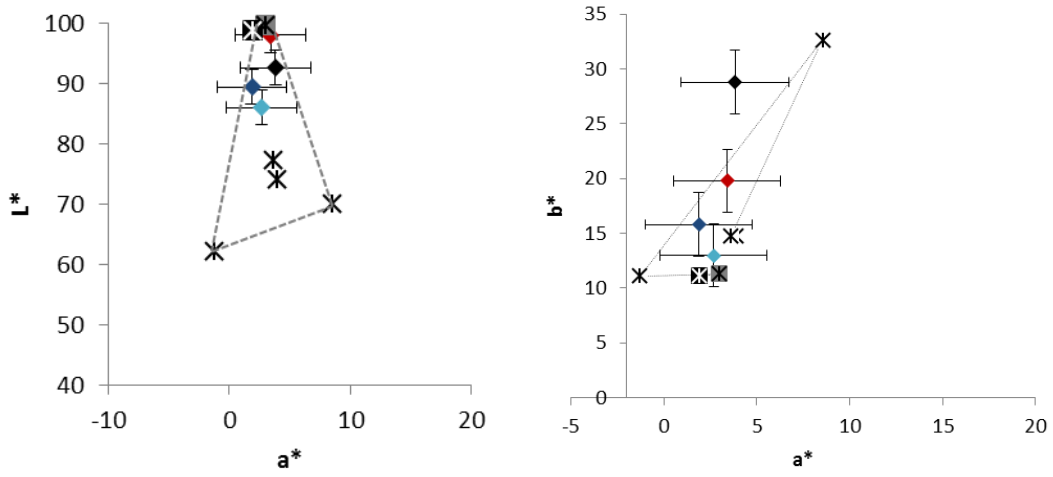

Fig. 7.6 A-B The CIELAB coordinates of every stone, and of every sand and binder in the database. The binders NHL5 and NHL 3.5 are represented as *filled stars*, the *black stars* are sands. *Black diamond* Maastrichter, *red diamond* Savonnières, *blue diamond* Avesnes, *light blue diamond* Obernkirchener. The bars indicate the tolerance range allowed for a total colour difference $\Delta E^* < 5$.

Table 7.6. Table representing the mortar recipes proposed by the tool, which were considered for production. The v% given by the tool were transferred into mass [kg] in order to be able to produce the mortars precisely. The graph represents the quantity of sand, binder and water used, as well as the spread measured on the mortar.

Component [kg]	**Ober**		**Savonn**		**Avesnes**		**Maast**	
	-3	**-4**	**-1**	**-2**	**-1**	**-2**	**-3**	**-4**
NHL 3.5	-	0.475	-	-	0.651	0.643	0.685	0.510
NHL 5	0.556	-	0.819	0.869	-	-	-	-
Rhin gros	-	-	-	0.388	-	-	0.641	-
Rhin fin	-	-	1.277	1.296	1.812	1.865	-	1.704
Yellow	1.681	-	-	-	-	0.369	1.129	-
Green	0.437	2.926	0.398	-	0.381	-	-	0.464
Water	0.579	0.625	0.638	0.607	0.528	0.501	0.867	0.872
Spread [mm]	100	100	200	200	150	110	180	n.d.

Table 7.7 represents the properties each mortar recipe is estimated to have after 90 days of curing. The last three columns of Table 7.7 point out the difficulty and complexity of choosing one mortar recipe amidst the mortar recipes proposed. The first selection parameter of favouring permeability and colour is clearly visible. As expected, the estimated resistance of mortar recipes based on this database is not high enough, leading to large differences between target and estimated value.

In addition, the results also point out that the ranking of individuals is relative to the other individuals in the population, making it as such possible that a mortar recipe with a difference of nearly 100% for one property can find himself amidst the best mortar recipes of the population.

It is also not surprising that the estimated water permeability for the Maast mortars is very distant from the targeted water permeability, since the Maastrichter stone is a very permeable stone.

The large estimated colour difference for the Maast mortar recipes could be expected, since the stone lies out of the theoretical volume (L*a*b*) the database can cover in terms of colour. However, better results were expected for the Savonnières and Obernkirchener, both with colours that theoretically can be made with the provided database. Two elements might have not played in this colour estimation's favour however: (a) the system is bound by the constraints which were set, such as the amount of sand, binder and water which can be added, and (b) the system needs to find mortar recipes which have properties close to all targets which are demanded.

Fig.7.8 shows that both Maast-3 and Ober-4 estimated colours are situated on the border of the theoretical L*,a* area the database can cover.

Table 7.7. Property values from each mortar, as estimated by the tool. The three columns on the right indicate the relative distance the mortars are *estimated* to be from the stone properties. Consider that the E_{stat} values are the values that were calculated after the run.

Mortar	k_{water} [10^{-12} m²]	f [-]	D1 [10^{-7} m]	[L*,a*,b*]			Fc [MPa]	E_{stat} [MPa]	**Δk_w [%]**	**ΔE * [-]**	**ΔF_c [%]**
Ober-3	4.22	0.43	7.75	86.86	4.91	21.00	2.26	307.81	**36.3**	**8.4**	**97.5**
Ober-4	1.88	0.30	8.72	86.06	0.52	11.81	0.62	84.58	**40.1**	**2.5**	**99.3**
Savonn-1	2.79	0.39	6.70	90.96	2.77	13.36	2.71	368.92	**71.5**	**9.6**	**81.2**
Savonn-2	7.38	0.49	15.9	91.56	3.39	13.69	3.30	448.77	**28.3**	**8.9**	**77.1**
Avesnes-1	2.78	0.36	6.84	89.27	2.39	13.65	4.31	586.54	**32.1**	**2.2**	**74.0**
Avesnes-2	4.73	0.36	12.0	89.37	3.43	15.62	4.14	562.49	**15.7**	**1.6**	**75.1**
Maast-3	11.9	0.57	19.6	89.21	5.38	19.32	1.37	186.92	**99.8**	**10.2**	**31.3**
Maast-4	4.58	0.37	8.93	89.14	2.79	13.75	0.79	106.94	**99.9**	**15.5**	**60.7**

7.3 Laboratory-based verification of the estimation

The mortars proposed by ReMO v0.0 were tested after 90 days on colour, elasticity and compressive strength, porosity, water and gas permeability and pore size distribution, according to the methods from the experimental campaigns from chapters 3, 4 and 5. No cylindrical samples were made available for this set of mortars, so cylinders had to be drilled out of the bars. Some mortars proved however not resistant enough, and another means had to be found to be able to test these mortars on their porosity and permeability. Therefore, little bars of 25 x 25 x 50 mm were sawn, and their edges were rounded by sanding paper. By turning the sample regularly, a cylindrical shape could be obtained.

7.3.1 Permeability and pore-related properties

Pycnometry tests were followed by gas permeability and water permeability tests. Both pycnometry and gas permeability tests evoked fissures and cracks in some samples, especially in the Ober mortar series: only one sample of the Ober-3 mortar could be measured for both permeability tests, and three Ober-4 samples broke during the water permeability test, so no water permeability could be measured for this mortar. Also Avesnes-2 showed a very high water permeability, which is not in balance with its measured gas permeability (Fig.7.7 & 7.8). It might be that some fissures were formed during the water permeability tests, thereby increasing the water permeability artificially. Since its gas permeability values are in comparison much lower, it might be that the water permeameter test also has caused small fractures which were used as preferential pathways in the sample by the water.

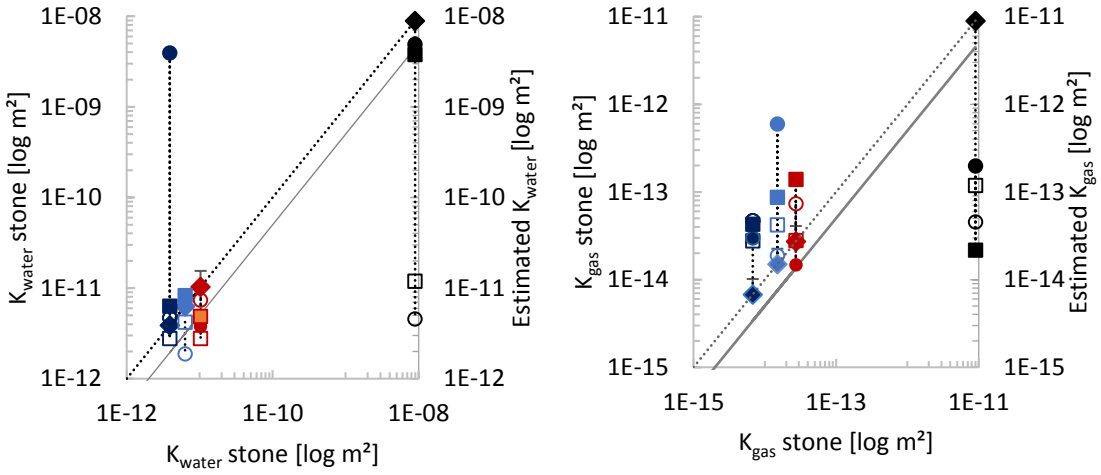

Fig. 7.7 & 7.8 Error bars represent the standard deviation on the measured stone permeability. The minimum allowed permeability for the compatibility tolerance range is indicated with a grey full line. The estimation was better for water permeability values than for gas permeability estimation. *Black diamond* Maastrichter, *red diamond* Savonnières, *blue diamond* Avesnes, *light blue diamond* Obernkirchener. *Empty square* and *circle* the estimated value of 1st and 2nd mortar. *Filled square* and *circle* the measured value of 1st and 2nd mortar (Fig. 7.12 E for the complete legend).

Because some mortar water permeability results are not reliable due to assumed fissures, the estimation quality of permeability will be compared based on the gas permeability measurements $\Delta K_{g\ m\text{-}e}$ for all mortars, on the water permeability for the reliable results. Fig. 7.8 shows that the gas permeability for 4 out of 8 mortars is underestimated. Three out of four mortars that were overestimated, have the lowest difference values: Avesnes-2 with 54%, Savonn-2 with 80% and Maast-3 with 81% (Table 7.8). Only the Maast-4 mortar is both overestimated and has a high difference between estimated and measured value. When comparing estimated values with the actually measured properties, the water permeability is underestimated for 5 out of 6 mortars (excl. Ober-4 and Avesnes-2 for erratic results).

In addition, the estimations for both porosity and pore throat diameter were compared to the measured values. The MIP analysis showed that the mortars have a bimodal pore size distribution, except for the Ober mortars (unimodal). A comparison between both estimated and measured values show that the first modal pore diameters in 5 out of 8 mortars was overestimated with an average perpendicular distance of 2.4E-7 m; the second modal pore diameters were overestimated, with an average perpendicular distance of 4.3E-8 m (Fig. 7.9 & 7.10).

Table 7.8. Pore-related properties measured on the mortars as well as the relative difference with the targeted value, $\Delta K_{w\ m\text{-}s}$, represents the relative difference between the measured mortar and measured stone permeability values, the $\Delta K_{w\ m\text{-}e}$ the relative difference between measured and estimated mortar permeability values, and $\Delta K_{w\ e\text{-}s}$ the difference between the estimated mortar and measured stone permeability values.

			Measured				Estimate
	$\Delta K_{g\ m\text{-}e}$ [%]	**$\Delta K_{w\ m\text{-}s}$ [%]**	K_w [10^{-12} m²]	f [-]	D1 [10^{-7} m]	K_{gas} [10^{-14} m²]	ΔK_w [%]
Ober-3	**107.16**	**31.54**	8.29	0.3719	5.95	8.74	36.25
Ober-4	**3066.20**	-	n.d.	0.4091	4.04	59.6± 30.5	40.06
Savonn-1	**400.76**	**52.73**	4.87± 0.66	0.5186	9.86	14.0± 19.1	71.54
Savonn-2	**80.00**	**63.05**	3.81± 0.23	0.4852	10.6	1.48± 0.52	28.25
Avesnes-1	**54.36**	**62.64**	6.33± 0.65	0.3643	9.66	4.29± 0.71	32.06
Avesnes-2	**54.44**	**100965.04**	*393± 0.23*	0.3570	10.8	3.00± 0.36	15.74
Maast-3	**81.76**	**57.69**	378± 25.2	0.3931	17.7	2.18± 0.05	99.84
Maast-4	**335.56**	**45.16**	490± 75.3	0.3833	15.6	1.99± 4.96	99.95

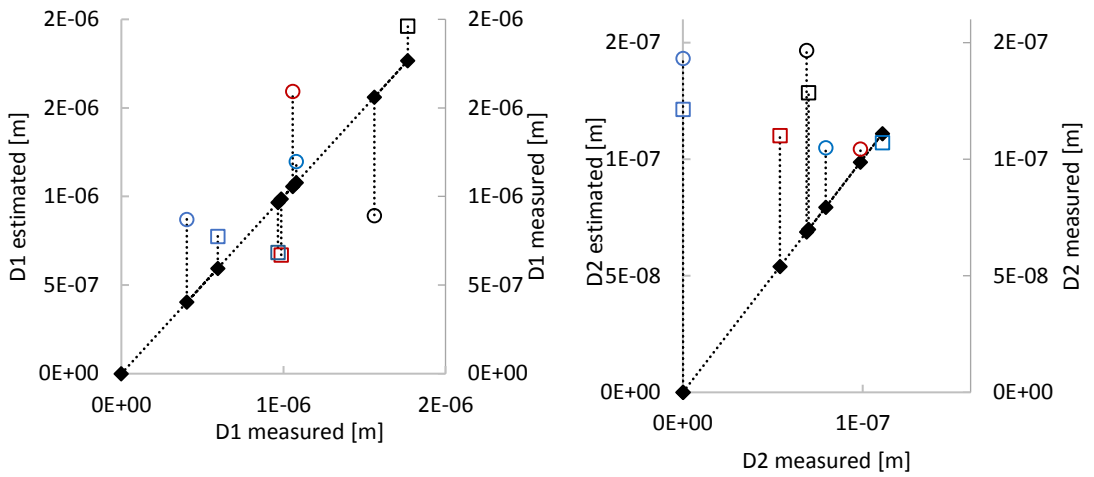

Fig. 7.9 & 7.10 The estimated pore diameters D1 approach the measured D1 pore diameters (cross), while the D2 pore diameters (cross) are generally overestimated. Both Ober mortars have a unimodal pore size distribution and have therefore no D2 pore diameter. The *empty square* and *circle* represent the estimated value of first and second repair mortar respectively, the *black diamonds* are the measured values of the repair mortars. *Light blue* is the Ober series, *red* the Savonn series, *dark blue* the Avesnes series, *black* the Maast series.

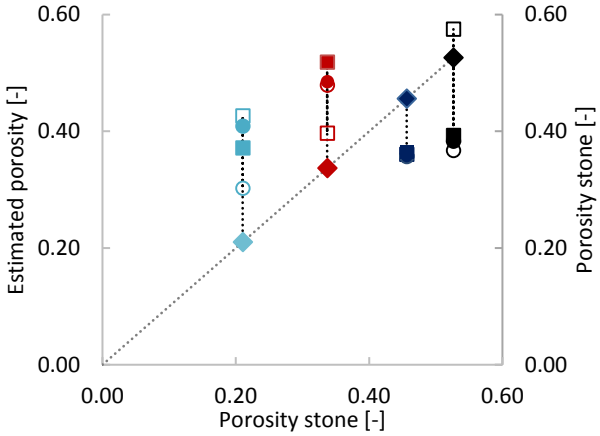

Fig. 7.11. The porosity of the mortars, both estimated and measured, and the porosity of the stone. *Black diamond* Maastrichter, *red diamond* Savonnières, *blue diamond* Avesnes, *light blue diamond* Obernkirchener. *Empty square* and *circle* represent the estimated value of 1st and 2nd mortar, *filled square* and *circle* the measured value of 1st and 2nd mortar (see Fig. 7.12 E for the complete legend).

Six out of eight mortars had their porosity underestimated (Table 7.8, Fig. 7.11). The best estimations of porosity were underestimations: estimations for Avesnes mortars were closest to the actual measured values, with a difference of 0.4 and 0.1% respectively. Porosity estimation of Savonn-2 and Maast-4 were not far from the actually measured porosity value (0.6 and 1.6%) either. The other 4 mortars had a difference larger than 5% (max. 18%), two were underestimated (Ober-4, 10%; Savonn-1, 12%) and two were overestimated (Ober-3, 5.5%; Maast-3, 18.2%).

Conclusively, the permeability is generally underestimated. Porosity is generally underestimated, the pore diameter overestimated.

If we compare the measured mortar permeability with the permeability of the stone $\Delta K_{w\ m\text{-}s}$, 5 out of 8 mortars perform better than was initially estimated (Table 7.8). Taking the tolerance range allowed for permeability into account, Ober-3 falls into the tolerance range set and Avesnes-1 and Savonn-1 and -2 mortars fall just out of the tolerance range. Since the pore structure of Avesnes-2 and both Maast mortars was assumed to be altered by the water permeameter test, only their gas permeability is taken into account here. In that situation, the Avesnes-2 mortar falls into the permeability tolerance range, the Maast mortars do not.

7.3.2 Colour

The measured [x,y,Y] coordinates were converted into [L*,a*,b*] coordinates using the CIE 1976 calculation method [6] in order to calculate the total colour difference. The first column of Table 7.9 indicates that the difference between measured and estimated colour $\Delta E^*_{m\text{-}e}$ is acceptable for some, but large for other mortars. For 4 out of 8 mortars, this difference is lower than 5 colour difference values: the estimated and the measured colour would thus be judged as the same colour. The estimation for the Savonnières mortars, the Avesnes-1 and Ober-4 mortars performed better than the estimation for the Ober-3 mortar, Avesnes-2 or Maastrichter mortars. These last four mortars show estimation errors between 6 and 10.4: the colours are thus distinctly different.

Table 7.9. The difference in chromaticity (ΔC*) and total colour (ΔE*) is represented for the pair measured-stone ($\Delta E^*_{m\text{-}s}$), estimated-stone ($\Delta E^*_{e\text{-}s}$) and measured-estimated ($\Delta E^*_{m\text{-}e}$). Colour coordinates per mortar recipe are also given. The chromaticity difference was calculated as $\Delta C^*_{i-j} = \sqrt{(\Delta a^*)_{i-j}{}^2 + (\Delta b^*)_{i-j}{}^2}$.

				Measured			Estimated	
Mortar	**$\Delta E^*_{m\text{-}e}$**	**$\Delta E^*_{m\text{-}s}$**	**$\Delta C^*_{m\text{-}s}$**	L*	a*	b*	$\Delta E^*_{e\text{-}s}$	$\Delta C^*_{e\text{-}s}$
Ober-3	**13.17**	**20.34**	**19.51**	80.264	4.740	32.396	8.35	8.31
Ober-4	**4.11**	**5.29**	**4.96**	80.264	-2.013	13.779	2.47	2.47
Savonn-1	**4.59**	**9.05**	**8.43**	94.734	0.649	11.830	9.58	6.47
Savonn-2	**3.39**	**8.12**	**7.30**	94.479	2.030	12.627	8.90	6.10
Avesnes-1	**4.92**	**5.40**	**2.82**	93.999	1.159	13.087	2.22	2.22
Avesnes-2	**9.35**	**9.24**	**9.03**	91.320	3.106	24.759	1.56	1.56
Maast-3	**10.39**	**3.59**	**1.39**	89.266	4.870	29.693	10.18	9.60
Maast-4	**6.03**	**16.50**	**16.35**	94.776	0.916	12.699	15.46	15.08

Remark that all measured L*,a*,b*- values (Table 7.9) show a shift towards higher luminance (L*↑), slightly greener range (a*↓) and mostly, to a more yellow range (b*↑). Four mortars actually lie out of the area which, according to Grassmann theory, should be theoretically feasible to achieve with the selected database (Fig.7.12 A-E). These mortars are assumed to lie out of this area mainly because of the shift in L*, and b* values. This trend might be related to two elements: the diffusivity of the surface which is not

taken into account in the estimation method of Grassmann and to the light used in the black room, which is not entirely equal to a D65 light source (Appendix 4.1), and is more yellow than a D65 light source.

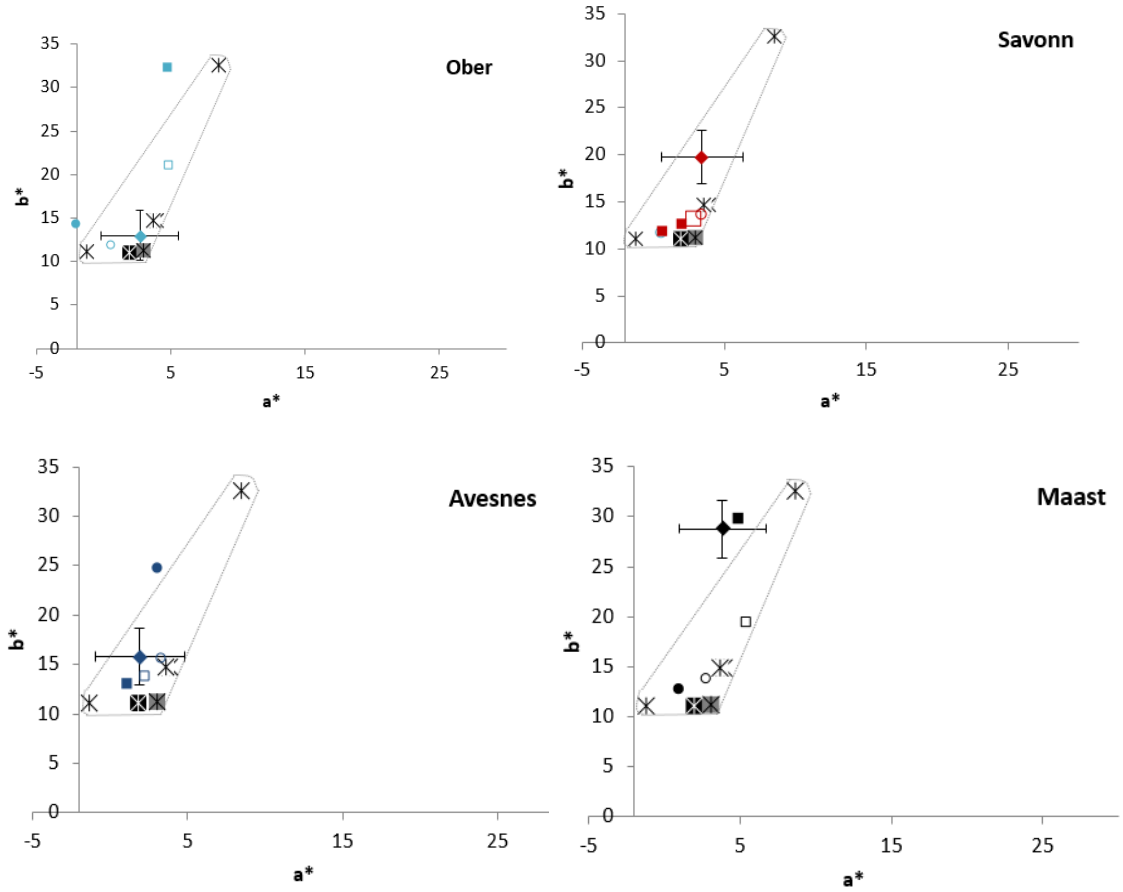

Fig.7.12 A-D. These four graphs represent the a*,b*-coordinates of the stone and the tolerance range attributed to it, as well as the coordinates for the estimated and measured mortars. The binders NHL5 and NHL 3.5 are represented as *filled stars*, the *black stars* are sands. *Black diamond* Maastrichter, *red diamond* Savonnières, *blue diamond* Avesnes, *light blue diamond* Obernkirchener (see Fig. 7.12 E for the complete legend). The range which can be theoretically achieved based on these binders and sands is the area bounded by the dotted line, taking into account an approximation of the error on the measurement.

The crushed mortars and stones used for the colour measurement are represented in Fig.7.13. Consider that the algorithm proposed these mortar recipes based on the xyY coordinates of binders and sands, and estimated the colour of the mortar mix based on the adapted Grassmann theory (as in November 2015). Comparing the measured mortar colour with the colour of the stone (Table 7.9), only Maast-3 has a colour close enough to fall in the narrow tolerance range of <5 (3.59). Both Ober-4 and Avesnes-1 (5.3 and 5.4) have a difference which can just be distinguished as a different colour. The difference in colour of stone and mortar for both Savonnières mortars, Ober-4, Avesnes-1 and the Maast-4 mortar approached the values of the expected difference (Table 7.9). The difference in colour with the stone was however larger for the Ober-3 mortars (20.34 instead of the estimated 8) and smaller for the Maast-3 mortar (3.39 instead of the estimated 10.2). These

large difference are assumed be due to the two elements stated above (light source and diffusive surfaces).

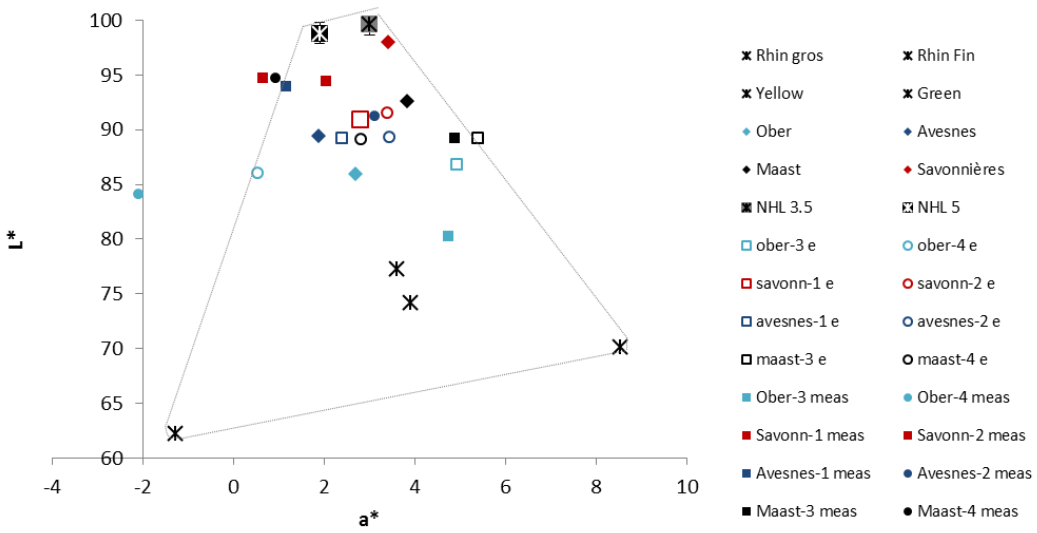

Fig. 7.12 E This graph represents the L*,a*-coordinates of the stones, and of the estimated mortar and measured mortar. The dotted line takes the approximation of the error on the measurement into account, the range which can be theoretically achieved based on these binders and sands is the area bounded by this line. Two estimated colours lie on this line. Four mortars produced fall out of this theoretically possible area.

A. FLTR: Oberkirchner stone, Ober-3, Ober-4

B. FLTR: Savonnières stone, Savonn-1, Savonn-2

C. FLTR: Avesnes stone, Avesnes-2, Avesnes-1

D. FLTR : Maastrichter stone, Maast-3, Maast-4

Fig.7.13 Photographs of the mortars and the stones.

7.3.3 Elasticity and compressive strength

Since the compressive strength was used as objective function for these validation runs, the compressive strength will be compared (Table 7.10) and the static elasticity is shown for indication.

The compressive strength of 6 out of 8 mortars was underestimated, only the Avesnes mortars showed a lower compressive strength than initially estimated (Table 7.10). The difference between estimated value and measured value varies significantly, between 2.5 and 60% with an outlier of 186% for Ober-4 mortars. Not taking into account this outlier, the average error on the estimation is 37.4 % (±17.3%).

The compressive strength of the mortars is mainly dependent of the real resistance of the NHL binders, it was unlikely to assume that the mortars would approach the actual compressive strength of the stones. Conclusively, all mortars are less resistant than the stones.

When comparing the measured mortar compressive strength with the stone's compressive strength, the tolerance range for compressive strength (20-100%) was assumed to be similar to the tolerance range for elasticity, which leads us to the conclusion that all mortars lie within the tolerance range for stone, with the exception of the Ober mortar series (Fig.7.14). This was as expected: the compressive strength of the Ober mortars show the lowest compatibility with the Obernkirchener stone, since the Obernkirchener stone shows a very high compressive strength (Fig. 7.14). The Maast-4 mortar achieved best the aimed-for value, i.e. 60% of the stone's compressive strength.

Table 7.10. Elasticity and compressive strength of the mortars.

			Measured		Estimated
	ΔFc m-e [%]	**ΔFc m-s [%]**	Fc [MPa]	Estat [MPa]	ΔFc e-s [%]
Ober-3	**2.54**	**97.42**	2.32 ±0.06	185.34 ±39.57	97.49
Ober-4	**186.04**	**98.02**	1.78 ±0.12	260.43 ±23.29	99.31
Savonn-1	**37.15**	**74.16**	3.72 ±0.09	553.91 ±112.23	77.54
Savonn-2	**59.69**	**63.41**	5.27 ±0.24	938.78 ±289.71	72.68
Avesnes-1	**47.96**	**86.46**	2.24 ±0.09	292.52 ±90.71	73.99
Avesnes-2	**29.40**	**82.39**	2.92 ±0.56	425.40 ± 37.74	75.05
Maast-3	**27.61**	**12.30**	1.75 ±0.14	149.87 ±56.18	31.28
Maast-4	**57.44**	**38.10**	1.24 ±0.05	233.72 ±80.90	60.09

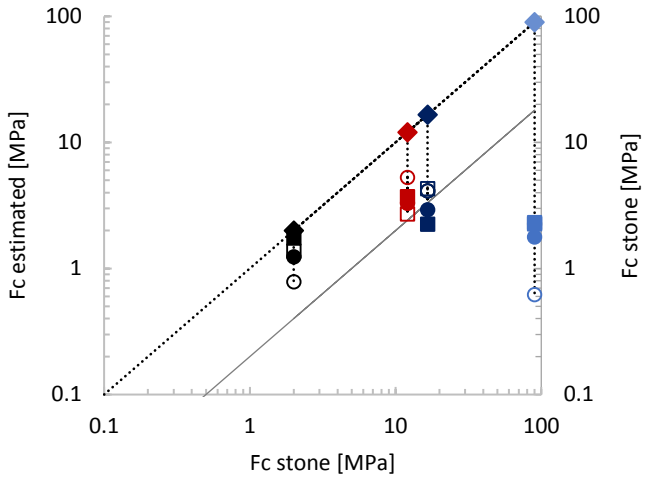

Fig. 7.14 The compressive strength of the mortars. The minimum allowed compressive strength for the compatibility tolerance range is indicated with a grey full line. *Black diamond* Maastrichter, *red diamond* Savonnières, *blue diamond* Avesnes, *light blue diamond* Obernkirchener. *Empty square* and *circle* the estimated value of 1st and 2nd mortar. *Filled square* and *circle* the measured value of 1st and 2nd mortar (see Fig. 7.12E for the complete legend).

7.4 Algorithm exploitation run ReMO v1.0

7.4.1 ReMO v1.0: improvements and features

ReMO was improved on various aspects. Firstly, the objective functions were adapted: the permeability estimation function was improved, the compressive strength estimation function was improved and transformed into the elasticity estimation function and the colour estimation function was improved. Secondly, an indication of the spread is now given for every mortar recipe. It is also this version of the system for which a GUI and the standalone application was made.

7.4.2 Comparison between ReMO v1.0 and ReMO v0.0

7.4.2.1 Approach for the comparison

For every stone, five new runs were performed with the ReMO v1.0. In order for a good comparison, the mechanical property to achieve was here compressive strength Fc, the property target also used in ReMO v0.0. The targets set for every stone in this new system were as such the same as the targets set in the older system. The individual labelled by the system as the 'best recipe' was retained. As such, the two older mortar recipes from ReMO v0.0 were compared with the five 'best mortar recipes' from ReMO v1.0 per stone. The mortar recipes were compared on their composition and on their estimated difference with the target values.

Below, a comparison is made between the different recipes per stone type. This comparison is more elaborate for the first stone discussed, the

Maastrichter stone, in order for the reader to comprehend which elements have been compared with each other throughout the entire section. The 'old' mortars refer to the mortars produced and tested in section 7.3, the 'new' mortars to the mortars proposed as best mortar recipe by ReMO v1.0.

7.4.2.2 Comparison of Maastrichter mortars

The new version of the system gives slightly different recipes for the Maastrichter stone than the two mortars made previously, that is, the components proposed are similar, the quantities are however different. Fig. 7.15A shows the composition of the old mortars in comparison with the five new mortars. As for the old mortar recipes, 4 out 5 new best recipes are made with NHL 3.5. The most preferred sand is the yellow sand (3 of 5), a sand type also used in the two old mortar recipes. The preference for Rhin gros or Rhin fin sands is less clear. The 3_NL mortar is most similar in components and quantities to one of the old mortars, Maast-3. The largest difference is that the quantities for Rhin fin and yellow sand are inverse. The 2_NL is the new mortar recipe which is furthest in composition of any of the two old mortar recipes: the only sand in this recipe is the green sand, and the quantities for both binder and water are much lower.

Comparing these values, certain trends show (Fig. 7.15B):

- The new mortar recipes should all approach the targeted Fc values much closer than the old recipes. When comparing the estimated Fc value of the most similar mortar recipe 3_NL (1.23 MPa) with the actual measured Fc values of Maast-3 (1.75 MPa), the estimation for Fc appears to have improved.
- The new mortar recipes are estimated to perform similar or better in colour difference than the old recipes. When comparing again recipe 3_NL with Maast-3, the estimated colour from 3_NL seems to be closer to the actual measured colour (ΔE^*_{est} 5.7 '3_NL', ΔE^*_{est} 10.18 and ΔE^*_{meas} 3.59 for 'Maast-3'). Hence, the colour estimation appears to have improved as well.
- The estimated permeability difference is still as high as estimated for the older mortar recipes, which is mainly due to the fact that the database is still the same and that the permeability of the Maastrichter stone is very elevated. No comparison can be made here with the measured samples, since the samples are thought to have altered during the permeability test.

Looking at the estimated differences with the target values and the composition of the mortar recipes, NL_3 appears to be the best performing new recipe of these 5, because of its use of yellow sand, NHL 3.5 and its estimated properties. However, the spread indicator estimates a spread of ±245 mm, which is very liquid. The other new mortars have a spread estimation between 200 and 300 mm. The least adapted mortar recipe appears to be 4_NL, it is estimated to perform worse on colour difference and does not perform better on any of the other targets. It contains green sand, for a yellow-coloured stone.

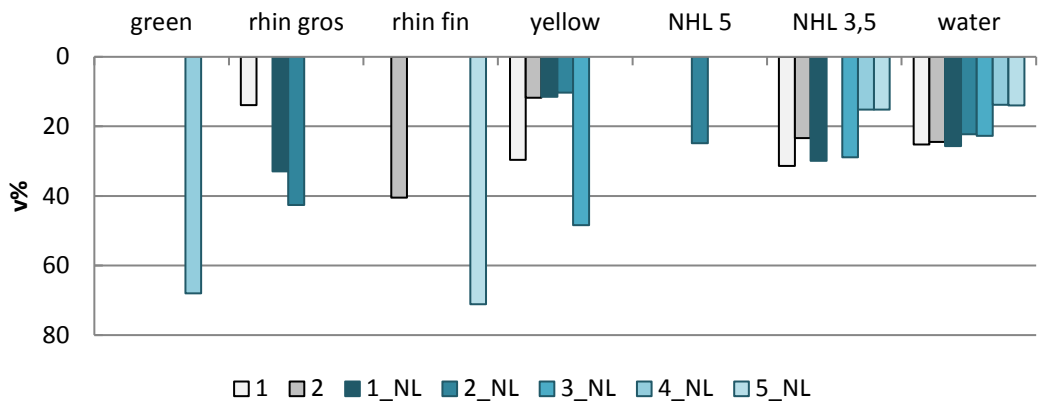

Fig. 7.16A Recipe composition in v% of every mortar component of the various new 'best mortar' recipes proposed by ReMO v1.0 (1_NL to5_NL), and the recipe composition for the Maast-3 and Maast-4 mortars, called 1 and 2 respectively.

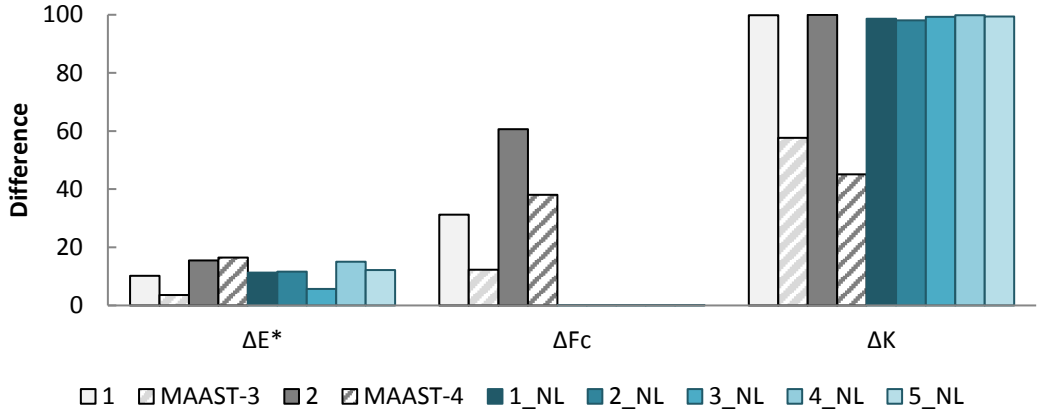

Fig. 7.16B Performance in compatibility of the various new 'best mortar' recipes proposed by ReMO v1.0 (1_NL to 5_NL), the *estimated* compatibility for the Maast-3 and Maast-4 mortars, called 1 and 2 respectively and the *actual* measured values for the Maast-3 and Maast-4 mortars. Remark that the ΔFc values from the new mortars are very low.

7.4.2.3 Comparison of Savonnières mortars

In ReMO v1.0, different mortar recipes are proposed for the repair of the Savonnières stone (Fig. 7.16A). The mortars differ in lime binder proposed (NHL 5 instead of NHL 3.5) and principal sand type (Rhin gros instead of Rhin fin) and in quantities for the sand types. A comparison of newly estimated values with the measured (old) mortar samples is therefore more difficult to make.

Comparing the *estimated* values, the estimated differences of the new mortars indicate that these new mortars should perform better, and approach the target values more than the old mortar recipes (Fig. 7.16B). This is the case for all three properties. Only 1_NL mortar recipe performs worse in terms of compressive strength, and is therefore it is also considered the least adapted recipe to the stone. The best mortar recipe is believed to be the 2_NL mortar recipe, because of its general better performance for all three properties, its estimated spread (±137 mm, vs. 130 to 180mm for the other

mortars). This mortar recipe is composed of the same sand types as Savonn-2, which performed reasonably acceptable.

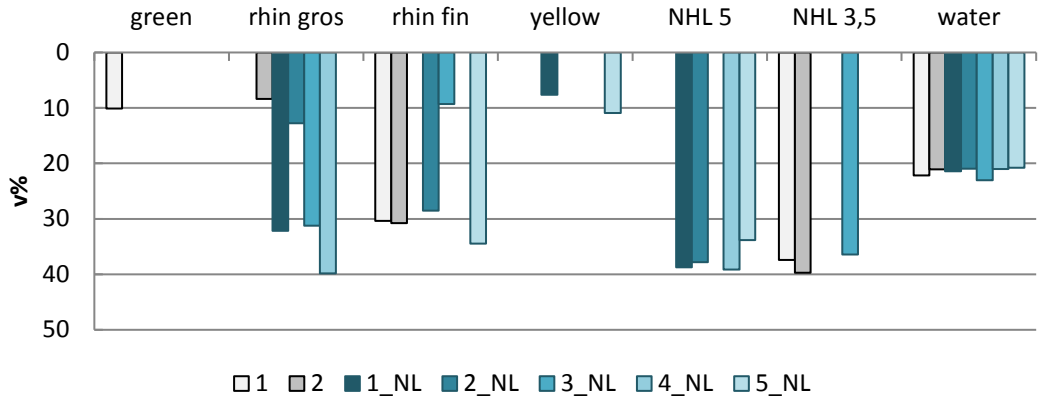

Fig. 7.16A Recipe composition in v% of every mortar component of the various new 'best mortar' recipes proposed by ReMO v1.0 (1_NL to5_NL), and the recipe composition for the Savonn-1 and Savonn-2 mortars, called 1 and 2 respectively.

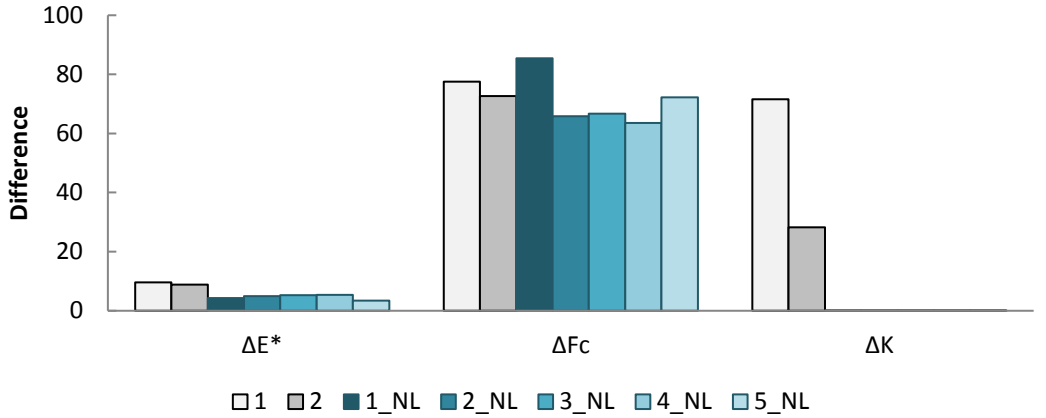

Fig. 7.16B Performance in compatibility of the various new 'best mortar' recipes proposed by ReMO v1.0 (1_NL to5_NL), and the estimated compatibility for the Savonn-1 and Savonn-2 mortars, called 1 and 2. Remark that the ΔK values for the new mortar recipes is very low.

7.4.2.4 Comparison of Avesnes mortars

In ReMO v1.0, different mortar recipes are also proposed for the repair of the Avesnes stone (Fig. 7.17A). The variability in type of components is rather large. Three out of five mortar recipes use NHL 3.5, the other two use the same binder as used by the older mortar recipes, NHL 5. The principal sand type used is the Rhin gros and yellow sand. Rhin fin is the main sand type for one mortar. This is in contrast to the mortars of ReMO v0.0, which contain a high quantity of Rhin fin, and some yellow sand. Additionally, the quantity of water and binder is lower in the new recipes. Conclusively, also here, no comparison will be made with the measured values of the (old) mortars.

Comparing the *estimated* values, some trends appear (Fig. 7.17B):

- Both ΔE* and ΔFc values from the new mortar recipes are higher than the values from the old mortar recipes.

- The ΔK values however, indicate this mortars should approach much more closely the targeted permeability.

This lower compatibility in colour and compressive strength is believed to be a direct consequence of the excellent performance in permeability and of the way a 'best recipe' is chosen by the algorithm. The best adapted individual to the target values appears to be 3_NL, because of it performs as one of the best out of these five recipes in terms of colour and compressive strength (permeability is nearly attained for all five recipes), and has a reasonable estimated spread (±162 mm vs. 171 to 243 mm for the other mortars). The least adapted individual appears to be 2_NL, because it is estimated to perform worst in colour and compressive strength.

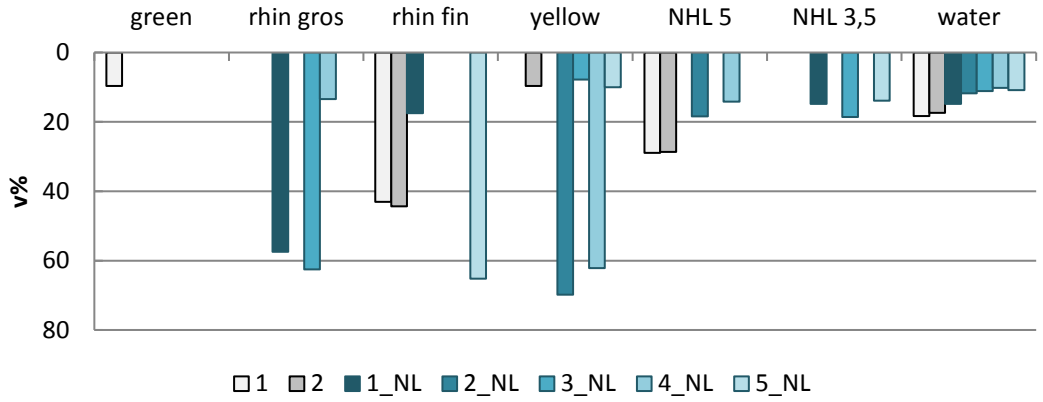

Fig. 7.17A Recipe composition in v% of every mortar component of the various new 'best mortar' recipes proposed by ReMO v1.0 (1_NL to5_NL), and the recipe composition for the Avesnes-1 and Avesnes-2 mortars, called 1 and 2 respectively.

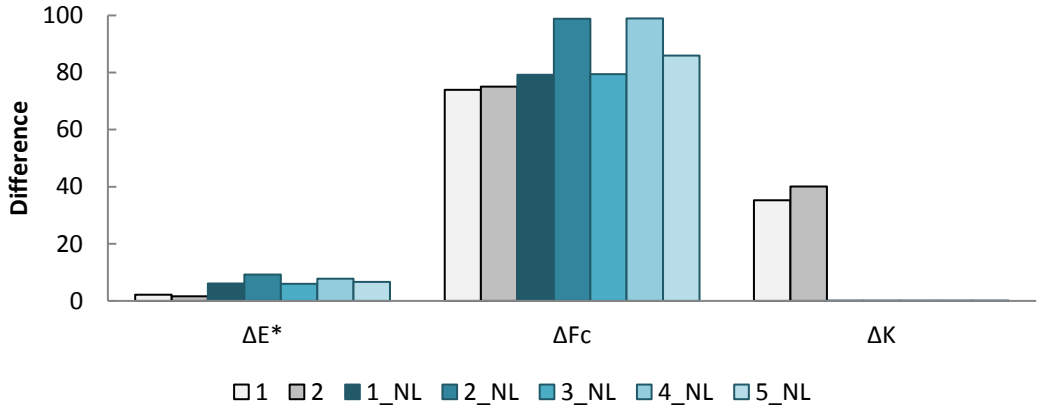

Fig. 7.17B Performance in compatibility of the various new 'best mortar' recipes proposed by ReMO v1.0 (1_NL to5_NL), and the estimated compatibility for the Avesnes-1 and Avesnes-2 mortars, called 1 and 2. Remark that the new mortar recipes have low ΔK values.

7.4.2.5 Comparison of Obernkirchener mortars

The new version gives similar to different recipes for the Obernkirchener stone, that is, 1_NL is similar in composition to Ober-4 and quantities are slightly different. Fig. 7.18A shows the composition of the old mortars in comparison with the five new mortars. The principal sand type is

mainly Rhin gros (3/5), but also Rhin fin and Yellow sand are proposed in large quantities for the other mortars. The old mortar recipes contained green sand and Rhin gros sand. As with the old mortars, the binder type varies as well (2 mortars with NHL5, 3 with NHL3.5). The quantity of water used is in general lower than the water quantity of the old mortars.

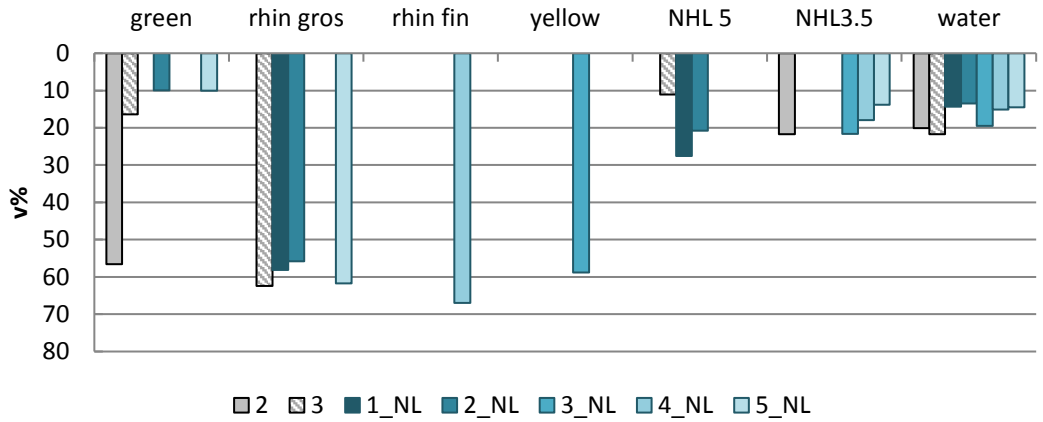

Fig. 7.18A Recipe composition in v% of every mortar component of the various new 'best mortar' recipes proposed by ReMO v1.0 (1_NL to5_NL), and the recipe composition for the Ober-3 and Ober-4 mortars, called 1 and 2 respectively.

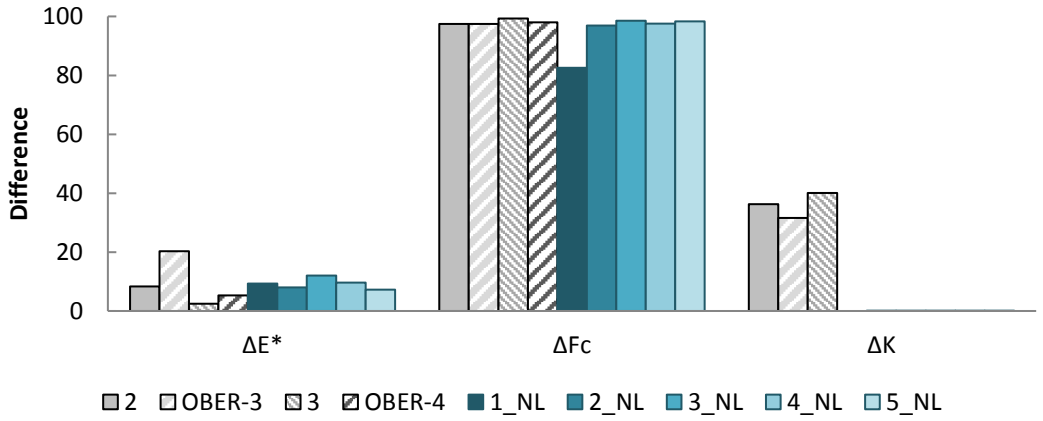

Fig. 7.18B Performance in compatibility of the various new 'best mortar' recipes proposed by ReMO v1.0 (1_NL to5_NL), the *estimated* compatibility for the Ober-3 and Ober-4 mortars, called 1 and 2 respectively and the *actual* measured values for the Ober-3 and Ober-4 mortars. Remark that the new mortar recipes have low ΔK values.

The estimated differences from the new mortars indicate that these mortars should perform better for compressive strength and permeability (Fig. 7.18B). These new mortar recipes are not estimated to perform necessarily better in terms of colour than the old mortar recipes. When comparing 1_NL with the estimated and measured property values of the Ober-4 mortar, the new estimations are better: the estimated colour (ΔE^*_{est} 9.29 '1_NL' in contrast to 'Ober-4' ΔE^*_{est} 2.47 and ΔE^*_{meas} 20.34) and estimated compressive strength (Fc_{est} 2.5 MPa '1_NL' in contrast to 'Ober-4' Fc_{est} 0.6 MPa and Fc_{meas} 1.8 MPa) is closer to the measured value than the initially estimated value of the Ober-4. The water permeability was not measured on the Ober-4 mortars, so a good comparison is thus not possible.

Both estimated values do not vary much (K_{est} 6.3E-12 m² '1_NL' in contrast to 'Ober-4' K_{est} 1.9E-12 m²).

The most compatible new mortar recipe is most likely 1_NL due to its permeability, best compressive strength difference and acceptable spread of 122 mm (versus 176 to 360 mm). The 5_NL is probably the least adapted mortar recipe, mainly due to the high estimated spread (360 mm), even though its colour estimation is with a ΔE^*_{est} of 7.2 the lowest of the 5 mortars.

7.5 Discussion

For the exploitation of this system, four stones were chosen. Two of these stones proved to have properties which were very pronounced: the Maastrichter stone was very permeable, the Obernkirchener had an elevated compressive strength. In both cases, the system had tried to converge towards these extreme properties, but had not succeeded. This attempt would however later have (negative) repercussions on the general quality of the mortar and on the other estimated properties of the mortar.

For example, the high demand of compressive strength made that Obernkirchener mortar recipes included a high amount of sand. This high amount of sand was probably proposed, since the F_c estimation equation also considers the influence of the sand on the compressive strength. In turn, this led to the mortars having a very low spread, impeded a good coring of cylinders and increased the formation of fissures during permeability tests. Contrary to the purpose behind the higher amount of sand, the mortars had a very low strength. In the case of the Maastrichter repair mortars, the high permeability target had to be answered too, leading to very liquid mortars.

The colour estimation was acceptably close (i.e. $\Delta E^* < 5$) for 4 out of 8 mortars to the actual measured colour. The estimation was not sufficient for one Ober mortar, both Maast-mortars and one Avesnes mortar. One explanation is possible for both the Ober and Maast mortar series (see above), but not for the Avesnes mortar.

Water permeability was generally underestimated which is better for the compatibility of the stone-mortar: the mortars are more permeable than estimated. In 4 out of 8 mortars the difference was less than 2 orders of magnitude, the other 4 lower than 1 order of magnitude. Other similar estimation methods for permeability of (cement) mortars have an error of 1 to 2 orders of magnitude, or around 40-60% [7–10]. The minimal difference between estimation and measurement was 50% difference, and the method can thus still be improved.

The compressive strength estimation difference was larger than 40% for 4 out 8 mortars. Mortars were underestimated as well, even though, ideally, compressive strength should always be lower than the stone it is repairing, since it would give an indication on whether the actual produced mortar

would have a higher compressive strength than the stone. Also here, more research is likely to improve the method.

A logical consequence is that the system was best in estimating mortars for natural stones with moderate properties. The Avesnes mortar estimation scored best overall. Secondly, the Savonnières mortars, third the Maastrichter mortars and fourth the Obernkirchener mortars. The Obernkirchener's high demand for compressive strength impeded a good compatibility for the other properties and the Maastrichter series suffered from the higher demand in permeability.

In comparison with the stones, the mortars created were in the accepted compatibility tolerance range for (gas) permeability, with of course, the exception of the Maastrichter stone, since the Maastrichter stone is much more permeable than lime mortars. The mortars created were also situated in the accepted compatibility tolerance range for compressive strength, with the Avesnes mortar being on the limit of acceptable. The Ober-mortars did not lie in the tolerance range of compressive strength.

The colour of one of eight mortars was situated in the colour difference accepted tolerance range, two were just out of this range (5-6%).

Conclusively, overall, Avesnes and Savonnières mortars can be considered more compatible with their stone than the Maastrichter and Obernkirchener mortars.

Where a comparison between new estimations from ReMO v1.0 and measured values was possible, the comparison seemed to indicate that the estimations for the various properties made by ReMO v1.0 are closer to reality or similar in some cases than the initially estimated values of ReMO v0.0. Of course, the comparison is not complete: the mortar recipes proposed by ReMO v1.0 should ideally also be produced and tested at 90 days of curing. Only this would allow to see whether there is an improvement of the estimation. Additionally, the Avesnes runs show that this system is not a computer-*directed* decision tool, but a computer-*aided* decision tool. Next to the 'best mortar' recipe proposed by the algorithm, there are 49 other mortar recipes in the last population which might provide an acceptable compatibility of *all* properties. This should be taken into account when selecting mortar recipes.

For some stones, mortar composition changed between ReMO v0.0 and ReMO v1.0. This is most likely due to the adaptation of the estimation methods. Another factor also plays a determining role: there is a certain randomness which has an influence on the final results: every run starts with a random distribution of individuals, and the mutation operator for example also uses randomness. Conclusively, every run can be different than the previous one, even with the same targets and input parameters.

7.6 Conclusion

It can be concluded that finding exactly the right repair mortars for some stones proved more difficult to achieve than others. The stone's properties are as such because of a series of events which eventually led to its diagenesis. On the other hand, the mortars proposed by the algorithm are created by meeting constraints and by ranking them on their overall compatibility. Colour estimation did not meet the expectations. The colour property has a very narrow tolerance range, and in order for the mortar's colour to be compatible with the stone, the estimation should be excellent. This was not the case, and some total colour differences between measured and estimation are high. This difference might be due to a combined effect of the light source, which is close but not identical to a D65 light source, and the diffusivity, which is not taken into account in the estimation method. The diffusivity is assumed to play a role in the lightness, the light source on the chromaticity.

In addition, the reader should bear in mind that this experimental campaign was performed using mortar recipes of ReMO v0.0. In the meanwhile, improvements on the system have led to ReMO v1.0.

The comparison between the two (ReMO v0.0 and ReMO v1.0) indicate that the new system is an improvement of the old system (estimation methods), and that the elements which have been added (spread indication, GUI) lead to a better interpretation of results. The comparison also pointed out that this is a computer-aided decision system, where the 'best mortar' recipes are not necessarily the ones the user would like to apply. In addition, it also allows to point out that the recipes proposed by one run from this algorithm are not the only recipes which might be compatible with the stone. Another run might give recipes which are as good or better.

When seen in its larger context, ReMO v1.0 is a system which can be applied in general: its set-up is as such that for a number of stones potentially repair mortar recipes can be proposed. It suffices to adapt the target values. Nevertheless, results show that more certainty concerning the proposed mortar recipes is required (e.g. through a larger exploitation) in order to use the system with confidence. If this system is compared to other approaches, for example, if this thesis would only have focussed on the development of one repair mortar for one natural stone, the compatible recipe finally found might possibly be better than the recipes proposed by the system here, but it would have been found based on trial and error processes.

The implementation of some specific elements might improve the system in the future. One solution to improve the quality could be expanding the database with a binder and sand selection adapted to the stones (e.g. a lime-cement mix for increased strength or an air lime-hydraulic lime for increased permeability). Future research with other binders in the database might help this mechanical compatibility, but in that case, the reactive

components of these new binders have to be considered in the permeability estimation.

As seen in this chapter, some target values appeared difficult to attain for the algorithm using this database. A weight might be attributed to the targets: the stone's property which is more difficult to achieve with the database or which is of lower interest, could as such be put last in ranking. This should lead to repair mortars that are less influenced in composition by this property. Instead of applying a weight, the user could modify the 'difficult' target to achieve as such that it becomes achievable with the proposed database. As such, repair mortar recipes proposed are more likely to be closer to the targets of the other two targets.

Bibliography

[1] Dusar M, Dreesen R, De Naeyer A. Natuursteen in Vlaanderen, versteend verleden. Mechelen: Kluwer; 2009.

[2] Cnudde V. Exploring the potential of X-ray tomography as a new non-destructive research tool in conservation studies of natural building stones. Ghent University. Faculty of Sciences, 2005.

[3] Nijland T, Dubelaar C, Hees R Van, Linden T. Black weathering of Bentheim and Obernkirchen sandstone 2003:179–95.

[4] Derluyn H. Salt transport and crystallisation in porous limestone: neutron - X-ray imaging and poromechanical modeling. ETH Zürich, 2012.

[5] Sasse HR, Snethlage R. Methods for the evaluation of stone conservation treatments. In: Baer NS, Snethlage R, editors. Dahlem Work. Sav. our Archit. heritage, Conserv. Hist. stone Struct., John Wiley & Sons Ltd.; 1997, p. 223–43.

[6] Bartleson CJ, Bertrand G, Chalmers AN, Fink X, Gentile C, Hunt RWG. CIE 15.2:1986 Recommendations on Colorimetry. 1986.

[7] Wong HS, Zimmerman RW, Buenfeld NR. Estimating the permeability of cement pastes and mortars using image analysis and effective medium theory. Cem Concr Res 2012;42:476–83. doi:10.1016/j.cemconres.2011.11.018.

[8] Katz AJ, Thompson AH. Quantitative prediction of permeability in porous rock. Phys Rev B Condens Matter 1986;34:2–4.

[9] Nokken MR, Hooton RD. Using pore parameters to estimate permeability or conductivity of concrete. Mater Struct 2007;41:1–16. doi:10.1617/s11527-006-9212-y.

[10] Hamami AA. Vers une prédiction de la perméabilité au gaz à partir de la composition des matériaux cimentaires. Université de la Rochelle, 2009.

Chapter 8 Conclusion and Perspectives

Restoration interventions with repair mortars for stone can have several advantages, such as the cost and the preservation of original material. Repair mortars should, like any other restoration material, fit in the conservation principles: ideally, they should be durable enough, but compatible as well with the original material it should repair. The presented thesis aimed to improve the development of repair mortars, by (a) the reasonable estimation of mortar properties based on the knowledge from mortar components, and (b) the introduction of a genetic algorithm that would help find a mortar recipe compatible to the stone. This genetic algorithm was based on data from estimation methods in order to compose a mortar recipe that, once hardened at 90 days, would exhibit values close to the demanded property values.

This chapter answers the research questions defined in the introduction, based on the information and conclusions gathered from the entire thesis.

8.1 Conclusions

The first step in the research was defining the properties which would influence compatibility most. Based on literature, this thesis presented a ranking in which fluid migration, colour and elasticity head the list. This thesis therefore focused on those technical properties. The choice was motivated by the logic of first understanding the mortar's properties which are either perceived first (colour) and/or determining for the quality of the intervention (permeability, elasticity). The three properties were selected based on their influence on the durability and on the compatibility of a repair mortar intervention.

- Repair mortars should have a fluid migration capacity adapted to the stone, since the presence of water in the stone can contribute greatly to the deterioration of stone. Tolerance ranges for compatibility indicated that fluid migration capacity should be equal or higher than that of the stone [1]. A mortar capable of transporting less water, could thus accelerate stone decay. Properties indicating fluid migration capacity

are therefore found to be of vital importance for the quality and durability of the restoration intervention. The capacity to store or transport water in the mortar depends on the pore size distribution and total pore volume.

- The second property, colour, was selected since it is an important factor for the public's appreciation and comprehension of the building. Moreover, literature study proved that mortars were regularly chosen mainly for their compatibility in colour, regardless of their other properties, e.g. [2,3]. Only colour was discussed in this thesis, and did not include texture. It was assumed that the aim for a compatible texture might prohibit finding a compatibility in any of the two other properties. For example, the aggregate grain size, which was found influential for both elasticity and fluid migration capacity, is also assumed to be determining for the texture. Since a wide spectrum of colours can be perceived up to a detailed level, the tolerance range allowed for colour is narrow in comparison to the other compatibility properties, e.g. 5% for colour instead of 40% for elasticity.

- Elasticity was the third property judged important for the compatibility between repair mortars and stone. The tolerance range for compatibility indicated that the repair mortar should have a lower stiffness than the stone. As such, formation of cracks would be avoided, making the restoration intervention more durable. The quality and durability of the restoration intervention thus also depend on the compatibility in elasticity. The mortars with elasto-plastic behaviour are considered over mortars with only elastic behaviour more appropriate for conservation purposes due to their higher deformability.

The experimental campaign in this thesis was composed of NHL mortars. Two binders, classified as NHL3.5 and NHL5, were chosen because of their use in restoration practices e.g. [4–7]. Experimental results showed however that their difference in resistance was rather small, and their XRD analysis showed that reactive components of both lime mortars were not very different. This observation led to the conclusion that the actual composition and resistance of the binders should be tested in every mortar campaign, since they give more pertinent information than the more general classification of NHL2, 3.5 or 5. It appeared to be a challenge to identify the pore-related properties of the lime mortars in this campaign: the low resistance and the elevated porosity demanded some new approaches for testing, such as the immersion of samples in water right before the water permeability test. The pore network was analysed through a combination of MIP and micro-CT and led to assume that the lime mortars in this study had large ink-bottle pores with smaller pore throat entrances. Due to their high permeability values, the lime mortars were assumed to have a well-

connected pore network, even though this could not be confirmed by micro-CT. It might be possible to visualize and quantify better the entire pore volume - which now partially remained unresolved in the scans- through micro-CT analysis of resin-embedded lime mortar samples.

An estimation method was developed for each compatibility property. Since these methods had to be implemented into an algorithm afterwards, the models proposed for this research are limited in complexity, whilst seeking acceptable results. For every property which had to be estimated here, no existing estimation method could be used as such for lime mortars. This thesis therefore proposed a new estimation method for permeability or adaptations to existing methods for colour (Grassmann) and elasticity (De Larrard) [8,9].

- The approach to estimate permeability as a product of porosity and the critical pore diameter, was taken from already existing permeability estimation methods [10–13]. This method belongs to the large group of existing estimation methods which are all based on this product expression. Such an approach was chosen since it could be implemented into the algorithm. The advantage of this method over a simulation model is that this model does not require to be fed by analysis using several (time-consuming) high-end techniques in order to function. It thus also allows that validation of this model is easier to perform. As such, the effect of various grain size distributions and binders is understood faster. In addition, this 'simple' approach permitted it to be introduced easily into the algorithm, without creating additional calculation time or demanding other software and/or high-end performing computers. The estimation method for porosity and critical pore size diameter was based on data derived from both literature and the experimental campaign performed on lime mortars of 90 days of age in this research. This indicated that there was an influence of mortar components on pore-related properties. The error margin of the method, namely 1 to 2 orders of magnitude, was found to be similar to other estimation methods for permeability such as [10,13,14].

- The method used for colour estimation is an adapted version of the general Grassmann theory. However, in reality, mortar mixes did not only follow the additive Grassmann theory, but the binder proved to play an additional role as 'polluter' of the sand particles. The experimental campaign on mortar component mixes in Chapter 4 indicated that adding a pollution factor might make the Grassmann theory adapted for mortars. Results of chapter 4 and later on, of the exploitation of the system in chapter 7 indicated that the colour estimation for some mortars varied from close to far from the actual measured colour. Nevertheless, by want of any other valuable method, this method was implemented

into the system. Another estimation method which might be more precise, could be the Kubelka-Munk estimation method. This method could not be applied due to practical limitations, but once these are overcome, it might prove very useful for the colour estimation of mortars, because of its different approach starting from diffuse surfaces [15,16].

- The experimental campaign on the lime mortars in this research indicated a clear linear correlation between the static elasticity and the compressive strength. An estimation method for compressive strength found in literature, used the influence of the mortar components. The static elasticity of the lime mortars was estimated based on a combination of these two elements: the empirical linear correlation and the estimation for the compressive strength. The estimation method, once adapted to lime mortars, showed a lower error range for higher elasticity, the estimation for the mortars with a very low elasticity and compressive strength differed much more with the actual measured value, on average 20%, for the mortars with higher elasticity. The mortars with least well-estimated values showed low compressive strength and elasticity values. The method appears currently to be limited to normal to high strength mortars. Future research might concern the effects leading to decreased strength, e.g. curing conditions or decreased binder/aggregate ratio. This estimation method was chosen because it uses properties from mortar components, and does not require another, additional estimation of any of the other properties of the various mortar elements (ITZ, bulk paste, aggregates) in order to estimate, finally, elasticity. The latter would certainly increase the uncertainty of the estimation. The estimation method proposed here showed acceptable correlations with the lime mortars tested experimentally in this research. More research on other mortars would have to point out the advantage of this estimation method for (lime) mortars in general.

The last step to attain the goal of this thesis, was to implement each estimation method into an algorithm. The algorithm used in this study was a NSGA II genetic algorithm, which aims for the best individuals by non-domination and the ranking into fronts according to the crowding distance [17]. Other optimisation methods were likely to have taken longer in calculation, and give uncertainty over the final results, i.e. whether they are solutions in a local minimum or whether they are actually solutions belonging to the global minimum. The estimation methods were implemented into the algorithm, and scripts were added so that the algorithm could use an external database. The system will be able to be used by users with no programming experience, since a GUI and .exe file were made. This might allow researchers with experience in (repair) mortar development, but not necessarily in encoding or in genetic algorithms, to use the system. Their

experience could then be used to improve the system and adapt it more to the needs of users.

The final chapter of the thesis discussed the exploitation of the entire system, by demanding the system to present compatible mortar recipes for four different sedimentary stones. The exploitation of ReMO v0.0 showed that the colour estimation method is the weakest link of the entire system; with colour differences of 2-20% instead of the allowed 0-5%. However, this also points out that the demands for colour compatibility are much higher than for the other properties. The algorithm itself functions as is expected and can create mortar recipes for these stones.

The comparison of ReMO v0.0 with ReMO v1.0 seems to indicate that the improved features add value to the system. Nevertheless, the improvements made on e.g. the three estimation methods, now also have to be compared with actual measured values in order to complete the assessment of the ReMO v1.0.

This comparison also clearly indicated that the mortar recipes proposed by the system are there to guide the user to potentially compatible mortar recipes. First of all, the tolerance ranges are no part of the system, so the best mortar recipe, according to the system, is thus the recipe which shows the smallest (total) distance. This may not represent the actual choice of the user, who would like to have a mortar recipe balanced in all its properties. In addition, the system is a guide and help to the user, because, inherent to its conception, several runs of the algorithm will not necessarily create the same recipes.

8.2 Perspectives

The selection of stones used in this work illustrated that the system is limited by the database it can use. In the future, an extended database should give more possibilities. The algorithm could then be chosen among more and different sands, and an extension of the binders would permit to explore a larger range of permeability and elasticity values. Moreover, if the string of variables in the algorithm is adapted so that it can use more than one binder, combinations can be made between these various binders. As such, lime-cement binders can be created. The estimation of colour would not have to be adapted when the database is expanded. The estimation method of permeability only requires the addition of reactive components of the binders used, and the estimation method for elasticity itself does not require any modification. An experimental campaign is still advised to then verify the capacities of these estimation methods. This expansion of the database might evolve in two directions, either with a focus on one range of stones with similar colour, or to a rather larger range of various colours. The last would have as advantage that the system as such could be used for a larger range stones, however, it would require more time to find the sands and

binders required for such a large group, and to make the system function well. The first approach would make the system very useful for, for example, the small range of lime-sandstones who easily deteriorate and thus require more quickly a repair mortar. Adapting a database for these stone types would also require an expansion of the database, but it would be easier to conceive.

The expansion of the database coupled to an additional target in the algorithm would also permit to introduce a fourth parameter, which until now was left aside: the mineralogy of the mortar. For example, if additional information is introduced into the database of each sand, e.g. specific minerals such as glauconite, or the presence of bioclasts, and an additional target is introduced into the algorithm for mineralogy, then the algorithm would search to promote the use of sand(s) containing this mineral (given that it is present in the database).

Naturally, future research perspectives should take into account the (final) goal of the subject. This research was performed in order to create a system that would help the user in his/her choice for repair mortars. This system has always been intended for the larger restoration projects, since only these projects (unfortunately) permit to have a multi-disciplinary team: in order to use this system at its best, the team should consist of both restorers with knowledge of on-site practices, and scientists, with access to some analysing techniques (e.g. grain size distribution, packing density, colorimeter) in order to complete the database and fill in the targets. Nevertheless, the system as it exists now, does not yet permit these users to apply the system: the spread estimation should be verified more in depth, the database should be expanded, the colour estimation method should be adapted, etcetera. On the other hand, the system might also be further elaborated and improved, e.g. adding the mineralogy in the components.

It is therefore interesting to not only continue the development of the system in order to improve and elaborate it, but also allow other users to test this ‘beta’ version. Their output and opinion will give direction to the adaptations for the better use of the system.

First of all, the aspect of mineralogy seems in terms of further improvement an interesting feature to implement. It is believed to require a minimal effort to implement this element into the tool. This aspect can then be combined with the expected durability and the effect of ageing in properties of both mortar and stone. The mortars proposed by the algorithm should then be subjected to ageing and weathering tests such as freeze-thaw tests. In such tests, it seems advisable to test both algorithm-proposed mortars and the stones they should repair and a reference mortar. Results should then point out the performance of the proposed mortars in comparison to the stones and reference mortar in durability, colour and other properties such as porosity and permeability. A comparison of properties between mortar and stone should then be able to indicate whether the mortars are still compatible with the stone.

Secondly, a larger exploitation of the system could be performed, which would only be beneficial for the use of the entire system. This exploitation is estimated to take up a considerable amount of time and effort, since various mortars have to be produced, cured, tested, and compared in properties with what was initially estimated. This can be combined with the expansion of the database.

Thirdly, complementary data, valuable for the user, can be extracted from the system. This information would not be used as additional objective or constraint, but merely bring added value to the mortar recipes proposed by the system. A first step was made by demanding the system to estimate the spread based on the empirical relation. This relationship is based on results from this experimental campaign, and is therefore not sufficient for a larger range of mortars. Logically, the establishment of complementary data would come after the larger exploitation of the system. Additional research should as such give complementary data, e.g. the adhesion and an indication for surface roughness. The research towards adhesion should be combined with mortar-stone sample tests, and with research into various application techniques. Eventually, the user would like to know whether or not the mortar proposed here is a mortar with good adhesion to the surface. It would only be possible to answer to this question once an acceptable estimation can be given concerning the spread or workability of the mortar.

The surface roughness indication would be valuable for the user since it would indicate surface finishes possible with this mortar, and the expected heterogeneity of the mortar, the work of Govaerts et al. (2014) might be in that aspect prove to be useful [18].

As last, future research might also look into the aspect of age. If the permeability of mortars is measured after, for example, 3, 6, 12, 24 and 36 months, the influence of time could be incorporated in the estimation method. In that case, one should also reflect on the effect of curing conditions on the permeability and other pore-related properties. In this research, age as well as curing conditions have been kept constant. However, in reality, not only age plays a role, but also the curing conditions and the period of time the mortars is subjected to these conditions. Hence, if future research tries to include the influence of age, it would be advised to also take into account the influence of the environment on the curing of the mortar.

Conclusively, this thesis demonstrated that it is possible to optimize mortar development: the algorithm creates mortar recipes and estimates three relevant properties. The thesis also demonstrated that the research towards the estimation methods for lime mortars is not finished, and that additional experimental campaigns, including ageing tests and research into the mineralogy of the mortars might be a pertinent continuation of this research.

Bibliography

[1] Sasse HR, Snethlage R. Methods for the evaluation of stone conservation treatments. In: Baer NS, Snethlage R, editors. Dahlem Work. Sav. our Archit. heritage, Conserv. Hist. stone Struct., John Wiley & Sons Ltd.; 1997, p. 223–43.

[2] Schueremans L, Cizer Ö, Janssens E, Serré G, van Balen K. Characterization of repair mortars for the assessment of their compatibility in restoration projects: Research and practice. Constr Build Mater 2011;25:4338–50. doi:10.1016/j.conbuildmat.2011.01.008.

[3] Ramge P, Kühne H, Meng B. Entwicklung von modularen Instandsetzungsmörteln für den Einsatz an denkmalgeschützten Natursteinbauwerken. Tagungsband 52. DAfStb-Forschungskolloquium, Berlin: BAM; 2011, p. 247–55.

[4] Gulotta D, Goidanich S, Tedeschi C, Nijland TG, Toniolo L. Commercial NHL-containing mortars for the preservation of historical architecture. Part 1: Compositional and mechanical characterisation. Constr Build Mater 2013;38:31–42. doi:10.1016/j.conbuildmat.2012.08.029.

[5] Smith BJ, Gomez-heras M, Viles H a. Underlying issues on the selection, use and conservation of building limestone. Geol Soc London, Spec Publ 2010;331:1–11. doi:10.1144/SP331.1.

[6] Maravelaki-Kalaitzaki P, Bakolas A, Karatasios I, Kilikoglou V. Hydraulic lime mortars for the restoration of historic masonry in Crete. Cem Concr Res 2005;35:1577–86. doi:10.1016/j.cemconres.2004.09.001.

[7] Grilo J, Faria P, Veiga R, Santos Silva A, Silva V, Velosa A. New natural hydraulic lime mortars – Physical and microstructural properties in different curing conditions. Constr Build Mater 2014;54:378–84. doi:10.1016/j.conbuildmat.2013.12.078.

[8] Larrard F de. Concrete Mixture Proportioning: A Scientific Approach. London: E & FN Spon; 1999.

[9] Grassmann H. Zur Theorie der Farbenmischung. Ann Der Phys Und Chemie 1853;165:69–84. doi:10.1002/andp.18531650505.

[10] Katz AJ, Thompson AH. Quantitative prediction of permeability in porous rock. Phys Rev B Condens Matter 1986;34:2–4.

[11] Hamami AA, Turcry P, Aït-Mokhtar A. Influence of mix proportions on microstructure and gas permeability of cement pastes and mortars. Cem Concr Res 2012;42:490–8. doi:10.1016/j.cemconres.2011.11.019.

[12] Glover PW, Walker E. Grain-size to effective pore-size transformation derived from electrokinetic theory. Geophysics 2009;74:E17–29. doi:10.1190/1.3033217.

[13] Nokken MR, Hooton RD. Using pore parameters to estimate permeability or conductivity of concrete. Mater Struct 2007;41:1–16. doi:10.1617/s11527-006-9212-y.

[14] Wong HS, Zimmerman RW, Buenfeld NR. Estimating the permeability of cement pastes and mortars using image analysis and effective medium theory. Cem Concr Res 2012;42:476–83. doi:10.1016/j.cemconres.2011.11.018.

[15] Kubelka P, Munk F. Ein Beitrag Zur Optik der Farbanstriche. Zeitschrift Für Tech Phys 1931;12:593–601.

[16] Capo-Chichi KTE. Materiaux complexes et couleur: hiérarchisation des paramètres et prévision de la couleur dans un béton coloré. Université Montpellier II, 1996.

[17] Deb K, Agrawal S. A fast elitist non-dominated sorting genetic algorithm for multi-objective optimization: NSGA-II. Parallel Probl Solving from Nat PPSN VI, Lect Notes Comput Sci 2000;1917:849–58.

[18] Govaerts Y, Meulebroeck W, Verdonck A, de Bouw M. Measuring the colour of rendering mortars. Opt Sens Detect Iii 2014;9141:91411D. doi:10.1117/12.2052309.

A. Appendix

A2. Appendix for chapter 2

A2.1 X-ray diffraction analysis of binders

The binders used are the Chaux Pure Tradi 100 and Chaux Pure Blanche LC, both from St Astier, France, and classified as NHL5 and NHL 3.5 according to EN 459-1 (2010). Figures A2.1 A-B represent the X-ray diffractogram for both binders, analysed with a Bruker D8 Advance ECO equipped with an energy dispersive position sensitive LynxEye XE detector. The XRD pattern was recorded from 3 to 70° 2θ with a step size of ca. 0.01° 2θ. An automatic divergence silt and air-scatter knife was used to collimate the primary beam to a fixed beam length of 17 mm and reduce background noise at low diffraction angles respectively. Operating voltage and current were 40kV and 25mA. The red line indicates the reference, the grey line the measured value. The black line below indicates the difference between the reference and the analysed sample.

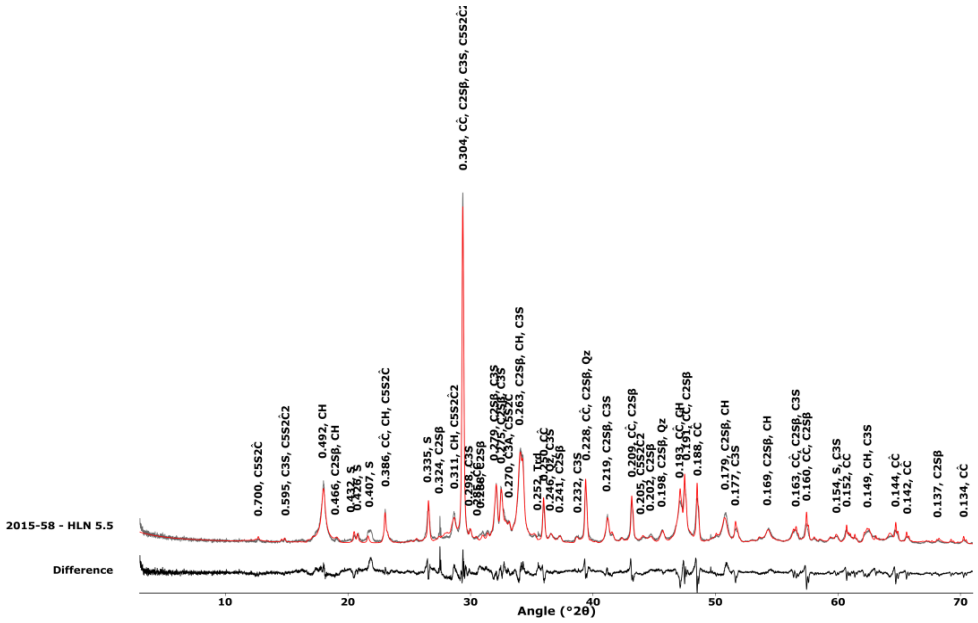

Fig. A2.1A. The diffractogram for the NHL5 binder used in this study.

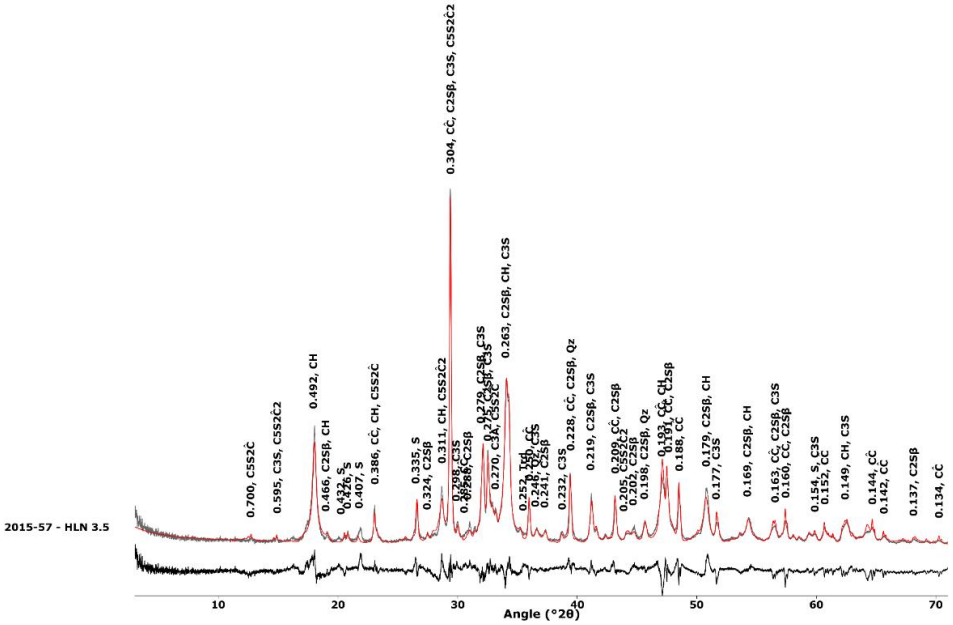

Fig. A2.1B. The diffractogram for the NHL3.5 binder used in this study.

A2.2 Grain size distribution of both binders

Figures A2.2 A-B represent the grain size distribution measured through laser grain size analysis with a Mastersizer 2000. The binders were dissolved in propan-2-ol for the analysis.

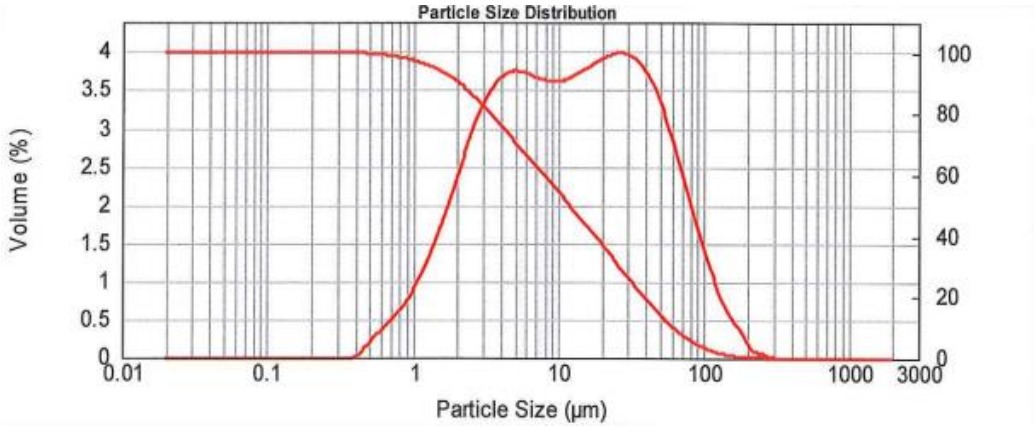

Fig. A2.2A. The grain size distribution for the NHL5 binder in this study.

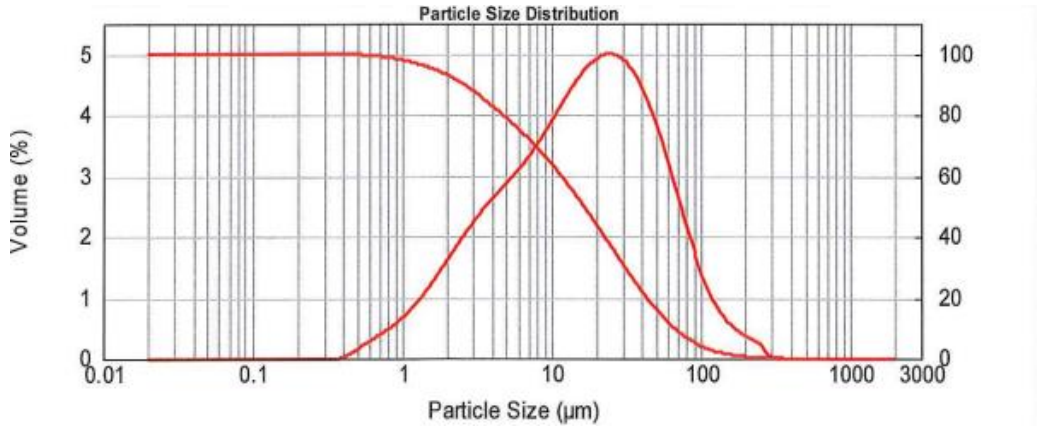

Fig. A2.2B. The grain size distribution for the NHL3.5 binder in this study.

A3. Appendix for chapter 3

A3.1 Pore-scale properties of lime mortars

Following tables represent the measured pore-scale properties of the lime mortars of the W/B mortar campaign. These values have been represented as figures in chapter 3: Fig.3.11-3.15 and Fig.3.25-3.30.

Table A3.1.1 Table with open porosity and apparent density values for each mortar mix at 90 days of age.

Name	App density [kg/m³]		Open porosity [%]		Name	App density [kg/m³]		Open porosity [%]	
	av	st dev	av	st dev		av	st dev	av	st dev
5-N-2	1882.20	0.02	27.56	0.70	**3.5-N-2**	1469.00	0.27	43.18	10.64
5-N-4	1767.12	0.09	33.95	1.22	**3.5-N-4**	1319.28	0.02	45.33	9.48
5-N-6	1786.36	0.08	31.51	3.01	**3.5-N-6**	1358.02	0.02	47.90	1.03
5-N-8	1683.04	0.03	35.95	0.79	**3.5-N-8**	1286.40	0.04	50.53	1.36
5-G-2	1643.85	0.05	36.80	1.67	**3.5-G-2**	1199.96	0.09	52.95	4.36
5-G-4	1675.80	0.14	35.80	5.14	**3.5-G-4**	1236.40	0.14	51.95	5.38
5-G-6	1585.18	0.04	39.60	1.60	**3.5-G-6**	1161.92	0.03	55.05	1.30
5-G-8	1928.00	0.09	26.11	4.04	**3.5-G-8**	1140.98	0.02	55.96	1.00
5-F-2	1341.25	0.05	48.77	1.72	**3.5-F-2**	1101.36	0.02	57.24	0.83
5-F-4	1433.53	0.18	45.04	6.79	**3.5-F-4**	1092.46	0.03	58.01	0.90
5-F-6	1264.10	0.06	51.88	2.12	**3.5-F-6**	1082.88	0.01	58.03	0.40
5-F-8	1269.10	0.04	51.32	1.08	**3.5-F-8**	1045.86	0.02	59.69	0.80
5-Y-2	1124.52	0.02	56.82	0.89	**3.5-Y-2**	935.64	0.03	63.73	0.91
5-Y-4	1085.10	0.04	58.59	1.40	**3.5-Y-4**	933.38	0.01	64.22	0.70
5-Y-6	1059.33	0.03	59.55	1.19	**3.5-Y-6**	908.76	0.03	65.02	1.45
5-Y-8	1026.33	0.01	60.93	0.39	**3.5-Y-8**	874.53	0.01	66.60	0.51

Table A3.1.2 The intrinsic permeability $k_{intrinsic}$ calculated from water permeability measurements and helium gas permeability k_{gas}.

Name	$k_{intrinsic}$ [10^{-12} m²]	k_{gas} [10^{-13} m²]		Name	$k_{intrinsic}$ [10^{-12} m²]	k_{gas} [10^{-13} m²]	
		av	st dev			av	st dev
5-N-2	2.46	5.92	0.46	**3.5-N-2**	2.91	5.92	0.50
5-N-4	3.32	3.56	0.83	**3.5-N-4**	2.65	3.56	0.26
5-N-6	1.95	4.01	1.84	**3.5-N-6**	2.87	4.01	0.21
5-N-8	3.50	2.46	1.60	**3.5-N-8**	4.22	2.46	0.60
5-G-2	2.59	3.53	1.86	**3.5-G-2**	3.48	3.53	0.35
5-G-4	4.14	2.20	0.79	**3.5-G-4**	2.93	2.20	0.81
5-G-6	6.69	1.80	1.33	**3.5-G-6**	4.23	1.80	0.16
5-G-8	3.99	2.60	1.04	**3.5-G-8**	3.65	2.60	0.20
5-F-2	3.56	2.49	0.88	**3.5-F-2**	3.44	2.49	0.66
5-F-4	3.22	1.99	0.77	**3.5-F-4**	3.43	1.99	0.64
5-F-6	3.99	1.84	0.75	**3.5-F-6**	4.86	1.84	0.91
5-F-8	3.70	2.02	0.55	**3.5-F-8**	6.69	2.02	0.26
5-Y-2	4.86	2.93	0.72	**3.5-Y-2**	5.22	2.93	0.39
5-Y-4	4.55	2.13	0.44	**3.5-Y-4**	0.00	2.13	0.12
5-Y-6	7.81	1.91	0.58	**3.5-Y-6**	5.17	1.91	0.45
5-Y-8	0.00	2.12	0.64	**3.5-Y-8**	0.00	2.12	0.37

Table A3.1.3 The intrinsic permeability $k_{intrinsic}$ calculated from water permeability measurements, helium gas permeability k_{gas}, water absorption coefficient C and compressive strength R_c of the studied lime mortars.

Name	**C ($g.m^{-2}.s^{-1/2}$)**		Name	**C ($g.m^{-2}.s^{-1/2}$)**	
	av	st dev		av	st dev
5-N-2	62.25	1.62	**3.5-N-2**	95.66	9.17
5-N-4	79.82	3.65	**3.5-N-4**	102.59	8.75
5-N-6	65.57	0.18	**3.5-N-6**	100.00	3.53
5-N-8	81.88	1.29	**3.5-N-8**	86.85	10.35
5-G-2	75.48	0.91	**3.5-G-2**	107.63	5.59
5-G-4	71.65	1.11	**3.5-G-4**	106.22	9.24
5-G-6	78.03	4.08	**3.5-G-6**	124.43	14.21
5-G-8	70.68	2.00	**3.5-G-8**	115.33	16.45
5-F-2	77.38	1.48	**3.5-F-2**	125.69	11.58
5-F-4	86.51	2.72	**3.5-F-4**	125.22	5.62
5-F-6	92.41	1.05	**3.5-F-6**	135.31	4.38
5-F-8	89.65	1.95	**3.5-F-8**	136.22	6.10
5-Y-2	100.88	0.81	**3.5-Y-2**	121.44	1.37
5-Y-4	112.23	1.88	**3.5-Y-4**	122.80	3.16
5-Y-6	116.12	3.15	**3.5-Y-6**	124.67	9.16
5-Y-8	123.06	1.16	**3.5-Y-8**	139.85	1.95

Following figures represent the pore size distribution of the W/B mortar series, obtained through MIP analysis.

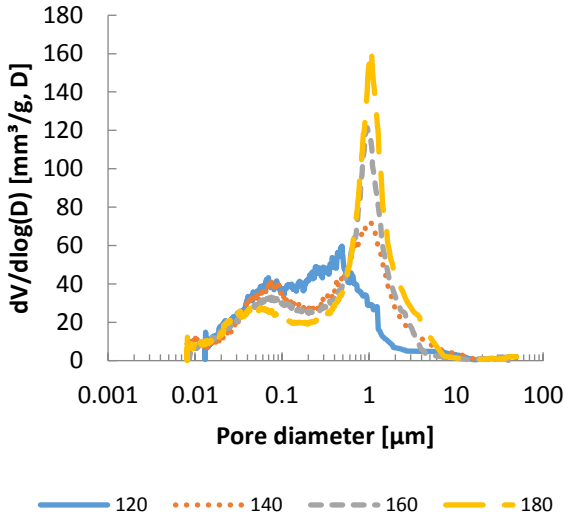

A. The differential specific volume of the various reference sand mortar mixes.

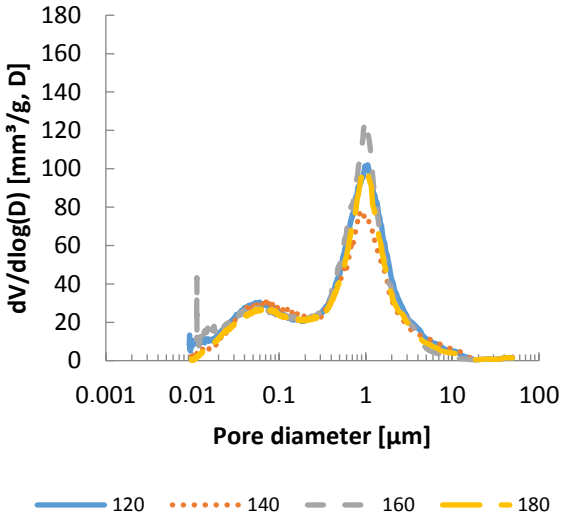

B. The differential specific volume of the various Rhin gros sand mortar mixes.

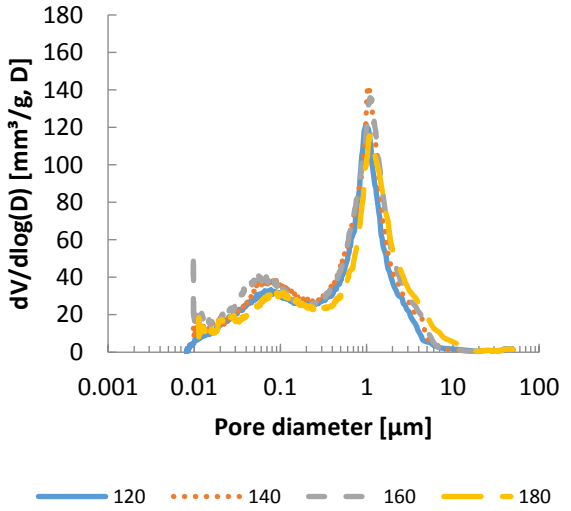

C. The differential specific volume of the various Rhin fin sand mortar mixes.

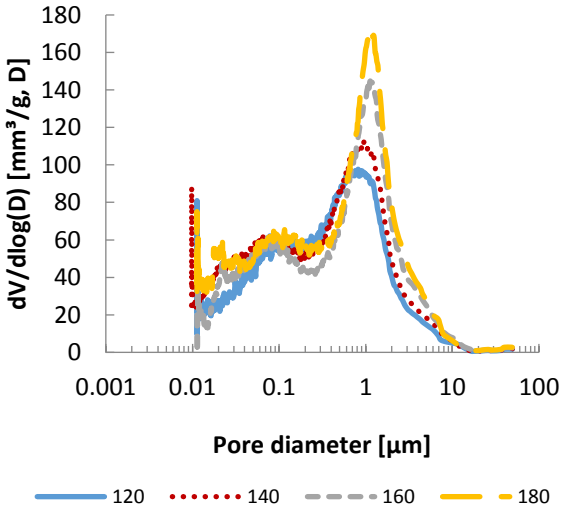

D. The differential specific volume of the various yellow & green sand mortar mixes.

Fig.A3.1.1 A-D. Differential specific volume of each NHL 5 W/B mortar mix. The increase in spread was clearly visible in the reference sand mortars, while it seemed absent or non-existent in the samples of both Rhin sands.

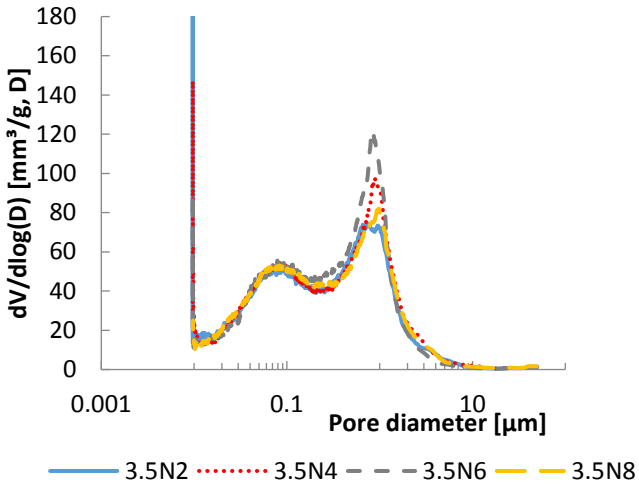

A. The differential specific volume of the various reference sand mortar mixes.

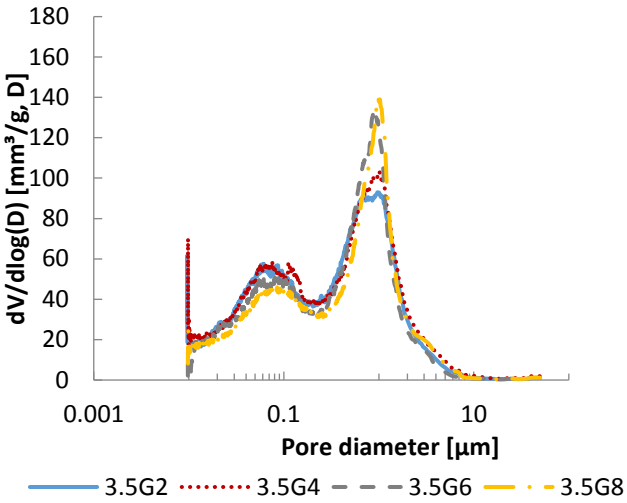

B. The differential specific volume of the various Rhin gros sand mortar mixes.

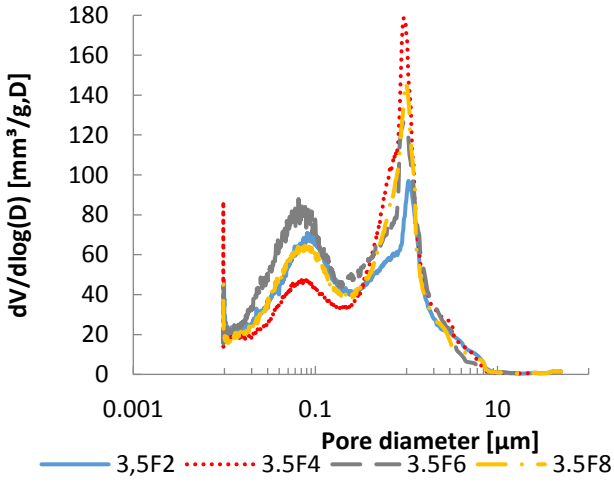

C. The differential specific volume of the various Rhin fin sand mortar mixes.

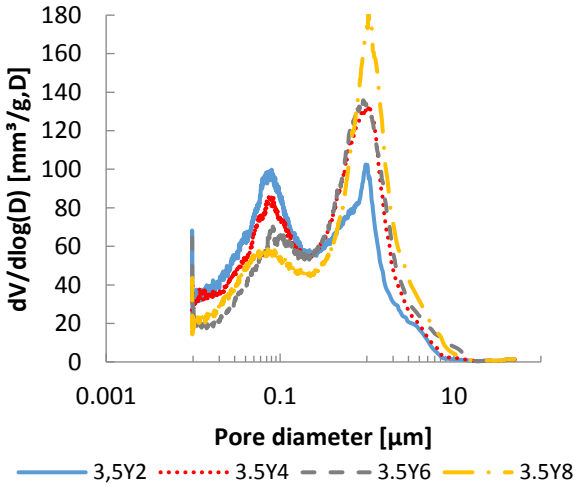

D. The differential specific volume of the various yellow & green sand mortar mixes.

Fig.A3.1.2 A-D. Differential specific volume of each NHL 3.5 W/B mortar mix. The increase in spread was clearly visible in the reference sand mortars, while it seemed absent or non-existent in the samples of both Rhin sands.

A3.2 Exploitation of Hamami estimation method for cement mortars

Hamami proposes that the permeability of cement mortar K_{mortar} can be calculated according to eq.3.11, based on his own model for cement pastes (eq. 3.12) and already existing equations which studied the influence of aggregates in a mortar such as proposed by Caré et al. or Garboczi et al. [19,62,63,71]. The influence of the aggregates is incorporated using the volume of the interfacial transition zone (ITZ), the more porous zone around the aggregate grains. The mortar permeability can then be calculated according to eq.A3.1:

$$K_{mortar} = K_{paste}\left(\frac{2V_{paste}}{300-V_{paste}}\right)\left(1+\alpha\frac{V_{ITZ}}{V_{paste}}\right) \qquad \text{(eq.A3.1)}$$

with V_{paste} the volume of the paste, V_{ITZ} the volume of ITZ, and α a parameter depending on ITZ properties. As can be seen in eq.A3.1, the paste volume of the mortar has a significant share in the estimation of the permeability of the mortar. The volume of the ITZ zone and the reactivity of the cement is also taken into account [71]. A cement grain radius r_a is calculated using the specific density and the specific Blaine surface of the cement.

The pore network is then narrowed by replacing all the anhydrous cement grains with the hydrated cement grains, assuming a grain volume increase due to hydration. The hydrated cement grain radius r_h is calculated using the Le Châtelier contraction and the hydration degree. The porosity is calculated, depending on the W/B ratio and the hydration degree.

Permeability was then defined as the product of the (measured) porosity f and the critical *pore* diameter D_c and correction coefficient 0.64 (eq.A3.2)

$$K_{paste} = 0.64\, f\, \left(\frac{D_c}{2}\right)^2 \qquad \text{(eq.A3.2)}$$

K_{paste} can now be used in the equation of K_{mortar} (eq.A3.1). The additional input parameters for the estimation of mortar permeability are the aggregate volume, the aggregate grain size distribution, the aggregate density, and the (assumed) ITZ thickness.

White Portland cement CEM II A-LL 42.5N was used for 6 cement pastes with varying W/B ratios (0.3-0.6) and 3 cement mortars with W/B 0.5, 0.6 and 1.16 with fine yellow and green sand in a 7:2 ratio. The cement's specific Blaine surface, 4244 cm²/g, was measured according to EN 196-6 (2010), the cement's specific density, 3119.5 kg/m³, was calculated through helium pycnometry on the anhydrous cement powder.

The mixes were cast as bars of 16 x 4 x 4 cm³ and vibrated for 10 to 15 s, and consequently cured in water for 28 days at 20 ± 2° C according to EN 196-1. Cylindrical cores (Ø 2.5 by 5 cm) from the bars were tested with helium pycnometry for their open porosity. Since the estimation method requires a value as hydration degree, the hydration degree was assumed to be 1.6, a value Hamami proposed for 28-day-old mortars.

The estimated porosity values of the pastes are, except for the 0.6 paste, close to the experimentally measured porosity values. The difference between the measured and estimated values of the mortars is noteworthy. Hamami estimated the water-measured porosity of the sample. This type of test was avoided in this study since hydration might occur during the test. This difference in testing method might therefore explain up to some extent the difference between estimation and measurement, but other elements, e.g. the amount of aggregates or the amount of water used, influence as well: the aggregates present in the mortar are believed to influence the porosity. The paste porosity is most likely not equal to the porosity of the mortar.

With the GasPermEdu nitrogen gas permeameter (Vinci Technologies) it was only possible to measure the permeability of the cement mortar of W/B 1.2; the other samples were not permeable enough for the permeameter present (minimal limit at 10^{-15} m²). Conclusively, the permeability of the mortars by Hamami's method was largely overestimated.

Table A3.2.1. Comparison of experimental and calculated values.

	Estimated		Measured values			
W/B ratio	f_{estim} [%]	K_{estim} [10^{-15} m²]	f_{open} [%]	CI_{95}	K_{gas} [10^{-15} m²]	CI_{95}
P-0.3	17.4	4.86	19.5	1.9		
P-0.35	23.5	8.81	26.2	1.7		
P-0.4	28.8	13.83	30.5	0.3		
P-0.45	33.5	19.90	34.4	0.6		
P-0.5	37.5	27.01	39.7	0.7		
P-0.6	44.3	44.44	40.5	0.2		
M-0.5	37.5	3.89	17.9	0.7		
M-0.6	44.3	5.49	18.2	0.5		
M-1.2	42.5	10.56	39.1	0.7	3.89	0.82

*P: paste, M: mortar, -X: the W/B ratio, f: porosity, K: permeability, CI 95: confidence interval at 95%. The ITZ thickness was assumed to be 30 µm.

The use of binder and aggregate properties in the estimation model indicates that in this model most mortar components influence the final mortar permeability. The aggregate grain size distribution and the reactivity of the cement particle were assumed to be amongst the most important factors.

Porosity is overestimated for the mortars, and the permeability appears to be overestimated for both pastes and mortars.

A3.3 Confrontation of the permeability estimation method

A3.3.1 Estimated and measured permeability

Tables A3.3.1-2 represent the estimated permeability and the measured permeability for every mortar mix.

Table A3.3.1 The estimated permeability for NHL 5 mortars in comparison to the measured permeability.

Name	Estimated permeability		Measured	Measured
	k_{gas} [10^{-14} m²]	$k_{intrinsic}$ [10^{-12} m²]	$k_{intrinsic}$ [10^{-12} m²]	K_{gas} [10^{-13} m²]
5-N-2	1.94	1.94	2.46	5.92
5-N-4	3.34	3.34	3.32	3.56
5-N-6	3.46	3.46	1.95	4.01
5-N-8	7.19	7.19	3.50	2.46
5-G-2	6.85	6.85	2.59	3.53
5-G-4	7.57	7.57	4.14	2.20
5-G-6	8.04	8.03	6.69	1.80
5-G-8	8.81	8.81	3.99	2.60
5-F-2	6.51	6.51	3.56	2.49
5-F-4	7.44	7.44	3.22	1.99
5-F-6	8.78	8.78	3.99	1.84
5-F-8	9.76	9.76	3.70	2.02
5-Y-2	6.94	6.94	4.86	2.93
5-Y-4	8.39	8.39	4.55	2.13
5-Y-6	9.19	9.19	7.81	1.91
5-Y-8	1.36	1.36	0.00	2.12

Table A3.3.2 The estimated permeability for NHL 3.5 mortars in comparison to the measured permeability.

Name	Estimated permeability		Measured	Measured
	k_{gas} [10^{-14} m²]	$k_{intrinsic}$ [10^{-12} m²]	$k_{intrinsic}$ [10^{-12} m²]	K_{gas} [10^{-13} m²]
3.5-N-2	2.75	2.91	2.91	5.92
3.5-N-4	2.87	2.65	2.65	3.56
3.5-N-6	3.27	2.87	2.87	4.01
3.5-N-8	3.55	4.22	4.22	2.46
3.5-G-2	5.85	3.48	3.48	3.53
3.5-G-4	6.31	2.93	2.93	2.20
3.5-G-6	6.95	4.23	4.23	1.80
3.5-G-8	8.90	3.65	3.65	2.60
3.5-F-2	5.27	3.44	3.44	2.49
3.5-F-4	6.01	3.43	3.43	1.99
3.5-F-6	6.80	4.86	4.86	1.84
3.5-F-8	7.65	6.69	6.69	2.02
3.5-Y-2	4.95	5.22	5.22	2.93
3.5-Y-4	5.73	0.00	0.00	2.13
3.5-Y-6	6.92	5.17	5.17	1.91
3.5-Y-8	7.51	0.00	0.00	2.12

A3.3.2 Study to the presence of interfacial transition zones in lime mortars

The ITZ zone around the aggregates for every binder type was analysed through SEM-EDS.

One NHL 3.5-RF-4 and one NHL 5-RF-4 cylindrical sample were cut to 25 mm in diameter and 10 mm in height. They were then 6 months old (conditions 20 °C, ±70 % RH). Samples were left to dry at 40°C during 4 days after which they were impregnated under vacuum with a Struers Citovac and polished up to 0.3 µm. 10 BSE images per sample were taken (x500, 20 keV high vacuum, spot size 11 to 15) with a size of 512 x 512 pixels, at a working distance of 20 mm.

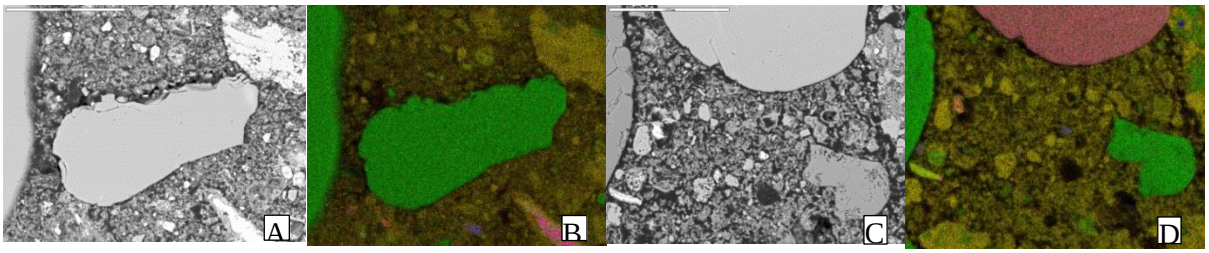

Fig. A3.3.1 EDS surface mapping of NHL mortars. NHL5 BSE image (A) and its respective mapping (B), NHL3.5 BSE image (C) and its respective mapping (D). Legend: yellow: Ca, green: Si, red: Al, magenta: K, blue: Fe. The scale bar represents 100 µm.

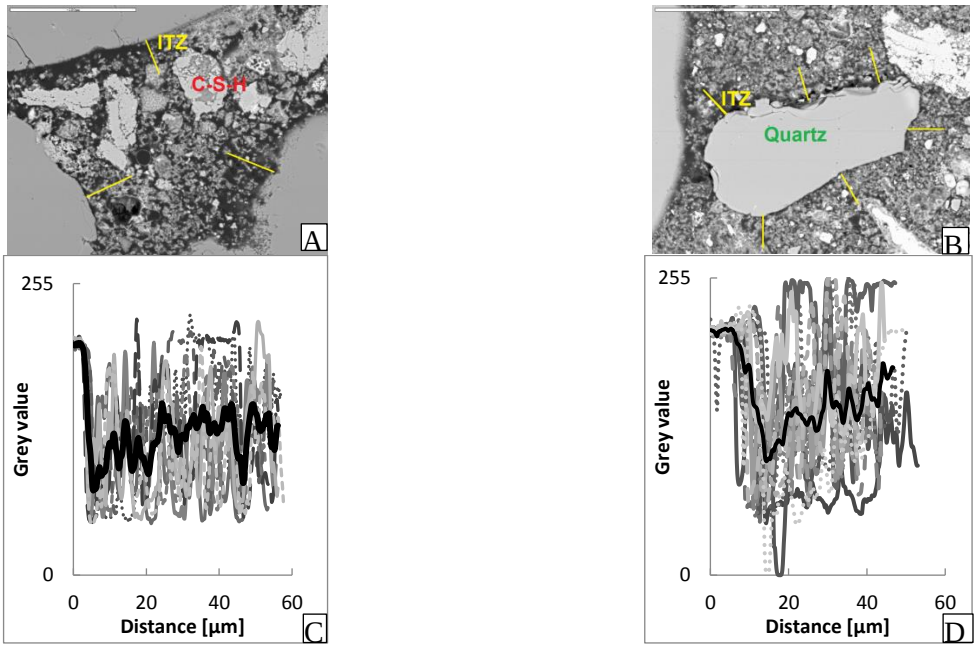

Fig. A3.3.2 A BSE image of NHL 3.5 & B BSE images of NHL 5 (at 500x) showing the zone considered ITZ region based on grey value plots around the aggregate.
C & D Grey value plot of a region of 60 µm around an aggregate in NHL 3.5 (C) and in NHL 5 (D). The aggregate ends at ± 8µm. The local depression in white values, and thus the local increase of porosity in the region next to the edge of the aggregate becomes more apparent through the black line, representing the mean value of all the measurements.

Three surface mappings were performed on each sample, at 20 keV in high vacuum and at a spot size of 17-19. Each EDS mapping was composed of 10 scans. Ca and Si are the main components, but also K, Al and Fe were detected (Fig. A3.3.1). The grains are mostly pure Si (quartz) grains, but also

some occasional phyllosilicate (as in Fig.A3.3.1B-D) were seen. The matrix mainly consists of Ca and Si, with some presence of Al and Fe. Whiter well-outlined areas in the paste were identified as calcite or unreacted portlandite; light grey blurred areas contain a higher percentage of Si, indicating the presence of C-S-H gel (Fig. A3.3.1 & A3.3.2A). Grey value plots of the region around various aggregates were made for both mortar types (Fig. A3.3.2). The edge around various silicate grains was analysed using line plots (from grain edge into the paste) with an interval of 20 µm. All plots were plotted on the same curve, after which a mean grey value curve was added to the plot. The average value shows the general trend of the presence of a higher porosity zone next to the aggregate, and a denser paste further away from the aggregate. As such, the ITZ thickness of the NHL 5 mortar varied between 0.05 and 20 µm, with an average of 15 µm. The ITZ thickness of the NHL 3.5 mortar varied between 0.05 and 80 µm, with an average of 37 µm. This is of course only an indication of the ITZ thickness, since image analysis of a plane section only discusses one transection of an aggregate and its ITZ [1,2].

A4. Appendix for chapter 4

A4.1 Background information on the experimental set-up for the colour measurement

A4.1.1 Colour temperature of the illuminant in the black room

The light source of the black room was characterized by measuring the incident light send out from the light source with the luxmeter-chromameter. The light was measured on a horizontal plane, some 65 cm from the light source. This position had previously been determined as the point with the maximal intensity of incident light on the optical eye [3].

The measured x and y values of the light source (x=0.318, y=0.333) were compared to the coordinates of a reference illuminant D65 (x=0.33, y=0.33). Figure A4.1.1 illustrates the x,y coordinates of the light source of the black room in comparison to a standard black body locus under a D65 illuminant. The light in the black room gives a slightly greener and more yellow colour than the D65 illuminant, but is still very close to the referent illuminant.

The XYZ coordinates of the D65 illuminant are (95.047, 100, 108.883), the XYZ coordinates of the light source in the black room are (95.495, 100, 104.057).

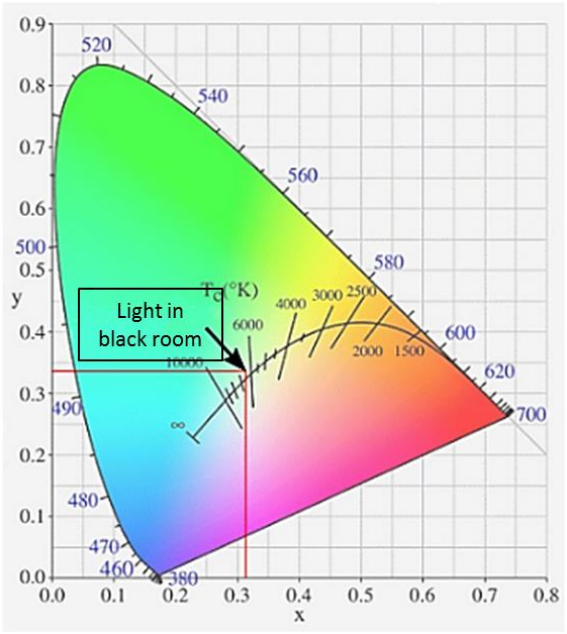

Fig. A4.1.1 The coordinates of the light source in the black room used for experimental measurements, in comparison to the black body locus in the x,y diagram.

A4.1.2 Colour change of the illuminant in the black room

The stability of the lights was verified by measuring the temperature of the illuminant through four testing sequences of two hours each. After two hours the maximal temperature was by and large achieved. Every minute, both colour and temperature were noted down (Fig.A4.1.2). Even though x and y values remained the same during time and increasing temperatures, the Y value changed. Before 50°C, the Y value would increase with increasing temperature, after that point, the Y value showed a decreasing trend [3]. In order to be able to compare values at different light tube temperatures, two measures were taken:

- The operator is to take measurements only after the light tubes had reached a temperature of 50°C
- A correction law, based on the four testing series, and for an arbitrarily chosen temperature of 70°C is to be applied on all Y coordinates (eq. A4.1.1). The measured Y value Y_m and the corresponding temperature T_m [°C] can as such lead to the corrected Y value Y_{corr}:

$$Y_{corr} = Y_m + 0.3423\,{T_m}^2 - 27.842\,T_m + 271.67 \qquad \text{(eq.A4.1.1)}$$

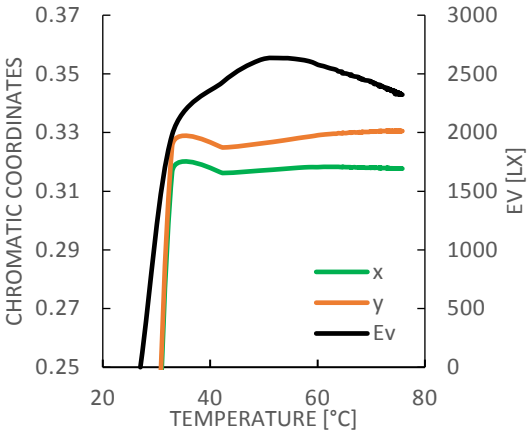

Fig.A4.1.2 Evolution of the Ev and x and y curve in function of the temperature measured, for one run.

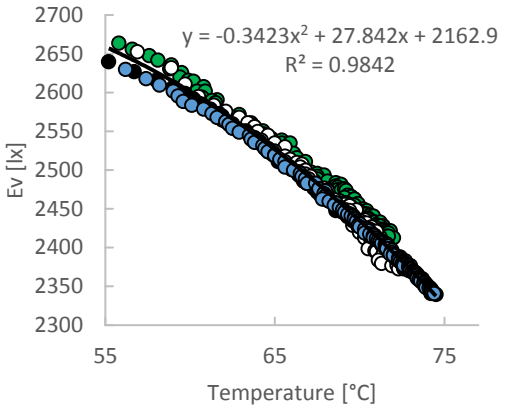

Fig. A4.1.3 The four runs with the trend line, for the Y value in function of temperature. The polynomial function was used for the correction factor.

A4.1.3 Comparative study between the colour of mortar and grinded mortar

This experimental study on 8 different lime mortars illustrates that the main difference between the surface colour and the colour of a grinded mortar lies in the Y value of the xyY coordinates.

For this study, first, the surface of mortar samples were measured (Table A4.1.1). These samples were grinded afterwards with mortar and pestle into a fine powder (diameter < 80 µm), and powdered samples were measured again. The powder was contained in a small transparent container of 7 x 10 cm³. When comparing the results on both sample types of the various mortars, it becomes clear that there is a difference in lightness detected, and that the difference in chromaticity is much lower (Table A4.1.1). It can thus be concluded that the difference is only due to the surface finish of the sample, an element excluded of this study.

Table A4.1.1. Colour measurements of 8 NHL mortar samples of 90 days of age. The same sample was measured once on its surface and once after it was grinded as a powder. The powder was placed in transparent cups of 7 x 10 cm² for measurement. The Δ in bold indicates the absolute difference between the two measured values.

Sample	x	y	Y	Sample	x	y	Y
1-Powder	0.3349	0.3505	0.6426	5-Powder	0.3696	0.3790	0.4508
1-Surface	0.3345	0.3505	0.6948	5-Surface	0.3748	0.3819	0.5095
Δ	**0.0003**	**0.0000**	**0.0522**	Δ	**0.0052**	**0.0030**	**0.0587**
2-Powder	0.3348	0.3470	0.8878	6-Powder	0.3333	0.3499	0.6129
2-Surface	0.3379	0.3510	0.6980	6-Surface	0.3364	0.3519	0.6539
Δ	**0.0030**	**0.0041**	**0.1898**	Δ	**0.0031**	**0.0020**	**0.0409**
3-Powder	0.3358	0.3576	0.4118	7-Powder	0.3357	0.3507	0.8237
3-Surface	0.3374	0.3602	0.4861	7-Surface	0.3376	0.3526	0.6333
Δ	**0.0016**	**0.0026**	**0.0743**	Δ	**0.0020**	**0.0019**	**0.1904**
4-Powder	0.3710	0.3818	0.2654	8-Powder	0.3580	0.3703	0.4185
4-Surface	0.3855	0.3920	0.4130	8-Surface	0.3622	0.3735	0.5674
Δ	**0.0145**	**0.0102**	**0.1476**	Δ	**0.0042**	**0.0032**	**0.1489**

A4.1.4 Comparative study between the colour of the cured mortar and the unhydrated binder-sand mix

Table A4.1.2 gives the colour measurements of white cement mortars and the dry mix of sands and binder, with the same proportions and components as the cured mortar [4]. A comparison between grinded cured mortar and dry powder mix shows that the difference between the two can mainly be attributed to the lightness: Y shows in general the largest absolute difference. The addition of yellow sand in the mortar appears to decrease this effect.

Table A4.1.2. Colour measurements of various mortars. The binder used was a white cement CEM II A-LL 42.5N, the sands used are noted each time Y= yellow, R= Rhin fin, G=green. The mortars were crushed and measured after 28 days of curing.

		Mortar 28 days			Dry mix			Δ		
Mortar type	B/A	x	y	Y	x	y	Y	x	y	Y
CEM-Y	1/2	0.364	0.380	0.616	0.346	0.366	0.604	0.0182	0.0147	0.0120
	1/4	0.369	0.383	0.525	0.355	0.371	0.500	0.0145	0.0116	0.0246
CEM-75Y/25 R	1/2	0.3558	0.373	0.592	0.344	0.364	0.605	0.0121	0.0088	0.0127
	1/4	0.3616	0.3776	0.564	0.349	0.368	0.515	0.0129	0.0097	0.0493
CEM-50Y/ 50R	1/2	0.353	0.371	0.581	0.342	0.363	0.606	0.0115	0.0084	0.0245
	1/4	0.361	0.377	0.561	0.347	0.366	0.517	0.0133	0.0111	0.0439
CEM-25Y/75 R	1/2	0.333	0.356	0.689	0.337	0.359	0.634	0.0034	0.0030	0.0553
	1/4	0.338	0.359	0.610	0.340	0.361	0.541	0.0021	0.0019	0.0687
CEM-G	1/2	0.326	0.355	0.658	0.327	0.355	0.603	0.0007	0.0007	0.0544
	1/4	0.3275	0.3587	0.588	0.327	0.356	0.525	0.0002	0.0027	0.0632

A4.2 The influence of grain size on the binder polluting effect: experimental study

The experimental campaigns had demonstrated that the Grassmann theory could not be applied on mortars without taking into account the polluting effect observed from the binder.

An experimental study was carried out on the presence of a relation between the aggregate grain size and the binder grain size. For this purpose, crushed grey-blue limestone was sieved and 5 different grain sizes (0.3, 0.6, 3, 6 and 12 mm) were set apart. Every grain size was mixed with white cement binder CEM II A-LL 42.5N (D_{50} = ±20 µm) separately, and for every grain size, the experimental threshold V_{tr} was defined [3]. The apparent density of the crushed blue limestone was 2711.62 kg/m³. Figure A4.2.1 indicates the experimental results in orange, as well as the theoretical model as explained in chapter 4, equations 4.8.1-11.

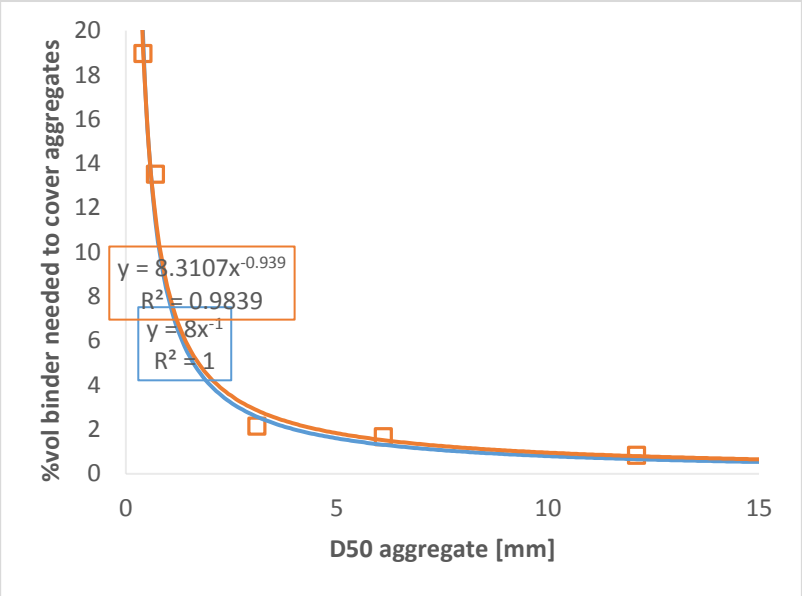

Fig.A4.2.1 Graph representing the influence of the polluting effect of the binder in function of the aggregate grain size.

A5. Appendix for chapter 5

A5.1 Composition of mortars in the E14 campaign

The following Table A5.1.1 presents the composition of the mortar campaign E14, performed by [5].

Table A5.1.1 The composition of the mortars in the mortar campaign E14

	Type			Mass [g]			
	Binder	Sand 1	Sand 2	Sand 1	Sand 2	Binder	Water
E3 135 90	NHL5	yellow	green	2737	747	1162	1203
E3 230 90	NHL5	yellow	green	2737	747	1162	1834
E3 255 90	NHL5	yellow	green	2737	747	1162	1906
E3 I 90	NHL5	yellow	green	2737	747	1162	1162
E3 II 90	NHL5	yellow	green	2737	747	1162	1307
E3 III 90	NHL5	yellow	green	2738	747	1161	1452
E3 V 90	NHL5	yellow	green	2737	747	1162	1742
E I 90	NHL3.5	yellow	green	2737	747	1162	1161
E II 90	NHL3.5	yellow	green	2737	748	1162	1307
E III 90	NHL3.5	yellow	green	2738	748	1161	1452
E V 90	NHL3.5	yellow	green	2738	747	1162	1742

A5.2 Measured and estimated mechanical properties

Tables A5.2.1-4 present the static elasticity and compressive strength as measured on the lime mortars.

Table A5.2.1 E14 mortars and their static elasticity and compressive strength

Name	E_{stat} [MPa]		F_c [MPa]		Estimated	
	average	C.I. 95%	average	C.I. 95%	E_{stat} [MPa]	F_c [MPa]
E3 135 90	164.58	17.81	1.91	0.30	362.23	2.66
E3 230 90	5.13	0.60	0.62	0.04	198.91	1.46
E3 255 90	20.24	1.26	0.72	0.04	187.06	1.37
E3 I 90	256.55	47.01	2.58	0.15	378.51	2.78
E3 II 90	115.22	34.92	1.35	0.40	325.23	2.39
E3 III 90	71.86	15.32	1.11	0.06	281.17	2.06
E3 V 90	77.39	19.86	0.78	0.04	215.40	1.58
E I 90	162.50	12.36	1.93	0.08	434.26	3.19
E II 90	102.69	6.31	1.27	0.07	373.54	2.74
E III 90	77.19	8.56	0.90	0.04	323.61	2.37
E V 90	162.50	12.36	1.93	0.08	248.76	1.82

Table A5.2.2 B/A mortars and their static elasticity and compressive strength

Name	E_{stat} [MPa]		F_c [MPa]		Estimated	
	average	C.I. 95%	average	C.I. 95%	E_{stat} [MPa]	F_c [MPa]
5-RF-25	384.49	114.26	2.53	0.12	574.53	4.21
5-RF-30	477.06	87.17	3.57	0.14	376.15	2.76
5-RF-45	951.41	210.81	5.64	0.20	838.84	6.15
5-RGY-25	73.44	7.30	1.55	0.04	506.91	3.72
5-RGY-30	87.65	8.45	1.98	0.11	326.08	2.39
5-RGY-45	174.72	33.71	2.99	0.16	749.03	5.50

Table A5.2.3 NHL 5 W/B mortars and their static elasticity and compressive strength

Name	E_{stat} [MPa]		F_c [MPa]		Estimated	
	average	C.I. 95%	average	C.I. 95%	E_{stat} [MPa]	F_c [MPa]
5-N-2	1479.70	104.78	9.14	0.74	1452.15	10.65
5-N-4	1152.48	219.59	10.58	0.28	1165.0	8.55
5-N-6	979.35	95.97	5.90	0.18	1147.55	8.42
5-N-8	701.73	106.10	4.74	0.08	816.49	5.99
5-G-2	1130.12	117.66	7.82	0.30	934.22	6.85
5-G-4	738.86	173.72	5.73	0.40	892.15	6.55
5-G-6	617.32	151.28	5.03	0.29	867.63	6.37
5-G-8	1350.56	47.52	8.13	1.33	830.72	6.09
5-F-2	1088.67	107.97	6.73	0.16	859.31	6.30
5-F-4	886.81	110.69	5.84	0.21	803.12	5.89
5-F-6	821.95	92.50	4.58	0.18	737.05	5.41
5-F-8	830.37	130.70	4.40	0.43	697.03	5.11
5-Y-2	438.19	35.74	4.03	0.34	424.09	3.11
5-Y-4	173.84	28.06	2.94	0.18	382.90	2.81
5-Y-6	193.36	69.45	2.59	0.25	364.32	2.67
5-Y-8	109.49	8.77	1.64	0.05	315.39	2.31

Table A5.2.4 NHL3.5 W/B mortars and their static elasticity and compressive strength

Name	E_{stat} [MPa]		F_c [MPa]		Estimated	
	average	C.I. 95%	average	C.I. 95%	E_{stat} [MPa]	F_c [MPa]
3.5-N-2	1336.37	84.97	10.07	0.49	1257.36	9.22
3.5-N-4	1285.80	47.09	9.01	0.24	1228.42	9.01
3.5-N-6	1258.77	39.31	8.34	0.24	1141.95	8.38
3.5-N-8	891.02	179.10	8.14	0.36	1090.34	8.00
3.5-G-2	992.75	109.65	8.57	0.39	1027.90	7.54
3.5-G-4	972.56	157.95	7.53	0.33	984.288	7.22

3.5-G-6	804.28	114.29	6.82	0.20	929.936	6.82
3.5-G-8	614.06	194.72	5.35	0.27	799.917	5.87
3.5-F-2	1442.51	66.73	8.99	0.17	965.09	7.08
3.5-F-4	863.88	232.61	6.39	0.47	885.50	6.50
3.5-F-6	1060.14	79.50	6.66	0.36	814.53	5.98
3.5-F-8	737.52	260.26	5.54	0.45	751.03	5.51
3.5-Y-2	680.32	178.14	5.11	0.32	489.54	3.59
3.5-Y-4	524.53	78.34	3.94	0.25	442.62	3.25
3.5-Y-6	286.27	30.96	3.02	0.10	387.52	2.84
3.5-Y-8	257.32	26.17	2.26	0.14	365.52	2.68

A5.3 Preliminary study on the De Larrard method

A preliminary study was performed, where cement mortars were used, in order to determine whether this estimation model would be valid for cement mortars using Betonlab software, which estimates the compressive strength of cement mortars based on the estimation of De Larrard.

The mortar strength estimation according to De Larrard's model was compared with experimental results obtained on 12 mortars with various W/B and B/A ratios. The mortars were obtained by mixing white Portland cement CEM II A-LL 42.5N and three different dry sand types: yellow, green and Rhine sand. Their grain size distribution is given in Chapter 2. The recipes are presented in Table A5.3.1. They all had a reasonable workability which allowed fresh mortar to be cast into prismatic moulds (16 x 4 x 4 cm^3). The samples were cured in water tanks during 28 days at a temperature of 20 ± 2°C. The compressive strength was then measured on 10 samples per mortar mix according to EN 1015-11. Next, BetonLab software was used in order to obtain the estimated value of fc_{28}. For cement, the effective strength value is 51 MPa, the packing density of cement β_c is 0.483. The grain size distributions of the sands as well as the maximum diameter and the packing density of sand β_s per sand type are presented in Table A5.3.2. The computed values for mortar are presented in Table A5.3.1 and Figure A5.3.1.

The results indicate that the De Larrard's model is suitable for estimating the compressive strength of a hardened mortar based on the recipe and on specific properties which can be measured on the raw ingredients. The experimental study with cement mortars proved that the model proposed by De Larrard can be used for the estimation of compressive strength for cement mortars.

Table A5.3.1. Estimated compressive strength values compared with the measured values. Mortars were made with yellow (Y), green (G) or Rhine sand (R).

Sand	# set	Mix ratios		Compressive strength [MPa]		
		B/A Ratio	W/B Ratio	Estim	Meas. av.	st. dev.
Yellow	Y1	0.46	0.69	15.00	15.19	0.36
Yellow	Y2	0.37	1.00	8.14	9.07	0.98
Yellow	Y3	0.31	1.31	3.95	3.98	0.35
Yellow	Y4	0.23	1.69	2.18	2.72	0.18
Green	G1	0.52	0.79	11.49	11.69	0.44
Green	G2	0.38	1.00	7.27	6.93	0.35
Green	G3	0.31	1.19	4.90	4.82	0.24
Green	G4	0.22	1.58	2.54	2.85	0.11
Rhine	R1	0.36	0.90	8.50	8.84	0.46
Rhine	R2	0.27	1.12	5.28	5.65	0.38
Rhine	R3	0.22	1.34	3.64	4.28	0.27
Rhine	R4	0.16	1.80	1.81	1.95	0.25

Table A5.3.2. Grain size information, packing densities β and adherence coefficient p per sand type.

Sand	D_{max} [µm]	$S_{80µm}$ [%]	β_s [-]	p [-]
Yellow	500	2.6	0.527	0.583
Green	280	6.3	0.567	0.497
Rhine fin	630	8.3	0.614	0.517

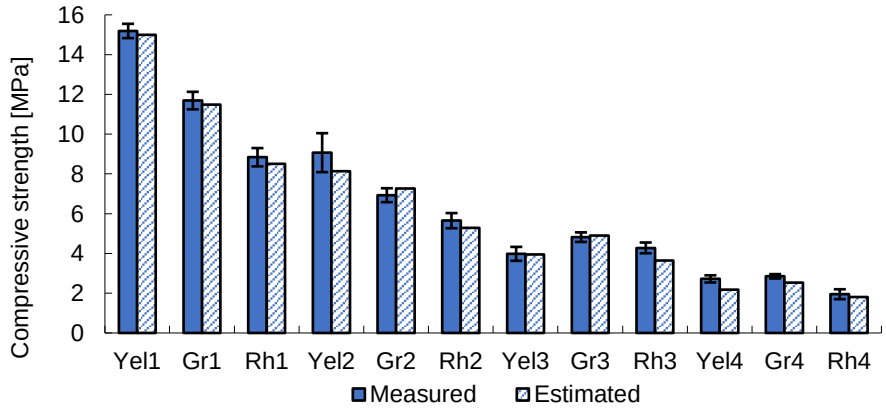

Figure A5.3.1. Estimated versus measured compressive strength per mortar mix.

A5.4 Preliminary study concerning the influence of the mixed-in air volume for the De Larrard estimation method

A preliminary study was performed in order to know whether the mixed-in air volume would influence the final compressive strength. Since the air volume is not known before making the mortar, a loop was created in order to estimate the mortar without using the equation given by De Larrard, where the air volume is calculated based on De Larrard's assumption that the air volume is mainly dependent on the volume of sand. Therefore, for a

specific amount of water and binder, only a specific combination of sand and air can exist. The volume of air calculated as such, varied between 0 and 4.5% of the total mortar volume, with an average of 2.2%, which corresponds to the air volume De Larrard calculated for his concrete samples, between 0.5 and 6% [6]. Excluding the V_a out of the estimation equation for the matrix' compressive strength (eq.7.2) does lead to a higher estimated compressive strength, which is more important for small estimated F_c values with an average increase of 115%, but lower for the higher estimated F_c values (on average 108%) (Table A5.4.1).

Table A5.4.1 Results of the preliminary study on the volume of air included into the mortar and its effect on the final compressive strength estimation of the mortar. The value calculated by Betonlab is given first, followed by the transcripted version of the method with the loop in order to calculate V_a, and the estimation without V_a. The difference is largest for the mortars with the smallest resistance.

Green	**R1/4**	**R1/3**	**R1/2.5**	**R1/2**
Betonlab SR	3	6	9	14.7
Fc with V_a	2.99	6.01	8.74	14.23
Fc without V_a	3.48	6.62	9.50	15.00
Rhin fin	**R1/4**	**R1/3**	**R1/2.5**	**R1/2**
Betonlab SR	2.3	4.6	7	11.2
Fc with V_a	1.88	3.89	6.02	9.59
Fc without V_a	2.25	4.49	6.64	10.35
Yellow	**R1/4**	**R1/3**	**R1/2.5**	**R1/2**
Betonlab SR	2.4	4.4	8.4	18.5
Fc with V_a	2.29	4.39	8.40	17.14
Fc without V_a	2.90	5.14	9.16	18.37

A6. Appendix for chapter 6

A6.1 General set-up of the algorithm

The design variables of each individual are created at random by the script 'initialize variables'. The randomness of the creation is guaranteed by a shuffle function, which imitates the re-initiation of values which Matlab® needs to create a 'random' population.

The evaluation script then determines the fitness of these individuals, i.e. the distance of the individuals towards the target. The fitness evaluates their objective functions (Table 6.2) using the continuous and discrete variables present in each individual. This file also includes constraints (Table A6.1.1), which force the algorithm to perform a first elimination of individuals.

The constraints refer to several minimal and maximal ratios for mixing. The first three are necessary for some estimation functions: for example, for colour, a minimal of binder volume is required (see Chapter 4). The W/A and W/B ratios are a translation for the workability of the mortar, based on Fig. 2.6 in Chapter 2 Because the mortar recipes are expressed in vol%, the

W/B and W/A ratios in this constraints file are expressed in vol% as well and not in mass, as usual. Constraints are best expressed as inequalities, since inequalities are less restrictive than equalities [7]. As stated in the introduction, the search space is subdivided by these constraints into feasible and infeasible regions. It might therefore be expected that, when running the algorithm, some zones in the search space will remain unexplored, since they are considered to bring only infeasible individuals.

The method used here to determine feasibility comes from [7], where the feasible individuals are clearly distinguished from the infeasible ones, by attributing a penalty to the infeasible individuals (eq. 6.1), from [7].

$$\mathcal{F}(x) = \begin{cases} f(x), & if\ g_i(x) \geq 0 \quad \forall i \in I; \\ f_{max} + \sum_{i=1}^{I} \langle g_i(x) \rangle, & otherwise. \end{cases} \qquad \text{(eq. 6.1.1)}$$

$$f_{max} = \max f_j(x) \qquad \forall i \in I \qquad \text{(eq. 6.1.2)}$$

Where the parameter f_{max} is the maximum function value of all feasible solutions in the population, with *j* the objective function and *i* the individual of population *I*. The operator $\langle\ \rangle$ returns the operand, if the operand is negative and returns a value zero, otherwise. The fitness of a feasible solution is equal to the function value *f(x)*.

All constraints are considered in a sequence, and when sufficient feasible individuals are found which satisfy the constraint, the next constraint is considered. This allows each constraint to direct the population in the region of its feasibility [7]. For any infeasible individual only the constraint violation is defined, and not the objective functions. Then, two individuals are compared according to the tournament selection operator, where:

- Any feasible individual is preferred over an infeasible individual
- Over two feasible individuals, the individual with the better objective function value is favoured
- Over two infeasible individuals, the individual with the smaller constraint violation is favoured

If the number of feasible solutions is large enough to fill the entire population, the infeasible solutions are eliminated, since they will have lost the tournament.

After evaluation, individuals are selected, based on the crowded tournament selection. Subsequently, individuals are subjected to crossover and mutation operations on both binary and real numbers. Consequently, individuals are evaluated again, and ranked according to the non-dominating elitism principle. Individuals are ranked and the best individuals are used for the generation of a new population (starting from 'decode'). The final evaluation will add additional information to each individual, so that the *.txt* file containing the last population will also contain information concerning

the actual properties of the mortar, and not merely the objective functions, i.e. difference between the target and the estimated property.

Table A6.1.1. Constraints in the evaluation script.

Sum of binder and water volume is smaller than 1	$g(1) = 100 - vol_b - vol_w$
Binder volume has to be larger than 10% sand volume	$g(2) = vol_b - 1.6\ vol_s\ \frac{D50_b}{D50_s}$
Sand volume not lower than 30%	$g(3) = vol_s - 30$
Minimal water/aggregate ratio	$g(4) = \frac{vol_w}{vol_s} - 0.05$
Maximal water/aggregate ratio	$g(5) = 0.6 - \frac{vol_w}{vol_s}$
Minimal water/binder ratio	$g(6) = \frac{vol_w}{vol_s} - 0.5$
Maximal water/binder ratio	$g(7) = 1.5 - \frac{vol_w}{vol_b}$

Table A6.2 represents which parameters can be adapted in the algorithm. The crossover and mutation probability for this algorithm were based on the information available in [7]. The crossover probability value depends on the type of genetic algorithm (GA), i.e. a binary GA or real GA. The binary GA is more restrictive, with a probability value between 0.9 and 0.99, than the real GA, with a probability value between 0.5 and 1. Since this multi-objective problem has both real and binary decision variables, the value should respect both. The crossover probability was therefore set to 0.9. This means that approximately 90% of all strings in the population are used in the crossover operation, and 10% are simply copied to the new population [7]. Single-point crossover is performed for the binary strings. Since for real parameter GA, few studies exist [7], the real value crossover operation is actually a simulated binary crossover, a method set up by Deb et al. [7].

The mutation probability is subdivided in the mutation probability for the binary and for the real numbers. The binary mutation probability can vary between minimally 0 and the inverse of the length of the 'field' maximally, i.e. the length of the chromosomes, the mortar recipe. In this optimisation problem, the chromosome length is defined at 10. The binary mutation probability is therefore 1/10 or 0.1. The real mutation probability should be set between 0 and the inverse of the number of variables. The variables in this problem are the quantity and type of constituents of the mortar (Fig. 6.2), and are 6 in this case. Also here, the maximum mutation probability was kept, and is thus 1/6 or 0.166667. By using this approach, the algorithm should be able to calculate the probability an individual is subjected to both operations.

Next to the probability of both operations, the distribution index should be defined as well, which defines the distribution of the crossover operation or mutation operation for the real values. The distribution index for real crossover should be situated between 1 and 100. This distribution index was

kept at 5. The distribution index for real mutation was kept at 250; when minimal and maximum values are set at 1 and 500.

Table A6.2. Parameters in the algorithm. The 'probability of cross-over' can be adapted depending on the type of algorithm, real-coded or binary-coded. Since the algorithm used here combines both binary and real values, the constraints of the binary coding should be taken into account. $l_{chromo,max}$ is the maximum number of bits in a chromosome, and n_{var} is the number of variables.

	Suggested values		
Parameters to modify	Min	Max	Selected
Probability of crossover BGA RGA	0.9 0.5	0.99 1	**0.9**
Distribution index real crossover	1	100	**5**
Binary mutation probability	0	$1/l_{chromo,max}$	**0.1**
Real mutation probability	0	$1/n_{var}$	**0.166667**
Distribution index for real mutation	1	500	**250**

The indication for the spread was determined based on the empirical linear relation between the W/B ratio and the measured spread of the mortars, produced in this experimental campaign.

As shown in Fig. A6.1.1, the mortars appear to be largely influenced by the W/B ratio and the grain size: the mortars made with fine grains are situated in the upper region of the graph, while the mortars made with larger grains or with a better grain size distribution, are situated in the lower region of the graph. A linear trend line for the W/B mortar series of both NHL5 and NHL3.5 YG mortars is indicated on Fig.A6.11. Another trend line was drawn for the W/B mortar series made with N, RG and RF sands. Both trend lines were used as basis for the empirical relation in order to estimate the spread. A generalized function was used, where a distinction in c in eq. A3.1.1 is made for mortars made with either fine or coarse-grained sands. The empirical relation established is thus determined by the grain size class and the W/B ratio.

$$S = \left(\frac{W}{B} - c\right) \frac{1}{0.003} \qquad \text{(eq.A3.1.1)}$$

$$if\ D_{50} < 250\ \mu m, \quad then\ c = 0.4$$
$$if\ D_{50} > 250\ \mu m, \quad then\ c = 0.3$$

Where S is spread [mm] and W/B are expressed in [g].

The reader should consider that this spread estimation is a mere indication, because of the empirical set-up of the estimation equation and because of the limited number of mortars it is based on. In fact, the correlation already decreases sharply once mortars with similar sand types from the other mortar series (B/A and from mortars produced in chapter 7) are added.

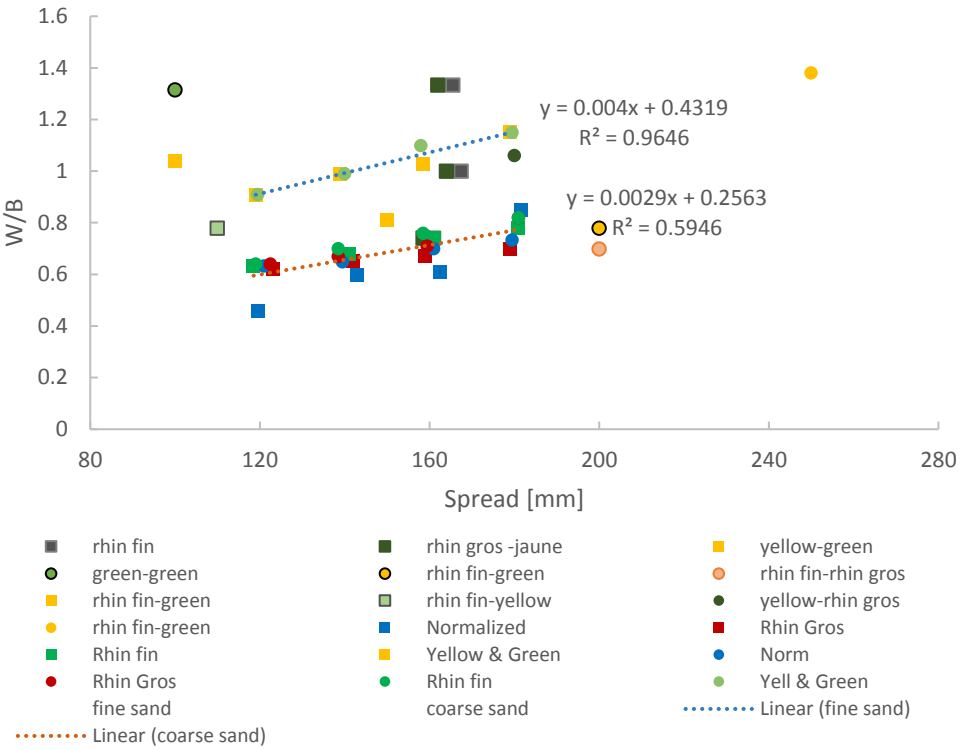

Fig. A6.1.1 The relation between the W/B ratio and the spread measured on the mortars of the experimental campaign. Remark the difference in mortars with green and yellow sand (upper) and the mortars made with the Rhin or Reference sands (lower). The mortars made with a mix of Rhin and yellow or green sand find themselves between these two groups.

A6.2 Validation of the algorithm: Evolution for every population size

Following graph sequences present the evolution of every population size, for each generation.

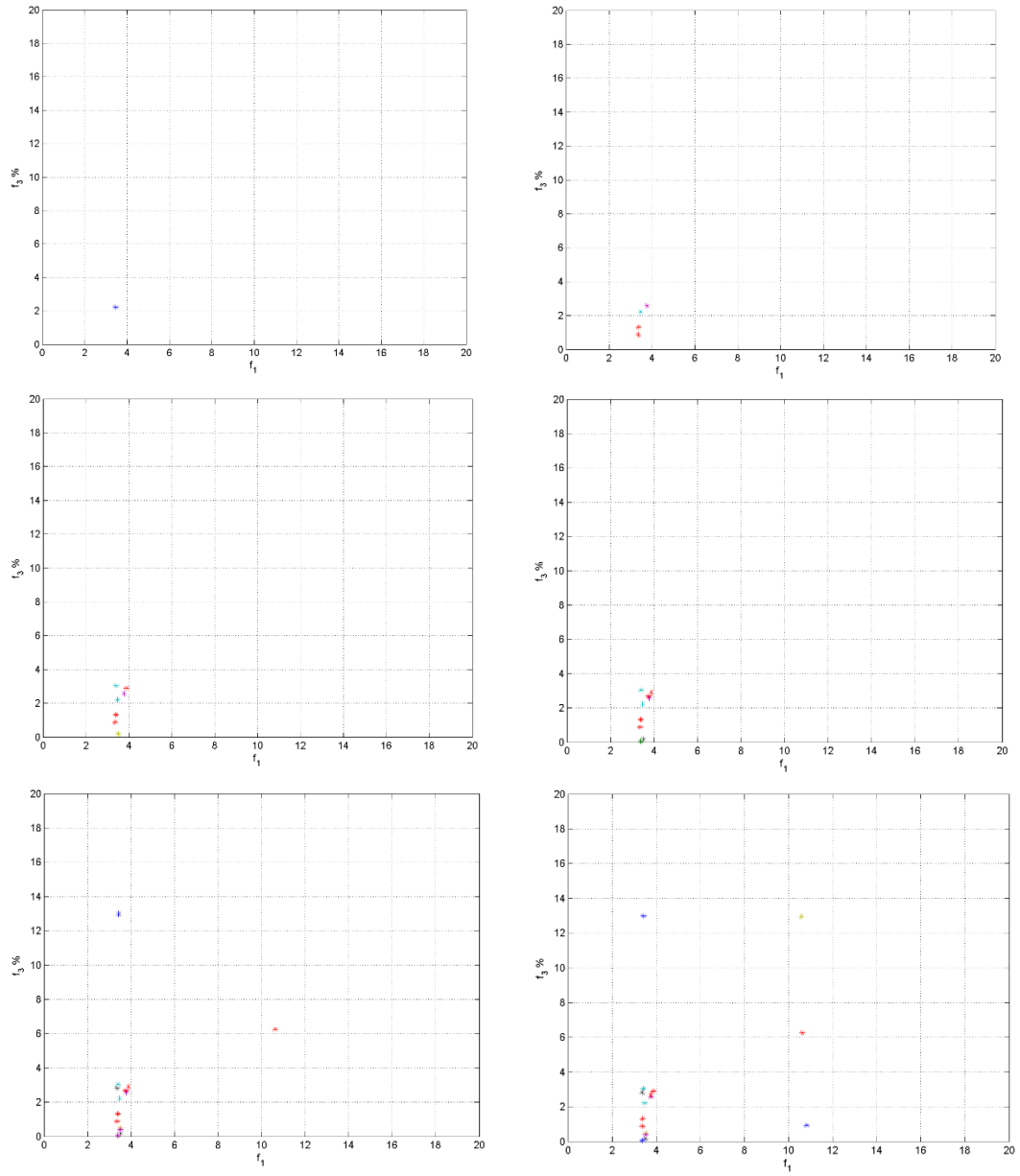

Fig. A6.2.1 Run 2 of the algorithm with N=6. A-F represent convergence of the individuals towards a minimal distance between the targets, here f1= ΔE^* [-] and f3%= ΔK_w [%], after 1, 10, 20, 30, 40 and 50 generations respectively.

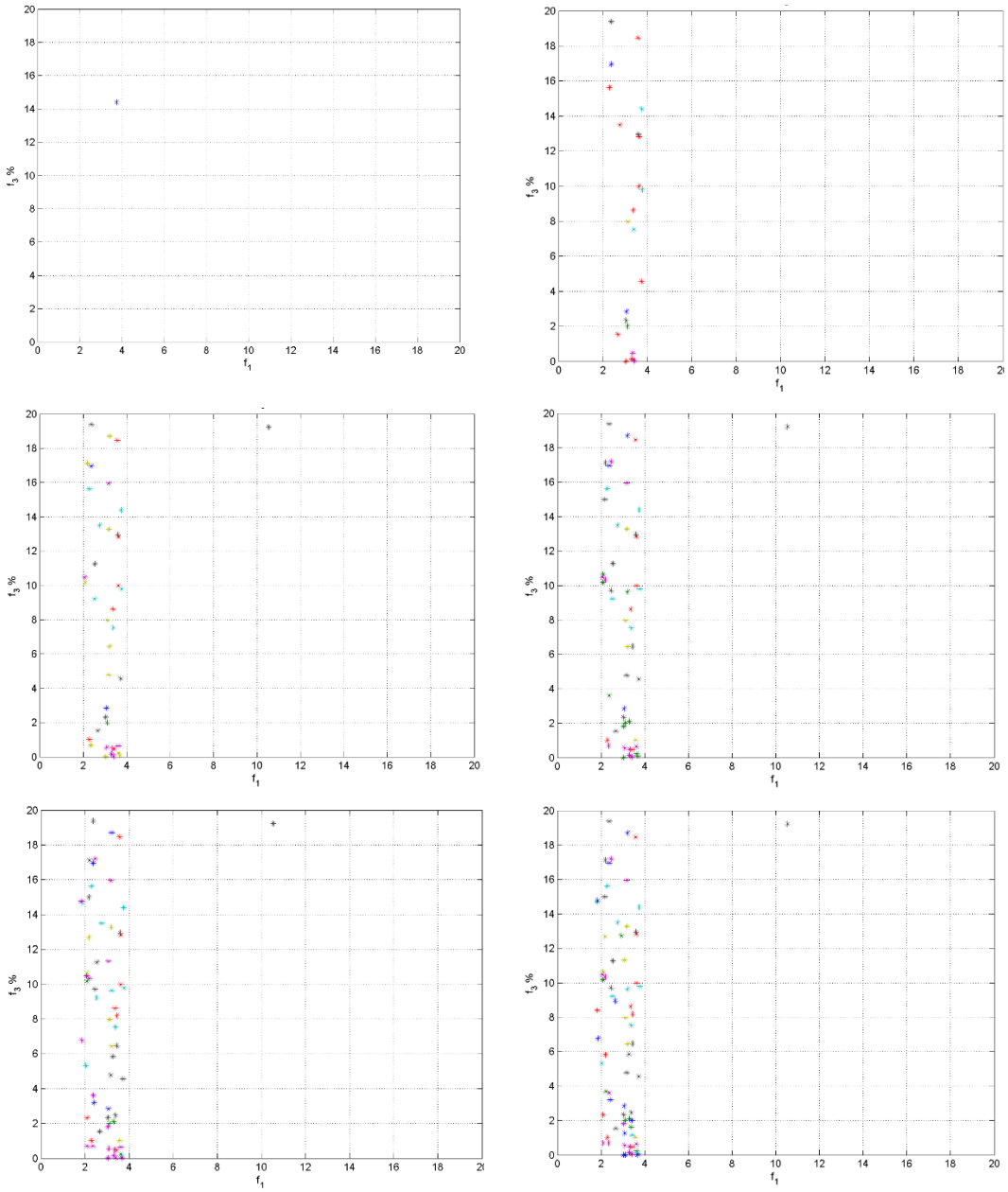

Fig. A6.2.2 Run 2 of the algorithm with N=30. A-F represent convergence of the individuals towards a minimal distance between the targets, here f1= ΔE* [-] and f3%= ΔKw [%], after 1, 10, 20, 30, 40 and 50 generations respectively.

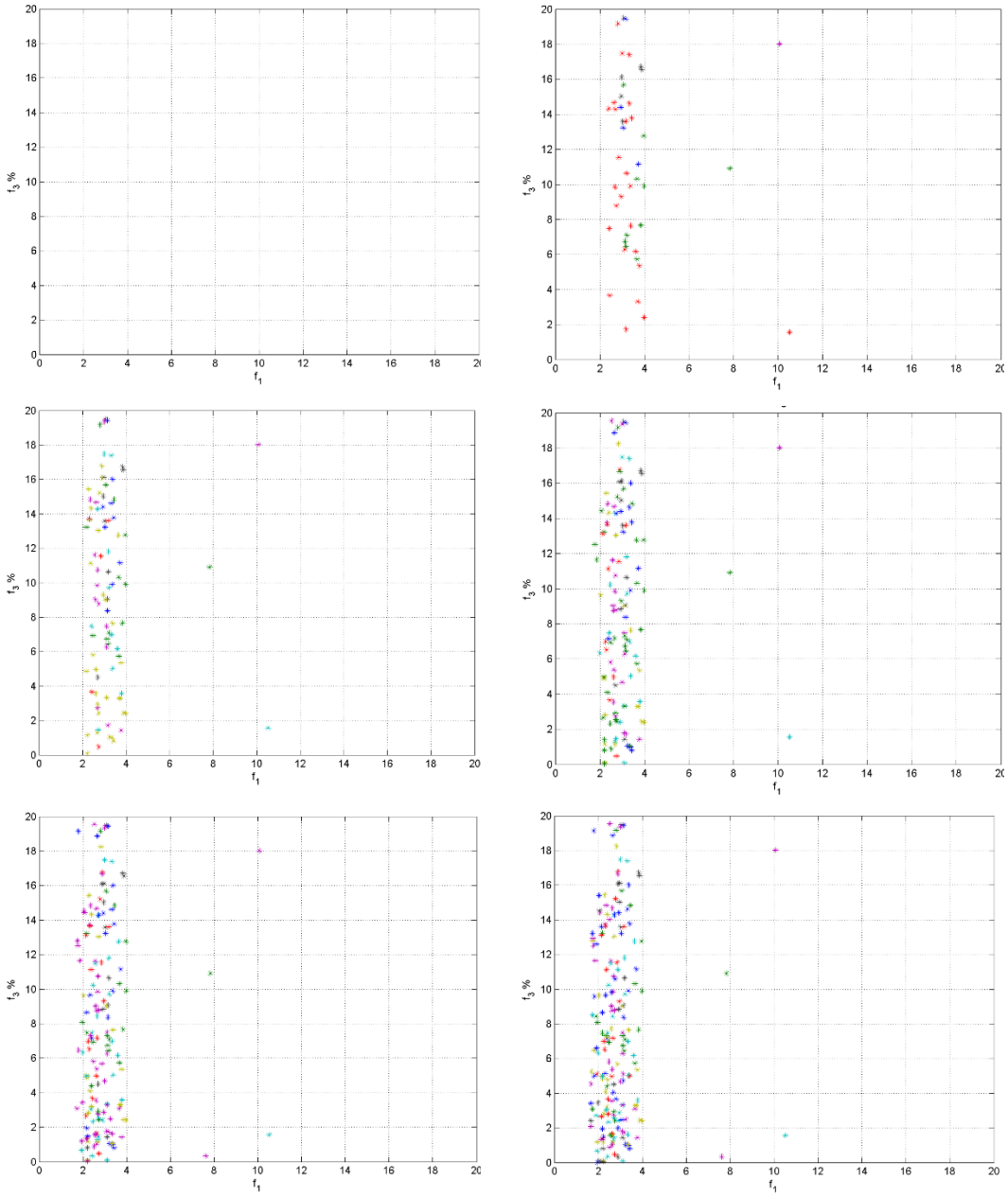

Fig. A6.2.3 Run 2 of the algorithm with N=60. A-F represent convergence of the individuals towards a minimal distance between the targets, here f1= ΔE* [-] and f3%= ΔKw [%], after 1, 10, 20, 30, 40 and 50 generations respectively.

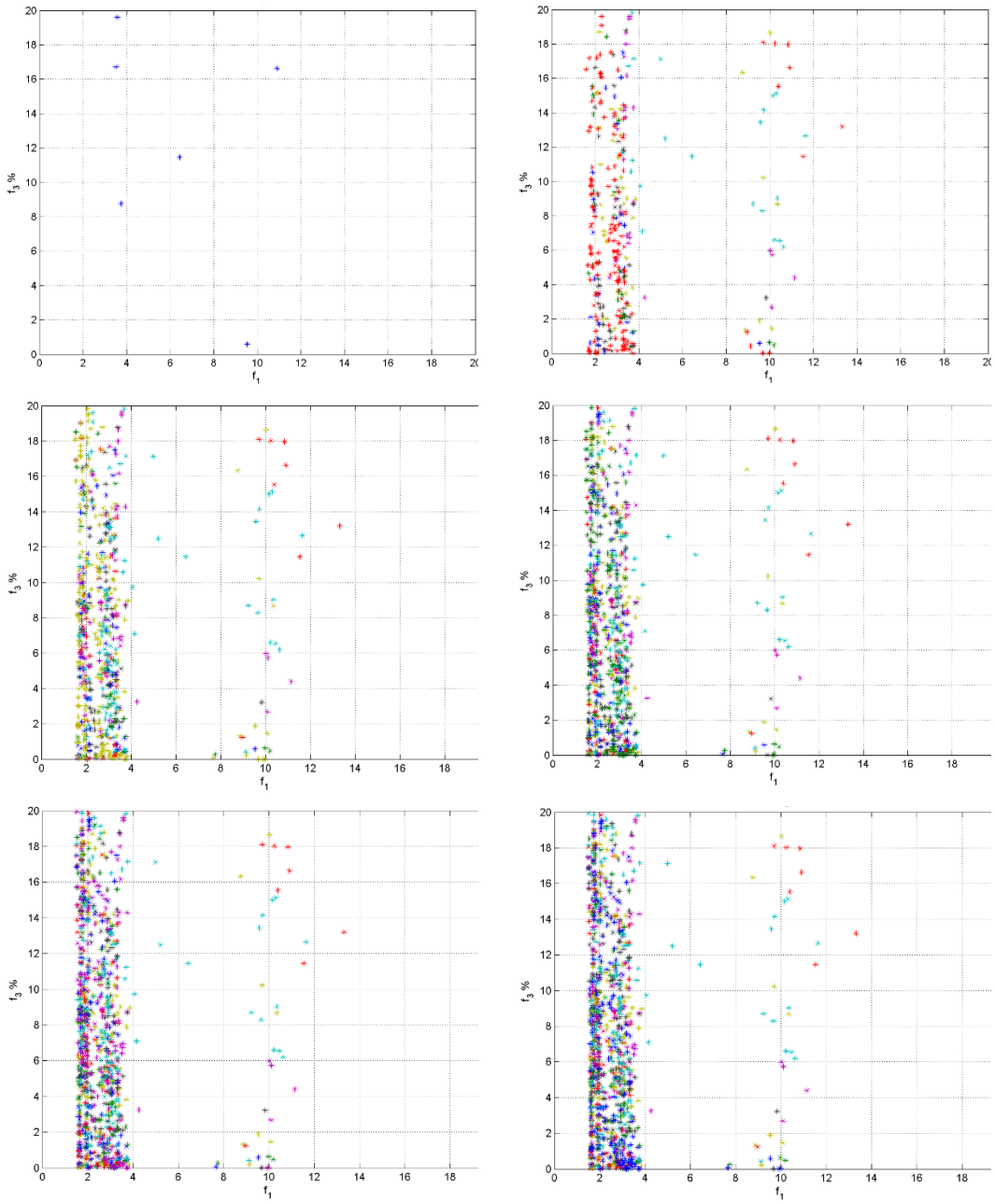

Fig. A6.2.4 Run 3 of the algorithm with N=300. A-F represent convergence of the individuals towards a minimal distance between the targets, here f1= ΔE* [-] and f3%= ΔKw [%], after 1, 10, 20, 30, 40 and 50 generations respectively.

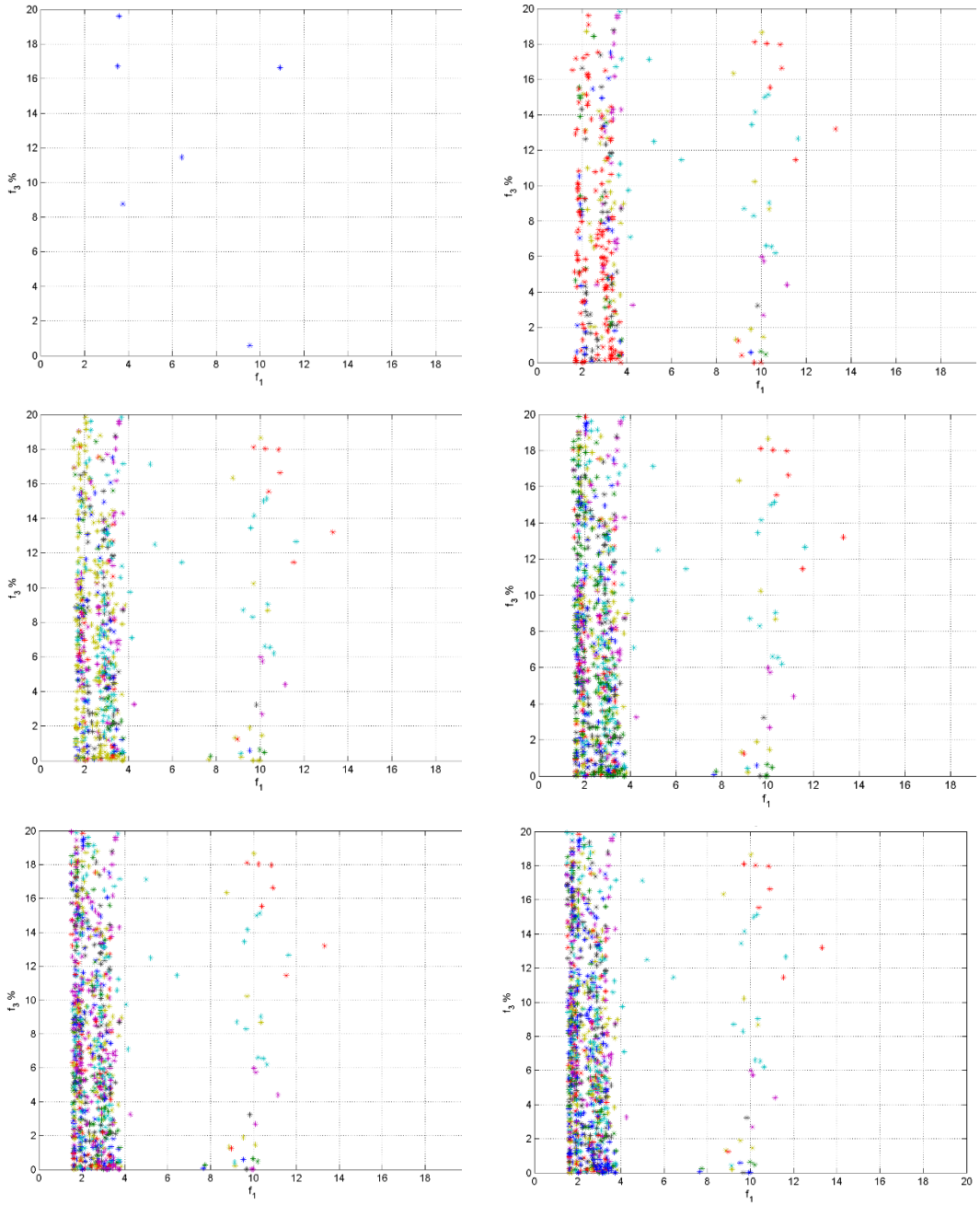

Fig. A6.2.5 Run of the algorithm with N=3000. A-F represent convergence of the individuals towards a minimal distance between the targets, here f1= ΔE* [-] and f3%= ΔKw [%], after 1, 10, 20, 30, 40 and 50 generations respectively.

A6.3 Determining the best individual of a run through ideal point X

Following table A6.3.1 gives the coordinates in the objective function space (ΔE^*, ΔE_{stat}, ΔK) of the ideal point X. This point is determined for each run: its coordinates depend on the lowest fitness for each objective function found during that run. The individual with the smallest distance towards this ideal, fictional point is considered the best mortar recipe.

Table A6.3.1 Coordinates of the ideal point X for every run. The variation of this point is low for colour and elasticity, but varies for permeability

	ΔE^*	ΔE_{stat}	ΔK		ΔE^*	ΔE_{stat}	ΔK
R1-T1	0.706	0.003	0.023	R1- T2	0.076	32.167	0.000
R2-T1	0.719	0.005	0.001	R2- T2	0.217	32.882	0.002
R3-T1	0.708	0.008	0.011	R3- T2	0.224	32.196	0.003
R4-T1	0.732	0.002	0.015	R4- T2	0.217	32.198	0.004
R5-T1	0.757	0.002	0.007	R5- T2	0.220	31.384	0.000
R6-T1	0.701	0.000	0.002	R6- T2	0.217	32.276	0.001
R7-T1	0.687	0.001	0.007	R7- T2	0.234	32.080	0.005
R8-T1	0.689	0.004	0.043	R8- T2	0.217	32.856	0.002
R9-T1	0.732	0.001	0.000	R9- T2	0.136	32.781	0.000
R10-T1	0.704	0.001	0.002	R10- T2	0.167	32.076	0.002
Average	0.714	0.003	0.011	Average	0.192	32.290	0.002
St. Dev.	0.022	0.002	0.013	St. Dev.	0.051	0.454	0.0017

A7. Appendix for chapter 7

A7.1 Background information of the natural stones used in the exploitation of the tool

A7.1.1 Avesnes stone

Origin

During the Cretaceous, continents spread out, leading to a general high sea water level. The climate was warm. These favourable conditions of shallow warm seas led to an increased number of carbonate-forming organisms. This stone is a chalk limestone which are typically formed by microscopically small organisms of marine plankton [8]. The formation is due to the deposition of calcite after every yearly algal bloom. This deposition had to take place in more profound seawater of some ten metres deep, below wave base, since no distinct deposition layers are visible. The sea bottom was habited by digging and crawling organisms which caused bioturbations in the Avesnes stone. The remains of shellfish and fish which lived in the upper water column can also be found [8]. Due to rotting organisms, the sea bottom was poor on oxygen, permitting the formation of glauconite in hollow calcite spheres. The glauconite in this stone therefore obtained a typical round shape [8]. Due to sedimentation and compaction, the glauconite was concentrated in the bioturbation [8].

Table A7.1 gives more information concerning the name, varieties, and geological age of the Avesnes stone.

Table A7.1 General information concerning the Avesnes stone [8,9]

Type natural stone	Sedimentary stone –limestone
Other names	*Pierre d'Avesnes-le-Sec*, pierre de Hordain, craie grise de Hordain, but also *bonne pierre de Valenciennes, pierre de Loos, pierre de Lézennes, calcaire d'Artois*. Remark that the name 'Avesnes stone' was used rather generally for chalky limestones from the same region (Fig.A7.1) with a more or less similar outlook, but which are from a different age and/or region. The Avesnes stone in the strict sense, concerns the *pierre d'Avesnes-le-Sec* and *pierre de Hordain* (also called *craie grise de Hordain*).
Quarry	The Avesnes stone *sensu stricto* was quarried in Scheldt basin, region of Hainaut-Cambrésis-Artois (FR) in e.g. Avesnes-le-Sec, Hourdain, Masnières. The *pierre de Loos* and *~Lézennes* are quarried in the Leie and Deule basin, near Lille (FR) in Lézennes and Loos-lés-Lille. For both, the last quarries closed at the end of the 18th C., beginning of the 19th C.
Geological age	All so-called Avesnes stone are from the Mesozoic, Upper Cretaceous. The Avesnes stone s.s. is from the Turonian (93.3-89.8 Ma), the stone from Lézennes and Loos from the Coniacian (98.8-86.3 Ma).

Description

The stone of the convent is white to light grey. Grains are sometimes visible with a small loupe, and bioturbations are visible with the naked eye (Fig. 7.1). Round bioturbation can be clearly distinguished since it is darker than the rest of the stone.

The thin section shows laminations which are visible even when holding the thin section towards the light, without microscope. These laminations can be distinguished through zones which are rich in micrite or glauconite. The glauconite-rich zones contain generally less bioclasts and micrite, and contain more glauconite.

The Avesnes stone is mainly composed of a micrite matrix, and a variety of bioclasts: echinoderms, crinoids, foraminifers and gastropods can easily be distinguished. The glauconite grains are rounded and green with sometimes a white rim at the edges. The stone also contains calcium phosphate, and a sieve texture typical for fish scales was observed. Very few grains of quartz were detected (<5%), which were angular, and of detritic origin. The stone contains in general well sorted grains, with a directional texture due to the glauconite-rich and micrite-rich layers. In accordance with literature, the stone was classified as an biomicrite wackestone [8]. The combination of micrite matrix, bioclasts, the presence of the calcium phosphate from fish scales or bones, as well as the rounded glauconite grains are considered to be distinguishable features of the Avesnes stone [8].

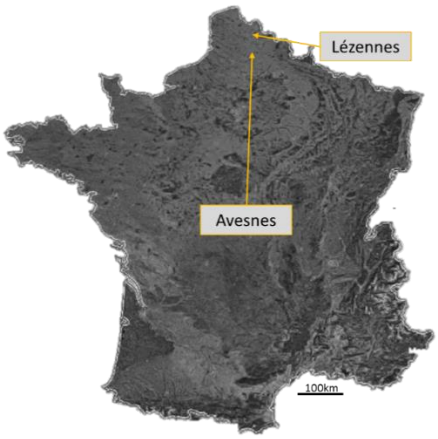

Fig. A7.1 Map of France. The provenance of Lézennes and Avesnes are indicated with a yellow arrow. Figure made based on information from Google Maps 2016.

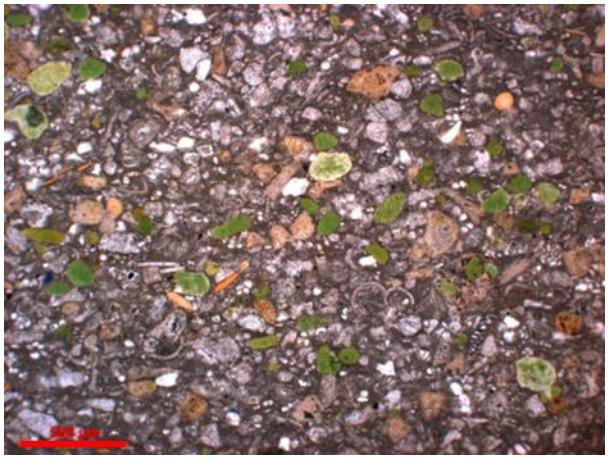

Fig. A7.2 Microscopic view of the stone from the Couvent des Ursulines, Mons, in plane polarized light. The scale bar represents 500 µm. A matrix of micrite is present, surrounded by bioclasts such as foraminifers, large glauconite and phosphate grains and some angular quartz.

Use

The Avesnes stone is a soft stone and was used for sculptures and ornamental structures on buildings. The stone of Avesnes is reported to be quarried since the middle Ages (11th C.), and was at the height of its popularity between the 15th and 17th Century [8]. The stone has not been quarried for long, the bulk of quarries closed down at the beginning of the 19th C., the last quarry closed in 1863 in Hourdain, and the last use of quarried stone from Avesnes-le-Sec was reported in 1903, when it was used for the restoration of the St Peter's Church in Douai. All types of buildings were constructed with Avesnes stone, religious, civil and vernacular buildings, in the region of Douai, Cambrai and Valenciennes. The stone was most likely not competitive anymore with the cheaper bricks for building purposes.

Quarries were either at the Scheldt River, or a little further away (Avesnes-le-Sec). The stone was often shipped off from Valenciennes, and became as such also known as stone of Valenciennes. This stone was used in the surrounding region of Artois, but, since the river runs northwards, the stone was also used in the regions now known as Belgium. The stone reached the town of Leuven, and was used for its town hall in the 15th C.

The stone was quarried underground, at a depth of 12 to 15 m, where a large network of galleries permitted to excavate the stone. Since quarries were closed down once the good banks had been exploited, and the last quarries closed nearly two centuries ago, the extent of the excavations is not precisely known, but it is assumed that they must have been significant. At present, only some 10% is still judged accessible.

It was used more generally as ashlar stone in façades, and in combination with another dark-coloured stone or brick, it formed the typical gothic polychrome combination of Flanders known as 'spek' layers [8]. It was used for the Cathedral of Our-Lady in Tournai (14th C.) or the Basilica

of Our-Lady in Halle (14th C.), and thus also in the convent and chapel of the Ursuline order in Mons (early 18th C.) (Fig.7.1-2). Since the stone is not quarried anymore, various stones have been used for replacement in restoration projects, e.g. the white limestones of Thénac, Migné, and Crazannes [8,9]. Pierre de Lens and Portland stone are also cited as possible replacement stones [8]. The use of a repair mortar might reshape and sharpen original architectural details and features, which might be lost due to the rounding or general weathering of the stone.

Weathering

According to Dusar et al. (2009), the sensitivity of the stone to weathering can vary significantly [8]. In general, the stone has a high porosity and due to its composition, the stone is sensible for weathering agents. It is reasonably to very frost sensitive and also sensitive for acid agents leading to rounded shapes of the building blocks [8]. As Fig. A7.4 shows, its soft character can lead to deterioration patterns such as blistering, powdering and scaling. The stone does not have a patina as such, but often has a more yellow outlook in the exterior due to oxidation reactions with glauconite for example. Historic use of this stone often included the painting or oiling of the stone if it was to be used in the exterior. Naturally, once this protective layer is removed, accelerated decay might be expected on the lower friable stone (Fig. A7.4).

Fig. A7.3 The chapel of the Ursuline convent in Mons (BE). The white elements are assumedly all Avesnes blocks. Any possible replacement stones cannot be distinguished from the original stone, since the surfaces are painted over.

Fig. A7.4 One part of the façade is still to be restored (visible as last part of the building on Fig. 1), and the Avesnes stone is visible here. Old paint layers are visible on the stone. This is a detail of a niche on which weathering such as blistering, powdering and scaling is visible. The black deposit appears to be present on the superficial paint layer only.

A7.1.2 Maastrichter stone

Origin

Maastricht limestone is formed from the remains of microorganisms. A sea covered Belgium and the Netherlands throughout the Cretaceous. At the end of the Upper Cretaceous, the sea began to withdraw, leaving shallow sea basins behind. The remainders of micro-organisms such as foraminifers, algae and bivalves, which had been deposited on the seafloor were now exposed to the turbulence of waves: they partially dissolved into calcium carbonate grains. They were deposited at the bottom of these basins, forming Maastrichter limestone [8]. The stone therefore consists of bioclastic sand, and contains fossil fragments and bioclasts from silt to gravel size [8,10]. The stone is homogeneously bioturbated [8,10]. Flint nodules can occur in certain layers. The stone was likely subjected to a very low burial depth (<50 m) and was therefore only subjected to a very low lithostatic pressure.

The Maastricht Formation is maximally about 100 m thick and can be subdivided into different limestones (top to bottom): limestone of Valkenburg, limestone of Gronsveld, limestone of Schiepersberg, limestone of Emael, limestone of Nekum and limestone of Meerssen. Two different facies can be recognized: "Maastricht facies" in the South-West of Southern Limburg (NL), while in the eastern part there is the 'Kunrade facies'. The 'Kunrade facies' is a hard, well cemented limestone, alternated with soft limestone with some clay content. The 'Maastricht facies' consists of soft stone, with bioclasts of sand size, and is also known as the "the tuffaceous chalk of Maastricht". Used as building stone, the Maastrichter can be subdivided in Zicher, Kanner and Sibbe blocks. Although these stones have a similar origin and evolution, the Sibbe stone is found to have a greater durability [8].

Table A7.2 gives more information concerning the name, varieties, and geological age of the Avesnes stone.

Table A7.2 General information sheet concerning the Maastrichter stone

Type	Sedimentary limestone
Other names	Limestone of Maastricht, Sibbestone, *Sibberblok*, *Kannerblok*, *Roosburgblok, Zicherblok* (commercial names in 20th c.). Other names which are preferably not used, since they are geologically incorrect: Maastrichts tuff stone, *Mergelsteen*, *Krijt van Maastricht*, *tuffeau de Maastricht* (FR)
Quarries	In the region between Tongeren and Valkenburg, and used in South-Limburg (NL), South-East of Limburg (BE), and adjoining communities in the province of Liège (BE). One quarry is still open in Sibbe.
Geological age	Mesozoic, Upper Cretaceous, Maastrichtian (72.1-66 Ma)

Fig. A7.5 Map of Belgium. The provenance of Maastrichter stone is marked in yellow. Figure made based on information from Google Maps 2016.

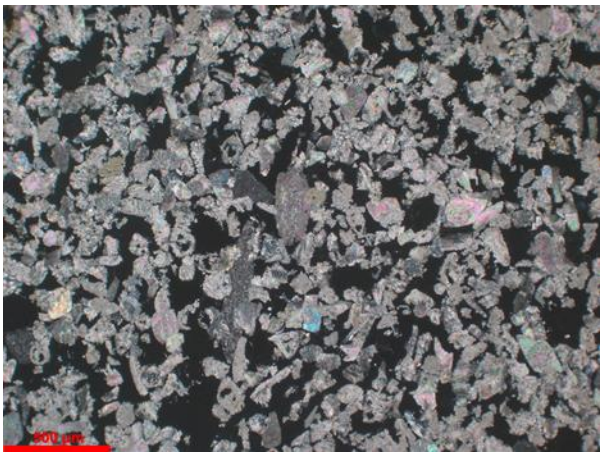

Fig. A7.6 Microscopic view of the Maastrichter stone in cross-polarized light. The scale bar represents 500 µm. The calcite grains of bioclasts show almost no compaction.

Description

The Maastrichter limestone used in this study is yellow coloured and fine to coarse grained. No laminations or heterogeneities are visible with the naked eye or loupe.

The stone is mainly composed of calcite, and on some occasions, the fossil remains are larger than the general 'fossil mud' visible in the stone. They were however still too small to be able to be recognized with certainty, but literature makes reference of foraminifers, algae, bryozoan and bivalves [8]. The grains hardly seem to touch each other in some zones of the thin section, and the voids visible between the grains are thus also large (Fig. A7.6). No cement could be distinguished, which is in accordance with findings in literature [8,11]. An occasional quartz grain was identified. The stone was classified as a bioclastic grainstone.

Use

The Maastrichter stone is quarried underground, on a rather shallow depth, in order to remain above groundwater level. Many old quarries were as such created and various subsurface rooms and galleries still exist, but are blocked or unstable [8]. The ruling architectural styles of the 19th century demanded harder stones, and the Maastrichter stone was left aside. Most quarries stopped working after the post-World War II demand of building materials had ceased. Now, only one quarry is still left, producing Maastrichter blocks almost only for restoration purposes[8].

The Maastrichter limestone has been used as a building stone since the Roman age, and was used throughout the Middle Ages. Buildings were either completely erected in this stone, or the stone was used for decorative architectural details and window arches and sills [8]. An important example of such a building is the Gothic Our-Lady- Basilica and adjoining

Romanesque convent in Tongeren (Fig. A7.7) [11]. Although there are still some beds present in the South-East of Belgian Limburg, French stones such as Savonnières are most often used to replace Maastricht limestone in restoration projects. Repair mortars might be used for Maastrichter limestone when architectural details are lost due to weathering of the surface, or because of mechanical damage.

Weathering

Viollet-Le-Duc in 1864 already mentioned the formation of a characteristic 'calcin' layer on the surface of an exposed Maastricht limestone [11]. This thin and superficial layer of calcite is formed due to the dissolution and recrystallization of calcite on the surface of the stone. The calcin layer protects the stone against weathering, and can thus be seen as a naturally formed protective coating. Although this layer can protect the stone, due to the differences in properties between the calcin and the rest of the stone, the layer can delaminate (bladder), leaving the stone unprotected [8].

Fig. A7.7 Maastrichter stone was used to build Our-Lady-Basilica, in Tongeren, Belgium.

A7.1.3 Obernkirchener stone

Origin

Obernkirchener deposits were formed during the Lower Cretaceous, and these deposits spread from Hannover to the Dutch border, and from Bremen to the Rhine sedimentation basin. The Obernkirchener belongs to the group of stones deposited in the German Wealden facies, Late Berriasien (145.5 - 140.2 Ma) [8]. An isolated basin was created in north-western Germany due to regression of the North Sea. This basin was about 280 km long from East to West and about 80 km wide from North to South. Briny water and lake sediments were consequently alternated with thin marine sedimentations when the sea spread land inwards. Obernkirchener specifically was formed by deposition of sands in the coastal rim area of the basin, and its marine

origin can still be seen due to the presence of glauconite [8]. The stone is known to contain fossils of vertebrates, such as dinosaurs, and show well-preserved dinosaur tracks. Table A7.3 presents general information of the Obernkirchener stone.

Table A7.3 General information sheet concerning the Obernkirchener stone

Type natural stone	Sedimentary stone – sandstone
Other names	*Bremer Sandstein, Bückeberger Sandstein, Stadthagener Sandstein*
Varieties	Colour: grey with some iron banding or yellowish grey with grey banding, or yellowish grey with strong iron banding
Quarry	The sandstone can be quarried in the Bückebergen, the Harrl, Deister and Rehburger Bergen, Germany. There is an existing quarry in Bückeberg, near Hannover. The sandstone bank has a thickness of about 15m, and is horizontally embedded. Eight homogeneous beds, with a maximal thickness of 1m 20, are being quarried.
Geological age	Mesozoic, Lower Cretaceous, Berriasian (145- 139.8 Ma), Wealden facies

Fig. A7.8. Map of Germany with the quarry of Obernkirchen marked with the yellow arrow. Figure made based on information from Google Maps 2016.

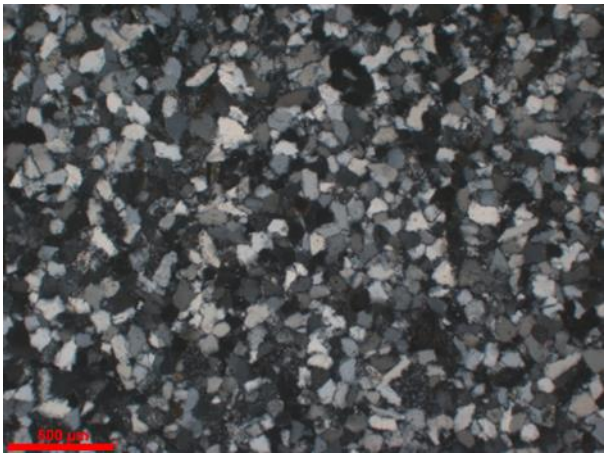

Fig. A7.9. Microscopic view of the Obernkirchener stone in cross-polarized light. The scale bar represents 500 µm.

Description

Macroscopically, the stone can be described as a light grey fine-grained compact stone. *Liesegang* patterns as described by Dreesen et al. (2009) and little specks of oxidized iron are also macroscopically visible [8]. Larger bioclasts of about a centimetre can occasionally be distinguished. Fig. A7.9 shows the thin section from the stone used in this study. The bulk of the stone is made out of quartz (80-95%). The cement consists mainly of syntaxial overgrown quartz. Convex-concave contact points are also clearly distinguished. Chalcedony, chert and tourmaline were occasionally detected in the thin section. The description is in agreement with literature [8,12,13], which indicate that the quartz percentage can vary from 76-95%, and that in addition mica, feldspar, heavy minerals, zircon and epidote also can be present, for less than 1% [8,12].

Use

The Obernkirchener sandstone is quarried since the 11th century in Obernkirchen, after which the stone was transported by river to the city of Bremen, from where it was transported to other regions, among which Belgium. Therefore, the stone was also traded and known as Bremer stone. The fine grains makes fine sculpting possible, and it was used in stone ashlars, certainly from the renaissance to the rococo period. The Obernkirchener stone was used frequently for Bremen buildings, e.g. the city hall, the Stadtwaage, the Bremer bank and the Baumwollbörse. The stone was also used very frequently in the Netherlands, mostly in the 16th - 17th C, for example for the Paleis op de Dam, the city hall in Amsterdam, and it occurs also in buildings in Delft (city hall) and Rotterdam (Museum Boijmans van Beuningen and the International Court of Justice). In Belgium, the stone can be found in some buildings, such as in Antwerp in the city hall, the house of the painter P.P. Rubens and the royal palace (Fig. A7.10). The stone was exported in the 19th Century to various countries such as the Netherlands, Denmark, Norway, Sweden, Russia, and the American continent but found competition from other sandstones. At present, the Obernkirchener sandstone is used as replacement stone for other, more fragile building stones [14].

Weathering

The stone is generally regarded as a very durable stone, resistant to weathering. Only the colour might change over time: it loses its light yellow-grey colour in due course, and becomes greyish. Nijland et al. (2003) mention Obernkirchen as one of the stones which can form distinct thin black weathering layers when exposed to (polluted) environments [12]. Analysis (PFM, SEM, chemical) showed that the thin black weathering is made up of gypsum, micro-organisms, iron hydroxides and oxides, encapsulated airborne materials and heavy metal compounds and salts [12]. The problem is however less explicit in comparison with the Bentheimer sandstone.

Since the stone is quite resistant to deterioration, a repair mortar is in this case probably most useful for the repair of mechanical damage.

Fig. A7.10 The royal palace in Antwerp, known as *Paleis op de Meir*, by architect J.P. Van Baurscheit the Younger (18th Century). The façade is in Obernkirchener sandstone.

A7.1.4 Savonnières stone

Origin [8,15]

This finely grained stone is largely composed of ooliths, which were formed in the Paris basin, a shallow, clear subtropical sea. Ooliths are spherical grains made of $CaCO_3$, and have a diameter between 0.3 and 0.7 mm. They show a concentric layering around a nucleus of micrite. Tidal waves assembled these ooliths in calcareous sand banks, mixing them with crushed shell fragments and peloids, non-concentrically layered micrite-rich spheres. The ooliths and shell fragments dissolved quickly after deposition, after which fresh water calcite cemented the deposits. The *Brauvilliers* type of the stone contains a superior layer of silicified concretions, which protected the ooliths and shell fragments from dissolution. The stone banks can be found in a region of over 1200 km² [8].

Table A7.4 gives more information concerning the name, varieties, and geological age of the Savonnières stone.

Table A7.4. General information concerning the Savonnières stone

Type natural stone	Sedimentary stone – limestone
Other names	Brauvilliers
Varieties	*Savonnières demi-fine*, *Savonnières fine*, *Savonnières demi-fin coquililer*, *Brauvilliers liais*
Quarry	Savonnières-en-Perthois, département de la Meuse, Lorraine region, France
Geological age	Mesozoic, Upper Jurassic, Tithonian (152.1-145 Ma), Barrois Plateau limestone Formation

Description

The Savonnières stone is a beige medium to coarse grained stone. Pores are visible macroscopically. Under the microscope (Fig. A7.12), the dominancy of ooliths is clearly visible. The ooliths are held together with a calcite cement (dog tooth sparite). The cores of the ooliths are partially or completely dissolved (then only the rim is visible). The pore volume consists thus, as stated in literature [8,16], of the interparticle and secondary, intraparticle porosity.

Depending on the location of the stone in the bedding plane, more or less shell fragments are present. with a grainstone texture. The amount of shell fragments, often from bivalves, indicates the quality (variety) of the stone. Also intraclasts of micritic limestone and oxidized opaque minerals can occur [8].

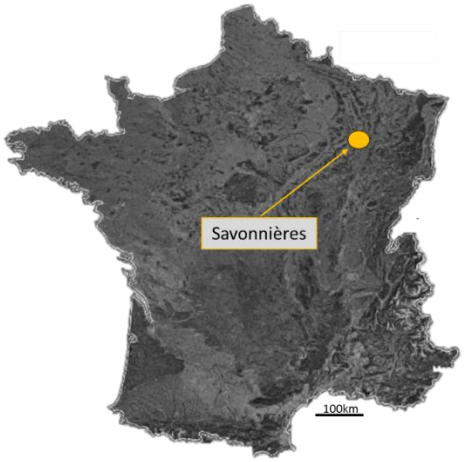

Fig.A7.11 Map of France with the provenance of Savonnières and Brauvilliers indicated in yellow. Figure made based on information from Google Maps 2016.

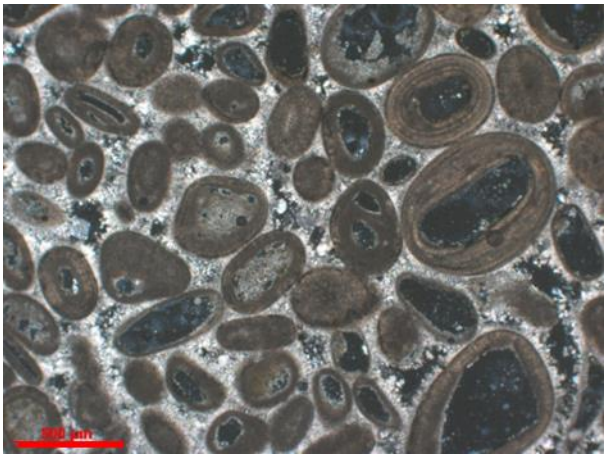

Fig.A7.12 Microscopic view of a Savonnières stone in cross-polarized light. The scale bar represents 500 µm. Ooliths are partially to completely dissolved, and are held together by calcite cement.

Fig. A7.13 Old postcard of the *Beurs*, the former stock exchange market, in Brussels, by architect L. Suys (19th Century).

Use

The stone is quarried since the Roman age, usually underground, since the exploitable layer for building stones is not higher than 3 m, at 20 m deep. Here as well, long quarry galleries are still present. The Savonnières and Brauvilliers are sometimes presented as two different stones, but it is actually the same stone bed, exploited in two different villages (Savonnières-en-Perthois and Brauvilliers) [8]. A distinction is made in quality, *fine* for the best quality, *demi-fine* if the grain size visibly varies, and *demi-fin coquillier* if shell-rich layers are present. Currently, a quarry is still operating in Couleuvre [15].

The stone has been found on a Roman excavation site in Tongeren (BE) and on a Medieval excavation site in Maastricht (NL) [8,15]. The stone was mainly used in the regions bordering the Meuse River, in the Barrois, Argonne, Aube and Haute-Marne region for the construction of vernacular

and religious buildings, and report has been made of its use for the Cathedral of Troyes [15].

The Savonnières stone was exponentially used in the second half of the 19th and first half of the 20th Century, where it was used for the then trending neo-styles, such as the neo-Gothic and neo-Romanesque styles [15]. In the Netherlands, Savonnières was used in the St John's Church (Maastricht) and the Munster Church in Roermond. In Belgium, Savonnières is one of the most frequently used French stones, alongside with the Massangis and Euville stone [16]. Savonnières was an important building stone in Belgium in the period of 1850-1925 [9], both for new build and for restoration of buildings constructed in local white stones, often in combination with other French limestones. Several important buildings in Brussels contain Savonnières: e.g. the Palace of Justice, the 'Beurs', the building where used to house the Brussels stock exchange (Fig.A7.13), and the train station of Brussels North [9].

Weathering

The stone has a white cream-coloured patina, but can show crumbling, alveolation and differential weathering where shell-rich layers stand out [8,15]. Occasionally, the opaque minerals oxidize and may stain the stone [8]. In some cases the stone is not very subjected to deterioration, since it dries rather quickly, due to its high porosity [8]. In other cases, the stone shows strong delamination, and a hypothesis suggests this would be due to a locally smaller pore structure [15]. Gypsum crusts of maximum 2 mm can occur. Repair mortars for Savonnières could be used to repair mechanical damage, and the repair damage by delamination, when the cause of the delamination is understood better.

A7.2 The best mortar recipes estimated by the algorithm

Figures A7.2.1-16 and Tables A7.2.1-4 represent the mortar recipes which were estimated to have the most compatible properties by the algorithm, as run for the exploitation of chapter 7.

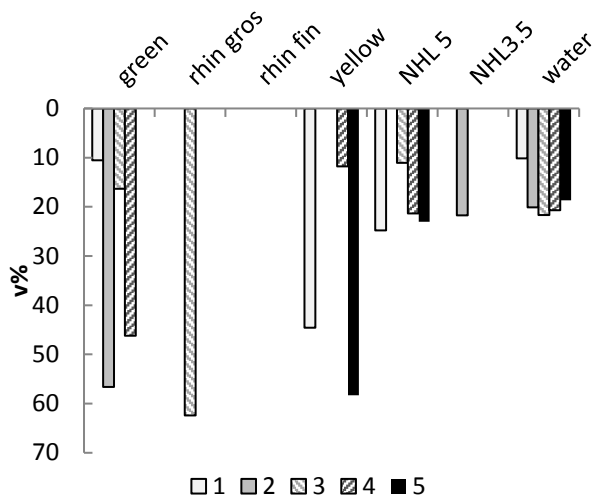

Fig. A7.2.1 The 5 best Oberkirchner mortar recipes, according to the algorithm as used for the exploitation. The mortars produced are 2 (Ober-3) and 3 (Ober-4).

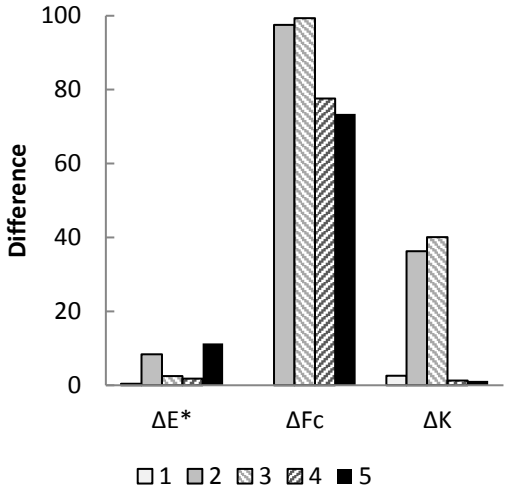

Fig. A7.2.2 The estimated properties of the 5 best Oberkirchner mortar recipes, according to the algorithm as used for the exploitation. The difference is in absolute values for ΔE*, in percentage for ΔFc and Δk. The mortars produced are 2 (Ober-3) and 3 (Ober-4).

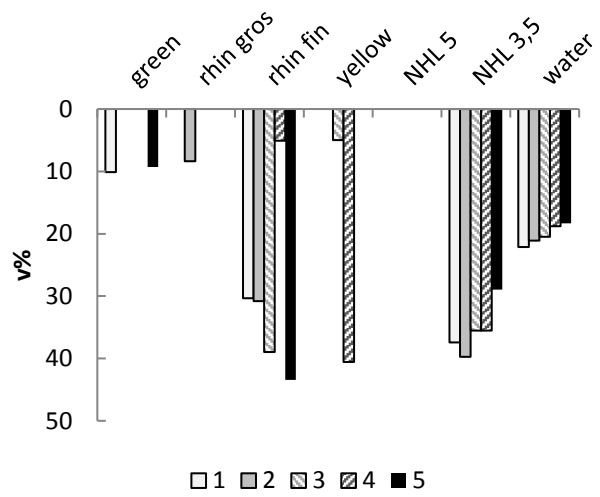

Fig. A7.2.5 The 5 best Savonnières mortar recipes, according to the algorithm as used for the exploitation. The mortars produced are 1 (Savonn-1) and 2 (Savonn-2).

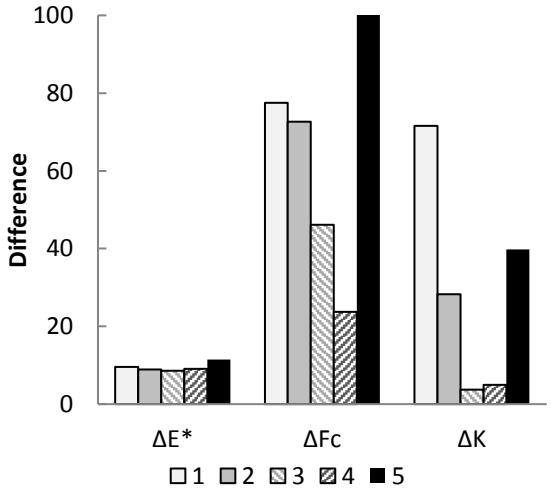

Fig. A7.2.6 The estimated properties of the 5 best Savonnières mortar recipes, according to the algorithm as used for the exploitation. The difference is in absolute values for ΔE*, in percentage for ΔFc and Δk. The mortars produced are 1 (Savonn-1) and 2 (Savonn-2).

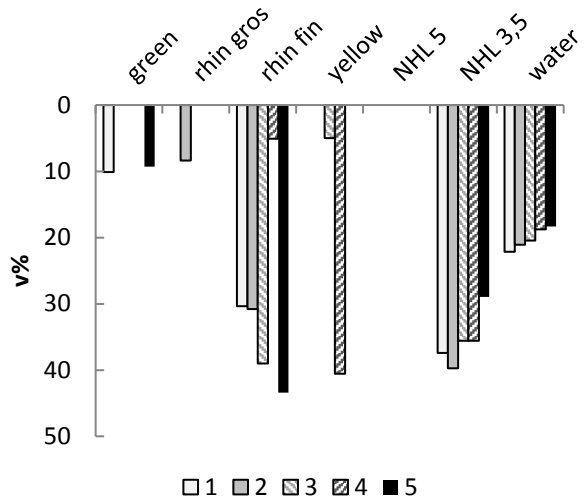

Fig. A7.2.9 The 5 best Avesnes mortar recipes, according to the algorithm as used for the exploitation. The mortars produced are 1 (Avesnes-1) and 2 (Avesnes-2).

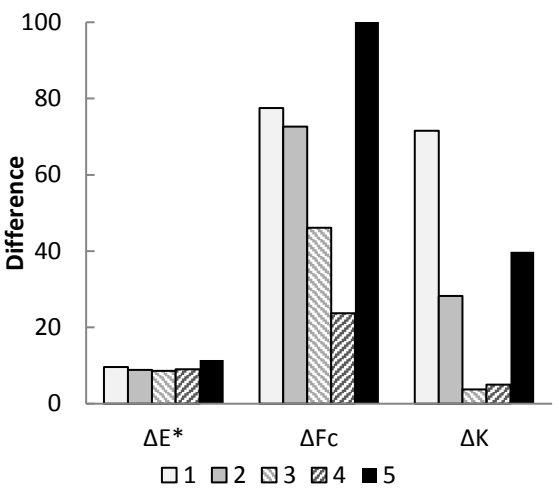

Fig. A7.2.10 The estimated properties of the 5 best Avesnes mortar recipes, according to the algorithm as used for the exploitation. The difference is in absolute values for ΔE*, in percentage for ΔFc and Δk. The mortars produced are 1 (Avesnes-1) and 2 (Avesnes-2).

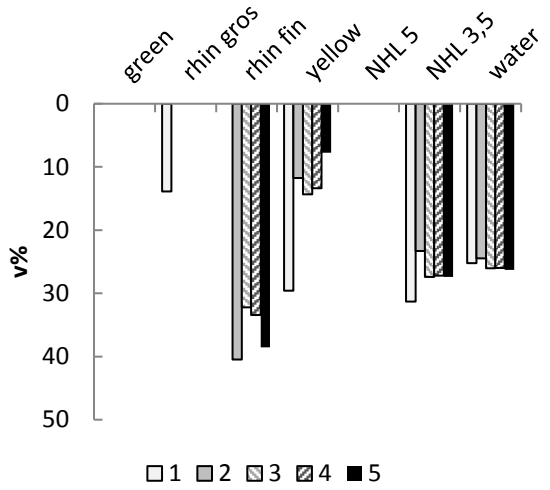

Fig. A7.2.13 The 5 best Maastrichter mortar recipes, according to the algorithm as used for the exploitation. The mortars produced are 1 (Maast-3) and 2 (Maast-4).

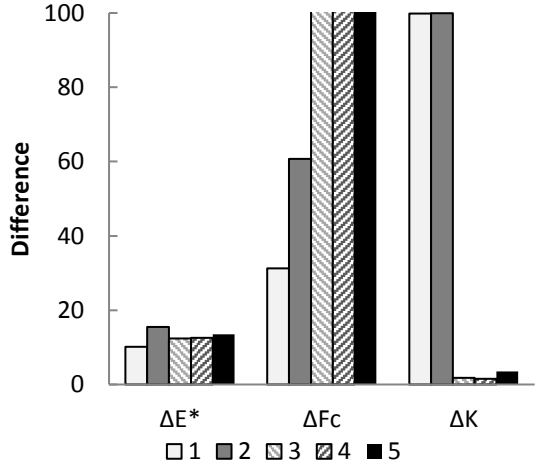

Fig. A7.2.14 The estimated properties of the 5 best Maastrichter mortar recipes, according to the algorithm as used for the exploitation. The difference is in absolute values for ΔE*, in percentage for ΔFc and Δk. The mortars produced are 1 (Maast-3) and 2 (Maast-4).

Bibliography

[1] Chen H, Sun W, Stroeven P, Sluys LJ. Overestimation of the interface thickness around convex-shaped grain by sectional analysis. Acta Mater 2007;55:3943–9. doi:10.1016/j.actamat.2007.03.009.

[2] Chen H, Zhu Z, Liu L, Sun W, Miao C. Aggregate shape effect on the overestimation of ITZ thickness: Quantitative analysis of Platonic particles. Powder Technol 2016;289:1–17. doi:10.1016/j.powtec.2015.11.036.

[3] Dessoy Q. Vers une maîtrise colorimétrique du béton. University of Mons, 2015.

[4] Ottaviani I. Contribution à la caractérisation colorimétrique des mortiers: méthodes de mesure et outils de représentation de la couleur des mélanges. University of Mons, 2010.

[5] Ecrepont S. Compatibilité des mortiers de restauration: contribution à l'étude de la migration des fluides. University of Mons, 2014.

[6] Larrard F de. Concrete Mixture Proportioning: A Scientific Approach. London: E & FN Spon; 1999.

[7] Deb K. Multi-Objective Optimization using Evolutionary Algorithms. Chichester: John Wiley & Sons Ltd.; 2001.

[8] Dusar M, Dreesen R, De Naeyer A. Natuursteen in Vlaanderen, versteend verleden. Mechelen: Kluwer; 2009.

[9] Dreesen R, Cnudde V, Dusar M, de Ceukelaire M, Bossiroy D, Groessens E, et al. In het voetspoor van Camerman: de opmars van de Franse steen in België. In: van Hees R, de Clercq H, Quist W, editors. 4de Vlaamse-Nederlandse Natuursteendag. Stenen van binnen, stenen van buiten natuursteen Jong. bouwkunst, Delft: Delftdigitalpress; 2012, p. 33–63.

[10] Cnudde V. Exploring the potential of X-ray tomography as a new non-destructive research tool in conservation studies of natural building stones. Ghent University. Faculty of Sciences, 2005.

[11] De Geyter G. De tuffeau van Lincent en de Maastrichtersteen. Bull van Belgische Ver Voor Geol 1991;99:177–83.

[12] Nijland T, Dubelaar C, Hees R Van, Linden T. Black weathering of Bentheim and Obernkirchen sandstone 2003:179–95.

[13] Stück H, Koch R, Siegesmund S. Petrographical and petrophysical properties of sandstones: statistical analysis as an approach to predict material behaviour and construction suitability. Environ Earth Sci 2012;69:1299–332. doi:10.1007/s12665-012-2008-1.

[14] Pätzold J, Wefer G. Naturbausteine der Bremer Innenstadt. Bremen: marum Bibliothek; 2002.

[15] Dubelaar W, Dreesen R, Lagrou D. Pierre de Savonnièrs: een historische bouwsteen in beeld gebracht. In: Van Hees R, de Clercq H, Quist W, editors. 4de Vlaamse-Nederlandse Natuursteendag. Stenen van binnen, stenen van buiten natuursteen Jong. bouwkunst2, Delft: Delftdigitalpress; 2012, p. 65–76.

[16] Cnudde V, Dewanckele J, de Ceukelaire M, Everaert G, Jacobs P, Laleman MC. Gent...Steengoed! Gent: Academia Press; 2009.

Repair mortars for stone : Increased compatibility through optimised development

Built heritage demands interventions in order for it to resist weathering and deterioration. The materials applied on built heritage are aimed to be compatible with the original building material. Repair mortars for stone also need to fulfil this demand: the properties of every mortar should thus depend on the properties of the stone. Repair mortars are however not always chosen for their adapted properties, mainly because time and budget do not permit to determine what mortar recipe is (most) compatible and durable.

In this thesis, a system is introduced which, based on the requirements of the stone, will propose several potentially compatible mortar recipes. The number of mortar recipes which should be produced and tested is as such reduced. The system focuses on three properties: permeability, colour and elasticity of the mortar, since in terms of performance they proved to be the most influential for compatibility. As the system should be able to present mortar recipes, this thesis discusses the effect of the mortar components on each of these three properties. Their effect is determined by theory and experimental campaigns. This knowledge is used in this thesis for the development of an estimation method for both permeability and elasticity and the adaptation of an estimation method for colour. These estimation methods were implemented into an optimisation algorithm, able to create mortar recipes based on a database and the established estimation methods. Finally, this system as a whole was tested on various natural sedimentary stones.

The thesis leads to the conclusion that the system presented here sets a solid base for an optimised mortar development. Future research can improve the system through the implementation of mineralogy as a compatibility parameter or by elaborating the estimation methods by including the effect of ageing.

Aurélie Isebaert

Aurélie Isebaert holds a Master in Conservation and Restoration from the University College Artesis, Antwerp (Belgium). She specialised in stone, plaster and terracotta sculptures and her Master thesis discussed the possibilities of removing synthetic polymers from marble. With a keen interest for materials and their influence on their surroundings, Aurélie Isebaert then started her research concerning the optimisation of repair mortars for natural stone as a joint doctoral research between the Faculty of Engineering at the University of Mons (Belgium) and the Faculty of Sciences at Ghent University (Belgium).

Université de Mons
20, Place du Parc, B7000 Mons - Belgique
Tél: +32(0)65 373111
Courriel: info.mons@umons.ac.be
www.umons.ac.be

UMONS Université de Mons | POLYTECH MONS | GHENT UNIVERSITY